OPEN ACCESS

University of BRISTOL

This electronic thesis or dissertation has been downloaded from Explore Bristol Research, http://research-information.bristol.ac.uk

Author:
Kalligas, K. P

Title:
The dynamic characteristics of two-dimensional spoilers at low speeds

General rights
Access to the thesis is subject to the Creative Commons Attribution - NonCommercial-No Derivatives 4.0 International Public License. A copy of this may be found at https://creativecommons.org/licenses/by-nc-nd/4.0/legalcode This license sets out your rights and the restrictions that apply to your access to the thesis so it is important you read this before proceeding.

Take down policy
Some pages of this thesis may have been removed for copyright restrictions prior to having it been deposited in Explore Bristol Research. However, if you have discovered material within the thesis that you consider to be unlawful e.g. breaches of copyright (either yours or that of a third party) or any other law, including but not limited to those relating to patent, trademark, confidentiality, data protection, obscenity, defamation, libel, then please contact collections-metadata@bristol.ac.uk and include the following information in your message:

• Your contact details
• Bibliographic details for the item, including a URL
• An outline nature of the complaint

Your claim will be investigated and, where appropriate, the item in question will be removed from public view as soon as possible.

UNIVERSITY OF BRISTOL

Department of Aeronautical Engineering

The Dynamic Characteristics of Two-Dimensional Spoilers at Low Speeds

Konstantinos Kalligas B.Sc. (Eng.)

A dissertation submitted for the degree of
Doctor of Philosophy in Engineering

December 1986

DEDICATION

To Helen

For adding the inspiration and taking the perspiration.

LIST OF CONTENTS

LIST OF FIGURES

Figure	Caption
5.5	Lift variation with steady spoiler angle
5.6	δ and C_L time histories for Run 3001 (extension of gapped spoiler on rear upper surface, $\alpha = 0°$, $U = 20\,m/s$, $\dot{\delta} = 990°/s$)
5.7	C_p time histories for Run 3001
5.8	C_p chordwise distributions for Run 3001
5.9	δ and C_L time histories for Run 3007 (as Run 3001, but $U = 10\,m/s$)
5.10	δ and C_L time histories for Run 3003 (as Run 3001, but $\dot{\delta} = 500°/s$)
5.11	δ and C_L time histories for Run 3009 (as Run 3001, but $U = 10\,m/s$, $\dot{\delta} = 500°/s$)
5.12	δ and C_L time histories for Run 3005 (as Run 3001, but $\dot{\delta} = 250°/s$)
5.13	Aerodynamic delay times for Run 3001 to 3009
5.14	δ and C_L time histories for Run 3201 (as Run 3001, but solid spoiler)
5.15	δ and C_L time histories for Run 2001 (as Run 3001, but perforated spoiler)
5.16	Aerodynamic delay times for Run 3001 to 3009, 3201 to 3209 and 2001 to 2009
5.17	δ and C_L time histories for Run 5001 (as Run 3001, but $\alpha = 14°$)
5.18	C_p time histories for Run 5001
5.19	C_p chordwise distributions for Run 5001
5.20	δ and C_L time histories for Run 5003 (as Run 5001, but $\dot{\delta} = 500°/s$)

Figure	Caption
5.21	Aerodynamic delay times for Run 3001 to 3009 and 5001 to 5009
5.22	δ and C_L time histories for Run 5101 (as Run 5001, but solid spoiler)
5.23	δ and C_L time histories for Run 4011 (as Run 5001, but perforated spoiler)
5.24	Aerodynamic delay times for Run 5001 to 5009 and 4011 to 4019
5.25	δ and C_L time histories for Run 3051 (as Run 3001, but retraction)
5.26	C_p time histories for Run 3051
5.27	C_p chordwise distributions for Run 3051
5.28	Aerodynamic delay times for Run 3051 to 3059
5.29	δ and C_L time histories for Run 3251 (as Run 3051, but solid spoiler)
5.30	Aerodynamic delay times for Run 3051 to 3059, 3251 to 3259 and 2051 to 2059
5.31	δ and C_L time histories for Run 5051 (as Run 3051, but $\alpha = 14°$)
5.32	Aerodynamic delay times for Run 3051 to 3059 and 5051 to 5059
5.33	Aerodynamic delay times for Run 5051 to 5059 and 4051 to 4059
5.34	δ and C_L time histories for Run 3103 (as Run 3001, but $\dot{\delta} = 500°/s$, also $\delta_i \neq 0°$)
5.35	Optimization of spoiler displacement profile
5.36	δ and C_L time histories for Run 3611 (as Run 3001, but $\dot{\delta} = 425\text{-}593\text{-}990°/s$)

Figure	Caption
5.37	C_p time histories for Run 3611
5.38	δ and C_L time histories for Run 3652 (as Run 3611, but solid spoiler, $\dot{\delta}$ = 330-600-900°/s)
5.39	δ and C_L time histories for Run 5631 (as Run 3611, but $\alpha = 14°$)
5.40	δ and C_L time histories for Run 3631 (as Run 3611, but $\dot{\delta}$ = 990-778-560-344°/s)
5.41	δ and C_L time histories for Run 3561 (as Run 3611, but retraction, $\dot{\delta}$ = 990-600-330°/s)
5.42	δ and C_L time histories for Run 3901 (as Run 3001, but short pulse, $\dot{\delta}$ = 990-790°/s)
5.43	C_p time histories for Run 3901
5.44	δ and C_L time histories for Run 9202 (extension of gapped spoiler on rear lower surface, $\alpha = 15°$, U = 20 m/s, $\dot{\delta}$ = 500°/s)
5.45	C_p time histories for Run 9202
5.46	C_p chordwise distributions for Run 9202
5.47	δ and C_L time histories for Run 9002 (as Run 9202, but solid spoiler)
5.48	δ and C_L time histories for Run 7102 (as Run 9002, but $\alpha = 20°$)
5.49	δ and C_L time histories for Run 9502 (as Run 9002, but $\dot{\delta}$ = 330-600-990°/s)
5.50	δ and C_L time histories for Run 9504 (as Run 9002, but short pulse, $\dot{\delta}$ = 330-600-900-990°/s)
5.51	C_p time histories for Run 9504
5.52	δ and C_L time histories for Run 9505 (as Run 9504, but long pulse)

ACKNOWLEDGEMENTS

I wish to express my sincere gratitude to Dr.D.L. Birdsall for his guidance, constant assistance and critical supervision.

In addition, I feel indebted to the following individuals and organizations:

The Ministry of Defence for their financial support and to Mr. D.G. Mabey of the Royal Aircraft Establishment, Bedford for his continuous interest and original ideas.

Dr. T.J. Cobbald for his valuable help and suggestions with regard to the development of the experiment-control hardware and software.

Prof. L.F. Crabtree for his inestimable support.

The technical staff of the Department of Aeronautical Engineering for their considerable assistance and craftsmanship, especially J. Hawkins, F. Wheeler and J. Burns of the Electronics Division.

Mrs. A. Palmer for her patience and willingness to keep late hours for typing this dissertation.

.....

Konstantinos Kalligas

DECLARATION

The work presented in this thesis was carried out solely by the author, under the supervision of Dr. D.L. Birdsall, at the Department of Aeronautical Engineering in partial fulfillment of the requirements for the Degree of Doctor of Philosophy.

The ideas and results are original except where otherwise acknowledged or referenced and no part of this work has been submitted previously to any University, College or other academic Institute.

.....

Konstantinos Kalligas

PERMISSION TO COPY

Konstantinos Kalligas

The Dynamic Characteristics
of
Two-Dimensional Spoilers at Low Speeds

Supervision: Dr. D.L. Birdsall

Department of Aeronautical Engineering
University of Bristol

I, the undersigned am willing that this thesis should be made available for consultation in Bristol University Library, for inter-library lending, for use in another library, or for photocopy in part or in full, at the discretion of the Librarian, and on the understanding that users are made aware of their obligations under copyright.

.....

Konstantinos Kalligas

SUMMARY

The dynamic characteristics of spoilers are notoriously non-linear. This is mainly due to the influence of a starting vortex induced by rapid deployment, causing an initial reversal of the desired lift response known as "adverse lift". A series of tests is presented from an experimental investigation into these dynamic characteristics for two-dimensional aerofoil-mounted spoilers at low freestream speeds. The results were obtained for two Reynolds numbers (2.8 and 5.6 x 10^5), and cover a range of angles of incidence, several spoiler positions and configurations and a range of rates of deployment (up to 1000°/sec). For the purposes of this investigation a real-time system for spoiler control and data acquisition was designed and built.

Chordwise pressure histories are presented individually and in integrated form. Good agreement is obtained with previous measurements regarding overall lift response characteristics and correlation of adverse lift and time for achievement of final lift in terms of the aerodynamic time parameter $\frac{UT}{c}$.

A technique for suppressing the adverse lift is explained and demonstrated with success. This technique is based on minimizing the change in rotation rate throughout deployment.

The usefulness of a lower-surface spoiler as an active control is highlighted. An increase in mean lift has been achieved by provoking a series of pulses of additional lift.

LIST OF SYMBOLS

C_L section lift coefficient at aerofoil centreline
$= \frac{\text{lift force}}{\frac{1}{2}\rho V^2 Ss}$

C_{L_a} net size of adverse lift

Cp local pressure coefficient $= \frac{p-p_o}{\frac{1}{2}\rho V^2}$

c aerofoil chord (410mm)

f frequency

p_o free stream static pressure

Re Reynolds number based on aerofoil chord

S wing area ($0.328m^2$)

s aerofoil span (800mm)

T time for spoiler rotation

t time from initiation of pressure measurements

t_a time to achieve adverse lift peak minus t_i

t_f time to achieve final lift minus t_i

t_i time to initiation of spoiler transient motion

t_o time for onset of lift change minus t_i

$\hat{t}$ $t-t_i$

U free stream velocity

x chordwise distance from leading edge

α angle of incidence

δ spoiler deflection

$\dot{\delta}$ spoiler rotation rate (deg/s)

$\bar{\dot{\delta}}$ spoiler average rotation rate (deg/s)

δ_i initial spoiler angle

δ_f final spoiler angle

Δ prefix denoting incremental change

ρ air density (1.225 Kg/m^3)

ω circular frequency = $2\pi f$

Notation Specific to Appendix B

a_o mean velocity of sound

C_p specific heat of fluid at constant pressure

i imaginary unit, $i = \sqrt{-1}$

J_n Bessel function of first kind of order n

K fluid conductivity

K_j polytropic constant for lumped volume elements

L_j length of the jth tube element

N number of tubes and volumes

n_j complex polytropic constant defined by Equ.(B.4)

P_r Prandtl number, $P_r = \mu C_p/K$

p_o amplitude of sinusoidal input pressure

R_j radius of tube element

V_j volume of tube element, $V_j = \pi R_j^2 L_j$

V_{vj} pressure transducer volume

α_j shear wave number, defined by Equ.(B.3)

γ specific heat ratio

μ fluid molecular viscosity

ρ_s mean density

σ_j dimensionless increase in transducer volume due to diaphragm deflection

ϕ_j complex variable defined by Equ.(B.2)

Special Abbreviations

ADC Analogue-to-Digital Convertor

DAC Digital-to-Analogue Convertor

DS/DD Double-sided, Double-density

DVM Digital Voltmeter

Kb Kilobyte = 1024 bytes

Mb Megabyte = 1024 Kb

MUX Multiplexer Circuit

PAD Packet Assembler-Disassembler

RAM Random Access Memory

S/H Sample-and-Hold Circuit

CHAPTER ONE

INTRODUCTION

1.1 General Background

Spoilers are currently in widespread use on aircraft as aerodynamic control devices. (A spoiler resembles a split-flap, only mounted on the upper surface of the wing, and is deployed in a similar manner). Spoiler deployment results primarily in local spanwise lift reduction and drag increase. Hence, current utilization involves (a) simultaneous extension of spoilers on both wings, causing net downward and rearward forces, i.e. a particularly desirable combination for use during the final landing phase; and (b) separate extension, producing a net rolling moment and thus assisting or supplanting the ailerons for roll control: the ailerons can then be reduced in span or eliminated in favour of longer- or full-span flaps, with consequent improvements in aircraft short-field performance. For the implementation of such applications, the aerodynamic phenomena associated with statically deflected spoilers have been widely investigated; extensive reference lists on the aerodynamic characteristics of spoilers can be found in the works of Hoerner (1975) and of Siddalingappa and Hancock (1980a). Until recently, such investigations have consisted entirely of ad hoc wind tunnel testing for particular wing-spoiler configurations, because of the previous failure to predict spoiler aerodynamic characteristics to any degree of accuracy (mainly due to difficulties in modelling the separated flow regions caused by spoiler deflection). A theoretical model, based on inviscid flow was presented by Brown and Parkinson (1973), its validity obviously restricted to low freestream speeds. This model has since been improved upon by Pfeiffer and Zumwalt (1981), by incorporation of some wake-mixing effects. Additionally, viscous effects have been considered by Le Balleur (1980) to help extend the prediction of spoiler (static) aerodynamics up to transonic speeds. Finally, the theoretical methods still apparently under development at ONERA, France,

are reported to show considerable promise:

In the course of the previous decade (1970's), a whole new dimension was added to the application of spoilers, inspired by ACT (Active Control Technology). High control effectiveness and the ability to provoke rapid lift changes made spoilers appear well-suited to exploits such as gust load alleviation, turbulence reduction, direct force control, and flutter suppression (i.e. raising flutter margins). Naturally a vital requirement for implementation of any of these applications was the extensive knowledge of the transient aerodynamic characteristics of spoilers (i.e. those associated with rapid spoiler motion). Now the enormously complex nature of the fluid mechanisms associated with spoiler transient motion precluded the use of theoretical methods to predict those characteristics. Furthermore, no documented research appeared to exist in this particular field, with the exception of some early water tunnel tests performed by Hoerner (and published much later, 1975) and low-speed wind tunnel and flight tests by Kramer et al (1951). So in response to the newly created requirement as above, recent experimental investigations have been carried out by Siddalingappa and Hancock (1979, 1980b) and Ahmed and Hancock (1983) using a spoiler-like surface deployed from a flat base, and by Siddalingappa and Hancock (1980c), Mabey et al (1982), and Consigny et al (1984) using aerofoil-mounted spoilers; in addition, flow visualisation tests involving a spoiler mounted on the floor of a water tunnel were performed by Garroch (1980), and cine films taken. The more fundamental findings stemming from these works are outlined in the following section.

1.2 Features of Spoiler Transient Aerodynamics

The dynamic characteristics of spoilers display significant non-linearities, which cannot be inferred or explained in terms of the associated static characteristics. Specifically, for a given airstream and conventional wing-spoiler

configuration, rapid spoiler deployment initially actually encourages the lift force to increase, before the intended response in the opposite direction is achieved. Apparently first observed by Kramer et al (1951), this phenomenon was at the time incorrectly linked with the equivalent camber effect produced at small angles of static spoiler deflection. In reality, this occurrence of lift reversal is purely dynamic in nature and will be outlined in some detail herein. Mabey et al (1982) refer to this phenomenon as the "adverse lift effect" and the same term will be used henceforth. These latter authors present extensive documentation of the adverse lift effect at various subsonic and transonic freestream speeds, while the same phenomenon was observed and discussed by Siddalingappa and Hancock (1980c) at low speeds, and, to a lesser extend, by Consigny et al (1984) at subsonic speeds.

A simple explanation of the adverse lift effect can be derived by examination of the associated fluid mechanism, as follows. Rapid spoiler extension causes the formation of a strong starting vortex immediately downstream of the spoiler. In turn, this vortex induces high local suctions which, for a conventionally-placed spoiler i.e. on the upper surface of the wing, cause a net lift increase. The vortex is then slowly convected downstream and is subsequently shed, to be replaced by the classical separation bubble asscciated with steady spoiler deployment. In the meantime, the overall circulation begins to re-adjust and lift gradually decreases to the steady value corresponding to the new static spoiler angle.

Conversely, rapid spoiler retraction apparently induces no starting vortex and comparable non-linear effects. As the spoiler closes, the separation bubble behind it contracts steadily and is eventually swept away as the spoiler aligns with the wing surface. Hence, no reversal of lift response is observed and the delay times for onset and ending of lift variation between the two steady conditions are rather shorter than for equal and opposite spoiler extension.

Early low-speed tests by Kramer et al (1951) showed that, providing that the airflow was always attached prior to deployment, incidence variation did not greatly affect the airflow response to spoiler motion. Finally, Mabey et al (1982), testing at speeds up to high subsonic, demonstrated that the non-dimensionalised delay times to maximum adverse lift, t_a/T, and to final lift, t_f/T, were unique functions of the dimensionless spoiler deployment time UT/c. Significantly, there appeared to be no Mach number or Reynolds number effects on those measurements.

1.3 Present Investigation

1.3.1 Retrospective view

This investigation was preceded by a number of smaller-scale related works in the same Department. Mainly taking the form of undergraduate projects, and although of undoubted value, these works were primarily of a qualitative nature and, of necessity, limited in scope. In contrast, this study was intended to provide higher-quality measurements as well as being more extensive in content. In broad terms, its purpose was to expand the knowledge of spoiler transient aerodynamics at low speeds. Some time after this investigation was embarked upon, a contract was awarded from the R.A.E. (Bedford), whereupon important additions were made to the pursued aims. In particular, the recommendations for further research made by Mabey et al (1982) were taken up. These included establishing the optimum spoiler geometrical configuration (i.e. utilization of gaps, perforations etc.) and spoiler displacement-time curve for minimum adverse lift, minimum response time delays and smoothest lift variations. Such a combination would be ideally suited to ACT-related applications such as gust load alleviation. A complete list of the objectives of the present investigation is presented in the following sub-section.

1.3.2 Objectives

The raison d' etre of this investigation was to promote the

understanding of the transient aerodynamic characteristics of spoilers.

Itemisation into the specific principal objectives, in order of precedence, follows:

(1) To study in some detail the fluid mechanisms associated with rapidly opening or closing spoilers.

(2) To observe and document the overall lift response to extending and retracting spoilers for a range of the aerodynamic time parameter UT/c. (N.B. Careful choice of range was to ensure sufficient overlap with results from Mabey et al (1982), so that direct comparison with, as well as extension of, that study could be achieved).

(3) To assess the relative merits of different spoiler geometries, concerning speed and smoothness of lift response.

(4) To investigate the adverse lift effect in particular as well as means of suppressing it.

(5) Ultimately, to explore other possible means of enhancing the potential of spoilers for gust alleviation or other comparable applications.

1.3.3 Approach

The subject to which this study was addressed appeared impracticably broad, considering the amount of human and material resources available within the context of university postgraduate research. As such, there was a need to narrow the field of pursuit in order to ensure that the investigation would be tractable. This was achieved by screening each of the relevant experimental parameters, in view of the objectives listed earlier. On the basis of this screening precedure, the following decisions were taken:

(1) To use a test model consisting of a two-dimensional aerofoil and spoiler.

(2) To restrict the fundamental experimental data to measurements of pressures from the aerofoil surface alone. So, from pressure time-histories the instantaneous chordwise pressure distributions could be obtained and, also, by integration of these instantaneous pressure distributions, lift and quarter-chord pitching moment histories could be deduced (though pitching moment was not to be investigated). Measurement of instantaneous spoiler angle was also necessary for reference.

(3) To confine testing to two Reynolds numbers and selected values of incidence, but at each of these there would be alterations to spoiler geometrical configurations and positions, and to spoiler angles and rates of rotation; details of these appear in Sec.4.2.

As a result of these decisions, the following topics were neglected:

- three-dimensional flow, e.g. around spoiler ends,
- interaction of a spoiler with high-lift devices and other control surfaces (in particular, the aerodynamic characteristics of spoilers are known to be considerably influenced by nearby flap deployment),
- aerodynamic loads on the spoiler (considered small by comparison with enertia forces),
- development of the boundary layer,
- structure of the wake,
- visualization of the flow field produced by spoiler deflection.

1.4 Guide to the Dissertation

Here follows a synoptic description of the remaining contents of this dissertation.

Chapter Two presents the two main discoveries made in the course of the present investigation and discusses their implications regarding the role of the spoiler as an active control.

Chapter Three discribes in detail the various components of the experimental setup.

Chapter Four explains the procedures covering pre-test system integrity checks, actual testing and, briefly, processing of the experimental data.

Chapter Five presents a cross-section of the primary experimental results while also interpreting these.

Chapter Six recapitulates the overall conclusions of the investigation and makes recommendations for further work.

The Appendices are concerned with experiment-related details; these were so transposed either because it was felt that their specialized nature rendered them of little interest to the average reader or simply because they would have otherwise disrupted the flow of the main body of the work.

CHAPTER TWO

PRINCIPAL FINDINGS AND THEIR SIGNIFICANCE

2.1 Introduction

Two discoveries were made in the course of the present investigation which outshone the remaining findings. Both of these discoveries were considered to be of wide significance in the field of spoiler transient aerodynamics, therefore deserving preferential presentation. It is this presentation that is the task of this chapter.

In the two sections to follow, the essence of both of these discoveries will be given, samples of relevant results will be shown, and possible applications will be outlined. A thorough account will be presented alongside the remaining findings in Ch.5 (specifically Sec.5.3.2 and 5.4, following the order of presentation here).

2.2 Suppression of Adverse Lift

The realization that the magnitude of adverse lift depends on the change of spoiler rotation rate, for a given aerofoil-spoiler combination and given freestream speed, led to the development of a technique to suppress this adverse lift.

Essentially, the usual single-ramp deflection profile was replaced by a series of steps to obtain a continuous but gradual deployment process, thereby reducing the change of rotation rate at any point within the period of deployment (see Fig.5.35(a) for such a deflection profile). The net result was a reduction in adverse lift. A comparative example of this is given in Fig.5.36 where the lift response for a 3-step rotation and that for a single ramp are superimposed. It is a reduction, not an elimination of adverse lift. Had it not been for the limitations of the actuation system (i.e. a limit on maximum rotation rate), this example could have shown a proper elimination.

It will be explained later how the lowest rate $\dot{\delta}_1$ (the first of the three steps) can influence the elimination.

The essence of this controlled lift-response characteristic is that if a powerful actuation system is available, the most undesirable feature of spoiler-induced transient lift can be prevented, thus widening the use of spoilers toward more ACT applications.

A related technique has been employed to augment adverse lift (Fig.5.40) and to minimize the lift response for a retracting spoiler (Fig.5.41).

2.3 Potential Of Lower Surface Spoilers

Tests for statically-deflected spoilers had shown that the lower-surface spoiler displayed superior control effectiveness at high angles of incidence (Fig.5.1 and 5.5, where the upper-surface spoiler at $\alpha < 0°$ is equivalent to a lower-surface spoiler at $\alpha > 0°$). Further, dynamic tests at high angles of incidence showed that the transient lift response for the lower-surface spoiler was as rapid as for the upper-surface spoiler, (e.g. compare Fig.5.44 with Fig.5.20). Therefore, the capacity for positive lift-enhancement from a lower-surface spoiler was seen to be at least as great as the spoiling capacity of a conventional spoiler and indeed it promised effectiveness over a wider range of incidence.

In addition, the combination of rapidity of lift response and direction (i.e. lift increase) could be exploited. In particular, if the lower-surface spoiler was "pulsed" (i.e. it underwent a complete cycle of rotation, with retraction following extension) it is shown that an increase in mean lift could be produced (see Fig.5.53).

Finally, but with little supporting evidence, it is suggested that an improvement on overall L/D ratio could be produced, during this sequence of pulses, because of the relatively slow response in the development of drag compared with lift.

CHAPTER THREE

EXPERIMENTAL ARRANGEMENT

3.1 Introduction

In the early stages of this work, it was envisaged that static and dynamic pressure measurements in the neighbourhood of a spoiler and its associated separation bubble would be taken from a flat-plate model. This arrangement would have allowed the use of a rather larger spoiler than would have been practical for a reasonably-sized wing in the same wind tunnel. This, in turn, would have eased the problems of interpretation of the mechanics of the local fluid phenomena associated with transient spoiler movement. Depending on the success of this early venture, a proper aerofoil model was envisaged; then, after having gained an insight into the aerodynamic mechanisms produced on the previous simpler setup, the more realistic chordwise pressure gradient and flow separation in the locality of the aerofoil-mounted spoiler could be met with greater confidence.

The flat-plate rig featured a hydraulically-driven spoiler and was mechanically complete, but still in need of the electronic control system as well as the microcomputer drive and data-collection apparatus which would serve any such rig. A considerably effort was expended in developing this control system even though it seemed unlikely that it would also serve a future aerofoil model. When an R.A.E. contract was awarded, urgency suggested that this development be abandoned in favour of a more comprehensive programme of tests involving a spoiler-equipped aerofoil rig.

The new rig consisted of a two-dimensional aerofoil which had been built for previous undergraduate research on spoilers. It was mounted on a simple frame for use in an open-jet tunnel and utilised a spring-loaded mechanism to move the spoiler impulsively between two pre-set deployment angles. Several modifications of this rig were necessary and, of course, a new actuation method was needed to allow

greater control of spoiler motion. This scheme would be fully integrated, as outlined above, to include a central microcomputer controller for data acquisition as well as actuation control. The requirements, general layout and major individual components of such a system will be described in the remainder of this chapter.

3.2 Wind Tunnel

The entire testing programme was carried out in a 3.5 ft. (1.07 m) diameter open working section, closed-circuit, low-speed (39 m/s) wind tunnel in the Department of Aeronautical Engineering at the University of Bristol (see Fig.3.1). The open working section tunnel was chosen, despite generally higher turbulence levels than a closed working section tunnel, because the open section allowed easier access to the model for various adjustments. Inevitably, some interference effects arose but no corrections were applied to the experimental measurements (see Appendix A for details).

3.3 Model

The model, shown in Fig.3.2, is a two-dimensional aerofoil of 800 mm span and 410 mm chord fitted with large end plates to preserve its two-dimensional flow. It has a NACA 0012-64 section, chosen for its symmetry and mid-section thickness. The latter feature simplified spoiler installation, whereas the aerofoil section symmetry effectively meant that the model, pitched to a negative incidence, was equivalent to a positively-pitched aerofoil with a lower-surface spoiler.

As stated earlier, the model was available from a previous study (Ref.5), however, extensive modifications were necessary before it could satisfy the requirements of this investigation. These modifications can be conveniently itemised as follows.

(a) The previously used 5% chord, ungapped, solid, full-span spoiler was replaced by an 8% chord, gapped (25% gap), perforated (22.5% open area), also full-span spoiler (Fig. 3.3), with the aim of approximating to the design employed at R.A.E. Bedford by Mabey et al (1982). The spoiler chord was tapered to retain reasonable leading edge thickness, yet fairly sharp trailing edge. Special attachments were built which could plug the spoiler gaps without the need to remove the spoiler; the perforations could be sealed, too, using a strip of adhesive tape for each spoiler surface. Thus a range of spoiler configurations could be tested.

(b) Previously, the spoiler could be mounted at one of two chordwise locations, with the leading edge at u/c = 0.15 or 0.70. Here, only the more common downstream location was required for the most testing. Thus, the cavity in the wing for the spoiler unit at the upstream position was filled in and the cavity at x/c = 0.70 was extended farther aft to accommodate the longer spoiler. The extension to the cavity was kept just deep enough for the retracted spoiler to be flush with the surface. The exposed cavity (not flush) beneath the spoiler when extended was not a source of any flow problems and, in any case, is typical of aircraft installations. In contrast, local surface quality is important and the aerofoil was polished and its smoothness generally improved all over. At the end of the main period of testing, the upstream gap was extended forward, to allow the spoiler to be moved forward to x/c = 0.13. A contour-following wooden block was then fitted into the cavity at the downstream location.

(c) The original 10 static pressure tappings were replaced by 25 new ones (see Fig.3.4). The distribution of these around the aerofoil was carefully chosen, not so much for obtaining the most accurate pressure integration, as for studying the pressures in the neighbourhood (and particularly downstream) of the spoiler. A better picture of the flow mechanisms associated with a rapid spoiler rotation could thus be obtained.

Lack of room inside the model dictated that the pressure transducers, used for both static and dynamic measurements be positioned outside, and on one side, of the aerofoil. The relatively long (630 mm) connecting PVC tubing from surface tappings to transducers would have been unsuitable on their own for dynamic measurements, being limited by the transfer function of the slender pneumatic path. A study was initiated to resolve the problem (see Appendix B for details) and ultimately 25 tubes were available for connection to transducers, just outboard of one end-plate.

3.4 Mounting Frame

Owing to the popularity of the open working section wind tunnel, the model had to be taken in and out of the working section at short notice. A lightweight dexion frame was used to be easily slid on the floor and on which the model was mounted for pitching to positive or negative incidences. Once positioned in the working section, weights were used to fix the frame against sliding. Even at the maximum tunnel speed used (20 m/s), vibration of the model on this frame was negligible.

3.5 Spoiler Control and Data Acquisition System Requirements

The basic requirement called for a system that would combine and synchronise rapid spoiler motion with transient pressure measurements. A more detailed specification is presented here.

3.5.1 Global experiment control

An effective system was required to serve at the heart of a test-management and data-collection scheme, for synchronization of all events in real time, during a complete test. The "hardware-intensive" approach, involving for example a set of transient recorders for data capture, was rejected on grounds of cost, so the "software-intensive" alternative was the obvious choice.

A microcomputer with the appropriate hardware and software was required and, in addition, hardware for this central scheme would include:

- serial and parallel input-output ports for communications (e.g. data transfer to another computer) and equipment control,
- Digital-to-Analogue Convertors (DAC), also for equipment control,
- fast Analogue-to-Digital Convertors (ADC) for data acquisition,
- a real-time clock facility for establishing a time-base for the test process, and
- adequate program and data storage facilities.

Software would include high-level and low-level programming languages and appropriate system software to enable program development.

3.5.2 Spoiler-actuation subsystem

The overriding requirement here was for a mechanism that was fully controllable by the microcomputer discussed above. The latter would specify accurately, not only the distance and rate at which the spoiler was to rotate, but also it would determine the shape of the rotation profile, including a change of speed or direction at mid-cycle. In addition, this mechanism needed to be capable of fast rotation rates (greater than 500°/sec), smooth operation, very rapid acceleration/deceleration, good damping and it would have to perform repeatedly with accuracy and reliability. It will later be shown that each run actually consisted of a pair of runs for which the mechanical operations (rotation of the spoiler according to a particular transient history) had to be virtually identical. Finally, the hardware local to the spoiler itself was required to be compact and light-weight, so it could be readily installed on the model/frame arrangement.

3.5.3 Data-acquisition subsystem

Fast pressure-signal sampling was called for in order to provide adequate signal "resolution" and to minimize the problems arising from frequency aliasing. The original signals would have to be suitably amplified, sampled and this digital form stored such that it could be transferred later to a larger computer for processing and permanent storage. Transient measurements of spoiler angle, $\delta(t)$, would be made simultaneously with the pressure measurements and treated in a similar manner.

3.6 Spoiler-Control and Data-Acquisition System Layout

A system was designed, assembled and its synchronous operation developed to satisfy the requirements laid out in the previous section. As identified in that section, the system equipment consisted of three major components:

(a) The central system controller, comprising:

- Cromemco Z2D 8-bit microcomputer, with appropriate computer boards, input/output facilities and disks for data storage, and
- Televideo TVI 920 "intelligent" VDU.

A detailed description of this follows in Sec. 3.7.

(b) Spoiler actuation subsystem, comprising:

- Sigma 17-series stepping motor, and
- Digiplan 1054 bipolar, bilevel stepping motor drive unit,

these being described in detail in Sec. 3.8.

(c) Data-acquisition subsystem, comprising:

- 12 Setra 207 fast-response pressure transducers,
- 12 isolated transducer power supplies,
- 12 channel differential amplifier unit,
- rotary potentiometer and power supply,

these to be described in Sec. 3.9. The applications software specially written to drive the entire system, and, also the data transfer programs, will be outlined afterwards (Sec. 3.10).

A wheeled console unit was built to accommodate the entire system instrumentation; a schematic drawing of this appears

in Fig. 3.5. The aim was to obtain a mobile, self-contained unit requiring only the minimum of electrical interconnections to conduct testing or data transfer. The layout reflected some thought for operational convenience, while keeping cabling short. Much of the cabling was trunked and guided through plastic tubing for neatness and reduction of possible electrical interference. Power sockets were provided at various points on the console, these served by a single mains supply to the whole unit.

3.7 Microcomputer Hardware

A Cromemco Z-2D microcomputer formed the main component of the spoiler-control and data acquisition system. Essentially, it consisted of a "motherboard", built around the IEEE 696 S100 system bus, into which various compatible computer boards could be inserted to enable the system to perform tasks beyond those capable by the basic computer or to improve the performance of those tasks within its normal capacity. In its final configuration, as used for testing, the microcomputer comprised the following:

- Zilog Z80A 8-bit microprocessor,
- 256K of Random Access Memory (RAM), configured as four 64K software-switchable banks (an 8-bit microprocessor can address only 64K at a time),
- 2 double-sided/double-density floppy-disk drives of 386K (formatted) capacity each, including their appropriate controller board,
- Winchester-type hard-disk drive of 18M byte (formatted) capacity, plus controller board. (This unit was procured not only to increase data storage capacity and to speed up storage rates, but also to obviate the annoying corruption of floppy disks in the dusty environment,)
- 3 serial-data input-output parts, linking to a Televideo TVI-920 "intelligent" VDU, a data transfer exchange unit, and a serial printer,
- a parallel-data input-output port for sending control data to the stepping-motor drive,
- a programmable interval timer, capable of generating

software interrupts at regular intervals (with 8μsec maximum resolution),

- 2 12-bit Digital-to-Analogue-Convertors (DACs) (Burr-Brown DAC80-CBI-V integrated circuits) with 3μsec claimed conversion time, linked to the X and Y inputs of an oscilloscope, for graphic display of collected digital data,
- a complete data acquisition integrated circuit (Burr-Brown SDM 856 KG), featuring a 16-to-1 Multiplexer (MUX), a Sample-and-Hold circuit (S/H), with 10μsec claimed acquisition time and 100nsec aperture time, and a 12-bit Analogue-to-Digital Convertor (ADC), with 25μsec claimed conversion time.

This configuration, including linkage to the rest of the system, is shown schematically in Fig. 3.6.

3.8 Spoiler-Actuation Subsystem

A combination of stepping motor and appropriate drive unit was selected to meet the spoiler actuation scheme requirement; a schematic diagram is shown in Fig.3.7. The Sigma 17-3437D200-F038 stepping motor and Digiplan 1054 motor drive unit were chosen on grounds of cost-effectiveness and compactness.

The stepping motor was a brushless, permanent magnet, two-stack design. Low-mass rotor construction resulted in high torque-to-inertia ratio for high start/stop rates and good damping characteristics. Full-stop angle was 1.8°, but by choice half-step drive (0.9°/step) was permanently engaged for increased resolution and smoother operation.

The motor drive unit, featuring a bipolar, bilevel bridge circuit with its own power supply had to be capable of matching the motor performance. CMOS logic circuits were available for interfacing at a strong signal level, but as the microcomputer parallel-data port (used for linking the two devices) issued lower-voltage logic signals (standard TTL signal level), open-collector amplifier transistors

were employed within the drive unit interface circuits to strengthen TTL logic to CMOS levels (N.B. This also inverted all incoming signals).

The motor was fixed to the outside face of one of the spoiler end plates (see Fig.3.8) and its shaft directly coupled (via a simple sleeve) to the spoiler end. A rotary potentiometer was installed beyond the other end-plate and similarly attached to the spoiler axle to monitor the spoiler displacement (see Fig.3.9). Signal digitisation of this transducing of spoiler rotations is described in the following section.

3.9 Data Acquisition Subsystem

A subsystem was constructed to monitor and collect the experimental data; a schematic diagram is shown in Fig.3.10.

Pressures from the model were monitored by 12 Setra Systems 237 0.1 psi (690 N/m^2) bidirectional, differential pressure transducers. These, arranged in a semicircle and fitted in a similarly shaped enclosure, were fixed onto one end-plate near the stepping motor (see Fig.3.11). Information and discussion on the geometry of the tubing arrangement connecting the transducers to the tappings can be found in Appendix B. The reference-pressure acting on the back face of each transducer was vented to ambient pressure via a length of plastic tubing. Also shown in Fig.3.11 are seals arranged around the transducer enclosure to minimise cooling of the transducers by the airflow within the tunnel jet, but outside the end-plates.

Cables to the transducers conveyed both the excitation (power supply) for integral electronics and the returning signals from the deflected diaphragms. The power-supply units were made especially for these transducers, allowing for this dual cabling, but also carefully designed to minimise "crosstalk" between neighbouring signals. The power supplies used the Burr-Brown type 700 dc-dc convertor and were current-limited to 30mA. A schematic circuit diagram

of a single supply appears in Fig.3.12.

Between the direct transducer signals and the sampling ADC was a bank of amplifiers designed to raise signal levels toward the maximum capacity of the ADC input stage, thus obtaining greater resolution than would have been the case for those pressure signals whose weakness produced only a low-voltage transducer output. Experience soon suggested amplifier gains for all signals in order to obtain this enhanced resolution in any testing configuration. The gains formed part of the stored data for later interpretation of sampled signals.

The amplifiers were specially made for this experiment. Of modular construction, and allowing for future expansion, the amplifier unit incorporated a mother cabinet into which was fitted six cards, each containing two single-ended amplifiers with a zero-offset adjustment and a variable (switchable) gain from 2 to 30; the common power supply incorporated an over-voltage protection. A circuit diagram for a single amplifier is shown in Fig.3.13.

The amplified electrical signals were connected to pins 1 to 12 of the microcomputer ADC input port, in single-ended configuration. At the same input, they were joined, on pin 16, by the signal from the rotary potentiometer mentioned in Sec.3.8. A power supply was selected for the potentiometer in order to provide outputs directly suitable for sampling at the ADC. In fact, the supply within the stepping-motor drive served this purpose quite adequately, but because this secondary function was so independent of the primary purpose Fig.3.7 and 3.10 do not acknowledge the dual role.

During data collection, the MUX scanned the input signals sequentially (pins 1 to 12, then 16), feeding them to the S/H where the signal voltage levels were sampled and then converted by the ADC into 12-bit digital values and made available to the computer microprocessor, which controlled the entire operation, including their storage.

3.10 Microcomputer Software

Software for the Cromemco Z-2D microcomputer was developed primarily as a cohesive set of programmes for utilization of the equipment described in the previous sections, i.e. for synchronized control of the spoiler, for sampling and initial storage of data, and for preliminary inspection of these records. A separate programme transferred the stored data to a more powerful computer for processing.

An existing program was modified to meet the data transfer requirement. This program used asynchronous, block-transmission to copy a data file directly from a micro-computer storage device to one in another computer.

Only a brief description of the principal software will be given here; reference may be made to App. C for a detailed account.

Essentially, different program modules, designed to perform specific tasks, were linked together by a master, menu-driven program. Thus, facilities available to the user included specifying the sequence of operations for a complete test, monitoring various test signals prior to the run, rotating the spoiler, collecting test data, or both, displaying the collected data in graphical or numerical form, and making a "temporary" or "permanent" record of the data.

3.11 Test Conditions

Tests were performed at two Reynolds numbers (Re). Based on the model chord, Re = 2.8×10^5 at a windspeed, U = 10m/s and Re = 5.6×10^5 at U = 20m/s. Ranges of variation for the other principal parameters are:

- angle of incidence, α ($-20°$ to $20°$),
- spoiler angle, δ ($0°$ to $40°$, usually),
- spoiler rotation rates $\dot{\delta}$ (t) (167°/sec to 1000°/sec),
- spoiler position (mainly at x/c = 0.70, but also at x/c = 0.13, and mainly on upper surface but also on lower surface),

- spoiler configuration (ungapped/unperforated , gapped/unperforated, and gapped/perforated).

3.12 Boundary Layer Transition Fix

Boundary layer transition was fixed at x/c = 0.055, by a trip wire, on both upper and lower surfaces. The wire diameter was 1.1 mm, giving a "roughness" Reynolds number (i.e. based on wire diameter) of 753 for V = 10m/s, (Re greater than 600 is recommended).

CHAPTER FOUR

EXPERIMENTAL PROCEDURE DETAILS

4.1 Introduction

The experimental set-up described in the previous chapter was employed to obtain the complete set of measurements required for this investigation. Both static and transient tests were carried out with different arrangements of the same model and the spoiler.

A series of system checks and preliminary tests was completed prior to the main programme of tests in order to confirm the integrity of the new spoiler-control and data-acquisition system, and to establish procedural techniques.

In the ensuing sections of this chapter, the tested configurations will be listed, system qualification tests briefly discussed, testing techniques explained, test procedures described and data processing methods summarised.

4.2 Aerofoil-spoiler Configurations

As described in Sec. 3.3 a number of combinations of aerofoil-spoiler configurations could be obtained by varying the aerofoil incidence and spoiler chordwise position and porosity, i.e. gap and perforations. Only a selection of the possible combinations was investigated, in the main because they were regarded as more likely to be applied in practice; these are listed in Table 4.1.

Henceforth, for the sake of brevity, the spoiler with gap and perforations sealed will be referred to as "solid"; when the gap is opened but perforations remain sealed it will be termed "gapped"; and when gap and perforations are opened it will simply be "perforated".

4.3 System Qualification Tests

Before the main programme of tests was embarked on, a series of system tests was executed, with the aim of confirming the capability and integrity of the experimental system.

4.3.1 Spoiler actuation trials

Exploratory wind-off, then wind-on tests were carried out, allowing for variation of spoiler rotation rate, rotation direction, initial and final angles and the transient deflection profile, in order to cover most of the likely situations in the proposed body of testing. Mainly using the signal from the rotary potentiometer fixed to the free spoiler end, the following observations were made:

The actuation mechanism itself was accurate, consistent, and coped with the high speeds demanded of it. Motor torque, both "holding" and at speed, was high enough to overpower the spoiler aerodynamic (drag) forces and thus to prevent slipping of the rotor. However, a problem emerged in the form of spoiler twist.

The problem was not unexpected, given the low torsional stiffness of the long, thin spoiler. The potentiometer signals showed that when one end was rotated rapidly, with a virtually impulsive start, the inertia and elasticity of the spoiler produced an inevitable lag in the rotation response at the other end, followed by an overshoot, when the driven end had stopped and the typical vibrational decay of the torsional action. In fact, the free end followed the deflection pattern imposed at the driven end quite closely, but with an additional damped oscillatory component at about 30 Hz, the initial overshoot half-amplitude being about 6° for an imposed rotation of 40° at the maximum nominal rotation rate of 990°/sec.

A two-part remedy was applied, namely:

- plasticine was unobtrusively packed along parts of the spoiler leading edge (the hinge-line), away from the pressure-measuring system, thereby providing a form of damping; and
- modifications were made to the final part of the transient rotation deflection profile issued to the stepper motor: the spoiler actuation signal was partly "inverted", the extent dictated by rotation speed, to counteract the first vibration peak.

These measures considerably improved torsional response.

Tests showed a much-attenuated oscillatory component and vibrational response, the initial overshoot having been reduced to a half-amplitude of 1.5° or less at maximum rotation rate, and negligible at slower rates. It must be remembered, of course, that only about half the distortion displayed at the spoiler free end would be expected at mid-span, where the pressure measurements were taken.

A couple of other, less significant, actuation problems were discovered, viz.:

- a mild form of motor resonance (inter-step vibration but no step-loss or stalling) occasionally occurred at rotation rates of around 250°/sec; this had no major effect and so was ignored; and
- motor step-loss consistently occurred in cases of reversal of direction during high-speed rotation; again this was of no real concern as such a deflection pattern requirement would seldom be necessary.

4.3.2 Data acquisition tests

A number of tests were made with a view to ensuring the integrity of collected data. These may be divided into isolated instrumentation component checks and tests on the apparatus as a whole.

Instrumentation component checks included:

- Calibration of pressure transducers and checks of linearity of their response (over 90% of their

pressure range), and electrical noise levels; also, monitoring of drift in the electrical output with time and temperature during the application of zero and non-zero gauge pressure loads.

- Monitoring of gain and phase response of the set of pressure-signal amplifiers to harmonic inputs. (A specially written computer program was used to monitor transducer and amplifier signals over periods as long as six hours, to ensure long term stability).
- ADC performance check (accuracy, resolution, conversion rates).

These tests were generally successful. Minor snags, e.g. a noisy transducer, were fixed whenever they occurred.

Tests on the apparatus as a whole included:

- Test data collection under different laboratory conditions to assess data susceptibility to electrical interference (i.e. low-frequency "noise" or high-frequency "spikes", or both) caused by external sources. It was found that under certain conditions e.g. another tunnel running, some interference, especially spikes, was picked up through the mains. Improved cable shielding cured this problem.
- Investigation of effect of spoiler dynamics on transducer signals (wind-off). It was thought that rapid spoiler motion might provoke vibrations of the aerofoil itself, perhaps inducing pressures at the tappings not strictly due to the aerodynamic mechanisms under study. Tests were carried out to assess the magnitude of such vibration-induced pressures; it was detectable but insignificant compared with normal wind-on spoiler-induced pressures.

4.4 Pressure Measurements and Repeatability

It was not possible to obtain the full set of pressure measurements around the aerofoil in a single pass because of the limited number of transducers (12 to serve 25 stations). So, a test was completed in two runs, one each for upper and

lower aerofoil surfaces. The wind was turned off between runs while the tapping-to-transducer connections were swapped at the transducer end. A particular transducer always served the same chordwise pair of tappings, first upper then lower surface or vice versa.

As a test consisted of two separate runs, repeatability was crucial and had to be established. Three factors were considered to compromise pressure measurement repeatability:

- unequal windspeeds,
- different spoiler deflection patterns, and
- the inconsistent nature of pressure transients.

The first two were comparatively easy to counter. Great care was taken in reproducing windspeeds, although tunnel turbulence did not always make that possible. An answer to tunnel turbulence was eventually developed (of which see later). Also, consistency had been an important requirement for the spoiler actuation mechanism; proving tests were satisfactory, as explained in the previous section. In any case, a noticeable difference in deflection pattern between runs would be spotted through visual examination of the spoiler displacement traces immediately after a test; the data would be discarded as a consequence and the second run repeated. If that screening failed, the discrepancy would be spotted by a more rigorous check at the processing stage. Usually, the data passed both checks.

The third factor posed a problem of a different kind. In effect, judgement had to be made whether from first to second run, in a pair, there had been "sufficiently accurate" duplication of the local aerodynamics to accept the pair as if it were a single run. In the early form of acceptance test, each part of a run pair was simply repeated and then their local pressure signals were compared. These comparisons proved to be very encouraging and agreement was generally good. The greatest differences occurred in the signals downstream of the spoiler, as expected, but that was not a major problem as these signals were from the same surface, therefore the same run.

Nevertheless, it was decided to install a permanent repeatability check, by connecting the two trailing-edge tappings on upper and lower surfaces, thus obtaining an averaged signal, and reading it on both runs of a pair. (Although a more "repeatable" signal could have been found upstream of the spoiler, the trailing edge was picked because no transducer needed to be dedicated to such a check). Again, immediate visual screening of data was available and hardcopy plots of pressure histories could be compared after processing.

4.5 Sampling Rates and Recording Times

Transient tests were always split into a number of segments; the concept of test segments is introduced in the discussion of experimental software, App.C. These could be classified as "static" and "dynamic" segments and, as implied, the former involved no spoiler motion. Thus, static segments were placed before the first and after the last dynamic segment in a test, in order to capture, respectively, the static conditions before spoiler deflection, and the post-deflection airflow response and the gradual establishment of new static conditions.

For dynamic segments, as described in app.C, the data sampling rate was dependent on specified spoiler rotation rate and varied between 400 and 1100Hz, when the maximum (and normally used) number of ADC channels was employed.

With static segments, the user had control of both sampling rate and segment duration. But there were some constraints in specifying these for the pre- and post-deflection test phases: sampling rate had to be high enough to prevent aliasing, and the duration of each phase was to be long enough to achieve its purpose, yet the volume of collected data would rise rapidly as rate and duration increased, thus posing handling and storage problems. Also, it was desirable to keep rate and duration of these phases constant from test to test for simplicity's sake. Thus the pre-deflection phase was fixed at 40 msec at a sampling

rate of 400 Hz. Tests to determine post-deflection parameters involved rotating the spoiler at the highest rate (990°/sec) in a number of situations and examining flow re-adjustment. As a result, post-deflection measurement time was set at 222 msec; it was split into two segments with the first 60 msec at 833 Hz and the remaining time at 556 Hz (the odd figures occur because of the need to select either a particular sampling time or rate). These recording times were used throughout the normal test programme.

4.6 Test Procedure

The same basic procedure was followed throughout the main test programme for transient and static tests. A step-by-step guide to the procedure for transient tests will be presented below; only steps relating to spoiler actuation would be omitted from static testing. It will be assumed that the experimental system described in Ch.3 was connected and its software running.

First, the software was configured for the particular test by specifying the following parameters:

- test number (for identification and classification purposes),
- initial spoiler angle (only for first test of session),
- number of ADC channels for pressure signals (the maximum of 12 was to be selected throughout the main testing, but see Sec.4.8),
- number of test segments,
- individual segment parameters determining spoiler deflection, rotation and sampling rates, and segment duration (for static segments; for dynamic segments it was computed from previous information).

Then, adjustments were made, as required, to the model, its spoiler, amplifier gains and tapping/transducer connections. Next, the wind-off pressure and retracted spoiler angle signals were monitored using the real-time VDU display and zero-offset averaged values obtained via the computer.

The required spoiler angle was then set and tunnel brought to speed. The actual test was executed (usually lasting no more than a half-second) and tunnel switched off. The collected data were then plotted on the oscilloscope screen, channel-by-channel, and checked for irregularities. Special attention was paid to the spoiler displacement trace for repeatability. This preliminary inspection was usually satisfactory.

If so, the data were stored in a floppy- or hard-disk file, usually the latter. Information was supplied about pressure-scanned aerofoil surface and windspeed, and stored alongside test configuration parameters and collected data. Occasionally, the data were shifted elsewhere in RAM and fetched after another run or series of runs for comparison of pressure or spoiler angle signals.

The above sequence, of course, would obtain only half the data required for a complete test. A second, identical run had to be made with swapped tapping/transducer connections to collect the remaining data from the opposite aerofoil surface.

At the end of a test session, all data files were dispatched, using the file-transfer program, to the mainframe computer, used for data processing. Data for a run pair (i.e. one complete test), usually stored in two separate disk files, were concatenated during transfer to form a single test data file.

4.7 Data Processing

The experimental data were transferred from the micro-computer to a Honeywell mainframe computer with Multics operating system, situated across the road from the Aeronautical Engineering Department. This computer was accessible via various computer terminals in the Department, and it was used for data processing and output in hardcopy graphical form.

Applications software was written to carry out these tasks. Briefly, the computer operator supplied the program with data file name and some appropriate configurational details. Then, the various necessary data sorting, checking and processing stages were executed and the operator was invited to choose a combination of graphical formats for the processed data, and required output device (i.e. VDU screen or hardcopy plotter). Reference may be made to App.D for a more detailed account.

4.8 Mid-course Testing Alterations

At the beginning of the main test programme the ADC circuit developed a fault, as a result of which the ADC channel corresponding to the pressure signal scanned last in a test cycle could not be read reliably. At that stage the fault had to be lived with, so one pair of signals had to be sacrificed. On the evidence of earlier tests, the pair at x/c = 0.50 was judged as least useful and bypassed, leaving 11 scanned pressure signals per aerofoil surface. Performance was not otherwise affected.

However, about halfway through the main testing, an in-situ repair was effected, restoring the 12th ADC channel. This, nevertheless, was not connected to the reserve tapping pair for the sake of consistency with previous results, and because a different use for this extra channel was envisaged by then.

A record of tunnel velocity during tests was desirable, so that turbulence levels could be monitored and comparisons made between the pair of runs making up a test. A simple pitot tube was installed upstream of the aerofoil leading edge, where it did not affect mid-span static pressures. Connected to the 12th pressure transducer and corresponding ADC channel, it provided a record of tunnel velocity signal data, to replace what was previously read as a "dummy" signal; thus, ADC performance in other respects was unaffected.

The test procedure following this modification was unchanged, except that these new velocity signals (a pair), were often compared using the oscilloscope screen, as was done for spoiler displacement signals.

The data processing software was modified to allow for optional processing of the velocity signal data, reporting of average upper and lower surface run velocities and instantaneous fluctuation errors, and use of the instantaneous velocity values in calculating all Cp, and therefore C_L, values.

After some experience with these velocity signals, the following observations were made:

- average measured velocity was about 3% lower than the nominal value deduced from tunnel manometer readings; independent measurements favoured the former;
- average velocity, from run to run, was reproduced accurately;
- velocity fluctuation error (deviation of instantaneous value from average) was normally below 3% (an indication of tunnel turbulence levels);
- there was no clear fluctuation pattern to suggest a dominant source;
- spoiler motion had no significant effect on the velocity signal within the duration of a test.

As a result of these observations, it was decided that whereas every pressure signal could have been reduced to coefficient form by using instantaneous velocity values from this extra probe, the constancy of velocity during the measuring period of a run led to the decision to use a single value for velocity. Therefore, none of the data presented in the following chapter imply the use of such instantaneous values.

CHAPTER FIVE

PRESENTATION AND DISCUSSION OF RESULTS

5.1 Introduction

This chapter is concerned with the presentation and discussion of experimental results from a representative cross-section of the test programme undertaken for the purposes of the present study, the test programme consisting of both static and dynamic tests. Static tests involved obtaining surface pressure measurements around the aerofoil for various incidences, but at steady angles of spoiler deployment, whereas dynamic tests captured the flow response to transient spoiler motion in the form of surface pressure histories. A selection of spoiler configurations was tested, as listed earlier in Sec.4.2.

Results from static tests are presented as time-averaged chordwise pressure distributions or alternatively, in integrated form, as lift force per unit span varying with angle of incidence or spoiler angle.

Results from individual dynamic tests are presented in one or more of the following forms:

(i) lift time history together with spoiler displacement profile for direct visual correlation,

(ii) a sequence of pressure signal time histories around the aerofoil,

(iii) a sequence of instantaneous chordwise pressure distributions taken in the course of a test.

All measurements for pressure and lift force are presented in non-dimensionalised form, i.e. as pressure coefficients or as section lift coefficients.

The variation of lift response with the aerodynamic time parameter UT/c is documented in terms of the aerodynamic delay times t_o/T, t_a/T and t_f/T (definitions follow in

Sec.5.3.1), which are presented for a range of UT/c; for this purpose several series of dynamic tests with different U or T were carried out, each series featuring a particular spoiler configuration.

In the remainder of this chapter, the results from static tests will be considered first, setting the scene for those from dynamic tests. As the latter tests formed the bulk of the experimental investigation, the corresponding presented material occupies appropriate portions of the chapter and for this reason, each portion is divided into a number of sections according to position of the spoiler on the aerofoil. The conventional upper-surface rearward spoiler position, which was investigated to the greatest extent, is given priority over the less orthodox cases. (In fact, the general order of presentation approximately coincides with testing chronological order, since later tests were often performed as a result of observations from prior, perhaps routine, testing).

5.2 Static Tests

Throughout the programme of static testing, the spoiler was fixed in the aft (70% chord) position and one wind-speed used (U = 20m/s) giving $R_e = 5.6 \times 10^5$. Unless otherwise stated, the spoiler is assumed to be on the upper surface of the aerofoil.

5.2.1 Spoiler retracted

Static tests with undeployed spoiler were performed in order to achieve the following:

(i) find the aerofoil lift curve characteristics, and

(ii) check the symmetricity of the aerofoil.

Results from these tests are presented in Fig. 5.1 and 5.2.

Fig.5.1 shows the aerofoil lift curve, i.e. lift as a function of angle of incidence with the spoiler completely retracted (flush with the aerofoil surface); for completeness, a similar curve with spoiler statically deflected at

δ = 40° is shown, but will not be discussed until later. Measurements for negative angles of incidence are included as they are of interest for later consideration of a lower-surface spoiler. Immediately apparent are the considerable under-estimation of maximum lift and over-estimation of stalling angle ($C_{L_{max}}$ = 0.61 at α_{stall} = 18°) when compared with standard data for this aerofoil (i.e. $C_{L_{max}}$ = 1.3 at α_{stall} = 15°). Largely responsible for the former discrepancy and entirely responsible for the latter was the absence of tunnel interference corrections to these plotted data, applicable at high angles of incidence, as explained and justified in App.A. A second factor contributing towards the indicated high-incidence lift deficiency was the error introduced by computation of lift from a limited number of pressures around the aerofoil. (Tests to evaluate this error were carried out at various angles of incidence using instead the wind tunnel balance arrangement to measure lift, and showed that the error was of the order 12-15% at high α , with $C_{L_{max}}$ = 0.71 while α_{stall} remained unchanged). However, this error too was ignored for the sake of consistency with dynamic tests (i.e. those performed at high α) where absolute static levels were of minor importance anyway. Therefore, further reference to angle of incidence and experimental measurements will be taken to mean the set value of incidence and the uncorrected values of lift, respectively, rather than the "actual" values which might come from a somewhat speculative correction.

Comparison of the negative lift curve with the positive equivalent shows that good agreement is obtained up to α = |16°|, i.e. just before the stall. The negative stall occurs slightly earlier and at a rather lower absolute C_L value(0.56, cf. 0.61 for positive α). However, examination of the corresponding series of chordwise pressure distributions showed the two stalling processes to be similar in character, i.e. originating and spreading from the leading edge, in flat-plate fashion. Flow visualization employing the helium-bubble technique confirmed these findings.

Fig.5.2 shows the steady pressure distributions on both surfaces of the aerofoil, at zero incidence and with retracted spoiler. Whilst in theory these should be identical, here discrepancies are observed at $0.10 < x/c < 0.40$ and $0.69 < x/c < 0.85$. The second of these may be attributed to interference caused by the presence of the spoiler and its associated recess, whereas the first appears to be due to poor manufacture of the model. Despite such inconsistencies, the areas under both curves are identical (hence, overall $C_L = 0$). All in all, the model was judged to be near enough symmetric to be treated as such.

5.2.2 Spoiler deflected

Static tests with deployed spoiler were performed in order to achieve the following:

(i) examine the typical static aerodynamic characteristics of spoilers,
(ii) observe the effect of incidence on spoiler characteristics,
(iii) compare the control effectiveness of different spoiler configurations in a qualitative manner,
(iv) briefly explore the potential of a lower-surface spoiler as an aerodynamic control surface, and
(v) generally establish boundary conditions for dynamic test measurements and enable later comparisons with these.

Results from this series of tests are presented in Fig. 5.3, 5.4 and 5.5.

Fig.5.3 shows the time-averaged steady pressure distributions for different deflection angler of the gapped (but unperforated) spoiler at zero incidence. A clear pattern is distinguishable, showing the classical trends of steady spoiler deployment, with the following main features:

(i) relatively large pressure increase on the aerofoil upper surface upstream of the spoiler, largely responsible for the spoiling action,

(ii) growth of a separation bubble immediately downstream of the spoiler, with associated negative (base) pressure region, and

(iii) relatively small pressure decrease over the lower surface.

Additionally, it is worth examining in some detail the pressure re-distribution process accompanying the step-by-step spoiler rise. For $\delta = 5°$, already some changes in pressures are effected relative to the levels for $\delta = 0°$, mainly of course in the neighbourhood of the spoiler. The trailing-edge pressure remains above free-stream pressure, indicating that the flow separating from the spoiler free edge reattaches, probably between $x/_c = 0.85$ and 0.90. The resulting disturbance extends with diminishing strength, upstream of the spoiler where it is felt up to about the quarter-chord position, as well as around the trailing edge and over the lower surface. As the spoiler rises to $\delta = 10°$, the separation bubble grows, apparently now closing (having merged with the boundary layer from the lower surface) in the wake, just downstream of the trailing edge, while the constant-pressure (i.e. base pressure) upstream part of the bubble appears to extend up to $x/_c = 0.95$. By now, the familiar characteristics associated with spoiler deflection, as outlined above, are established. Further spoiler extension helps only to augment those characteristics, gradually if not linearly, thereby causing the strengthening of the upper surface adverse pressure gradient extending from $x/_c = 0.40$ to 0.69 (immediately ahead of the spoiler leading edge) and the sudden favourable pressure gradient over the chord of the spoiler. Behind the spoiler, the separation bubble expands farther into the wake with increasing spoiler deflection, the constant-pressure region extending well past the trailing edge, and the base pressure ever decreasing. Apparent in the pressure signals recorded behind the spoiler, at high deflection angles, though not in the time-averaged values presented in Fig.5.3,

is some increase in pressure fluctuation levels that would normally be associated with such a bubble.

Looking at the lower surface, comparatively small pressure changes take place as signals relating to additional spoiler deflection are relayed via the trailing edge. Existing pressure gradients are barely modified, except near the trailing edge; there is a small-scale separation which appears at $\delta = 15°$, eventually extending forward to $x/_c = 0.85$ at merging in the wake with the above-mentioned bubble.

The net effects of such pressure re-distributions, following spoiler deployment, can be itemised thus:

(i) The main desired effect is an overall lift decrease (see separate treatment later in this section).

(ii) There is a drag increase: this results, in bluff-body fashion, from the additive effect of compression on the front face of the spoiler and suction (base pressure) on the back face. A relative measure of this (pressure) drag can be obtained from $\Delta C_p = (C_{p_u})_{0.69} - (C_{p_u})_{0.80}$ for $\delta > 10°$, which is also an approximate measure of total drag, since the pressure drag is much larger than the skin-friction drag component. (N.B. Consideration of spoiler-induced drag is generally beyond the scope of the present investigation. Some qualitative static measurements were obtained, using the wind-tunnel balance arrangement, to help put drag into perspective, but cannot justifiably be presented here as a sensible addition to lift responses.)

(iii) The pitching moment increases (nose-up).

(iv) Considerable variations in boundary layer displacement-thickness occur on the upper surface, due to the strong adverse pressure gradients upstream of the spoiler, where some local separation may be induced, particularly if there is no gap between the spoiler and the aerofoil. The flow should then reattach on the front face of the spoiler.

Comparable results were obtained for solid and perforated (gap and perforations opened) spoiler configurations.

Fig.5.4 is similar to Fig.5.3, but for $\alpha = 14°$ now (note the different ordinate scale, too). This angle of incidence was selected as the principal alternative to $\alpha = 0°$ for the main testing, including dynamic tests, because of its proximity to the stall; thus, the flow pattern here is quite different from zero incidence, but without any significant separation in the region of the (retracted) spoiler that would seriously impair control effectiveness. However, a certain amount of deterioration is to be expected vis-a-vis $\alpha = 0°$, mainly due to much greater boundary layer displacement thickness caused by the strong adverse pressure gradient upstream of the spoiler. Fig.5.4 confirms this view: all the characteristic tendencies identified in the previous case apply here, too, but the magnitude of the actual pressure changes is reduced. Therefore, a separate detailed account is not called for, but it is appropriate to summarize the essential differences from the effects of spoiler deployment at zero incidence, as described earlier:

(i) There is a reduction in spoiled lift (hence control effectiveness) and in pitching moment (nose up) due to the spoiler.

(ii) The increase in pressure drag appears to have been reduced.

(iii) It appears that the boundary layer displacement thickness is now virtually unaffected, in the absence of large pressure gradient changes.

In view of the apparent disadvantages of the present spoiler position at high angles of incidence, and with regard to static characteristics alone, a case can be made for a spoiler positioned in the high-suction area of the wing. However, aside from any structural problems that may arise, it will be seen later (Sec.5.5) that this position would probably induce undesirable dynamic characteristics.

Again, solid and perforated spoilers performed in a manner generally similar to this gapped spoiler.

Fig.5.5 shows steady lift as a function of spoiler deflection for all three spoiler configurations and for several angles of incidence. For $\alpha = 0°$, considering first the curve for the gapped spoiler (i.e. the integrated pressures of Fig.5.3), the lift appears to decrease linearly at first, but the rate drops slowly from $\delta = 15°$ onwards, displaying the early stages of the well-known fact that the majority of a spoiler's effectiveness is in the first half of a possible 90° rotation. Comparison with the curves for the other two spoiler configurations holds no surprises, placing those just on either side of the first one. With little to choose between any of them at $\delta = 5°$, nevertheless, the superior blockage area of the solid spoiler begins to show at $\delta = 10°$ and this configuration remains marginally the most effective up to maximum deployment. Conversely, the opposite effect of the porosity of the perforated spoiler does not show until $\delta = 25°$, when the holes begin to expose themselves in the direction of the main flow, and this configuration thereafter proves increasingly the least effective. For $\alpha = 14°$, all three curves are shallower, pointing to reduced control effectiveness and reflecting observations made from Fig.5.4; for example control effectiveness for the gapped spoiler is reduced to 73% of that for $\alpha = 0°$. A similar figure applies to the perforated spoiler which, as for $\alpha = 0°$, initially compares well with the previous configuration, but becomes less effective from $\delta = 25°$ onwards. Not unexpectedly, however, the solid spoiler is now much less effective (64% of original value), as the much thicker boundary layer at this incidence obliterates the advantage of the extra blockage area; indeed, the gap now appears to be completely immersed in inert air.

Though not formally monitored, as they were of no direct interest, the pressure fluctuation levels around the aerofoil could be observed from the recorded pressure signals.

As already noted for the gapped spoiler, pressure fluctuation levels behind the spoiler generally increased at high spoiler deflection angles. Such levels were slightly higher for the perforated spoiler, agreeing with results from Mabey et al (1982), where it was suggested that this was due to different bubble structures. However, fluctuations were much higher still for the solid spoiler tested here (about 4 times at the trailing edge for $\delta = 40°$ cf. with $\delta = 0°$), extended into the lower surface, and were dominated by a single frequency (about 100 Hz); the suspicion of vortex shedding was confirmed by a phase shift of 180° between the signals on either side of the trailing edge. This occurrence was not detected for any other configuration.

Overall, with complete regard to static characteristics, it would appear that the gapped spoiler is the best all-round compromise, being only slightly less effective than the solid spoiler, but possessing the least non-linear characteristics and inducing the lowest pressure fluctuation levels. Even so, the three configurations display generally similar characteristics and therefore, only one configuration (solid spoiler) was chosen to be tested at angles of incidence of lesser interest.

Still in Fig.5.5, it is quite clear that the spoiler has virtually no effect at $\alpha = 20°$; with the aerofoil displaying a leading-edge-type stall, the spoiler would be immersed in separated flow and rendered ineffective beyond that point. For $\alpha = -14°$ (or $\alpha = 14°$ for a lower-surface spoiler if the data values had their sign reversed), the spoiler appears <u>more</u> effective than at zero incidence (25% more), but displays much more non-linear characteristics; in fact, slight reversal of control effectiveness occurs in the range $0° < \delta < 5°$, where a modest <u>increase</u> in lift occurs before the expected spoiling begins. Far from uncommon, this phenomenon is a camber effect (see also Sec.1.2) and results from the apparent increase in camber caused by the flow separating from the spoiler free edge only to reattach upstream of the trailing edge. For $\alpha = -20°$ it appears that, despite the fact that the surface opposite to the spoiler

is completely stalled, the spoiler is still considerably effective; however, these results must be viewed as strictly qualitative, given the extent of tunnel interference at this incidence.

Now, a return to Fig.5.1 affords an alternative interpretation of the data presented therein The two curves are for spoiler angles of 0° and 40° and the separation of one from the other implies a control effectiveness which could be described as follows. Since the two curves are roughly parallel, the spoiling action is largely independent of incidence and the spoiler-induced lift as a percentage of normal lift is widely varied over the incidence range shown. At large positive incidence the spoiling is fractional; at about $\alpha = 7°$ the spoiling is 100%. For all negative there is already negative lift so further "spoiling" is actually an <u>enhancement</u> of lift.

It is here that the potential for an additional control surface is evident, suitable for ACT applications, perhaps particularly related to gust-alleviation and accurate flight-trajectory control. In fact, if we look at Fig.5.1 upside down and consider that portion which is presented for negative incidences, the spoiler is seen to be acting like a split flap on the <u>lower</u> surface of a wing at <u>positive</u> incidence. Not only is there lift enhancement, but the maximum available lift is increased substantially.

Clearly, there could be advantages in combining a traditional upper-surface spoiler with a lower-surface spoiler at the same $x/_c$, to form a gust-alleviation mechanism capable of dealing with gusts of both <u>sign</u>, as suggested by Mabey et al (1982). A more thorough treatment of this form of control is presented later in Sec. 5.4.

In conclusion, the steady measurements presented here provide the "boundary" steady-state conditions for the ensuing dynamic tests, i.e. they provide the starting and finishing conditions between which the transient measurements should move.

5.3 Dynamic Tests With Upper-Surface Rearward Spoiler

Dynamic tests using the conventional upper-surface rearward spoiler were performed at two nominal wind speeds, U = 10m/s and 20m/s, giving Re = 2.8×10^5 and 5.6×10^5. Unless otherwise stated, the more commonly used higher speed is to be assumed.

5.3.1 Ramp deflection profile

Dynamic tests using the simple ramp deflection profile, as is likely to be in practice with current spoilers, were performed in order to achieve the following:

(i) investigate the typical transient aerodynamic characteristics of spoilers, with particular emphasis on the "adverse lift" phenomenon,

(ii) examine the effect of the aerodynamic time parameter $\frac{UT}{c}$, and document the lift response times in terms of that parameter,

(iii) compare the characteristics of different spoiler configurations, and

(iv) examine the effect of angle of incidence.

Results from this series of tests are presented in Fig. nos. 5.6 to 5.33 inclusive. These results have been conveniently divided below according to direction of spoiler transient motion.

Before proceeding to present and discuss the contents of individual figures, it is appropriate to repeat here that measurements from an individual dynamic test were routinely plotted in a number of formats, as displayed for example in Fig.5.6, 5.7 and 5.8. It would be neither wise nor helpful to present <u>all</u> the formats for every test conducted, or indeed to present <u>any</u> format at all for many of the tests. Many ramp tests are represented merely by a single point on each of the curves for aerodynamic delay times versus $\frac{UT}{c}$, to help gauge the flow response for a variety of aerofoil-spoiler configurations.

(a) Spoiler extension

Fig.5.6, 5.7 and 5.8 display the transient measurements from a typical dynamic test, where the gapped spoiler is extended at a nominal rate $\dot{\delta}$ = 1000°/s with the aerofoil at zero incidence.

Fig.5.6(a) shows the spoiler displacement profile signals, with the effective signal for $\delta(t)$ at the measuring station on the wing being approximately midway between the two shown (see Sec.4.3.1 for details). The apparently large discrepancy between the two signals here (this test was from the earliest series of mainstream testing) was improved upon in later tests (e.g. see Fig.5.15(a)), yet proved to be of little significance. With the spoiler stopping slightly earlier (effectively, up to 3° lower than later tests as above), only the final static levels were slightly affected, being up to 6% lower. The spoiler free end begins to respond to inputs at the driven end at a time t_i, and reaches its final position after a time interval T. It is reasonable to assume that the spoiler mid-span position rotates for the same length of time, although it is actually set in motion slightly in advance (by about 3ms in this case). As T = 40 ms here, we have $\frac{UT}{c}$ = 2 approximately, i.e. the free stream travels about 2 chord lengths in the time it takes the spoiler to rotate fully.

Fig.5.6(b) shows the transient lift as a function of time, this signal being synchronized with the spoiler deflection signals and displayed directly below for ease of correlation. The definitions by Mabey et al (1982) for the aerodynamic delay times have been adhered to and are illustrated here, with t_o denoting the time to onset of lift response, t_a the time to maximum adverse lift, and t_f the time to final lift value (new steady state), all of these response times being measured from initiation of spoiler motion. The transient lift response shown here is typical of spoiler dynamic characteristics. Following activation (at t = 45 ms), a short time elapses before initial lift

response occurs in the positive direction (at t = 50 ms and $\delta(t) = 4°$) opposing the desired response and in contrast to the static characteristics (Fig.5.5). This "adverse lift" phenomenon, already explained in Sec.1.2, will be discussed in more detail later. A maximum is reached (called C_{L_a} henceforth) at t = 71 ms and $\delta(t) = 23°$ approximately, before the lift drops sharply and steadily to attain its final value at t = 102 ms, that is 12 ms after the spoiler reaches its final position, i.e. $\frac{U_{tf}}{c} = 2.8$.

So, the differences from quasi-steady aerodynamics can be summarized thus:

(i) delay in lift-response to initiation of spoiler deployment,

(ii) initial adverse lift effect (here, about 50% at eventual net ΔC_L), and

(iii) delay in establishing the new steady state.

All of these features are obviously undesirable and, while this sub-section is concerned mainly with understanding and documenting the dynamic characteristics of spoilers, efforts to reduce or eliminate their effect (particularly the adverse lift) will be presented later.

Meanwhile, Fig.5.7(a) to (d) shows the transient chordwise pressure time histories, also synchronized with the signals of Fig.5.6. (N.B. It must be remembered that these signals along with those from Fig.5.6, are not, as the graphical presentation suggests, continuous analogue traces, but are series of discrete points collected, processed and now connected sequentially by straight lines in order to reconstruct the original transient signals. However, in view of the high data acquisition rates and generally low errors, the assumption of dealing with the original continuous records will be made).

The presentation sequence of the pressure histories is in the direction of circulation about the aerofoil, starting from the leading edge and returning to it via the lower

surface. However, attention is focussed first on signal no.7 (Fig.5.7(b)), $x/c = 0.80$, i.e. immediately behind the spoiler free edge, where the flow is expected to react first to spoiler rotation. In fact, response is almost coincident with spoiler activation ($t = 45$ ms), with a barely detectable compression peak ($t = 48$ ms, $\delta(t) = 2°$) followed by a large, sudden suction peak ($t = 65$ ms, $\delta(t) = 19°$), to $C_p = -0.75$, then sharp reversal with the pressure reaching its new steady value at about $t = 94$ ms, approximately 9 ms after the spoiler reaches its final position, $\frac{U(t-45)}{c} = 2.4$; henceforth the symbol $\hat{t}$ will be used to denote the time following initiation of spoiler motion at mid-span. It is this kind of non-linear response that produces the adverse lift effect, and is provoked by the formation and rapid growth of a strong starting vortex just underneath the free edge of the fast-rising spoiler. This vortex induces a small compression ahead of it and a large suction below it, accounting for the observations just made, though a rather larger initial compression might be expected; it is thought that high-speed air drawn through the gap at the base of the spoiler may account for this partial suppression of the expected compression.

These vortex characteristics give important hints for monitoring its progress as it grows and is eventually convected downstream of the spoiler free edge. Examination of the "footprints" of the vortex on the pressure signal histories from $x/c = 0.80$ to $x/c = 1.0$ reveals that it begins to travel downstream well before the spoiler has stopped rotating. Because the spoiler free edge is at $x/c = 0.78$, it is fair to assume that the vortex is fully grown and just starting to travel by the time that minimum pressure, $C_{p_{min}}$, is recorded at $x/c = 0.80$ (the vortex is assumed to be directly above at this instant). As seen already, this occurs at $t = 65$ ms ($\frac{U\hat{t}}{c} \doteq 1$) while, $\delta(t) = 19°$ or at mid-deployment. The vortex passes over $x/c = 0.85$ at $t = 67$ ms, over $x/c = 0.90$ at $t = 71$ ms, over $x/c = 0.95$ at $t = 83$ ms, and altimately over $x/c = 1.0$ at $t = 87$ ms. (I.e. at $\frac{U\hat{t}}{c} \doteq 2$ which is almost simultaneous with the end of spoiler deployment, but this is only a coincidence).

Apparently the vortex is slowing down, but an average velocity of 4 m/s , or 20% of free stream velocity, applies. Also as an ever-decreasing C_{pmin} shows, the vortex gradually loses strength as it is convected downstream, presumably leaving vorticity in the newly-forming shear layer which is a characteristic of the final steady state. This thick viscous layer is situated between the separation bubble aft of the spoiler and the main stream flow and is associated with heavy flow mixing. Finally, the tiny compression peak occurring just before the large suction, observed earlier at $x/_c = 0.80$, grows appreciably towards the trailing edge, reinforcing the speculation about the cause of its original suppression, i.e. flow through the spoiler base gap.

Digressing from the main theme here, it is interesting to compare signals no.11 and 12 in Fig.5.7(b), both of which represent the transient pressure history at the trailing edge, but were recorded during <u>different</u> runs in similar conditions, as was the usual test policy (see Sec.4.4 for details). Therefore, given the nature of the test and the selected chordwise position, such comparison affords perhaps the ultimate check on test repeatability! Clearly, all important transient features are reproduced accurately in terms of both signal amplitude and phase. Generally, consistently high fidelity of signal reproduction was achieved, so all tests will be treated as single-piece runs with complete coverage of pressures around the aerofoil.

Now, away from the region of the spoiler, if the Kutta trailing edge condition was to be satisfied, the effects of the starting vortex would begin to propagate around the trailing edge and over the lower surface of the aerofoil. This is confirmed by examination of the pressure signals in Fig.5.7(c) and (d). These show that lower-surface pressures react progressively, starting from $x/_c = 1.0$ at $t = 55$ ms , up to $x/_c = 0.05$ 9 ms later; this propagation rate is much higher than that seen behind the spoiler, as it is associated with circulation re-adjustments, not vortex

convection. However, the general initial response is a small pressure increase, with the later decrease beginning to take effect only after t = 70 ms. (This observation reaffirms the initial development of net lift increase ("adverse lift"), i.e. suctions develop on the upper surface of the aerofoil, before the flow has had time to respond elsewhere). Not unexpectedly, the fastest-settling lower-surface pressures are not those nearest the trailing edge, for they remain influenced by the shed vortex which is slowly disappearing in the wake, but rather it is those around $x/_c$ = 0.8 (t = 89 ms). Also, the overall pressure change diminishes steadily towards the leading edge, reflecting the position of the origin of the disturbance, while the uncommon high-frequency content of these lower-surface signals at $x/_c$ = 0.05 and 0.10 is induced by the boundary layer trip wire situated nearby ($x/_c$ = 0.055).

Having initially ignored pressures on the forward part of the upper surface, we now turn to Fig.5.7(a). There are no surprises here if we recognise the absence of a passing vortex, but the distinct dam-like influence of the deployed spoiler which requires its own settling time. At $x/_c$ = 0.69, just ahead of the spoiler, a very small suction peak upon spoiler activation (due to air drawn through the gap), is succeeded by a large, steep compression (t = 51 ms, $\delta(t) = 6°$) up to the new steady state (t = 90 ms). Farther upstream, the pressure change is progressively attenuated and the response delayed until, at $x/_c$ = 0.05, the pressure finally settles at t = 108 ms (equivalent to $\frac{Ut}{c}$ = 3.1) Note that all of these approaches to steady state are part of a readjustment of circulation all around the aerofoil and there is no single "wave" of adjustments sweeping past or around the section. Evidence here is given by settling at t = 108 ms for $x/_c$ = 0.05, but slightly <u>later</u> at $x/_c$ = 0.25 which is <u>closer</u> to the spoiler. However, the small changes imposed on pressures so far upstream ensure that they have little bearing on overall lift response (Note that $\frac{Utf}{c}$ = 2.8, which is earlier than the 3.1 quoted above).

UNIVERSITY OF BRISTOL LIBRARY
ENGINEERING

A selection of the measurements of Fig.5.7 is shown in Fig.5.8, this time in the form of instantaneous chordwise pressure distributions. (N.B. Here, as for all figures of similar format, the values for δ (t) are derived from the signal for the spoiler's free end; therefore, the true values at mid-span will be a little higher that those quoted. Comparison with Fig. 5.3 highlights the contrast between the dynamic and the static spoiler characteristics: while the initial and final (steady) distributions in both cases compare well, the in-between transient distributions in Fig.5.8 display the severe non-linearities caused by the starting vortex. The transient trends that have already been described in detail are shown in summarized form here.

Although separate discussion is not appropriate, it is still interesting to note the effect of the starting vortex on the local pressures. In particular, the beginning of the separation bubble aft of the spoiler can be seen (t = 81 ms), extending from the spoiler free edge to x/c = 0.85, taking over from the vortex induced pressures as it convects downstream. When the vortex is shed from the trailing edge, the bubble merges with the boundary layer from the lower surface, so closing around the trailing edge, and marking the onset of the final steady state (of which this closed bubble is a prominent feature,as seen in Sec.5.2.2 and Fig.5.3).

The trends noted in these transient pressure measurements are generally in good agreement with the observations made by Siddalingappa and Hancock (1980c) and by Mabey et al (1982). However, in contrast with the remark made by Siddalingappa and Hancock, it has been found here that the overall lift decrease does not coincide with, or follow, the point when the starting vortex leaves the trailing edge. In reality, at that instant (t = 87 ms), considerable "spoilage" has already taken place (see Fig.5.6(b)). It appears that the event signalling the lift reversal (from adverse effect to favourable) is the time when the lower-surface pressures begin to decrease, i.e. very shortly

after the trailing-edge pressure decrease, influenced by the approaching vortex.

The foregoing has allowed scrutiny of typical dynamic characteristics of a conventional spoiler and our observation of well-known features in the aerodynamic response has established that the basic fluid mechanisms evident in the wind tunnel are consistent with those at full scale. We now have the task of extending the knowledge of transient aerodynamics by examining the influence of several parameters which govern the position or development of these fluid mechanisms. In particular, we shall look at the importance of the non-dimensional time $\frac{UT}{c}$, the transient deflection history, geometry of the spoiler and other factors which are seen to offer considerable potential for accurate lift control.

Initially, the previous combination of spoiler configuration and aerofoil incidence will be retained, so that the effect of varying $\frac{UT}{c}$ can be isolated. Fig.nos.5.9 to 5.12 inclusive illustrate this effect when compared with the "standard" case of Fig.5.6 (Run 3001). Identified by test code number, the transient lift history from that figure is superimposed on Fig.5.9, 5.10 and 5.11 for ease of comparison.

Fig.5.9 compares Run 3007 (U = 10 m/s, $\frac{UT}{c} \doteq 1$) with Run 3001 (U = 20 m/s , $\frac{UT}{c} \doteq 2$). The decrease in airspeed allows the spoiler-induced vortex to be more dominant and the non-linear rise to C_{La} is accentuated, here seen to be approximately doubled, as are the delay times t_a and t_f, so in effect $\frac{Utf}{c}$, or the number at aerofoil chord lengths travelled by the main stream before the lift settles to its new steady value, remains virtually unchanged (the value 2.73 is to be compared with 2.78). Note that the compression ahead of the starting vortex is strong enough to manifest itself here (t = 50 ms). (N.B. The lift response curve added for comparison purposes here (Run 3001) is shifted along the ordinate in order to compensate for a small difference in steady lift levels and thus enhance the comparison. This exercise is repeated in several other figures).

Fig.5.10 introduces Run 3003 (T = 80 ms, $\frac{UT}{c} \doteq 4$). As expected, the increase in deployment time has the opposite effect, suppressing the vortex strength seen in Run 3001. Whereas C_{L_a} is reduced by about 60%, t_a is unchanged, therefore, apparently independent of spoiler rotation time (or rate), and t_f is increased almost to suggest that the response is quasi-steady, i.e. the time required for settling is only marginally greater than T for deployment. (N.B. The apparent overshoot before reaching the final lift value seems to be due to increased tunnel turbulence; a longer overall signal-capture period would show an irregular wavering at low-frequency of this near "steady" value.)

Fig.5.11 introduces Run 3009 (U = 10 m/s , T = 80 ms, $\frac{UT}{c} \doteq 2$). Now both U and T have been varied so as to keep $\frac{UT}{c}$ constant, thereby providing a good check on the suitability of $\frac{UT}{c}$ as the <u>single</u> parameter which is best employed to correlate the aerodynamic delay times t_a and t_f. Comparison of the two transient lift histories shows that the C_{L_a} values are very similar and while both t_a and t_f for Run 3009 (53 and 110 ms) are about twice as long as for Run 3001 (26 and 57 ms), the <u>non-dimensionalised</u> values, $\frac{t_a}{T}$ and $\frac{t_f}{T}$, are virtually identical and thus very good correlation is achieved.

Finally, Fig.5.12 shows Run 3005 (U = 20 m/s, T = 163 ms, $\frac{UT}{c} \doteq 8$). Included for completeness only, the deployment rate for this test is at one quarter the speed of the standard case and the response to it appears to lie at the threshold of quasi-steady lift response, i.e. only the slightest suggestion of lift-reversal or other non-linearities is apparent and the transient lift shows no delay in settling to the final steady state.

The success in correlating $\frac{t_a}{T}$ and $\frac{t_f}{T}$ in terms of $\frac{UT}{c}$ exclusively, could very well be compromised by the separate influences of compressibility and Reynold's number. The former was precluded by use of low wind speeds, while the latter effect was minimised by the fixing of transition near

the leading edge. Now, with confirmation of such success, it appears a useful exercise to consider the above non-dimensionalised times from different tests as a function of the same aerodynamic parameter (Fig.5.13, where $\frac{t_o}{T}$ is included for completeness). As the range of test code numbers betrays, some of these tests have already been presented. Also, it will be noted that there are two points on each curve at $\frac{UT}{c} = 2$; these are from the tests of matched $\frac{UT}{c}$, both being included for visual comparison.

It can be seen that no distinct pattern emerges for the delay before initial lift response, which appears to be quite independent of $\frac{UT}{c}$. Seemingly, $\frac{t_o}{T}$ is very small (about 0.05) at low $\frac{UT}{c}$ and, paradoxically, large (about 0.1) at greater values of the same parameter. However, this would be a misleading conclusion, as at low $\frac{UT}{c}$ with strong adverse lift, the initial response is in the <u>wrong</u> direction. In such cases, the delay before changeover into the right direction is a more useful measure of an initial lift response time. However, the most convenient <u>well-defined</u> response time is t_a, for maximum adverse lift, because a suggestion of this response peak exists even for very slow deployment rates whereas general turbulence can obscure the time for a sign-change in the response. Fig.5.13 shows that excellent correlation is achieved for values of $\frac{t_a}{T}$ and, not surprisingly, $\frac{t_a}{T}$ tends to $\frac{t_o}{T}$ for high $\frac{UT}{c}$ (approaching quasi-steady deployment). For low $\frac{UT}{c}$, $\frac{t_a}{T}$ diverges hyperbolically.

A similar trend is observed in the values of final lift delay time, with $\frac{t_f}{T}$ predictably tending towards unity as quasi-steady conditions are approached, but increasing sharply as the opposite end of the range of $\frac{UT}{c}$. Correlation employing this aerodynamic time parameter is still good, although some scatter has been introduced because of the difficulty in determining t_f precisely.

The essence of the message conveyed by these results is that exteme care needs to be taken when designing an ACT system where a spoiler is intended to be rotated rapidly relative

to the velocity of the main stream. For example, it is currently envisaged that rapid operation in flight would be at rates of about 400%$_s$ so, typically, $\frac{UT}{c} = 5$ at $M = 0.5$. For such a value of $\frac{UT}{c}$, as Fig.5.13 shows, the transient non-linearities are relatively mild, but would be considerably amplified were the air speed to be reduced by half, say, without an equivalent reduction in deployment rate.

Now the characteristics of response to different spoiler configurations will be compared. All three configurations that were routinely tested, displayed essentially similar characteristics and, since the response of the "standard" gapped spoiler has already been extensively reported, it would be superfluous to apply similar treatment to the other cases. Instead, only the typical lift response for each configuration will be compared, followed by an overall comparison of the aerodynamic lift delay times.

Fig.5.14 compares Run 3201, for the solid spoiler, with its equivalent for the gapped spoiler from Fig.5.6, the "standard" case of Run 3001. The inferiority of the solid spoiler, at least in dynamic terms, becomes immediately obvious, for although the same trends apply, the magnitude of adverse lift is considerably greater for this configuration. Additionally, t_a occurs a little later (by 4ms) resulting in slower initial (favourable) lift response, even if faster subsequent lift development compensates, giving a similar t_f. It is believed that the reason for both of these differences is the fact that air is sucked through the base vent into the underside of the gapped spoiler as it rises, opposing the growth of the starting vortex and encouraging its convection downstream. Also, note the initial compression ahead of the starting vortex, strong enough to be discernible for the solid spoiler only.

Fig.5.15 introduces Run 2001, this providing an opportunity to compare the standard case with the perforated spoiler. The opposite effect is seen here: this configuration produces transient lift with <u>less</u> adverse effect and also responding more quickly with favourable lift (by 3 ms) <u>and</u> settling to

the new steady state earlier (by 11 ms) when compared with the gapped spoiler. The local pressure histories (not shown) revealed that the porosity of the spoiler accounts not only for a weaker starting vortex, but also for its faster convection (by about 50%) downstream of the spoiler presumably because of the deprivation of a solid screen from the main stream; these observations explain the above trends.

Fig.5.16 is comparable with Fig.5.13, but shows response characteristics for all three configurations and also includes measurements by Mabey et al (1982) for comparison. (They were obtained for a perforated spoiler of identical porosity at speeds in the range $0.25 < M < 0.70$.) The lift onset data $(\frac{t_o}{T})^{\cdot}$ are again included for completeness only.

In situations where adverse lift <u>does</u> appear (i.e. for $\frac{UT}{c} < 8$), the use of t_a as a measure of response time was mentioned and the variations with configuration noted above are echoed in Fig.5.16

So, the adverse lift occurs earliest for the perforated spoiler, except at $\frac{UT}{c} > 4$ where the gapped spoiler fares marginally better, while the solid spoiler consistently shows the tardiest response. These measurements compare quite well with those from Mabey et al (1982), particularly at lower $\frac{UT}{c}$. The differences in test conditions for Mabey's or the current tests are significant, e.g. Mach No., Reynolds No., wind tunnel (closed rectangular working section with slotted walls vs. open circular working section), yet the two sets of results go well together.

The final lift delay time ratios also reflect the observations made above for typical transient lift histories. Differences are small down to $\frac{UT}{c} = 3$, owing to quasi-steady final response $(\frac{t_f}{T} \doteq 1)$, but for lesser $\frac{UT}{c}$ the perforated spoiler produces the fastest final lift settling. There is little to choose between the other two configurations, except at $\frac{UT}{c} < 1.5$, where the gapped spoiler appears to account for the slowest settling times; this may be

attributed to the increasing difficulty in determining t_f at the lowest values of $\frac{UT}{c}$. Comparison with values from Mabey et al (1982) is now only fair at low $\frac{UT}{c}$, but remains very good at higher values. In addition, the same authors found similar trends when comparing a plain gapped spoiler with a perforated one.

Next, the effect of varying the angle of incidence will be investigated. Until now, all the tests presented and discussed have been at zero incidence, but an identical series of tests was performed for an indicated incidence $\alpha = 14°$. No significant changes in the basic shape of lift responses were expected, as suggested by the experiments of Kramer et al (1951), and indeed this proved to be the case. Therefore, given the comprehensive coverage already granted to the zero incidence results, only appreciable differences from those will be reported here. Results from this series of tests are presented in Fig.nos. 5.17 to 5.24 inclusive.

Fig.5.17 (Run 5001) is of the same format as Fig.5.6 (Run 3001) and shows a similarly-specified test. There are obvious differences that could be deduced from the steady-state characteristics (see Sec.5.2.2 for details), but the transient lift responses are very similar, at least in terms of delay times. Significantly, but not surprisingly, the adverse lift here is much smaller (about 50% of that for Run 3001). This can be explained in terms of a weaker starting vortex, due to locally-separating flow, inducing smaller suctions downstream of the spoiler. Evidence to support this view is provided in Fig.5.18, showing the individual pressure histories for Run 5001 (the same format as Fig.5.7, but at twice the scale for the ordinate). Thus, the signals recorded downstream of the spoiler, nos.7 to 11 of Fig.5.18(b), show suctions clearly attenuated relative to those for the same signals of Run 3001. As a result, the transient pressure changes around the aerofoil are generally smaller over the lower surface and near the leading edge, where the steady changes are small, the spoiler deployment is barely felt. The instantaneous pressure distributions (Fig.5.19) simply echo these features.

Fig.5.20 (Run 5003) is similar to Fig.5.10, and the comments made for it apply here also (see p.50), in particular when comparing this test with Run 5001 (Fig.5.17).

Fig.5.21 is similar to Fig.5.13 and includes the measurements presented in that figure. Thus, direct appreciation of the effect of angle of incidence on the aerodynamic lift delay times can now be gained. Confirming the observations from Fig.5.17, very good matching is achieved in Fig.5.21 for all delay times throughout the range of $\frac{UT}{c}$, except at the lowest values ($\frac{UT}{c} < 1.5$), where a rather faster response is achieved for $\alpha = 14°$. Also, very good agreement is obtained for tf with Hoerner's (1975) rapid spoiler deployment tests ($\frac{UT}{c} = 1.5$), performed in a water tunnel at $C_L = 1.0$.

Fig.5.22 (Run 5101) and 5.23 (Run 4011) are similar to Fig.5.14 and 5.15, allowing comparison of the typical transient characteristics of the different spoiler configurations. Fig.5.22 shows that at this incidence, the solid spoiler provokes an almost identical response as for the "standard" gapped configuration. Whereas at low incidence the solid spoiler was noticeably more effective, that additional effectiveness is lost at high incidence and the two curves in Fig.5.22 are as similar as can be expected (in an area of some unsteadiness), after the lift decrement. This behaviour is undoubtedly due to the poor quality of flow over the rear upper surface (thick boundary layer) and the consequent small influence of flow through a gap or, to a lesser extent, perforations. Note also that the magnitude of ΔC_L was about 0.3 in Fig.5.14 whereas it is about 0.2 here, indicating that the spoiled lift was already of lesser quality. The flow quality can also be blamed for the reduction of the adverse-lift peaks from about 0.10 (Fig.5.14) to about 0.05 here. Clearly the same spoiler rotation rate cannot induce a vortex of the same strength in a thick boundary layer.

Fig.5.24, like Fig.5.16, compares the aerodynamic lift delay for the different spoiler geometries, except that

measurements for the solid spoiler are omitted on the evidence of Fig.5.22. Now reflecting the indications from Fig.5.23, there is no discernible difference between the two configurations, save at low $\frac{UT}{c}$, where the adverse lift seems to occur slightly earlier for the perforated spoiler.

Finally, and predictably, it was found that spoiler motion had no effect at angles of incidence beyond the stall.

(b) Spoiler retraction

Fig.5.25, 5.26 and 5.27 display the transient measurements from a typical dynamic test (Run 3051), where the gapped spoiler is now retracted at a rate $\dot{\delta} = 1000°/s$ with the aerofoil at zero incidence. The measurements in these figures are presented as for Fig.5.6, 5.7 and 5.8 respectively.

As Fig.5.25(a) shows, spoiler retraction was effectively the process of extension in reverse, but with a minor difference, insofar as the spoiler was stopped slightly earlier in order to prevent slamming against the recess on the model surface, and therefore, resulting in a final spoiler angle slightly above zero. The transient response characteristics remained, of course, unaffected. Also note that the initial spoiler angle is set as $\delta = 37°$ so as to achieve consistency with the final steady state for spoiler extension.

Fig.5.25 shows the effect of the totally different dynamic features of spoiler retraction from those, now familiar, features of extension. There is no manifestation of any "adverse" effects here, though the lift response cannot be regarded as quasi-steady either. Following initiation of spoiler motion (assumed to be at $t = 45$ ms, as before, from interpolation of the two spoiler position signals), there is a short delay t_o ($t = 48$ ms, i.e. $t_o = 3$ ms, $\delta = 34°$) succeeded by quasi-linear lift increase consistent with, and lagging behind, the spoiler motion. Finally, following the completion of spoiler rotation ($t = 82$ ms, i.e. $T = 37$ ms

and $\frac{UT}{c}$ = 1.8) the lift eventually settles to its new steady value, after a time t_f from spoiler activation, giving $\frac{Ut_f}{c}$ = 3.4 (based on t = 115 ms).

Such a response is entirely typical of rapid spoiler retraction. No "adverse" effects could be provoked in the course of testing, even at the lowest value of the aerodynamic time parameter ($\frac{UT}{c} \doteq 0.9$). This is because the initial flow conditions for the retreating spoiler are completely different from those for the opening spoiler. Whereas in the latter case the direction of rotation was into "clean" airflow, now it is into a region of separated flow, which appears to close in the wake downstream of the trailing edge to form a bubble. The retreating spoiler can therefore be visualized as squeezing and pushing this bubble downstream, rather than inducing any vorticity. The effect of very high rotation rates cannot be predicted, however such rotation rates are impractical and hence "adverse" effects must not be expected on closing. Previous research programmes have yielded generally similar results, with the consequence that this phase of transient spoiler motion is often regarded as unworthy of investigation. Yet, the problem remains of trying to reduce delays in the initial lift response and in the final lift settling; in fact, as shown above $\frac{Utf}{c}$ is actually longer than for extension. This problem has been addressed as part of the present investigation and details will be given later.

Returning to Run 3051, examination of the chordwise pressure histories (Fig.5.26(a) to (d)) should at least give some hints regarding the fundamentally different character of the effects of spoiler retraction, when compared to extension. However, prior research and especially the flow visualization tests by Garroch (1980) have already suggested what might happen: as the spoiler closes rapidly, the bubble behind it contracts while being convected downstream and eventually is completely swept away to allow the new steady state to establish itself; obviously no starting vortex is involved in this motion. Such behaviour would explain the fairly monotonic increase in lift. Indeed, the pressure

histories confirm those findings. Looking at the pressure signals downstream of the spoiler (Fig.5.26(b)), there is no evidence of generation of vorticity and all signals react virtually simultaneously, i.e. sudden changes almost coinciding with spoiler activation (t = 45 ms). This near-simultaneous compression along the length of the bubble, suggests equally rapid initiation of its convection downstream. Signal no.7 ($^{x}/_{c}$ = 0.80) shows considerable overshoot in compression before settling to the new steady level, and this tendency is evident as far along as $^{x}/_{c}$ = 0.90. It seems clear that this overshoot, which is greatest near the spoiler hinge, and which peaks only 1-2 ms after the rotation is complete, is a manifestation of compression induced underneath the rapidly-closing spoiler. Generally the signals behind the spoiler, are unsettled until about t = 110 ms ($\frac{U\hat{t}}{c} \doteq 3.2$), this being rather later than for an equally swift extension $\frac{U\hat{t}}{c} \doteq 2.8$), thus betraying a relatively long convection time for the viscous bubble, and mirroring the previous observations viz. t_f (Fig.5.25). Elsewhere on the aerofoil, the initiation of pressure response is equally rapid, with the compression "pulse" being transmitted around the trailing edge and over the lower surface, losing strength in the process (see Fig.5.26(c) and (d)); a similar tale unfolds on the upper surface, with suction spreading forward from the spoiler front face (Fig.5.26(a)). Overall, the pressures on both surfaces appear to react in the "right" direction and approximately simultaneously, coinciding with initiation of convection of the bubble; these observations account for the relatively smooth transient lift development.

Fig.5.27 simply reiterates the main points of the above analysis. Additionally, an interesting comparison can be made with the transient pressure distributions for spoiler extension (Fig.5.8), immediately highlighting the difference in character between the two processes. The initial and final distributions of one are very similar to the other (in reverse order), but the intervening transient distributions are markedly different, reflecting the

contrast between the sharp effects of the starting vortex behind the rapidly-opening spoiler, and the gentler, more gradual influence of the viscous bubble being squeezed away by the rapidly-closing spoiler. Nevertheless, it is clear that in either case, viscous effects dominate the scene, and the conditions at the trailing edge are always of vital importance for monitoring these effects.

As for spoiler extension, the typical trends noted here compare well with the measurements of Siddalingappa and Hancock (1980c) and of Mabey et al (1982). (N.B. The former authors found the final lift delay time for retraction to be <u>shorter</u> than for extension, apparently contradicting the trend seen here. However, their measurements were for the lower value $\frac{UT}{c} \doteq 1$, and for that value the current tests showed a comparable response.

In view of the generally smooth transient response, in contrast to spoiler extension, it is felt that presentation of a wide range of retraction cases would not supply much additional information concerning transient trends. Instead, it appears sufficient to consider only the aerodynamic delay times from a range of tests as a function of the aerodynamic time parameter $\frac{UT}{c}$ (Fig.5.28). As for extension cases, the initial lift response delay seems to be quite independent of $\frac{UT}{c}$, though $\frac{t_o}{T}$ does appear to be longer for retraction, especially at the lower values of $\frac{UT}{c}$. (N.B. Again, this comparison is rather meaningless, as t_o for extension marks the onset of response in the <u>wrong</u> direction.) Here too, good correlation is achieved for the final lift delay ratio in terms of $\frac{UT}{c}$. Comparison with the equivalent measurements for extension (Fig.5.13) reveals generally similar trends, though t_f for retraction increases less slowly than the hyperbolic increase for extension, at very low $\frac{UT}{c}$. As a consequence of these differing rates of increase, t_f for retraction is about 40% greater at $\frac{UT}{c} \doteq 4$, whereas it is actually about 15% lower at $\frac{UT}{c} \doteq 5$.

The other two spoilers, solid and perforated, performed in

a very similar manner, showing near-identical transient lift response between the rather different initial and final levels dictated by their respective steady characteristics. Fig.5.29 emphasizes this similarity, showing Run 3251 for the solid spoiler together with its equivalent test for the gapped spoiler, the previously discussed Run 3051. Excellent comparability is obtained, therefore, further consideration of such individual tests for these different spoiler configurations is not presented explicitly.

Fig.5.30, showing the aerodynamic lift delay times for all three spoiler geometries, provides further evidence of common response characteristics. Comparison with the measurements of Mabey et al (1982), obtained for a perforated spoiler at speeds from M = 0.25 to 0.70, shows poor agreement for $\frac{t_o}{T}$, but the much more important values of $\frac{t_f}{T}$ compare very well.

By now, it might be expected that the effect of wing incidence would be small, at least on transient lift response. The set of tests performed at $\alpha = 14°$ confirmed this assumption. Fig.5.31 shows the typical response at this incidence, the configuration for this test (Run 5051) being specified as for the "standard" case at $\alpha = 0°$, Run 3051. Compared with that test, Run 5051 shows a similar lift-developement profile also, save a relative sluggishness in initial lift response.

Fig.5.32 allows an overall appreciation of the effect of wing incidence, being of similar format to Fig.5.28 and also showing the measurements presented in that figure. The earlier observation of longer t_o for a typical dynamic test at high incidence is reflected here, especially for low $\frac{UT}{c}$, but being of no great consequence, this small delay being made up later on. By contrast, excellent correlation is achieved for t_f throughout the range of $\frac{UT}{c}$.

As for $\alpha = 0°$, all spoilers at $\alpha = 14°$ provoked very similar transient lift responses to retraction. Some

evidence of this general similarity is presented in Fig.5.33, i.e. an orderly variation in t_f, but no other significant response characteristics to be timed. This figure, like Fig.5.24 for spoiler extension, shows the aerodynamic lift delay times for the perforated spoiler as well as those for the standard gapped spoiler from Fig.5.32. It can be seen that the delay times for the two configurations compare very favourably.

5.3.2 Multiple-step deflection profile

With the completion of tests using spoiler ramp-deflection profiles and analysis of the results, as described in the previous sub-section, the first three of the five major objectives of this investigation had been achieved (that is, briefly, studying the fluid mechanisms triggered by transient spoiler motion, examining the effect of $\frac{UT}{c}$, and assessing the relative performance of different spoiler configurations; also see Sec.1.3.2). In addition, the fourth objective, namely specially investigating the "adverse lift" phenomenon and possible methods of suppressing its effects had been met in part so that this phenomenon and its implications were already well understood. This sub-section is primarily concerned with the other part of the same objective. Hence, a method will be described of suppressing the transient lift-reversal observed at the initial stages of rapid spoiler extension, while afterwards different forms of the concept behind this method will be applied briefly in other related areas.

Previous suggestions for prevention of the initial adverse lift have generally been based on the assumption of a "datum" operating position of $\delta = 10°$. This would not only allow the spoiler to produce both positive and negative ΔC_L (by retraction or by additional extension), but also, because it began from a point at which the separation bubble downstream of the spoiler had already extended past the trailing edge, its further opening was expected not to generate the undesirable adverse effects. This scheme does

not work, as is convincingly illustrated by Fig.5.34 (Run 3103). The testing configuration for this run is exactly as for Fig.5.10 (Run 3003), except for the starting angle of $\delta \doteq 12°$. Even without comparing the two figures it is clear in Fig.5.34 that the adverse lift C_{L_a} remains strong and a starting vortex of some strength has been produced.

A fresh approach was obviously needed and this will now be outlined. As stated implicitly in Sec.5.3.1(a), the actual magnitude of adverse lift, C_{L_a}, is dependent upon the strength of the starting vortex. In turn, it was recognized that for a given aerofoil - spoiler combination and constant free-stream speed, the strength of the vortex was primarily dependent on the change in net spoiler rotation rate $\Delta\dot{\delta}$ (this being the single constant $\dot{\delta}$ for a ramp deflection) rather than the rotation time T. This dependence on <u>change</u> of rotation <u>rate</u> rather than T is supported by two observations:

1. whatever strength of vortex is produced by a single ramp rate, the vortex will begin to convect downstream before the spoiler rotation is complete at time T (unless T is very small),
2. the existence of distinct "packets" of vorticity in the fluid has been noticed as a direct consequence of sudden "impulses" imposed on the fluid by equally sudden changes in spoiler rotation rate.

These are certainly consistent with the flow visualization by Garroch (1980) and lend weight to the statement that adverse lift is not related to the aerodynamic time parameter $\frac{UT}{c}$, as in Sec.5.3.1(a), but perhaps related to an aerodynamic <u>rate</u> parameter $\frac{U}{\delta c}$. (N.B. The correlation in terms of $\frac{UT}{c}$ in Sec.5.3.1(a) <u>was</u> successful because the distance rotated through by the spoiler was kept constant, hence T <u>was</u> representative of δ).

Now, if it is assumed that the initial and final spoiler angles, δ_i and δ_f, as well as T are all given then the average rate of rotation will be

$$\bar{\dot{\delta}} = \frac{(\delta_f - \delta_i)}{T} \qquad (5.1)$$

and for a ramp deflection, $\dot{\delta} = \bar{\dot{\delta}}$. However, note that the same initial and final positions in the transient profile, namely from $\delta_i(\hat{t} = 0)$ to $\delta_f(\hat{t} = T)$, could be spanned by two successive ramps, the first at a rate lower than $\bar{\dot{\delta}}$, the second at a rate greater than $\bar{\dot{\delta}}$, but such that the change of rate between them will be less than $\bar{\dot{\delta}}$, i.e.

$$\dot{\delta}_1 < \bar{\dot{\delta}} < \dot{\delta}_2 \qquad (5.2)$$

and

$$\dot{\delta}_2 - \dot{\delta}_1 < \bar{\dot{\delta}} \qquad (5.3)$$

Thus both the initial step in rate and the following step would be less than the step in rate for the single ramp; the single vortex which produced adverse lift would now be replaced by two vortices, the first being proportional to $\dot{\delta}_1$ and the second proportional to $\Delta\dot{\delta} = (\dot{\delta}_2 - \dot{\delta}_1)$ i.e. the net <u>increase</u> in rotation rate. It can be deduced from (5.2) and (5.3) that each of the vortices would be weaker than the original single vortex, thereby resulting in an overall reduction in C_{L_a}. In the limit, an ever-accelerating spoiler following a hyperbolic displacement profile, to minimise $\Delta\dot{\delta}$ throughout the deployment, should be capable of eliminating the adverse lift effect, but there is also an implicit demand here on actuation capacity.

In the simplest terms, ACT requirements will be for very rapid production of ΔC_L, of either sign, and hence the rotation period T must be small. The foregoing shows that rotation rates just prior to t = T must be rather <u>greater</u> than $\bar{\dot{\delta}}$ if the initial rates are to be <u>less</u> than $\bar{\dot{\delta}}$. Clearly if T is going to be satisfactorily small then the rotation rate just before completion of the rotation could be very great indeed. Whatever this maximum rate may be, it will govern the deflection profile employed to prevent adverse lift.

Thus, if a given actuator could deliver a maximum rotation rate $\dot{\delta}_{max}$ (about $1000^{o}/_{s}$ nominal, here) and if the quasi-steady limit for a specific aerofoil-spoiler configuration was known ($\frac{UT}{c} = 8$ for a gapped spoiler, here), then for a given windspeed the maximum rate of rotation for which no adverse lift is manifested, $\dot{\delta}_{qs}$, could be calculated

($\dot{\delta}_{qs} \doteq 250°/s$ for U = 20 m/s, here). Then, as Fig.5.35(a) shows, the optimum spoiler displacement profile for minimization of C_{L_a} could be obtained by setting the initial rotation rate $\dot{\delta}_1 = \dot{\delta}_{qs}$ and the final rate $\dot{\delta}_n = \dot{\delta}max$, and then by computating a suitable set of intermediate rates for a smooth transition between the two. The following conditions would be satisfied:

$$\dot{\delta}_1 = \dot{\delta}_{qs} < \bar{\dot{\delta}} < \dot{\delta}_n = \dot{\delta}max \qquad (5.4)$$

and $$\Delta\dot{\delta}_i = (\dot{\delta}_i - \dot{\delta}_{i-1}) < \dot{\delta}_{qs} \text{ for } i = 2,3....,n-1,n \qquad (5.5)$$

Then, the single starting vortex of the equivalent ramp test at $\dot{\delta} = \bar{\dot{\delta}}$ would be replaced by a succession of much smaller vortices. Even if the combined effect of these vortices were to be additive, their physical spread in the chordwise direction would ensure a considerable reduction in adverse lift: the lower surface of the aerofoil, alerted by the arrival of the first vortex at the trailing edge, would now react well in advance of the full development of suctions on the upper surface, therefore partly cancelling their effect i.e. adverse lift. On the other hand, the other transient effects, the delay times t_o and t_f, would probably not be shortened and would possibly even be lengthened, relative to the ramp deflection.

The design specification of the experimental system constructed for the purposes of the present investigation already allowed for reproducing deflection patterns as shown in Fig.5.35 (see Sec.3.5.2 for the requirement for the spoiler-actuation sub-system and App.C for the specification of the appropriate software). Therefore, no modifications to software or hardware were required before the above hypothesis could be put to the test. Unfortunately, however, an insurmountable problem soon became apparent. As implied in Fig.5.35(a) and the related argument in the test, it would have been desirable to have a large $\dot{\delta}_{max}$ compared with $\bar{\dot{\delta}}$, but at the same time this average or standard rate $\bar{\dot{\delta}}$ had to be large enough to generate the undesired lift, if only for the sake of comparison. Thus for the "standard" gapped spoiler, a rate $\bar{\dot{\delta}} = 667°/s$ was called for. Given that $\dot{\delta}_{max} = 1000°/s$ nominal, it would have been impossible to

field the optimum multi-step deflection profile as outlined earlier. Nevertheless, the point could still be made even if partial suppression of the adverse lift could be achieved with a less than perfect deflection pattern.

Fig.5.36 shows Run 3611, a test employing such a deflection pattern. As can be seen from Fig.5.36(a), this was a three-step rotation with $\dot{\delta}_1 = 425°/s$ i.e. <u>not</u> as low as $\dot{\delta}_{qs} \doteq 250°/s$). Fig.5.36(b) shows its transient lift history, together with that for Run 3002, the single-ramp rotation at the same $\bar{\dot{\delta}} = 667°/s$. Clearly, the point <u>is</u> made here: C_{L_a} for Run 3611 is only about 50% of the value for the single ramp and it approximately coincides in time with that for Run 3002 (t = 73 ms). Not unexpectedly, there is same evidence of a second adverse lift peak (t = 92 ms), apparently due to the vortex for the second step, but there is no manifestation of the third vortex, its effect seemingly being countered by the suctions developing on the lower surface. The process of convecting a succession of starting vortices rather than only the one would account for the delayed onset of lift reduction (about 9 ms later), but the time to achieve the final lift steady value is very similar.

Fig.5.37 (a) to (d) shows the transient chordwise pressure signals for Run 3611, whereas the transient signals for Run 3002 are similar to those for Run 3001 (Fig.5.7(a) to (d)), if slightly attenuated by comparison. Looking at the signals downstream of the spoiler (Fig.5.37(b)), at least two distinct suction peaks are registered at any one station, betraying the formation and passage of an equal number of starting vortices, thereby confirming the earlier assumption to this effect. Further to this, the fact that these peaks are well-defined reaffirms that the particular change in spoiler rates here from one deflection step to another is too abrupt to eradicate C_{L_a} altogether, although these rates do reduce it. Even such a reduction is not apparent by sole examination of the signals behind the spoiler since, overall, sizable suctions are still

manifested. The answer lies in looking at the whole picture: by the time the largest suction peak is recorded at the trailing edge (t = 116 ms), suction is already established throughout the lower surface (Fig.5.37(c) and (d)), as is compression upstream of the spoiler (Fig.5.37(a)). Both of these effects tend to oppose the influence of that peak and the net result, shown by the transient integrated pressures in the lift history (see Fig.5.36), is that the peak is completely suppressed, hence the observed reduction in C_{L_a}.

Overall the technique has achieved the desired effect, endorsing the concept behind it; no obvious drawbacks have been highlighted except the need for rapid actuation. Tests at slightly different overall rates (down to $\bar{\dot{\delta}} = 500°/s$) yielded similarly encouraging results. There was no intention to carry out extensive testing with different spoiler configurations and at different angles of incidence, since there was no a priori reason why any such parameters should cause fundamental departures from the results quoted above. Nevertheless, selective tests were performed for a limited range of spoiler configurations and angles of incidence.

Whereas the perforated spoiler showed results similar to the gapped configuration, success was more limited with the solid spoiler, as Fig.5.38 demonstrates. This is not a surprising result, given the increased C_{L_a} caused at high $\dot{\delta}$ by comparison with the gapped spoiler; a higher $\dot{\delta}_{max}$ would therefore be required for the solid spoiler to match the present performance of the gapped one. Fig.5.38 shows Run 3652, for which $\bar{\dot{\delta}} \doteq 500°/s$, and the transient lift history for the equivalent single-ramp deflection is also shown. Apart from the small reduction in C_{L_a} for Run 3652, the "kinks" in lift development betray a sequence of vortices and, as previously, the initial lift response is delayed slightly, but t_f is identical.

Fig. 5.39 is similar to Fig.5.36 except now $\alpha = 14°$. Similar trends also are observed here, i.e. reduced C_{L_a},

delayed initial lift response and identical final lift settling time, thereby confirming that the technique has comparable consequences across the range of α.

Recapitulating, the adverse lift phenomenon can now be said to be quite well understood: the fluid mechanism that causes it is known, as are its effects and how they can be influenced by a number of important parameters. Further, and more significantly given its undesirability, a technique is now known for eliminating it. However, this technique does depend on a couple of important assumptions, namely:

(a) A spoiler actuation system is available to provide a maximum deployment rate that is large by comparison with the overall (ramp) deployment rate likely to be demanded to counter a gust, for example.

(b) The same actuation system is able to provide a fairly complex but well-defined spoiler deflection profile.

In practice, the initial stage of such a profile would be easier to reproduce than the equivalent single ramp, being less abrupt, but problems might arise at the final stage where a very sudden <u>stop</u> would be demanded. No attempt has been made here to determine or study desirable stopping-dynamics from the point of view of fluid mechanics, but there is the obvious structural problems of post-deployment vibrations to deal with. In the present investigation, the computer-controlled deflection profile included automatic adjustments by software to counter this particular problem.

Armed with a better knowledge of the adverse lift phenomenon and in view of the success of the multi-step technique in minimising C_{L_a}, it was not difficult to see the method that could be used to <u>maximize</u> C_{L_a}. Although of no immediately apparent practical value, such an exercise was still of interest, as it would be demonstrating the extreme case on the other side of the "standard" case of the ramp deployment; further, it could provide information of some use in the quest for increasing short-term manoeuvre lift, for example.

Essentially, this displacement profile would form the concave-downwards arc of a pair that brackets the single ramp, the concave-upward arc being for <u>suppression</u> of adverse lift. The two arcs are seen respectively in Fig.5.35(b) and 5.35(a). It follows that for this new profile, $\dot{\delta}_1 = \dot{\delta}_{max}$ and $\dot{\delta}_n << \bar{\dot{\delta}}$ ($\dot{\delta}_n$ is no longer of crucial importance). Also, the following conditions would be satisfied:

$$\dot{\delta}_1 = \dot{\delta}_{max} > \bar{\dot{\delta}} \qquad (5.6)$$

$$\Delta\dot{\delta}_i = (\dot{\delta}_{i-1} - \dot{\delta}_i) << \bar{\dot{\delta}} \qquad (5.7)$$

This time around, of course, there would be a single starting vortex, as for the equivalent ramp deflection ($\dot{\delta} = \bar{\dot{\delta}}$) but much stronger, as deduced from expression (5.6). Consequently, C_{L_a} would be increased accordingly.

Fig.5.40 shows a three-segment arc of the kind described above, for comparison with the equivalent single ramp (Run 3002) and whilst this profile is less than perfect it nevertheless confirms the above view. The response is largely as expected, with Run 3631 showing greater C_{L_a}, faster initial lift response, but also faster time to final lift.

Finally, a similar displacement profile in reverse could be applied for spoiler retraction this time. Although no effect comparable with adverse lift is induced during spoiler retraction, it was seen earlier (Sec.5.3.1(b)) that considerable aerodynamic time delays $\frac{t_o}{T}$ and $\frac{t_f}{T}$ existed during retraction, especially at the lower values of $\frac{UT}{c}$. In view of the fast response time seen in Fig.5.40 it is not illogical to suggest that this graduated deflection profile from high-rate to low-rate could improve on these time delays while <u>not</u> producing any undesirable effects. The suggested deflection profile is given in Fig.5.35(c), this to be compared with (b). The same general policy is applied in selecting rates between $\dot{\delta}_{max}$ and the final zero rate.

Fig.5.41, allowing comparison between such a multi-step profile (Run 3561) and the standard ramp (Run 3053 for $\dot{\bar{\delta}}$ = 500°/s), again illustrates the desired effect. The initial lift development is appreciably faster for Run 3561, whereas t_f is only slightly smaller. As an additional bonus, the much-reduced final rotation rate also reduces the risk (or the effect!) of impact as the spoiler approaches the wing surface beneath it.

In conclusion, therefore, it has been shown that the multiple-step deflection profile, in different forms and for different reasons, displays substantial benefits for both extension and retraction phases of transient spoiler motion and, in particular, it displays the capacity to eliminate the adverse lift phenomenon, the bete noire of transient spoiler aerodynamics.

5.3.3 Pulsed operation

The results presented so far have been concerned with one or other of the primary phases of spoiler operation, that is extension or retraction. However, in order to counter a sudden gust for example, the spoiler would have to undergo a complete cycle of rotation, opening rapidly and closing again after a certain delay, the length of which would be dictated by the duration of the gust. It follows from the findings that have been discussed in the previous section that the sequence for the optimum displacement-time history for such a cycle would consist of a multi-step deflection profile as shown in Fig.3.35(a) followed, after the appropriate delay, by the profile shown in Fig.5.35(c). Then the overall lift response to such an operation can be deduced by simply concatenating Fig.5.36 and 5.41; therefore, there is no need for presenting results to that effect. However, for comparison or to prove the case, it is worthwhile looking at the lift response to the extreme case of very rapid extension followed immediately by equally rapid retraction. It was hoped that such a "pulse" in spoiler deflection might

cause a lift response which gave a net <u>increase</u> in transient lift if it were possible to reverse the spoiler rotation from opening to closing <u>before</u> a lift decrease was obtained (hence, $\delta_f \doteq 20°$ now, not 40°). The initial transient lift reversal would then no longer be an "adverse" effect, but would seem to be favourable in the context of augmenting manoeuvre lift or of countering a negative gust.

Fig.5.42 shows Run 3901, where a deflection pulse as described above was employed. Clearly, the result is disappointing, showing in fact an overall small reduction in transient lift, i.e. the negative lift impulse is stronger than the positive lift impulse preceding it.

A glance at the transient pressure signals for Run 3901 (Fig.5.43(a) to (d)) is sufficient to reveal the reasons for this result. The suctions induced by the starting vortex aft of the spoiler (Fig.5.43(b)) are very short-lived as the convection of that vortex is aided by the compression wave following it, the compression itself being induced by the retraction process. While that compression is in the process of cancelling the overall effect of the vortex (i.e. lift increase), suctions over the lower surface (Fig.5.43(c) and (d)), and compressions ahead of the spoiler are added, to give overall a large negative lift peak before the more familiar response to retraction takes over to restore the original steady lift state.

This now concludes the discussion of the results for the main, conventional spoiler position, i.e. at the rear of the upper surface of the wing.

5.4 Dynamic Tests With Lower-Surface Rearward Spoiler

Dynamic tests using the lower-surface rearward spoiler were performed at a single nominal windspeed U = 20 m/s giving $R_e = 5.6 \times 10^5$.

Because of the shear volume of tests (and accompanying experimental data!) that were eventually carried out for the previous spoiler position, far exceeding the original estimates, the temptation to discuss this series of tests might have been irresistible, especially given the universal omission of this spoiler arrangement from modern aircraft. However, analysis of the previous results had already suggested that the lower-surface spoiler had its own merits for ACT-related applications, making it particularly worthy of investigation.

Firstly, not only does the lower-surface spoiler appear to share the capacity of its upper-surface equivalent to effect rapid lift changes, but it has the additional advantage that, by remaining in active flow at high angles of incidence, its effectiveness appears to be unimpaired up to the stall and, to a lesser extent, beyond it, as shown by Fig.5.1 and 5.5. Further, this spoiler's ability to counter gusts of opposite sign than the upper-surface spoiler would suggest that the pair could form the basis for an effective system for gust alleviation (i.e. countering the loads imposed by downgusts as well as upgusts).

Secondly, it became apparent from the tests with "pulsed" operation (Sec.5.3.3) that the overall small negative lift impulse resulting from such an operation (e.g. Fig.5.42) could have been greatly enhanced if the multi-step extension profile for minimising adverse lift (Fig.5.35(a)) had been employed, instead of the single ramp. With the initial positive lift peak suppressed, the net result ought to have been a negative lift pulse issued in response to the overall spoiler motion. Such behaviour would have been the opposite of the one hoped for at the time. However, if a lower-surface spoiler were to be deployed in a similar manner, a positive lift impulse ought to be produced, achieving the result originally required.

The dynamic characteristics of a lower-surface spoiler displayed no fundamental differences to those for an upper-surface spoiler. In fact, because of the symmetricity of

the aerofoil and identical chordwise distance, all findings for the upper-surface spoiler at $\alpha = 0°$ apply equally to the lower-surface spoiler, but with the sign for C_L reversed. Therefore, this section is concerned only with tests at high angles of incidence. (N.B. "High" now means "more negative": as already explained, the aerofoil was pitched at $\alpha < 0°$, but the upper surface was nominated as the lower surface and vice versa, so that in effect the upper-surface spoiler at $\alpha < 0°$ could be treated as one on the lower surface at $\alpha > 0°$. Henceforth, this latter notation will be used). Further, only a small selection of results from these tests will be discussed, which it was felt could make useful contributions to the wisdom already acquired, as hinted in the previous paragraphs. On this basis, single-ramp deflection tests will be for one incidence ($\alpha = 15°$) unless otherwise stated, one rotation rate ($\dot{\delta} = 500°/s$), and for an extending spoiler only. Retraction tests showed no unusual features and are therefore omitted, except implicitly, as the latter part of "pulsed" spoiler operations. The results from tests that <u>were</u> of interest are presented in Fig.5.44 to 5.53 inclusive.

Fig.5.44, 5.45 and 5.46 display the measurements from a typical dynamic test for extension of the gapped spoiler at $\alpha = 15°$ (Run 9202). The standard testing policy quoted above for this set (e.g. $\dot{\delta} = 500°/s$) is clearly a deviation from what was previously called "standard" (e.g. Run 3001, Fig.5.6, for which $\dot{\delta} = 1000°/s$ and $\alpha = 0°$). Nevertheless, comparisons can be made between <u>similar</u> sets of conditions, e.g. see Run 3003 in Fig.5.10. Also note that the scales and ranges employed for the graphs of those earlier cases are different from those being used now.

Fig.5.44 shows the transient lift history for Run 9202. Comparing with Run 3003, the overall "spoiling" effect is rather greater at this incidence ($\Delta C_L \doteq 0.4$ cf. with 0.3 for $\alpha = 0°$), though tunnel interference effects may well compromise the accuracy of this result. The transient lift

development is generally as for $\dot{\alpha} = 0°$, with the time for the lift to reach its final steady value being very similar for both tests (t_f = 90 ms, i.e. $\frac{Ut_f}{c} = 4.4$), and thus suggesting that t_f is independent not only of incidence but also of which surface has the spoiler; similar results are obtained for the upper-surface spoiler at $\alpha = 14°$, too. A significant difference does apply, though, in the development of "adverse" lift: this peaks later (t_a = 47 ms compared with 27 ms) and is larger (C_{L_a} = 0.08 compared with 0.04) than for $\alpha = 0°$. This is not entirely surprising as the flow over an upper-surface spoiler, at incidence, is such as to move away from the aerofoil surface downstream, whereas the direction of the freestream flow passing a lower-surface spoiler is nominally toward the downstream aerofoil surface. The consequence of this is therefore likely to be that the developing vortex is encouraged to stay attached to the spoiler tip for a longer period, and thus to become stronger, than for an upper-surface spoiler.

Fig.5.45(a) to (d) shows the transient pressure signals for Run 9202. These are generally as expected, reacting in a very similar manner to those for Run 3003 (not shown), with the exception of the signals immediately downstream of the spoiler (Fig.5.45(c)). They show clearly-defined suction peaks that betray the strong starting vortex deduced from Fig.5.44. However, the convection time for this vortex does not change from $\alpha = 0°$, thereby resulting in similar pressure settling times and, presumably, t_f as seen earlier.

Fig.5.46 shows the instantaneous pressure distributions for Run 9202 and is presented primarily for the completeness of a "typical" case. Nevertheless, there are certain features which deserve attention because the case has some uniqueness. In particular, we had previously seen the effect of a pressure-change at the trailing edge, sweeping forward over the lower (pressure) surface, whereas now as the separation-bubble reaches the trailing edge we find its effect sweeping forward over the upper (suction) surface in a more dramatic way, such that before or after t = 109 ms the pressure distributions seem to be in either

one state or another.

From the typical transient lift response shown above, it was demonstrated that the lower-surface spoiler can effect lift variations as rapid as its conventional counterpart on the upper surface of the wing. In fact, it was seen that t_f appears to be unaffected by spoiler position, upper or lower, at least for a symmetrical aerofoil. Furthermore, it was shown that the characteristics of lift development with spoiler motion are not attenuated at high incidence and the spoiler retains full control effectiveness. Unfortunately, the initial "adverse" lift, here of course being a lift decrease, so still opposing the desired effect, is not only preserved but actually augmented.

It could be predicted from the results for the upper-surface spoiler that the above augmentation of C_{L_a} would be even more pronounced when the solid spoiler was used. Fig.5.47, showing Run 9002 for the solid spoiler and being compared with the similarly-configured Run 9202 for the gapped spoiler, confirms that prediction: as was the case for the upper-surface position, responses are generally similar with identical t_f, but with C_{L_a} nearly doubled relative to the gapped spoiler. Because the range of tests for this spoiler position was limited and because the lower-surface position promised a rather unconventional display of transient aerodynamics, the solid-spoiler configuration was selected for the remainder of the cases to be presented here. The solid spoiler was also the only one to be fully tested statically.

Emphasising the point that some control effectiveness is retained even (just) beyond the stall is Fig.5.48, showing a test configured as for Run 9002, but for $\alpha = 20°$, i.e. 3° beyond the stall. Interestingly, apart from the usual transient trends, another "adverse" lift effect is observed here, only this time it follows the final stage of deployment. This effect was consistently reproduced and its absence from lift histories for static tests confirmed its dependence on transient conditions following deployment.

However, the time available did not allow proper pursuit of this peculiarity, although its repeatability was challenging.

A far more important proposition was to show that the "multiple-step" technique, explained and successfully demonstrated for the upper-surface spoiler in Sec.5.3.2, could also be employed here to suppress C_{L_a}. Fig.5.49 shows Run 9502, a test employing a multi-step deflection profile for which $\dot{\delta} = 500^{o}/s$, and which is therefore directly comparable with Run 9002 (Fig.5.47) of which the transient lift response is also shown. Clearly, the venture is a success, with C_{L_a} being reduced by about 40%, though t_f appears to be a little longer for Run 9502.

Such a success is of enormous significance for the prospects of the lower-surface spoiler. Given an actuation system capable of suppressing C_{L_a}, the road is open for many ACT-related applications, as highlighted at the beginning of this section. In particular, as explained there, the lower-surface spoiler now appears especially attractive for generating positive-lift (i.e. additional lift) impulses that, issued in succession, would have the effect of increasing the mean lift. The spoiler would be extended using the multiple-rate deflection profile and retracted immediately afterwards at the fastest rate available.

A test where such a pulse is issued (Run 9504) is presented in Fig.5.50. It is shown in Fig.5.50(a) that the extension part of the pulse is identical to the profile employed in Run 9502 (Fig.5.49); added to that after a short delay, is retraction at $\dot{\delta}_{max} = 1000^{o}/s$ nominal. The lift response to this pulse (Fig.5.50(b)) is exactly as hoped: a pulse of additional lift ($\Delta C_L = 0.4$), inevitably delayed somewhat, given the rotation rates involved.

The transient pressure signals for this test (Fig.5.51(a) to (d)) show quite clearly the effect of the pulsed motion of the spoiler, i.e. a pulse-like pressure disturbance originating in the locality of the spoiler (Fig.5.50(c),

signal nos.16 and 17, immediately behind and ahead of the spoiler respectively), and being gradually transmitted around the aerofoil. Comments apply here, generally similar to those made in Sec.5.3.3 for Fig.5.43. It is important to emphasize that the way in which positive lift is generated here is not purely dynamic, i.e. it is to be contrasted with previous attempts, using an upper-surface spoiler, to develop and hold a starting vortex over a period useful in flight dynamics. This fact is illustrated by Fig.5.52, showing a test similar to Run 9504, but with an elongated delay between extension and retraction (Run 9505). Clearly, the lift pulse is widened accordingly, but there is an additional important difference. The short pulse was so short that steady-state conditions could not be established and $C_{L_{max}}$ was only about 0.9 whereas the widened pulse did allow the greater value of $C_L \doteq 1.0$ to develop. To this extent the positive-lift pulse is a dynamic phenomenon, but in general we have another "rapidly-applied static phenomenon"; the lower-surface spoiler produces long-term positive ΔC_L just as the conventional spoiler produces long-term negative ΔC_L.

Although the transient drag development was not investigated, it is known that this takes longer to settle than the transient lift, and therefore the effect of the spoiler motion in Run 9504 is not only to increase the mean lift temporarily, but also to increase the ratio L/D temporarily. Hence, if a succession of spoiler pulses were to be issued, the improvement in L/D ought to be sustainable, as suggested by Fig.5.53. This is one of several features which show promise for the lower-surface position, but considerably more testing is due before conclusive statements could be substantiated.

5.5 Dynamic Tests With Spoiler In Forward Position

Dynamic tests using the spoiler in the forward position were performed at a single nominal windspeed U = 20 m/s, giving $R_e = 5.6 \times 10^5$.

Previous research, for example by Siddalingappa and Hancock (1980c) had already shown that the lift response for a rapidly-moving forward-mounted spoiler was considerably slower than for its aft-mounted counterpart. Not surprisingly, this was found to be due to the longer distance that the spoiler-induced starting vortex had to travel before reaching the trailing edge. The present investigation, however, was mainly concerned with the transient aerodynamics of spoilers with regard to ACT applications requiring fast response, such as gust alleviation. Therefore, it was decided to defer the series of tests employing a forward spoiler until the end of the main test programme that would feature the more promising rear spoiler. In the event, late developments (multiple-step technique, Sec.5.3.2 and lift augmentation method, Sec.5.4) forced the demotion of this series of tests, so that its objective was to introduce the dynamic characteristics of the forward-mounted spoiler and enable direct comparison with the more conventional aft position.

In the remainder of this section, only the measurements from two typical dynamic tests will be presented, one each for extending and retracting spoiler. For the sake of facilitating comparison with the aft position, a similar definition of "typical test" will apply, i.e. gapped spoiler rotating at $\dot{\delta} = 1000°/s$ nominal for $\alpha = 0°$. Results from these tests are presented in Fig.5.54 to 5.59 inclusive.

Fig.5.54 shows the transient lift history for such a typical test for an extending spoiler (Run 3401), similarly configured to Run 3001 (Fig.5.6) for a rearward spoiler. It is immediately obvious that no comparison can be staged, as a totally different situation is encountered here. The response to initiation of spoiler motion is about as rapid as for the rearward spoiler, but afterwards the transient lift development is completely different: a large "adverse-lift" peak develops relatively slowly, followed by a long settling process to a final apparently steady lift value that is slightly higher than the pre-deployment steady value. This behaviour can only be explained in terms of

a stronger starting vortex than for a rearward spoiler, that causes greater C_{L_a}, and a separation bubble following the vortex, this eventually reattaching on the aerofoil surface. This reattachment would then account for the final lift increase, as it would effectively introduce a camber effect.

Fig.5.55(a) to (d), showing the transient pressure histories for Run 3401, confirms these views. Fig.5.55(a) shows large suctions developing behind the spoiler, now hinging at x/c = 0.13, indicating the formation of a strong vortex (compare this with pressure signals for Run 3002, Fig.5.7(b)). However, this vortex loses its strength as it is convected downstream, having little impact on local pressures by the time it reaches the trailing edge (Fig.5.55(b)). Consequently, its effect over the lower surface is barely detectable (Fig.5.55(c) and (d)). The final mean levels for the signals behind the spoiler suggest the presence of a separation bubble (also see Fig.5.56), whilst the fluctuation levels suggest a long process of reattachment that explains the apparently long lift development times.

Fig.5.56 shows the instantaneous pressure distributions for Run 3401. No additional information is presented here, but rather a different viewpoint, and no further comments are due.

Now, Fig.5.57 shows the transient lift history for a typical test for a retracting spoiler (Run 3451), similarly-configured to Run 3051 (Fig.5.25) for a rearward spoiler. Again there is no correlation between the two responses, but this time there appears to be no obvious alternative explanation for the very large negative lift peak recorded before the final lift steady state is reached, this occurring in a short time when compared with the extending spoiler.

Fig.5.58(a) to (d) shows the transient pressure signals for Run 3451. Examination of the pressure signals as a whole, and particularly downstream of the spoiler, now

helps explain the odd transient behaviour shown above: the signals downstream of the spoiler all react very quickly following the initiation of motion of the spoiler, showing sharp compressions i.e. reflecting the very rapid convection of the bubble towards the trailing edge (almost at main stream speed). Then it appears that the large negative lift peak is due to the additive effect of the near-synchronized compressions behind the spoiler, while the rapid convection of the bubble would explain the relatively fast settling time. The spoiler is simply squeezing the air out behind it.

Fig.5.59 shows the instantaneous pressure distributions for Run 3451. Again, there is no additional information here, but the rapid convection of the separation bubble (Fig. 5.59(a)) can be seen rather more clearly here (e.g. observe the movement of the highest suction peak).

Overall, it has been shown here that, mainly as a result of reattachment, the transient characteristics at the forward spoiler are far removed from those for the rear-ward spoiler. Additionally, this spoiler would be associated with slow lift development due to increased convection time for this starting vortex, but also with more pronounced transient features, due to the strength of this vortex. As such, it would be worth investigating its potential as a lift-augmenting device. In any case, this spoiler position deserves to be treated rigorously in a separate investigation.

CHAPTER 6

CONCLUSIONS AND RECOMMENDATIONS

6.1 Conclusions

The main conclusions to be drawn from the present investigation that may contribute to the current knowledge of the transient aerodynamics of spoilers or even, perhaps, influence their application as active controls, can be itemised thus:

(1) The dynamic characteristics of a gapped and perforated spoiler are superior to those of a spoiler that is gapped but not perforated, (faster onset of lift change from initial steady state, also faster attainment of the final steady state, and smaller adverse lift). The latter, however, shows superior dynamic characteristics to a spoiler that is also ungapped (faster lift response as requested and smaller adverse lift). Nevertheless, all three configurations show similar transient trends.

(2) The angle of incidence can influence the <u>magnitude</u> of transient effects (the adverse lift is reduced at higher angles of incidence) but not the <u>timing</u> (initial lift response, time to adverse lift and final lift remain unchanged).

(3) The transient lift response at low speeds appears to be a unique function of the aerodynamic time parameter $\frac{UT}{c}$. Good agreement with previous measurements at speeds up to high subsonic indicates independence from Reynolds number, too.

(4) The adverse lift, in particular, appears to be a unique function of the aerodynamic <u>rate</u> parameter $\frac{U}{\delta c}$.

(5) Using the above observation, a technique has been devised, employing a variable-rate deflection profile, which can suppress the adverse lift. This has been demonstrated with success, and shown to be independent of spoiler configuration, spoiler position, and angle of incidence.

The application of this technique, however, assumes an actuation system capable of delivering higher rotation rates than would normally be required.

(6) Employing the same principle, it has been shown that the adverse lift can be increased, with possible implications for generation of dynamic lift. Similarly, it was shown that the initial lift response for a retracting spoiler can be speeded up.

(7) The potential of the lower-surface spoiler as an active control has been demonstrated, this perhaps complementing the upper-surface spoiler for gust alleviation for example.

(8) A method has been shown, whereby a lower-surface spoiler, undergoing a "tailored" pulsed motion, can provoke pulses of additional lift to increase the mean lift value, and possibly even increase the mean L/D ratio.

(9) Finally, the presently untapped potential of the forward spoiler, for example for generation of dynamic lift, has been pointed out.

6.2 Recommendations for Further Work

The present study is generally considered to have achieved its original objectives. Almost inevitably however, a variety of new topics of interest arose and shortcomings of the experiment became exposed in the course of the investigation. While it was possible to modify the original programme in order to satisfy some of these points, others have been ignored, as dictated by the available time or inherent limitations of the experiment or both. These are listed here as recommendations for future work.

(1) Measurements in the wake behind the model, to help establish the development of transient drag. Without this, an incomplete, and sometimes misleading, picture of transient characteristics can be obtained e.g. generation

of dynamic lift may well be accompanied by an equivalent increase in drag.

(2) A detailed investigation of the dynamic characteristics of a spoiler mounted nearer the leading edge. Such a spoiler, though possibly undesirable for gust alleviation for example (due to delayed lift response), may well prove promising in other areas e.g. augmentation of transient lift.

(3) Final endorsement of the suggested independence of transient measurements from the type of wind tunnel (i.e. open-, closed-, or slotted-walled etc.) used to obtain them. For example, an open-section tunnel might be enclosed or have slotted walls fitted and measurements repeated and compared.

(4) The "lip" of the collector of an open-section tunnel such as the one used here might be extended outwards, or the lower side of the section partly enclosed, to minimise lift "spillage" behind the model and associated errors in the measurements.

In addition, although deliberately omitted from this study on the grounds of complexities in data acquisition and handling, it would be extremely useful if three-dimensional effects were investigated, such as spoiler-end effects and sweep angle. In particular, the latter might seriously affect spoiler effectiveness.

APPENDIX A

Wind Tunnel Interference Effects

Interference in the wind tunnel could be due to a number of factors, such as, disturbances from model supports and other gear within the jet, airstream irregularities caused by non-uniformity, unsteadiness or turbulence, and due to the model itself. Only the last factor will be discussed here, as it is believed to have been the most influential and easiest to quantify. The methods of Gardner et al (1966) have been used for all correction evaluations.

Steady model interference resulted from two distinct sources: (i) blockage i.e. due to body (solid) volume and wake volume, and (ii) lift interference i.e. associated with circulation around the model.

Blockage effects were very small for the particular tunnel/model combination. Solid blockage contributed an error to measured C_L ranging from negligible at zero incidence to less than +1% at high incidence, and even smaller corrections to stream quantities. Wake blockage, too, had negligible effect. (Note that a positive percentage quoted here means that the measured C_L must be corrected by applying a positive increment, in order to approach the "correct" value).

Lift interference, though by definition negligible at zero incidence, became considerable at high incidence. Corrections to high values of both C_L and α were calculated as +6% and -18% respectively. For example, the peak C_L shown in Fig. 5.1 to be 0.61 at an incidence of 18° ought really to be given as 0.65 existing at an incidence of about 15°. These calculations, however, ignored any effect of a vertical displacement of the jet at the collector ("spillage" effect) due to lift developed. There is considerable uncertainty with regard to this condition and its mathematical equivalent, but it was

estimated that, at (uncorrected) $\alpha > 11°$, such spillage would begin to cause serious departures from the corrections quoted above based on linearised theory.

No corrections were applied to the experimental data, as it would have been possible to apply corrections to static test measurements only, but then the correlation between static and transient data would have been lost. Thus, the accuracy of measurements obtained at high positive and negative incidences was compromised in terms of absolute static values of pressure and lift but not in terms of static or indeed transient trends, which were far more important in this investigation.

Unsteady interference effects due to rapid spoiler motion were thought possible, but could not be estimated. Also, it was assumed that the finite jet boundary did not significantly affect the flow structure around the aerofoil or its development due to spoiler motion. However, the possibility of influence on flow separation and reattachment points in the neighbourhood of the spoiler cannot be ruled out.

APPENDIX B

Dynamic Response of the Pressure Sensing System

The use of long and narrow tubing to connect the pressure transducers to the surface tappings allowed the bulky transducers to be housed away from the measuring section of the aerofoil while minimising the volume of air through which the pressure changes had to be transmitted. However, this arrangement had the disadvantage, because of this transmission, that the instantaneous pressure at the face of the transducer was not a copy of that on the aerofoil surface; distortion of signal amplitude and phase was introduced by the slender pneumatic path for dynamic signals. It therefore became imperative to relate the pressures at either end of the pneumatic path by a frequency-dependent transfer function. A twin requirement was formulated for this transfer function, namely:

(a) the amplitude curve to be as close to unity as possible, in order to prevent signal amplification or attenuation, and

(b) the phase shift to be linear with frequency, over the pressure signal frequency domain.

The following simplified argument is intended to clarify the second requirement:

A sinusoidal pressure signal component, $p_1(t)$, of frequency f and amplitude $A_1(f)$, can be expressed as

$$p_1(t) = A_1(f)\sin 2\pi ft. \qquad (B.1)$$

This signal would appear at the transducer diaphragm as

$$p_2(t) = A_2(f)\sin[2\pi ft + \phi f)] \qquad (B.2)$$

in which $A_2(f)$, different from $A_1(f)$, implies an amplitude distortion and in which $\phi(f)$ is the phase distortion which we normally expect to vary in a most non-linear fashion with frequency f, changing rapidly near a resonance, for example, if damping is low. The special point to be noted here is that we derive a useful relationshop if we can arrange to have a phase shift which is near enough linear

with frequency, i.e.

$$\phi(f) = 2\pi fK \qquad (B.3)$$

where, having included the 2π for later convenience, we must determine a value for the factor K which is conveniently called a time-constant. Then B.2 becomes

$$p_2(t) = A_2(f)\sin 2\pi f(t + K) \qquad (B.4)$$

now giving the same sinusoidal variation as the original signal, but with a constant time lag K, since in fact K<0. Clearly this time lag is itself independent of frequency so for every sinusoidal component of a pressure signal the delay is constant.

Further if we can also satisfy the first requirement above, namely that $A_2(f) = A_1(f)$, then the pressure at the transducer face becomes

$$p_2(t) = A_1(f)\sin 2\pi f(t + K). \qquad (B.5)$$

Now comparing (B.5) with (B.1), it can be seen that the new signal is simply a delayed version of the original, i.e. the transducer measures the pressure applied at the tube inlet, but after a constant delay of K seconds. The value of K can be determined from the phase response curve, using Equ. B.3, and be used to adjust the time-base prior to analysis of the recorded pressures, thus giving the true pressures that existed at the tappings.

As will be shown later, in the simplest pneumatic path configuration, i.e. a long narrow tube connecting tapping to transducer, the frequency response curve developed classical resonance characteristics, showing considerably amplified gain and associated non-linear change of phase lag in the region of the resonance peak. To alleviate this problem, a form of damping was introduced into this arrangement, in the shape of restriction devices (hence-forth called restrictors), inserted somewhere along the length of the connecting tubes; these were short lengths (about 26 mm) of metal tubing of unusually small internal diameter (0.305 mm). Correctly used, they had the effect of suppressing resonance peaks and extending the frequency range over which a unity amplitude and linear phase lag

transfer function was approximately attained. This method is now widely used, eg. by Cook at the U.K. Building Research Establishment, and Lawson of this Department; it was Lawson's experience with restrictors that provided confidence in the technique.

The theoretical analysis of Bergh and Tijdeman (1965), was used to predict the frequency response of a pressure sensing system. This was achieved by solving the fundamental flow equations governing the propagation of pressure waves in cylindrical tubes, viz, the Navier-Stokes equations, the equation of continuity, the equation of state for an ideal gas, and the energy equation. The following simplifying assumptions were made:

- the pressure disturbances are sinusoidal and small,
- the internal radius of the tube is small in comparison with its length, so that end effects are negligible, and
- laminar flow occurs throughout.

Further, the following boundary conditions were specified:

- zero radial and tangential velocity components at the tube wall and the wall assumed rigid,
- zero radial velocity at the tube centreline due to the axisymmetry of the problem, and
- zero perturbation temperature at the tube wall, assuming that the heat conductivity of the wall is large in comparison with that of the fluid.

Manipulation of the flow equations, simplified by these assumptions and conditions, yield an equation for the dynamic response of a set of N slender circular tubes, in series, interspersed with N narrow cylindrical volumes, as illustrated in Fig.B.1; the following general recursion formula relates the pressure perturbation in successive nodal volumes by the appropriate transfer function of the tubing between them:

$$\frac{P_j}{P_{j-1}} = \left[\cosh(\phi_j L_j) + \frac{V_{vj}}{V_j} \left(\sigma_j + \frac{1}{K_j} \right) n_j \phi_j L_j \sinh(\phi_j L_j) + \right.$$

$$\left. + \left(\frac{V_{j+1}}{V_j} \frac{L_j}{L_{j+1}} \frac{\phi_{j+1}}{\phi_j} \frac{J_0(\alpha_j)}{J_0(\alpha_{j+1})} \frac{J_2(\alpha_{j+1})}{J_2(\alpha_j)} \frac{\sinh(\phi_j L_j)}{\sinh(\phi_{j+1} L_{j+1})} \right) x \right.$$

$$\left. x \left(\cosh(\phi_{j+1} L_{j+1}) - \frac{P_{j+1}}{P_j} \right) \right]^{-1} \qquad \text{(B.6)}$$

where,

$$\phi_j = \frac{\omega}{a_o} \left[\frac{J_0(\alpha_j)}{J_2(\alpha_j)} \frac{\gamma}{n_j} \right]^{\frac{1}{2}} \qquad \text{(B.7)}$$

$$\alpha_j = i^{3/2} \left[\frac{\omega R_j^2}{\mu} \rho_s \right]^{\frac{1}{2}} \qquad \text{(B.8)}$$

and,

$$n_j = \left[1 + \left(\frac{\gamma - 1}{\gamma} \right) \frac{J_2(\alpha_j \sqrt{P_r})}{J_0(\alpha_j \sqrt{P_r})} \right]^{-1} \qquad \text{(B.9)}$$

Starting from the last tube element in the series (where p_{j+1} does not exist, so the last term in Eqn. B.6 is zero), and by successively putting j = N, N-1, ..., 2, 1 in Eqn. B.6, the overall transfer function for the tube/volume series is determined; thus, each complex pressure ratio p_j/p_o is given by

$$\frac{P_j}{P_o} = \frac{P_j}{P_{j-1}} \frac{P_{j-1}}{P_{j-2}} \cdots\cdots \frac{P_2}{P_1} \frac{P_1}{P_0} . \qquad \text{(B.10)}$$

It is worth noting that a tube radius discontinuity can be accounted for by considering the appropriate tube element as two elements; then, for the first element, say j, $V_{vj} = 0$.

Experimental evidence was obtained by Bergh and Tijdeman (1965) to support their theory; also by Samuelson (1967), Irwin et al (1979) and Gumley (1981). Overall, it was concluded that the theory predicted the dynamic response of pressure sensing systems to a high degree of accuracy. However, it was found that the theory tended to over-estimate the actual pressure amplitude ratio by 1-5% at each frequency. Bergh and Tijdeman suggested cancelling this tendency by performing the analysis with an effective tube diameter 2-5% smaller than the actual diameter. Additionally Tijdeman and Bergh (1972) found that air flow <u>across</u> the entrance of a tube system (i.e. tapping) affected the overall dynamic response, increasing system damping; they thereby introduced a modification to their recursive formula (Eqn.B.6) for the first tube element (j = 1). But Gumley (1981) expressed reservations regarding this modification, having found certain inconsistencies in the theory. Also, given that a maximum error of less than 5% for Mach no. M < 0.1 was predicted for a restrictor-optimised tube system, it was decided to ignore this development.

<u>A computer program</u>, employing the analytical equations as outlined above, was written to help design a tube-restrictor pressure measuring system. Only one or two systems needed to be designed, but, in view of this program's potential usefulness as a research tool, the program was developed to cater for a range of tube systems. The program was coded in FORTRAN 66 and run on a multi-user minicomputer (GEC4090); it used a line printer for hardcopy numerical output and a drum plotter for graphical records. The following facilities were available to the program operator:

- Flexible parameter input, including:
  - (i) frequency range (first, last and interval),
  - (ii) ambient pressure and temperature, with default values available,

(iii) length, diameter and, if applicable, end volume of each element in the tube system, including tapping, restrictor, and transducer connections.

Any of these input sections could be retained between program runs for saving input time.

- Choice of either calculating the dynamic response of a specific tube system geometry, or having the computer design an optimal system (a restrictor, as given by the program operator, was consecutively placed at each of 100 equispaced positions along the main tubing; the "best" position was suggested and the corresponding system response displayed; selection was based on the smallest maximum deviation of amplitude transfer function from unity over the specified frequency range).
- At the end of calculations, selection from one or more of the following options:
  - (i) listing the output data on VDU,
  - (ii) storing the input and output data in a data file,
  - (iii) plotting the calculated amplitude and phase frequency-response on graphics VDU or drum plotter (the graphical format will be presented later),
  - (iv) trying a different input configuration,
  - (v) leaving the program.

The integrity of program calculations was checked by inputting tube systems of known transfer function, given in the previously mentioned publications; duplication of response was achieved invariably. With confidence in the program established, attention was turned to the tube systems used in the present investigation; of these, the longest is shown schematically in Fig. B.2 (a). (N.B. effective tube diameters are shown, slightly smaller than actual diameters, in keeping with the recommendation by Tijdeman and Bergh). The calculated response of this system, presented as Fig. B.3, is typical of such slender pneumatic paths; it can be deduced from the amplitude transfer function that this arrangement is unsuitable for measuring signals with components at 20Hz or above, if signal distortion is not to exceed 5%.

For simplicity, only one tube system was designed; this was approximately as long as the simpler system above (see Fig. B.2(b) for dimensions), and was duplicated enough times to provide connections to all available pressure tappings on the model. As Fig. B.4 shows, signal distortion was minimised for frequencies up to 100 Hz, with maximum amplitude error below 2% and frequency lag very nearly linear with frequency; conversely, there was a sharp signal attenuation at higher frequencies. Considering the straight line fitting the phase curve over 0-100 Hz, and using Eqn. B.3, the system delay K was evaluated (K = 2.78 msec), and taken into account during data processing. Effectively, the tube system then functioned as a low-pass filter in the data acquisition circuit. The sensitivity of the transfer function to likely fluctuations in ambient conditions in the laboratory was tested by varying the appropriate program input parameters; only insignificant deflections of the amplitude transfer function (up to 2%) were produced by variations of either temperature or pressure. Small variations in tube dimensions were found more likely to influence the transfer function, so care was taken when producing the tube circuits to maintain a high standard of accuracy.

Finally, after effectively introducing low-pass filters in the data acquisition system, it became necessary to show that no dominant transient signal components existed above, say, 113 Hz (i.e. beyond where the amplitude error exceeded 5%). In order to find the frequency content of pressure signals, another computer program was written, which employed an FFT (Fast Fourier Transform) algorithm to calculate signal frequency spectra, then used a plotter to provide hardcopy graphical records; this program also was coded in FORTRAN 66 and run on the GEC 4090 minicomputer. A number of typical transient pressure signals around the aerofoil were obtained, with the optimised tube circuits in place, then analysed using this program; a couple of typical signal spectra are presented as Fig. B.5 and B.6, from pressure tapping positions near, and on either side, of the spoiler and hence more likely to display high-frequency content. Although the tube system low-pass filter effect is imposed on the signals, an inverse transfer function applied to the spectrum curves would still show that no

significant pressure signal components exist above about 70 Hz. Hence, the optimised tube system was judged suitable for the ensuing experimental work.

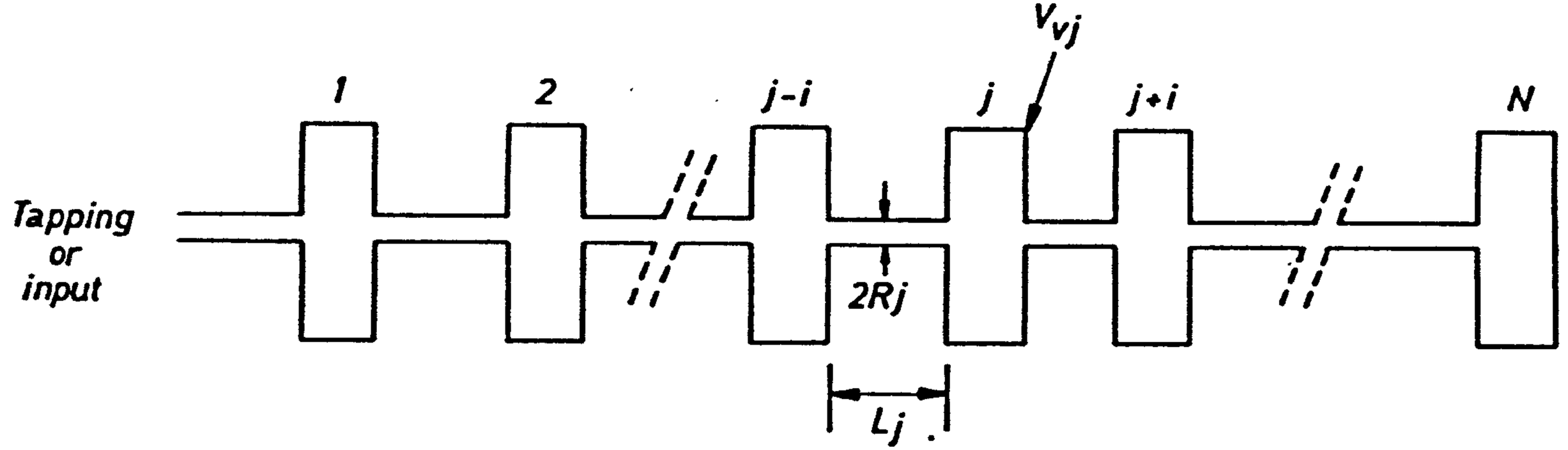

FIG. B1 SERIES CONNECTION OF TUBES AND VOLUMES

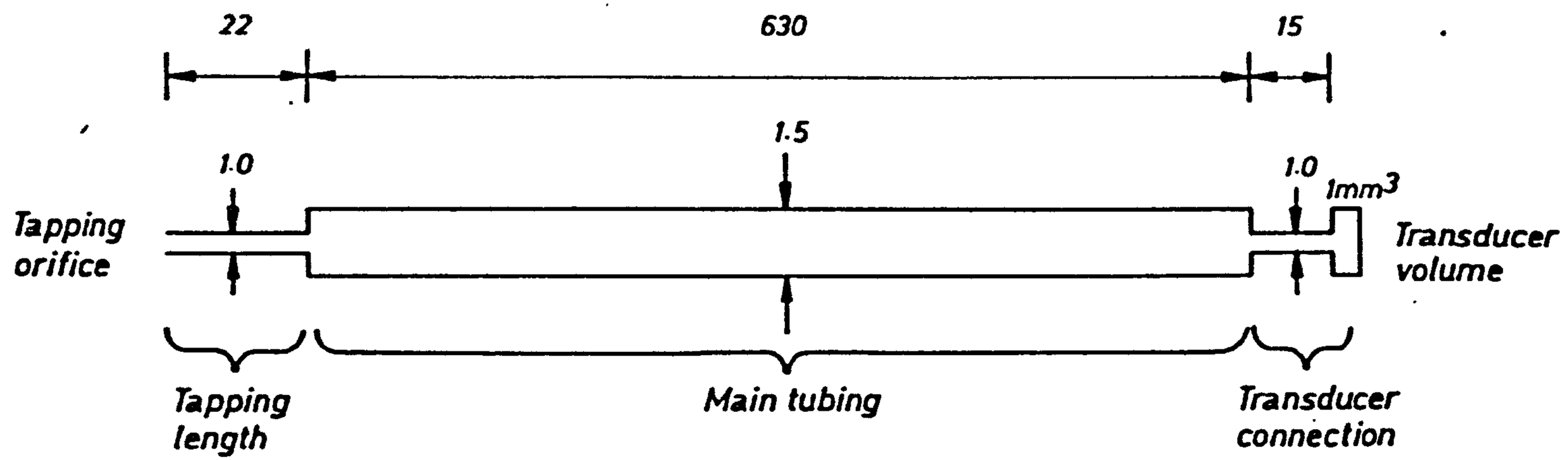

(a) Simple system

N.B Dimensions are mm unless otherwise stated

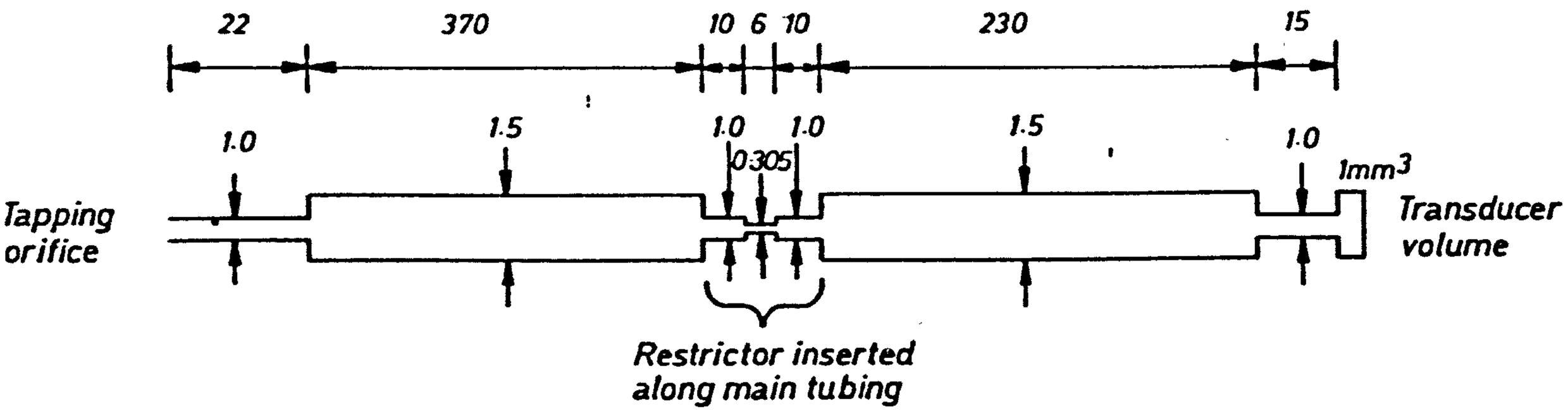

(b) Restrictor-optimised system

FIG. B.2 SCHEMATIC DIAGRAM OF TUBING CONFIGURATIONS FOR PRESSURE MEASUREMENTS

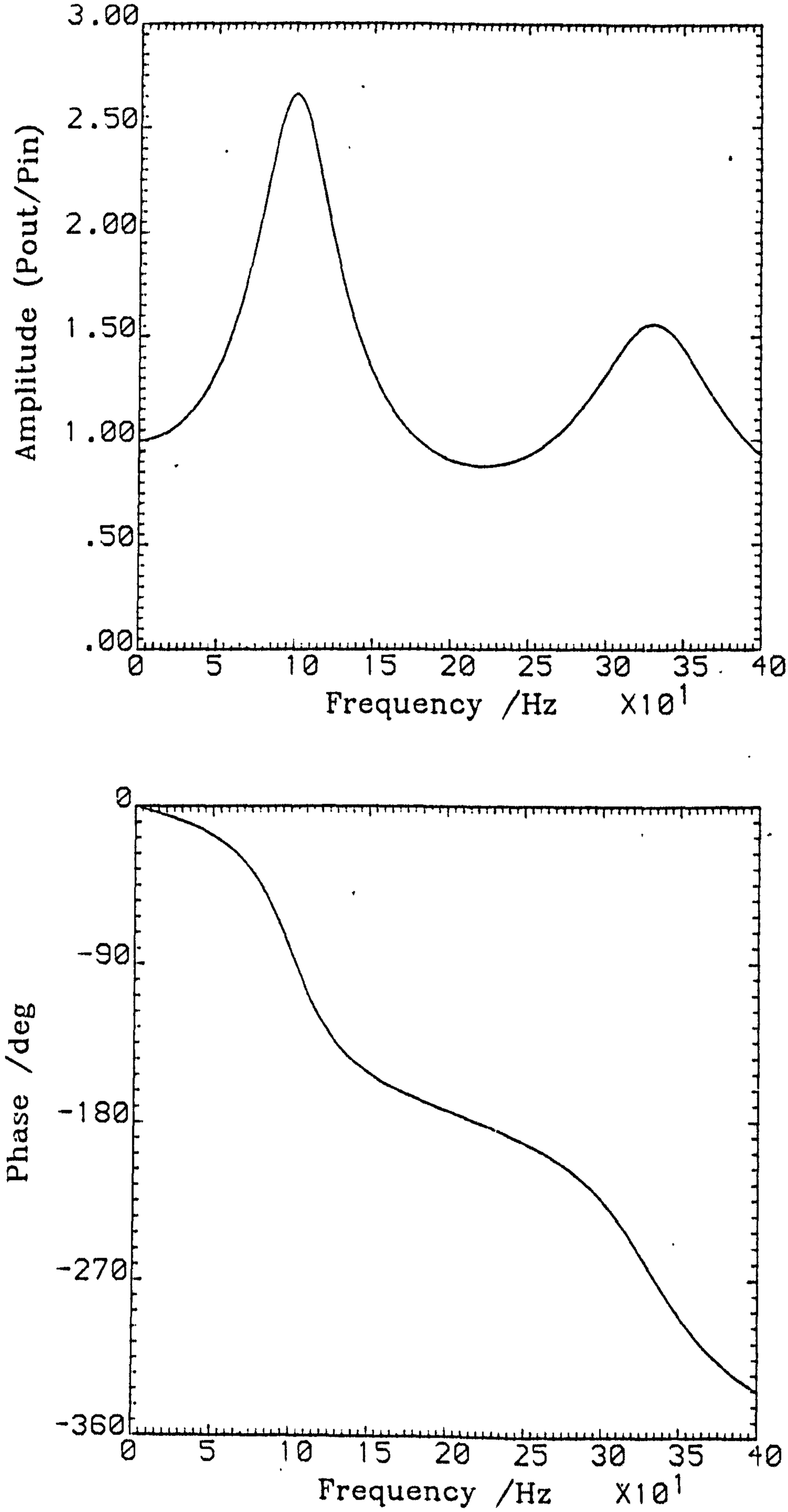

TUBING GEOMETRY
(Tapping end first)

Len (mm)	Dia (mm)	Vol (mm3)
22.0	1.000	0.0
626.0	1.500	0.0
15.0	1.000	1.0

Fig.B.3 Frequency response of pressure measuring system

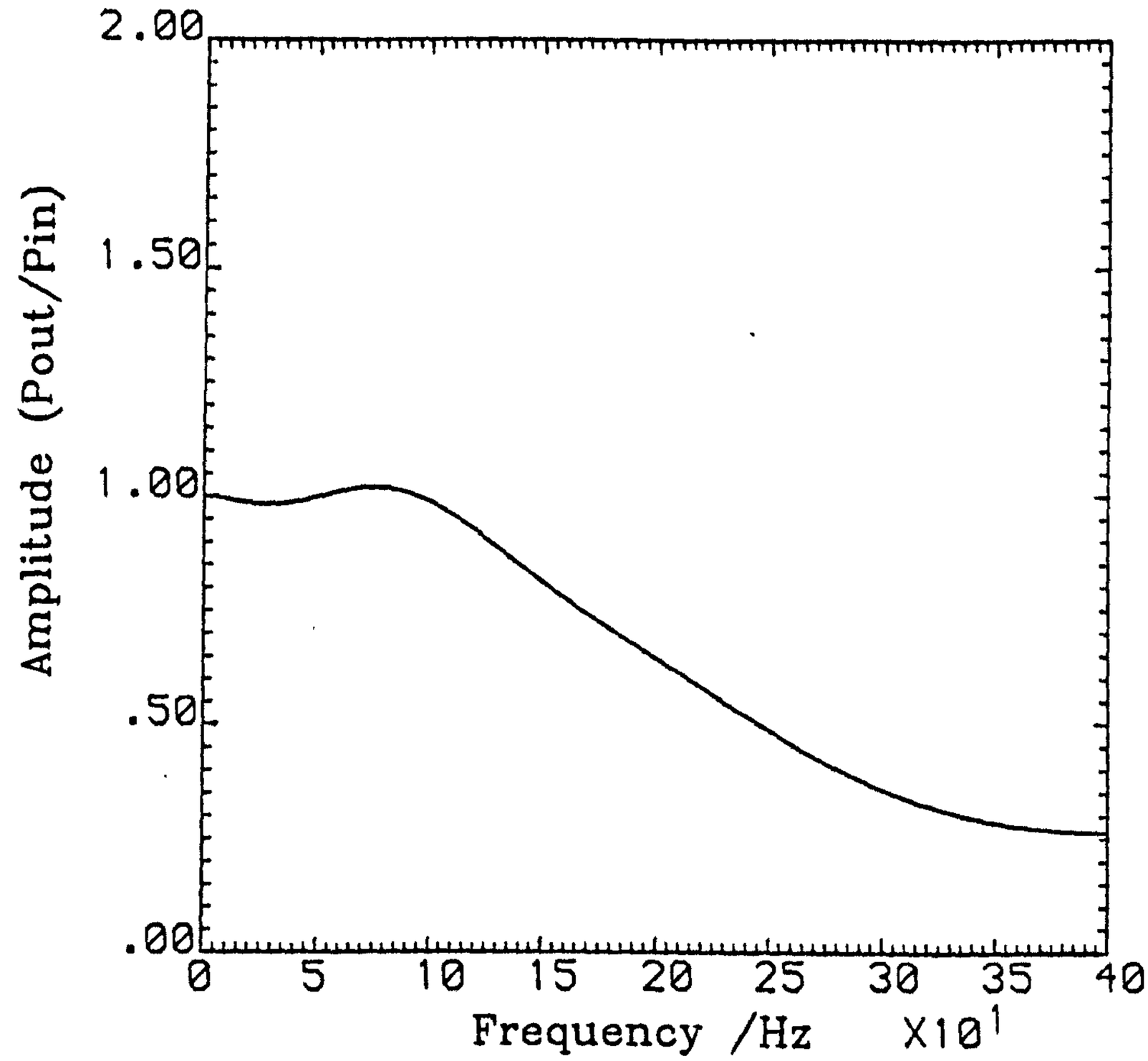

TUBING GEOMETRY

(Tapping end first)

Len (mm)	Dia (mm)	Vol (mm3)
22.0	1.000	0.0
370.0	1.500	0.0
10.0	1.000	0.0
6.0	0.305	0.0
10.0	1.000	0.0
230.0	1.500	0.0
15.0	1.000	1.0

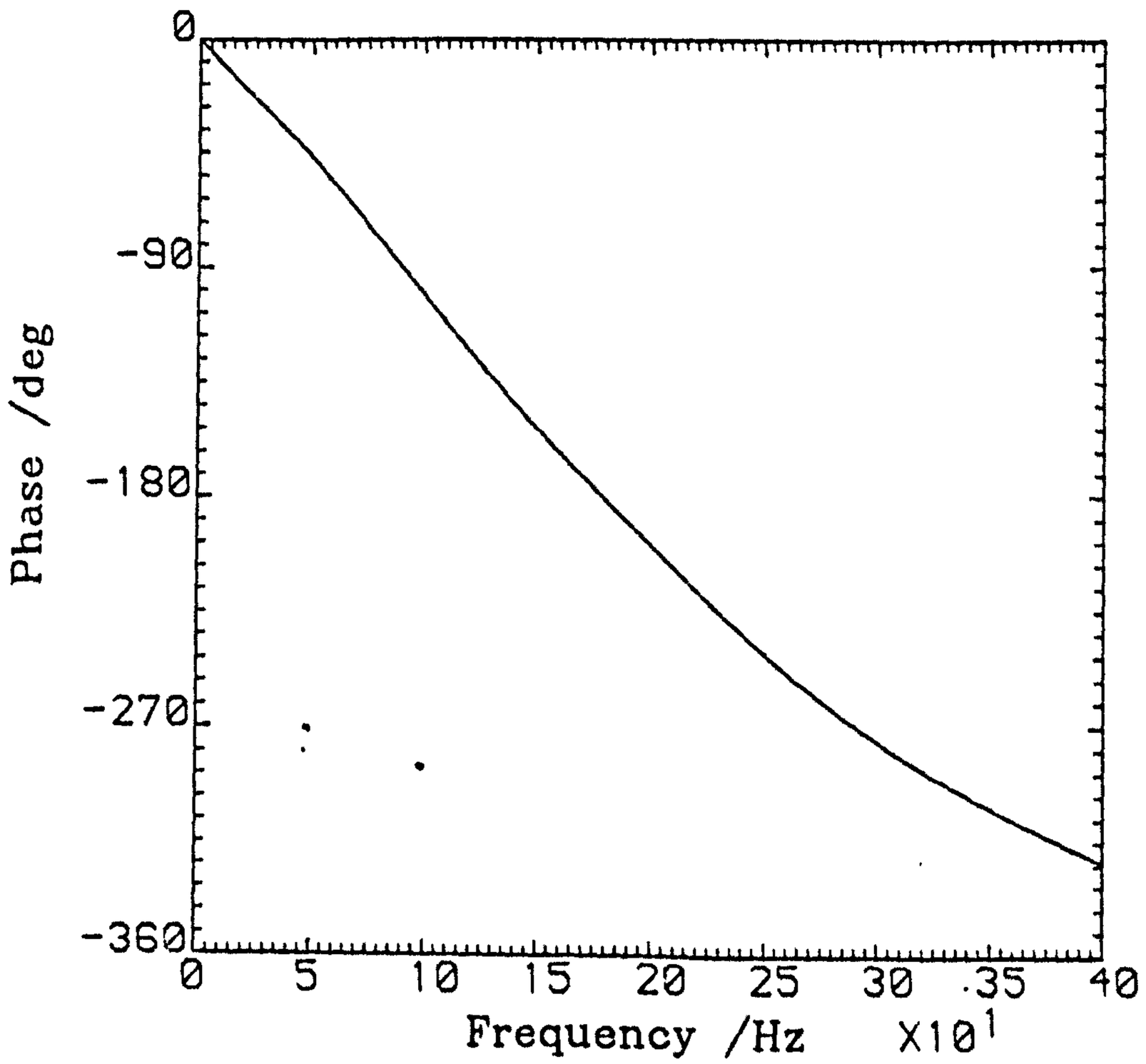

Fig. B.4 Frequency response of pressure measuring system

Origin of data analysed here:
Run 9506 (Pressure signal at x/c=0.69, u.s.)

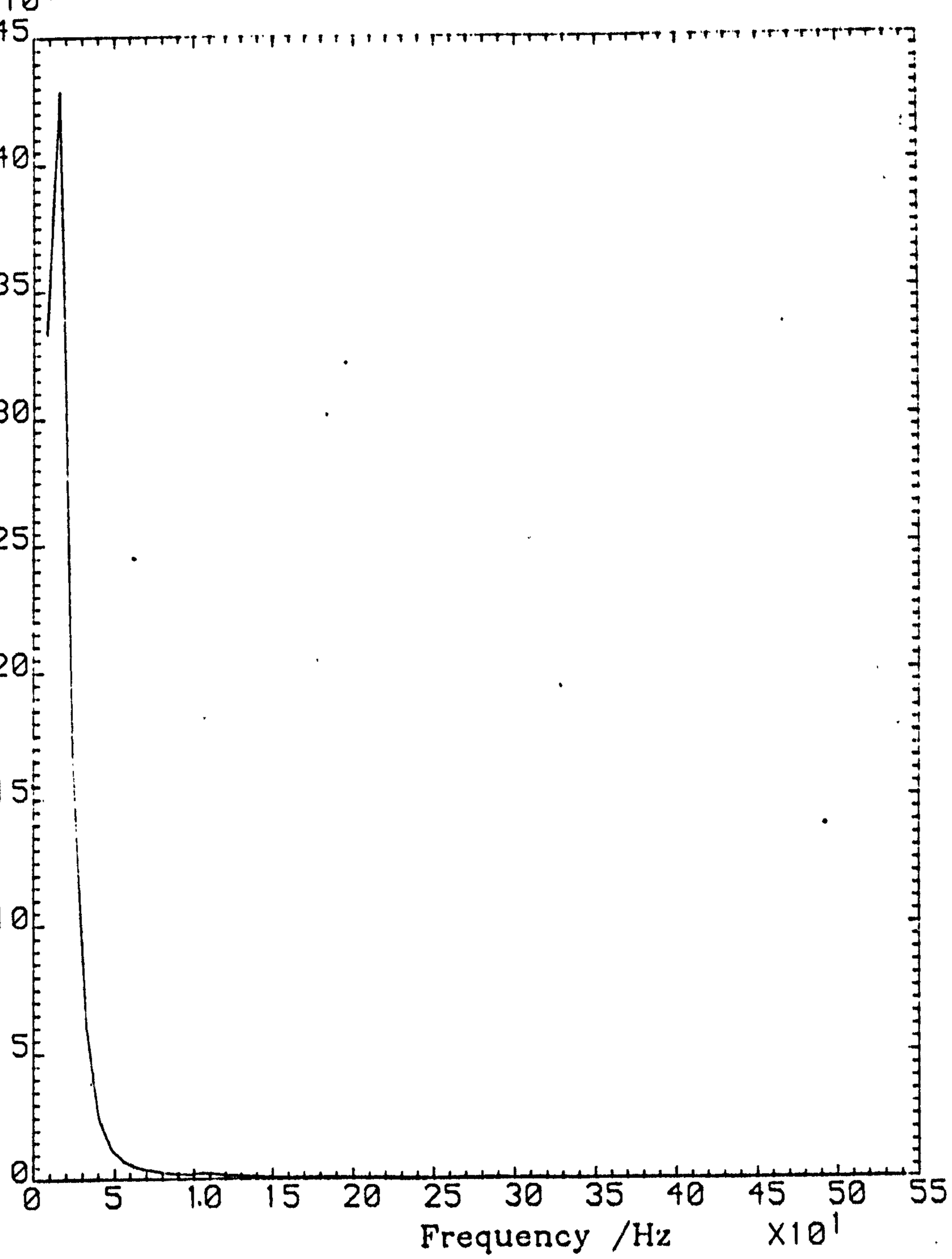

Fig. *B.5* Power spectrum analysis using FFT algorithm

Origin of data analysed here:

Run 9506 (t.e. pressure signal)

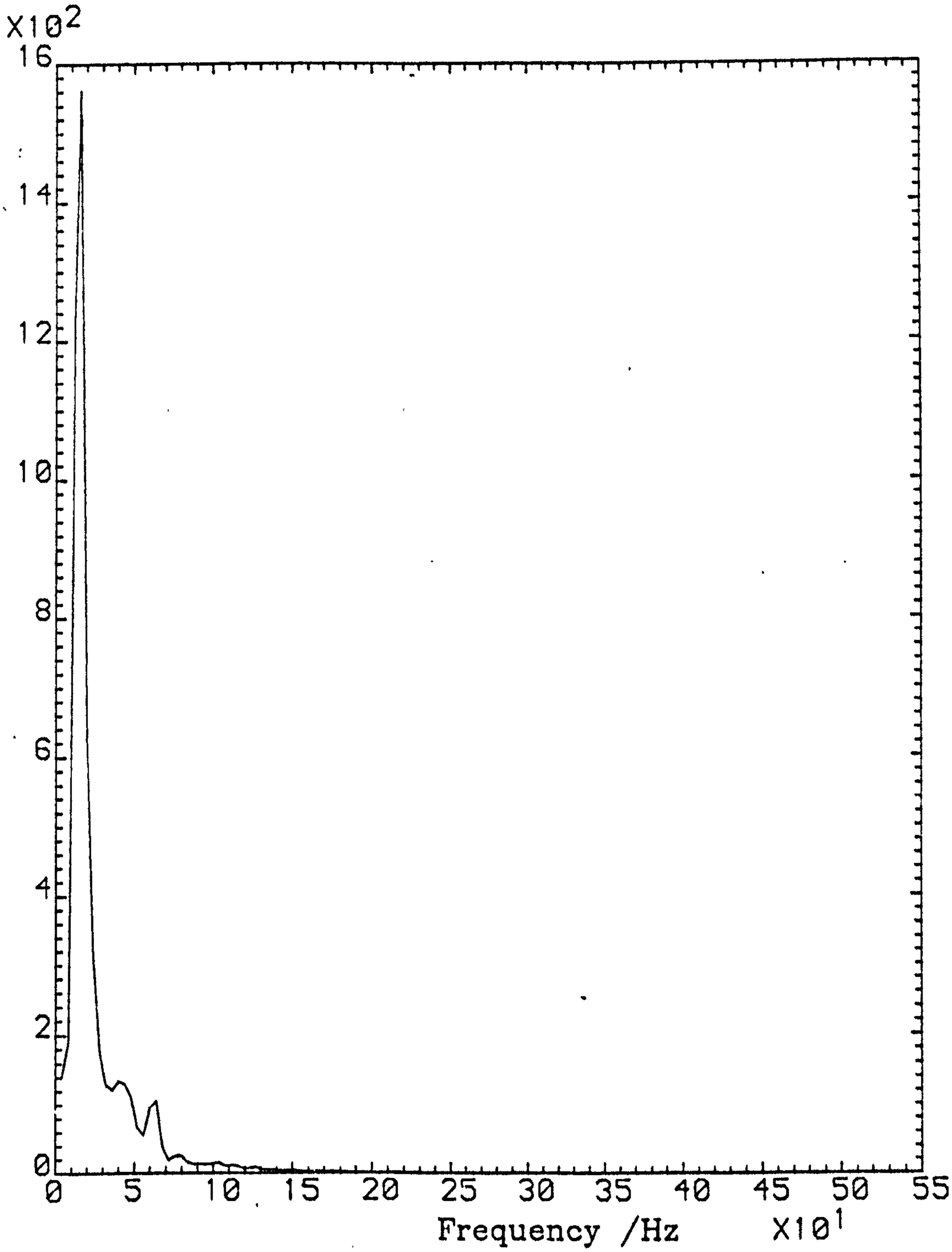

Fig. B.6 Power spectrum analysis using FFT algorithm

APPENDIX C

Spoiler Control and Data Acquisition Software

The various aspects of the spoiler control and data acquisition software are discussed here. A brief description is followed by a list of available facilities and a discussion of program structure and the function of individual program modules, finishing with a brief discussion of operating system modifications, memory occupation and concluding remarks.

The software was loaded by a single command and, while running, appeared to the user as a multi-function, menu-driven single program. In reality, it comprised a series of programs, each assigned a specific task and all chained together by a higher-level, organiser program.

The facilities available to the user included:

1. Flexible, foolproof test configuration allowing for
   - choice of 1 to 12 analogue input channels,
   - "segmentable" test sequence,
   - spoiler displacement, rotation speed and signal sampling rate being variable from one test segment to another.

2. Collection of zero-offset data from the pressure transducer signals prior to a run, plus averaging and automatic compensation for the test data that followed.

3. Real-time text display of data from all connected ADC channels.

4. Transient signal data collection.

5. Synchronised spoiler control and data acquisition.

6. Test initiation, either by operator command (always used) or trigger mechanism.

7. Detection and report of motor malfunction.

8. Graphic display of collected data (pressure or spoiler displacement traces).

9. Text display of collected data.

10. Temporary "storage" of data from several tests in RAM.

11. Storage of collected data on floppy or hard disk.

12. Option to interrupt execution of any program and return to menu in main program.

A high degree of modularity was adopted when writing this software, in order to facilitate development and, in particular, to simplify debugging. The whole programming scheme was structured as twelve modules and split into four levels; a schematic diagram illustrating this software structure is presented as Fig. C.1. The modules at the highest levels, 3 and 4, were written in Fortran 66, for speed of program development; however, it was found necessary to employ the Z80 Assembly language for the modules at the lower levels, mainly because of inadequate execution speed of the higher level language.
(N.B. The lower the "level", the more specialised was the module function).

A discussion of the function of each module now follows; reference may be made to Figs. C.2 - C.8 for the appropriate, if often considerably simplified, flowcharts.

The Main Module was not, as the name may imply, the principal or most important program, but did occupy a central organising position. Placed at the highest level, it served as an interface between the user and the rest of the

software. At the beginning of a session, having already defined the various data blocks and variables for common assess by different modules, this program displayed a menu of program facilities on the VDU; the user was thus allowed access to any module at level 3 (as shown in Fig. C.1) or the option to finish the session. When execution of a module ended, or was interrupted by the user, control reverted to the Main Module and the menu was re-displayed.

The Test Configuration Module allowed input of the parameters that determined how a test was performed. Many were assigned default values, and all were checked upon input for validity (i.e. values outside the program-specified limits were rejected). As indicated earlier, the user was allowed to split a test into different segments and vary test parameters from segment to segment. Thus, for example, complex spoiler displacement profiles could be investigated. Varying amounts of compensation, depending on spoiler rotation speed, were incorporated into the data forming the instructions to the spoiler actuation mechanism, in order to account for spoiler twist; refer to Sec. 4.3.1 for discussion of this problem.

The Signal Zero and Monitor Module covered standard pre-test procedures. A sub-menu allowed choice of three functions, namely:

- data collection for zeroing the pressure transducer signals, then later calculation and display of average values; a lower-level routine was called to do the actual reading of data,
- zeroing of the spoiler angle signal, and
- a real-time display of digital values (in "page" or overwriting mode) from all connected ADC channels; the same lower-level routine was used.

The Test Management Module would be selected in order to perform a test; as this was the most important piece of the software, it will now be described in greater detail.

With all 12 ADC channels scanned, the minimum cycle duration was 910 μsec (=1100 Hz sampling rate or 1100 pulses, 13,200 pressure values and 1100 spoiler angle values per second), and the maximum duration was about 400 msec (=2.5 Hz). Faster rates could be achieved, but only with fewer scanned channels.

Cycle rate was varied to obtain the desired motor pulse rate for example (hence, spoiler rotation rate). So, the maximum rotation rate at half-step driving mode (for the stepping motor) was

$$\frac{0.9°}{\frac{1}{2}\ \text{step}} \times \frac{1100\ \frac{1}{2}\ \text{step}}{\text{sec}} = 990°/\text{sec}$$

However, for the lowest spoiler rotation rates used it was not acceptable simply to reduce the cycle rate for all actions, because pressure signal sampling rate would thereby be reduced as well and signal aliasing could follow. The alternative procedure was to retain the high pulse rate, but to make a spoiler rotation pulse "active" only every second or third cycle. This allowed the pressure signal sampling rate to be maintained above the minimum of 400 Hz as an anti-aliasing precaution (also see Sec. 4.).

The Graphic Display Management Module and the associated lower-level routines provided a channel-by-channel graphic display of the collected test data. The two DAC's converted the data into analogue signals and continuously displayed them on a simple oscilloscope, set in the X-Y mode, to obtain a refreshed "vector graphics" display. Software "zoom-in" and "panning" facilities allowed a particular "window" of the signal to be examined. Thus, trasient pressure traces from points around the aerofoil and for the spoiler displacement profile could be visually checked on-the-spot, allowing an important preliminary data clearance or immediate rejection of the new data (also see Sec. 4.6).

The Peripheral Data Outward Module, selected after a successful test, offered choice of a text display of test

data on VDU or its filing on floppy- or hard- disk. The first option gave a scan-by-scan display of the data (overwriting) in page mode; the display could be frozen before completion, then restarted or abandoned. The filed data included all test configuration parameters and the collected data; time base and spoiler-control data were re-constructed at the processing stage to save space and transfer time. The data were stored in ASCII (American Standard Code for Information Interchange) format, as required by the data transfer program. About a dozen average datafiles could be stored on a single 5¼" floppy disk, and a total of 512 such files on the hard disk.

The Data Shift Module and Bank Switching Routines were used to transfer the test data to and from one of the three otherwise unused memory banks (due to the inability of an 8-bit microprocessor to directly address more than 64 Kbytes). It was thus possible, for example, to compare the spoiler displacement traces from several tests (an adapted Polaroid camera could photograph the oscilloscope screen), without the need to process or even store any data. The full 64 Kbytes per "storage" bank was available, except for the highest 128 bytes, taken up by the necessary transfer code.

Two modifications were made to the microcomputer operating system, CDOS. The first was to reduce its size, so that more memory space would be available for program object code and data (CDOS was necessarily resident in memory at all times); so, unnecessary portions of its code were deleted. The second consisted of implementing a multi-function "system call" to take advantage of the special "screen formatting" features of the VDU used (Televideo TVI920). A "library" of general-purpose functions was linked with the rest of the software, indirectly allowing any module to make this system-call along with some other such calls already featured in CDOS, thereby simplifying screen formatting etc.

Of the 64 Kbytes of addressable RAM, exactly 36 Kbytes were available after CDOS was loaded (discounting the 128 bytes required in high memory). The combined program object code occupied 21.4 Kbytes, and input parameters and other variables took a further 1.0 Kbyte. Therefore, 13.6 Kbytes was left for test input (ADC) and output (parallel part) data. Then 500 2-byte values were reserved for each of the 13 ADC channels and 500 1-byte values for output, i.e. these required a total of 13.2 Kbytes (in practice never filled). The small remaining space was not used.

A map of the microcomputer memory, with CDOS and all programs loaded, is shown in Fig. C9.

Although the discussed software was developed specifically for this study, an effort was made to enhance program versatility and "user-friendliness" so it could be operated by other users, in the same or closely-related experiment, or where transient signal measurements were required for comparable reasons.

FIG C.1 STRUCTURE OF SPOILER CONTROL AND DATA ACQUISITION SOFTWARE

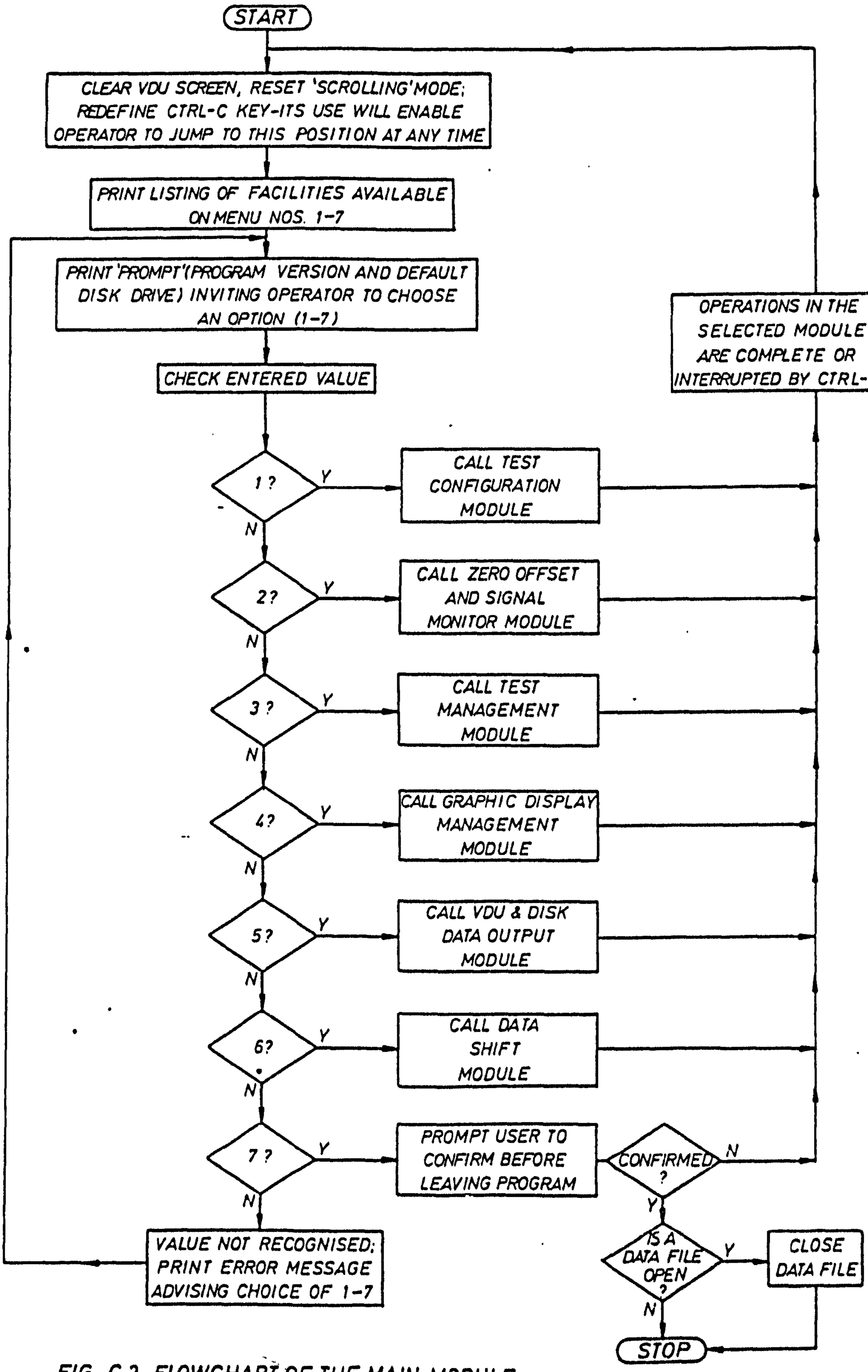

FIG. C.2 FLOWCHART OF THE MAIN MODULE

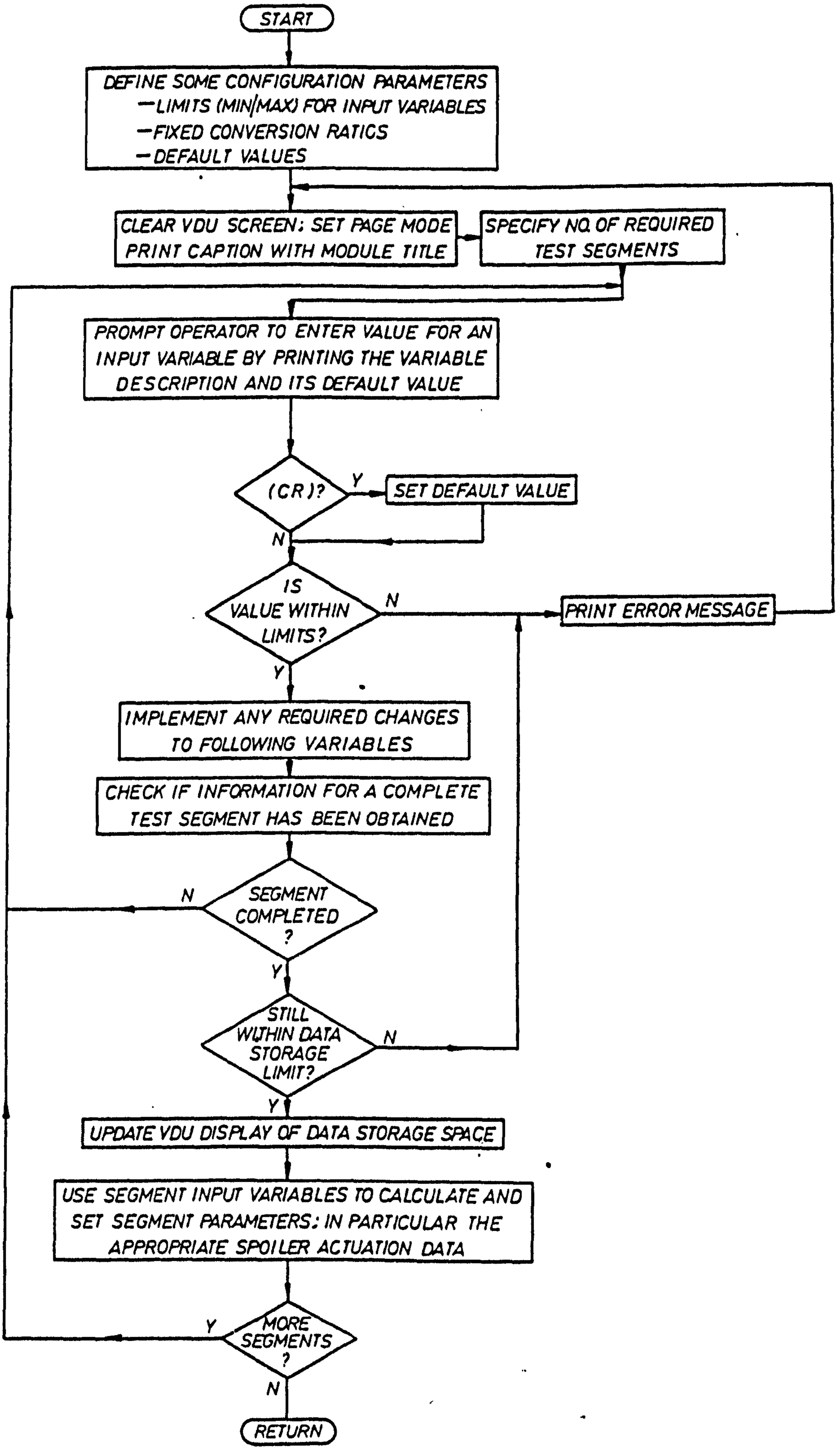

FIG C.3 FLOWCHART OF TEST CONFIGURATION MODULE

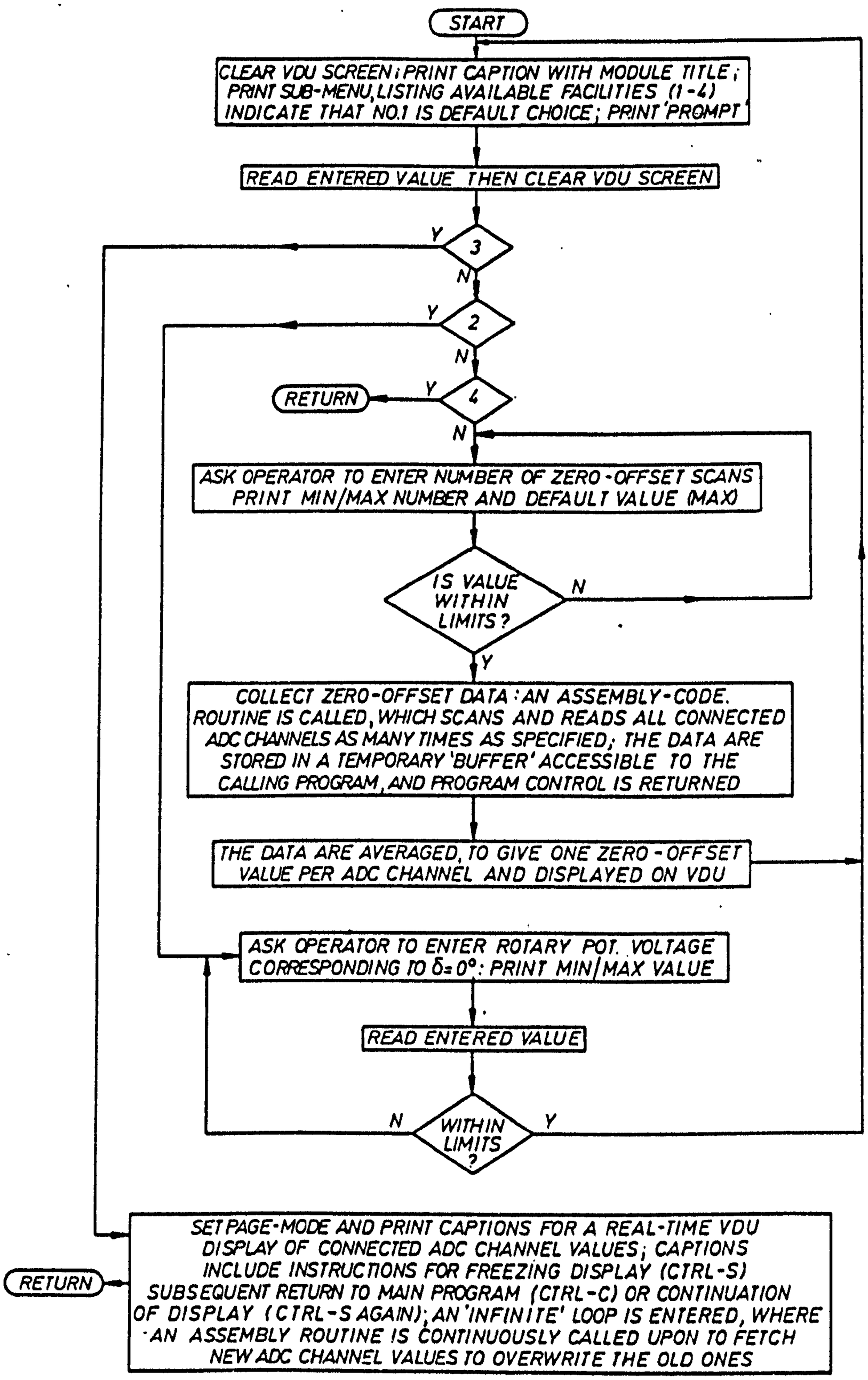

FIG. C.4 FLOWCHART OF SIGNAL ZERO AND MONITOR MODULE

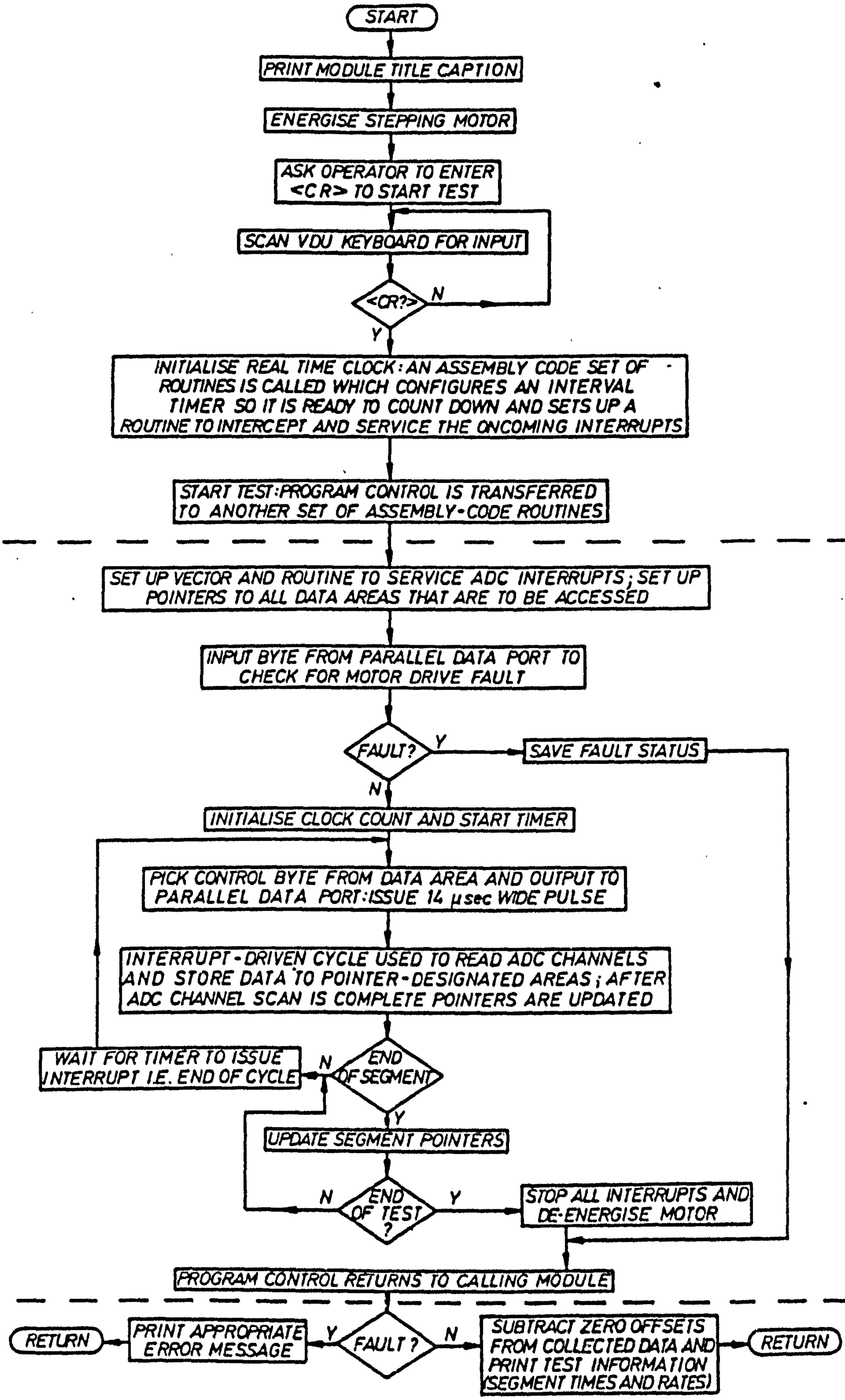

FIG. C.5 FLOWCHART OF TEST MANAGEMENT MODULE AND CALLED ROUTINES

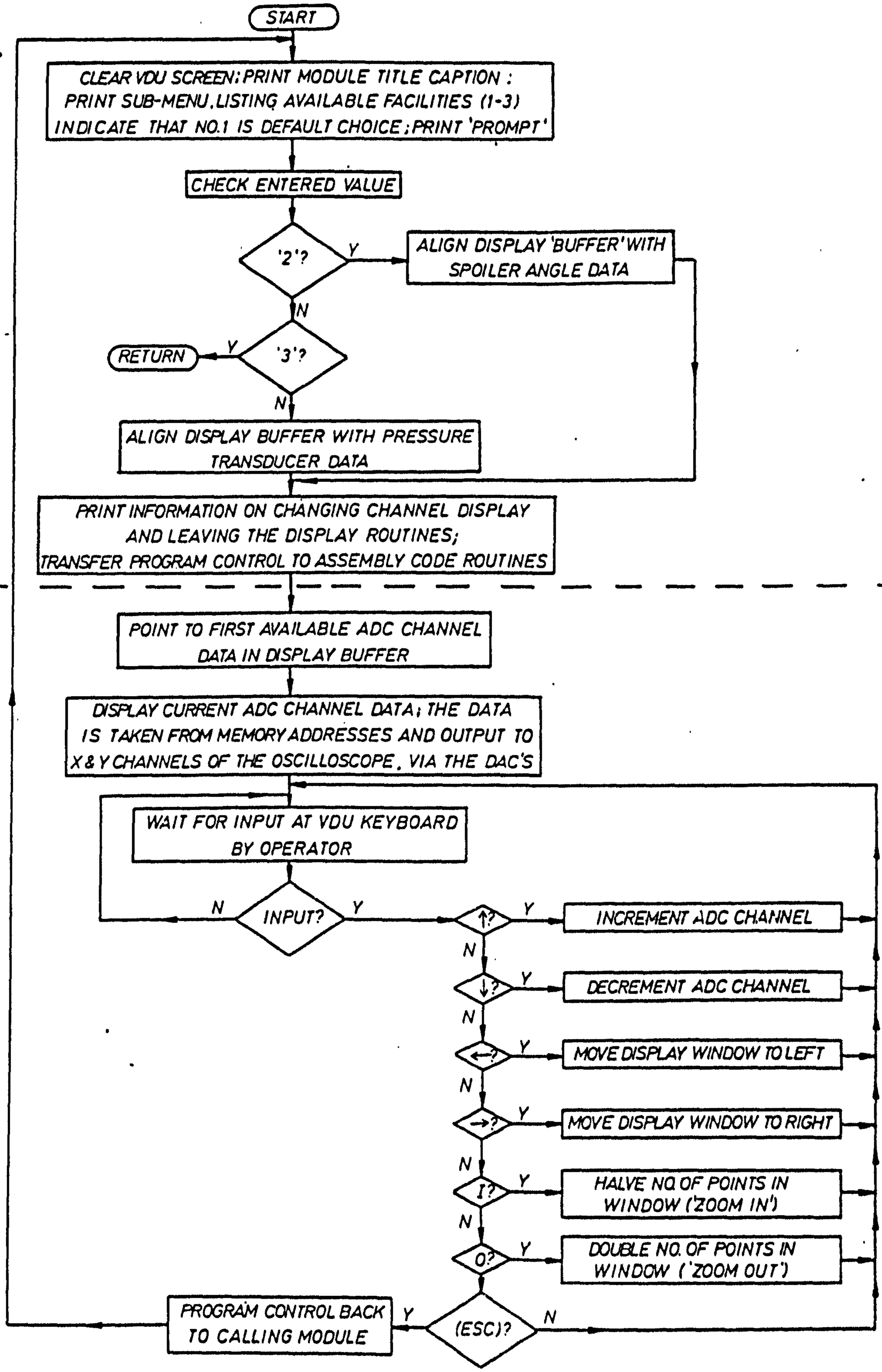

FIG. C.6 FLOWCHART OF GRAPHIC DISPLAY MANAGEMENT MODULE AND OSCILLOSCOPE GRAPHICS ROUTINES

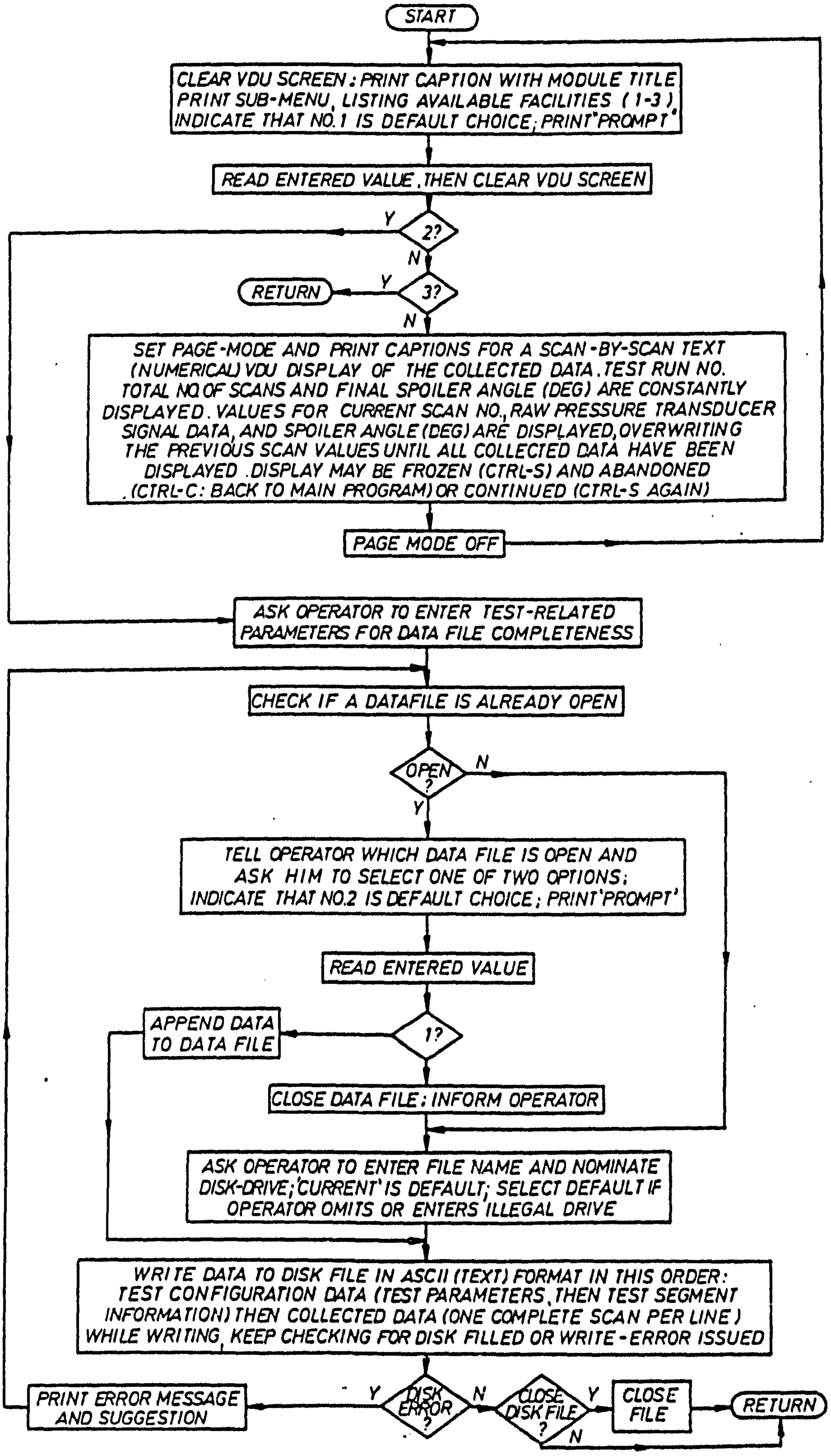

FIG.C.7 FLOWCHART OF PERIPHERAL DATA OUTPUT MODULE

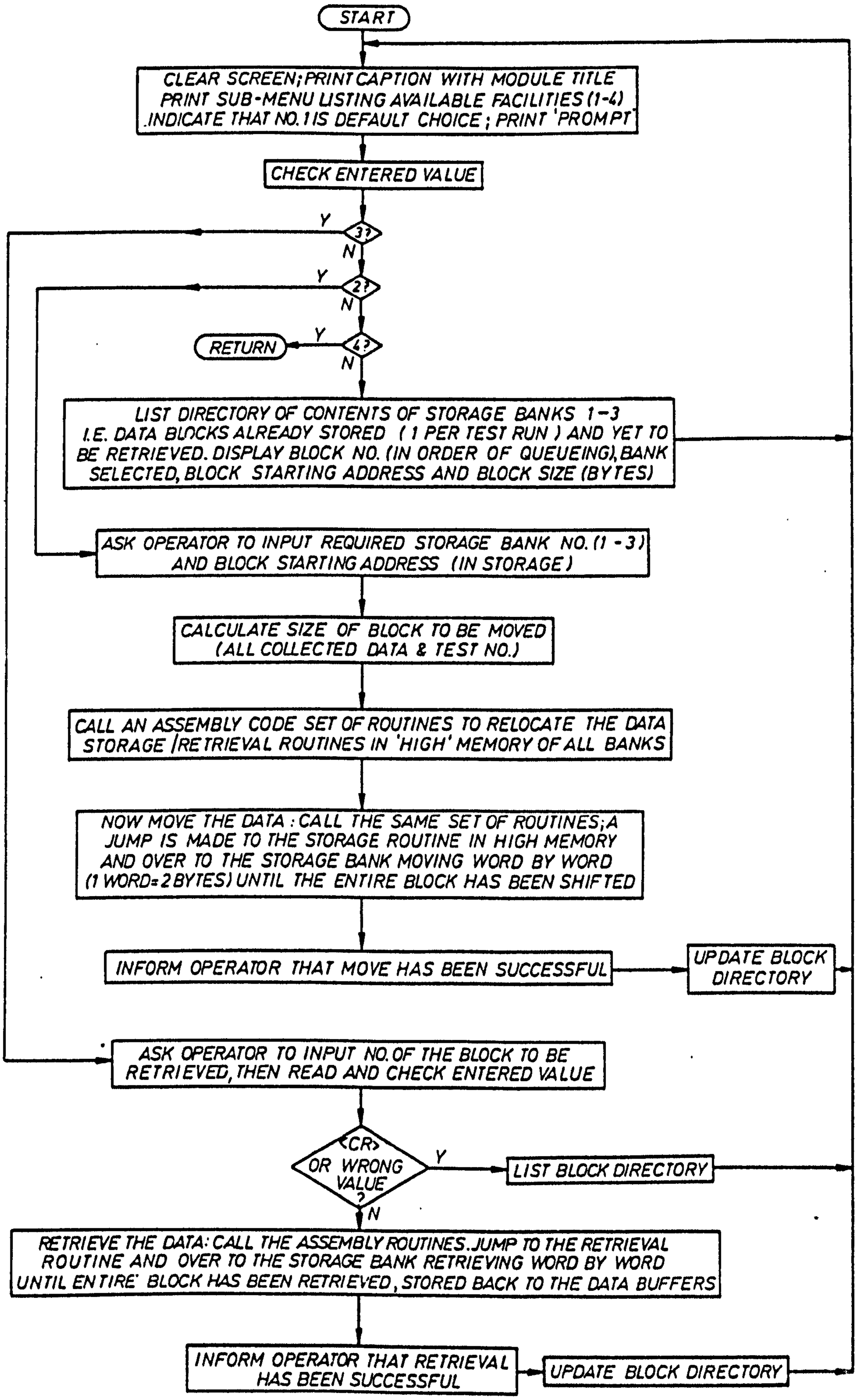

FIG. C.8 FLOWCHART OF DATA SHIFT MODULE

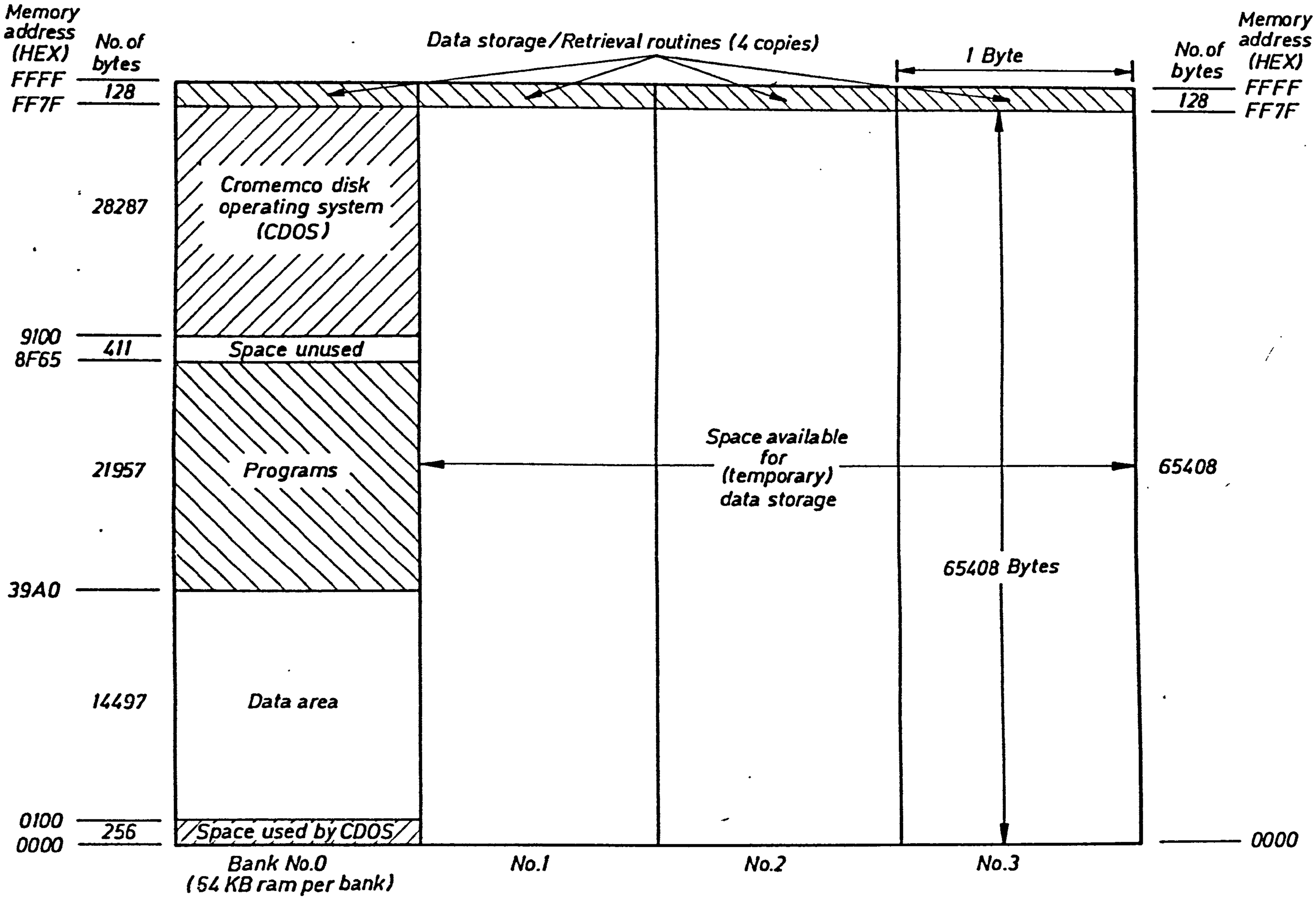

FIG.C.9 SCHEMATIC MICROCOMPUTER MEMORY MAP WHEN SPOOLER CONTROL AND DATA ACQUISITION PROGRAMS ARE LOADED

APPENDIX D

Data Processing Software

All experimental data obtained by the microcomputer-based laboratory system were processed by specially written applications software residing in the Honeywell mainframe computer; the same software supplied suitably coded information to a plotting device for producing hardcopy graphical records of the processed data.

This software was coded in FORTRAN 77 and consisted of two programs; the main program, and another effectively being a set of general-purpose graphics routines regularly called (via dynamic linkage) by the main program. Both programs used the GINO-F graphics package supported by Multics (the mainframe operating system).

During program execution, the experimental data underwent a number of sorting, checking and processing operations, and these are described next; but first a look will be taken at data-file structure.

A typical data-file contained eight blocks of data, i.e. four per run (a test consisted of a pair of runs, as explained in Sec. 4.4) as follows:

- "test-essential" configuration parameters (part of CPAR) for execution or identification;
- test segment parameters (SPAR);
- pressure transducer data (PDAT); and
- spoiler potentiometer data (SDAT).

The program would begin execution by requesting a data-file name; the file was opened and format checked. The "test-inessential" part of CPAR was then made up, partly by the program (fixed quantities e.g. pressure tapping chordwise positions) and partly by the operator (variable quantities e.g. aerofoil incidence).

The data from both runs were then read. All values in the CPAR and SPAR data block pairs were compared in order to

check various compatibilities necessary before accepting a run-pair. Upon completion, the data-file was closed and one each of CPAR and SPAR were deleted.

Next, the data in the PDAT and SDAT pairs were converted from two-byte integer format to four-byte real (floating point) format, allowing for six significant decimal places. The two PDAT data blocks were merged into a single two-dimensional array of data for ease of access; with one dimension being the number of data acquisition cycles and the other the total number of pressure signals, PDAT could now be referenced as a series of complete signal scans around the aerofoil (in terms of array "rows"), or complete signal records at a particular pressure tapping (in terms of array "columns"). The corresponding individual values in the pair of SDAT records were averaged and stored in a single array, this to be referenced to as ASDAT. A check was then carried out on spoiler profile repeatability: the ASDAT values were compared against the corresponding values in one SDAT block, and differences equivalent to 1° or greater were reported to the operator, thus allowing rejection of the run on the basis of profile differences. No further action was taken by the program on this matter.

Using SPAR, the spoiler actuation input data were then re-constructed, and transformed into a spoiler displacement signal, δ(in degrees); this will henceforth be referred to as spoiler input data (SIDAT).

Also using SPAR, the time-base for each test segment was calculated and a continuous time record (i.e. one value per data acquisition cycle) pieced together (in msec.); this record will be referred to as time data (TDAT).

Next, the collected data values in ASDAT and PDAT were transformed from ADC output format to δ (in degrees) and pressure coefficient form, Cp, respectively. Linear transformation, of the form $y = mx+c$, was used in both cases as the spoiler potentiometer and the pressure transducers showed linear response characteristics; no constant term c was involved in transforming pressure

values as those had already been "zeroed". The resulting transformed data sets will be referred to as spoiler output data SODAT) and Cp data (CPDAT).

As discussed in App. C, there was a 60μsec delay between sampling of successive pressure values in a data acquisition cycle. This delay was next accounted for, to make the pressure values in a complete cycle (i.e. one CPDAT scan) appear as if they had been collected in "parallel" i.e. simultaneously. This was achieved by linearly interpolating with respect to time, between the existing, recorded values for all ADC channels from the second to the last, in order to produce new data sets valid for sampling times which coincided with those for the first channel.

Thus, one CPDAT scan represented an apparently instantaneous chordwise pressure distribution at mid-span of the aerofoil. It was then possible to obtain, for each time, the single value for aerofoil sectional lift, C_l, by numerically integrating each CPDAT scan; the trapezium rule was used for this purpose. The resulting signal will be referred to as CLDAT.

The end of the first major program task i.e. data processing was reached. The processed data finally comprised the arrays SIDAT, SODAT, CPDAT, CLDAT, and TDAT.

At this stage, the operator was offered options to list or to store the processed data (not normally taken up), to restart or to end the program execution and finally the option introducing the other major program task i.e. presentation of the processed data in a number of graphical formats.

Only a brief description of the facilities provided by this part of the program follows.

The operator was offered any combination of the following plots:

(i) static pressure histories, one or six per A4 page (CPDAT signal records vs. TDAT),

(ii) aerofoil chordwise pressure distributions at various test stages, (selected CPDAT scans, or a single averaged scan if steady test, vs. percentage chord),

(iii) aerofoil sectional lift history (CLDAT vs. TDAT),

(iv) spoiler displacement histories (SIDAT and SODAT vs. TDAT), and

(v) combination of the above two within one A4 page.

Note that the scale of each plot and the range for plotting coordinates were automatically selected for optimum presentation, but there was an operator-override facility. There was also available a choice of plot output device (VDU graphics screen, high-resolution drum plotter, or A4-size flat-bed plotter).

A selection of the plots produced on the drum plotter are presented and discussed in Ch.5.

REFERENCES

1. Ahmed. S., Hancock, G.J. (1983)
"On The Local Flow About A Spoiler Undergoing Transient Motion at Subsonic Speeds"
QMC EP1050

2. Bergh, H., Tijdeman, H. (1965)
"Theoretical And Experimental Results For The Dynamic Response Of Pressure Measuring Systems"
Report NLR-TR F.238, NLR, The Netherlands

3. Brown, G.P., Parkinson, G.V. (1973)
"A Linearized Potential Flow Theory For Airfoils And Spoilers"
Journal of Fluid Mechanics, Vol.57,

4. Consigny, H., Gravelle, A., Molinaro, R. (1984)
"Aerodynamic Characteristics Of A Two-Dimensional Moving Spoiler In Subsonic And Transonic Flow"
Journal of Aircraft, Vol.21, Paper 9, pp.687-693

5. Davie, M.J., Davies, M.J. (1982)
"An Investigation Into The Transient Pressure Redistribution Around An Aerofoil Due To The Rotation Of A Spoiler"
B.Sc. Thesis, Department of Aeronautical Engineering, University of Bristol

6. Garner, H.C., Rogers, E.W.E., Acum, W.E.A., Maskell, E.C. (1966)
"Subsonic Wind Tunnel Wall Corrections"
AGARDOGRAPH 109, AGARD, NATO

7. Garroch, A.W. (1980)
Unpublished Private Communication

8. Gumley, S.J. (1981)
"Tubing Systems For The Measurement Of Fluctuating Pressures In Wind Engineering"
Oxford University, Engineering Laboratory Report No. 1370/81

9. Hoerner, S.F. (1975)
"Fluid Dynamic Lift"
Published by Hoerner Fluid Dynamics

10. Irwin, H.R.A.H., Cooper, K.R., Girard, R. (1979)
"Correction Of Distortion Effects Caused By Tubing Systems In Measurements Of Fluctuating Pressures"
Journal of Industrial Aerodynamics, Vol.5, pp.93-107

11. Kramer, M., Zobel, T., Erche, C.G. (1951)
"Lateral Control By Spoiler At The DVL"
NASA TM 1307

12. Le Balleur, J.C. (1980)
"Calcul des Ecoulements a Forte Interaction Visquense an Moyen de Methodes de Couplage"
Paper 1 in "Computation of Viscous-Inviscid Interactions", AGARD CP 291

13. Mabey, D.G., Welsh, B.L., Stott, G., Cripps, B.E. (1982)
"The Dynamic Characteristics Of Rapidly Moving Spoilers At Subsonic And Transonic Speeds"
R.A.E. Report TR 82109

14. Pfeiffer, N.J., Zumwalt, G.W. (1981)
"A Computational Model For Low Speed Flows Past Airfoils With Spoilers"
AIAA Paper 81-0253

15. Samuelson, R.D. (1967)
"Pneumatic Instrumentation Lines And Their Use In Measuring Rocket Nozzle Pressure"
Report No. RN-DR-0124 Nerva Progam, Contract JNP1
Aerojet - General Corporation

16. Siddalingappa, S.R., Hancock, G.J. (1979)
"Unsteady Aerodynamics Of Two-Dimensional Spoilers At Low Speeds"
Paper 21, AGARD CP 262

17. Siddalingappa, S.R., Hancock, G.J. (1980a)
"An Introduction To the Aerodynamics Of Spoilers"
Department of Aeronautical Engineering, Queen Mary College, University of London, QMC Report EP 1034

18. Siddalingappa, S.R., Hancock, G.J. (1980b)
"Some Qualitative Experiments On The Local Flow About Spoilers In Unsteady Motion At Low Speeds"
Department of Aeronautical Engineering, QMC, University of London, QMC Report EP 1035

19. Siddalingappa, S.R., Hancock, G.J. (1980c)
"Some Qualitative Experiments On The Flow About An Aerofoil Due To The Unsteady Motion Of A Two-Dimensional Spoiler"
QMC Report EP 1036

20. Tijdeman, H., Bergh, H. (1872)
"The Influence Of The Main Flow On The Transfer Function Of Tube Transducer Systems Used For Unsteady Pressure Measurements"
Report NLR MR 72023U, NLR, The Netherlands

X Tested
O Not tested

		Incidence		'Spoilered' surface		Spoiler position		Spoiler geometry		
		0°	14°	Upper	Lower	Rear	Fore	Solid	Gapped	Perf'd
Incidence	0°			X	O*	X	X	X	X	X
	14°			X	X	X	O	X	X	X
'Spoilered' surface	U	X	X			X	X	X	X	X
	L	O*	X			X	O	X	X	O
Spoiler position	R	X	X	X	X			X	X	X
	F	X	O	X	O			O	X	O
Spoiler geometry	S	X	X	X	X	X	O			
	G	X	X	X	X	X	X			
	P	X	X	X	O	X	O			

* Tested implicitly

Note : Under spoiler geometry, 'solid' means closed gap and perforations, 'gapped' means the the gap is opened, and 'perforated' means the perforations are opened too.

The spoiler with closed gap but open perforation was not investigated

TABLE 4.1 INVESTIGATED AEROFOIL-SPOILER COMBINATIONS

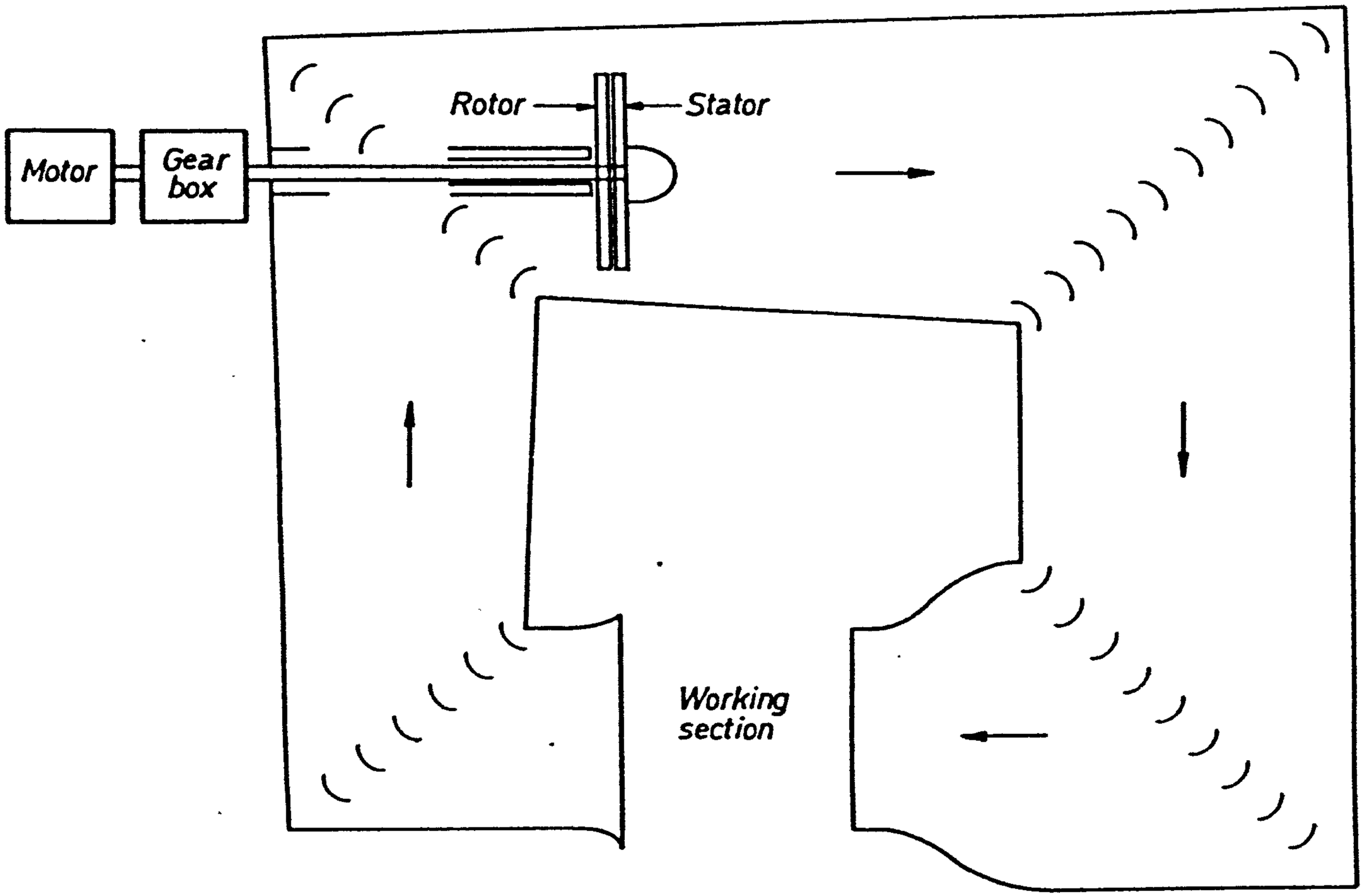

FIG. 3.1 SCHEMATIC DRAWING (PLAN VIEW) OF 3.5ft OPEN-SECTION WIND TUNNEL

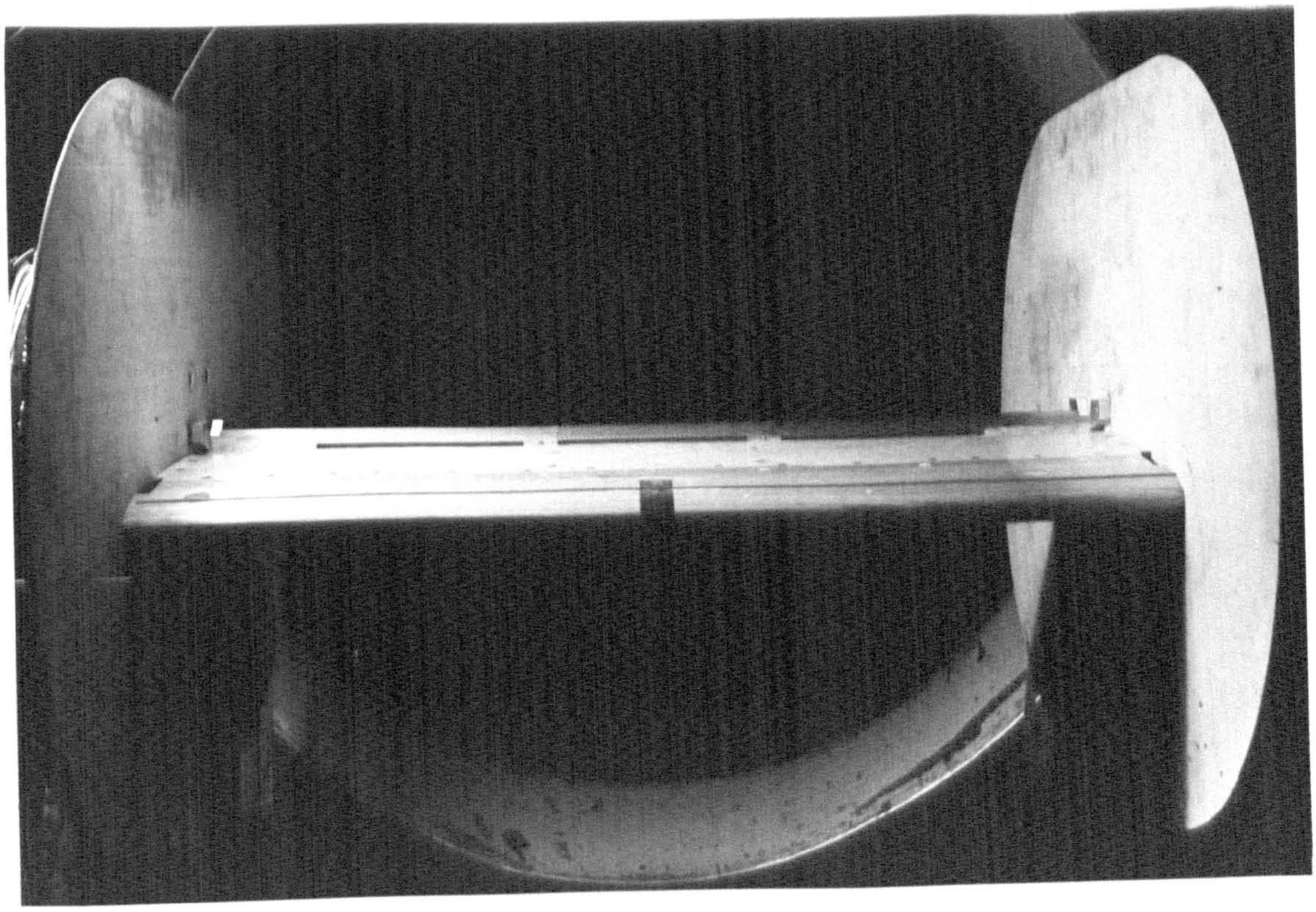

(a) Front view (Spoiler extended)

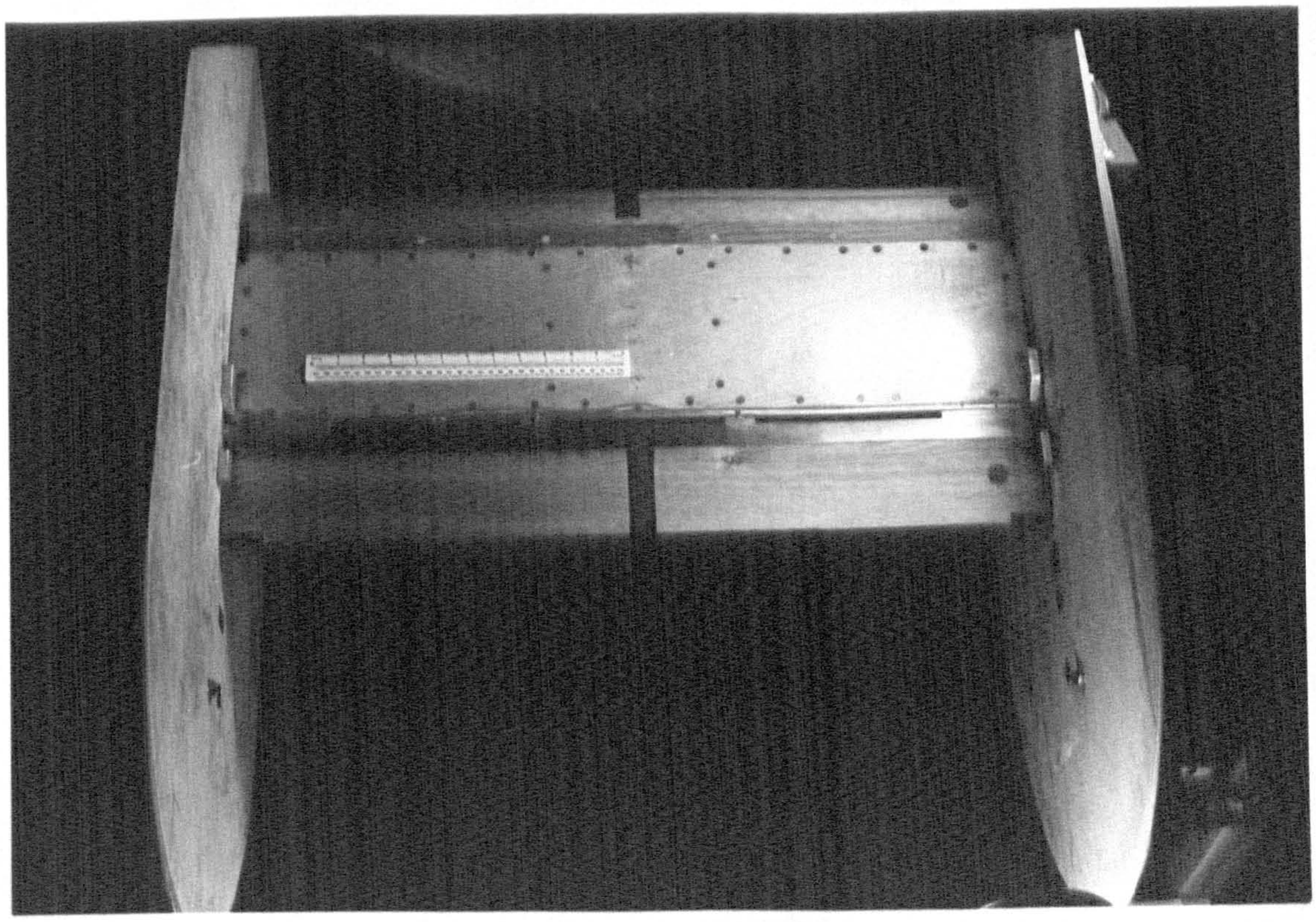

(b) Plan view (Spoiler retracted)

FIG. 3.2 MODEL IN WIND TUNNEL

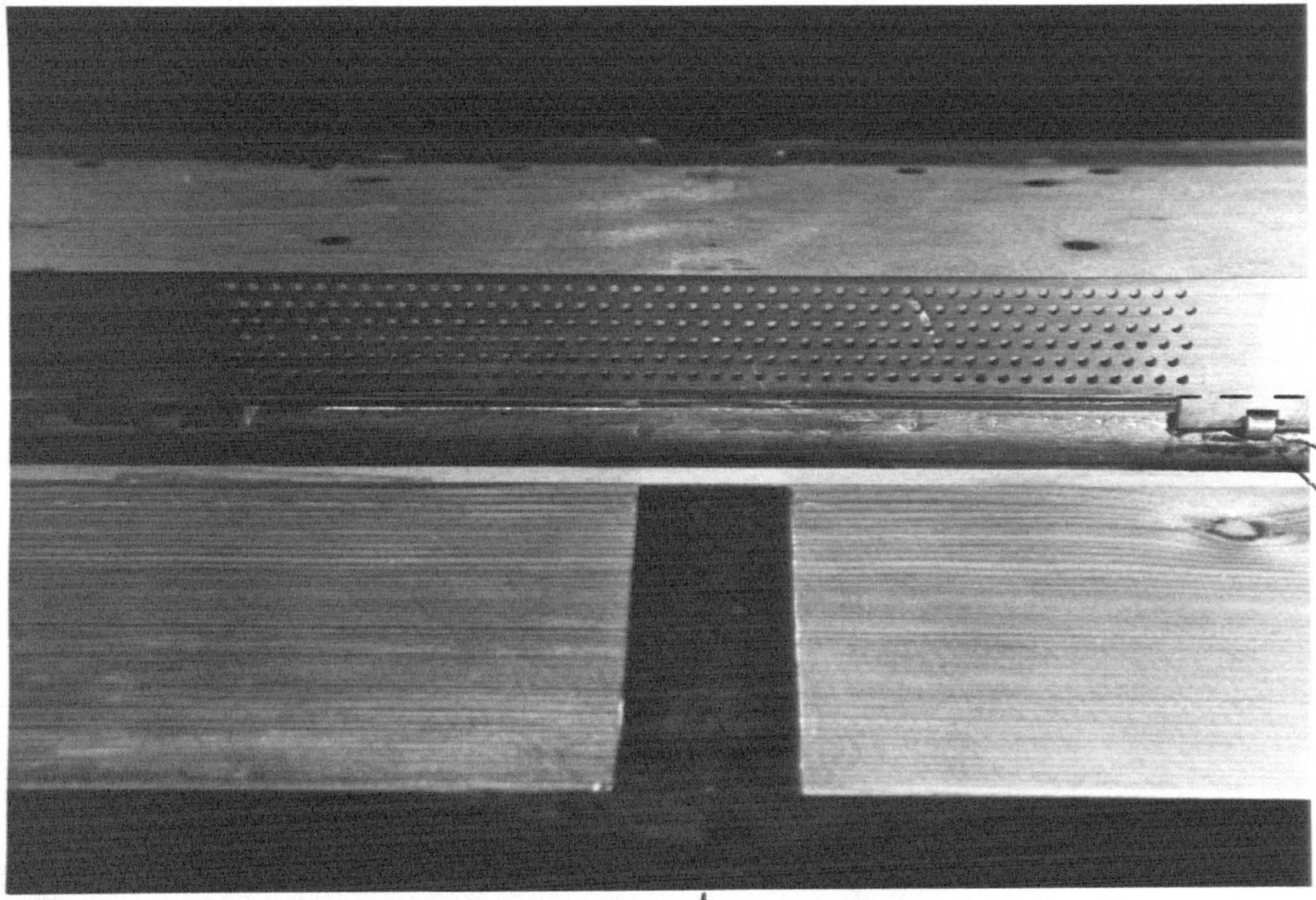

Aerofoil centre line
(tappings are just discernible)

(a) Spoiler viewed from trailing edge ($\delta = 90°$)

All dimensions in mm

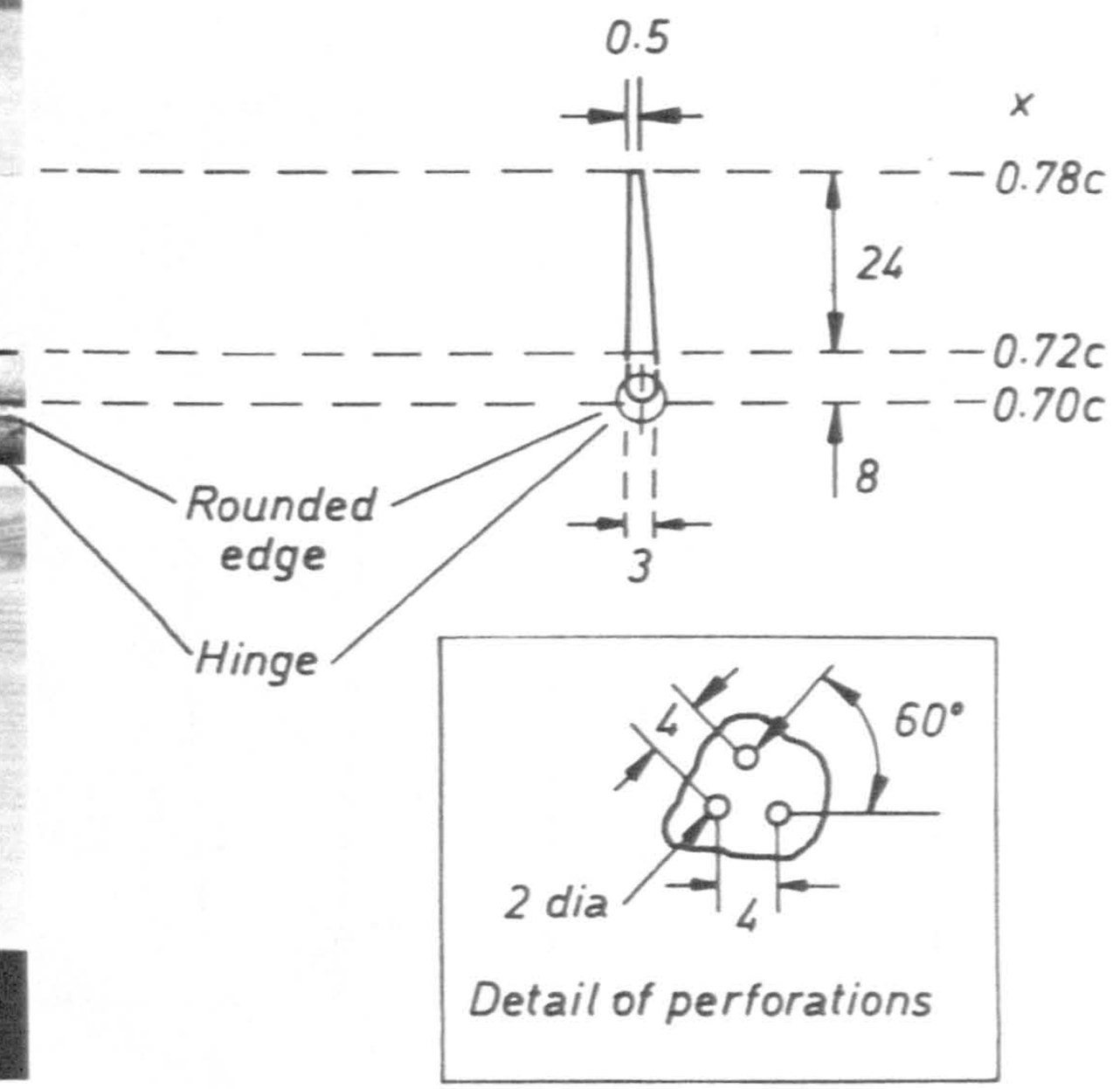

Overall length = 800mm

Perforated length = 170mm

(b) Spoiler geometry

FIG. 3.3 SPOILER ARRANGEMENT

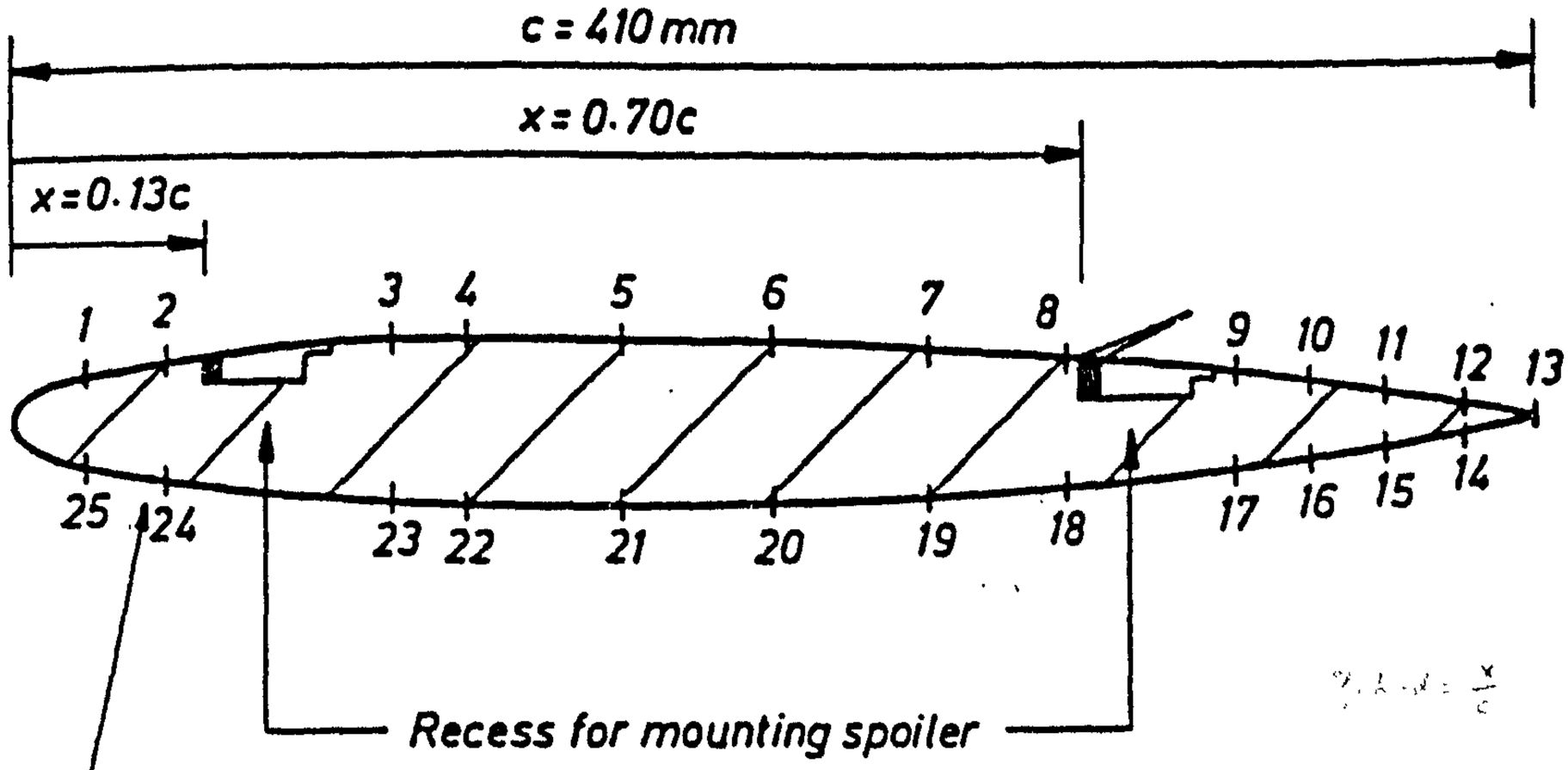

Pressure tapping Tapping no.	Chordwise location x/c	Utilization (for main testing) Rearward spoiler	Forward spoiler
1,25	0.05	X	X
2,24	0.10	X	X
3,23	0.25	X	X
4,22	0.30		X
5,21	0.40	X	X
6,20	0.50		X
7,19	0.60	X	X
8,18	0.69	X	X
9,17	0.80	X	X
10,16	0.85	X	
11,15	0.90	X	X
12,14	0.95	X	
13	1.00	X	X

FIG. 3.4 SPOILER POSITIONS AND PRESSURE TAPPING LOCATIONS

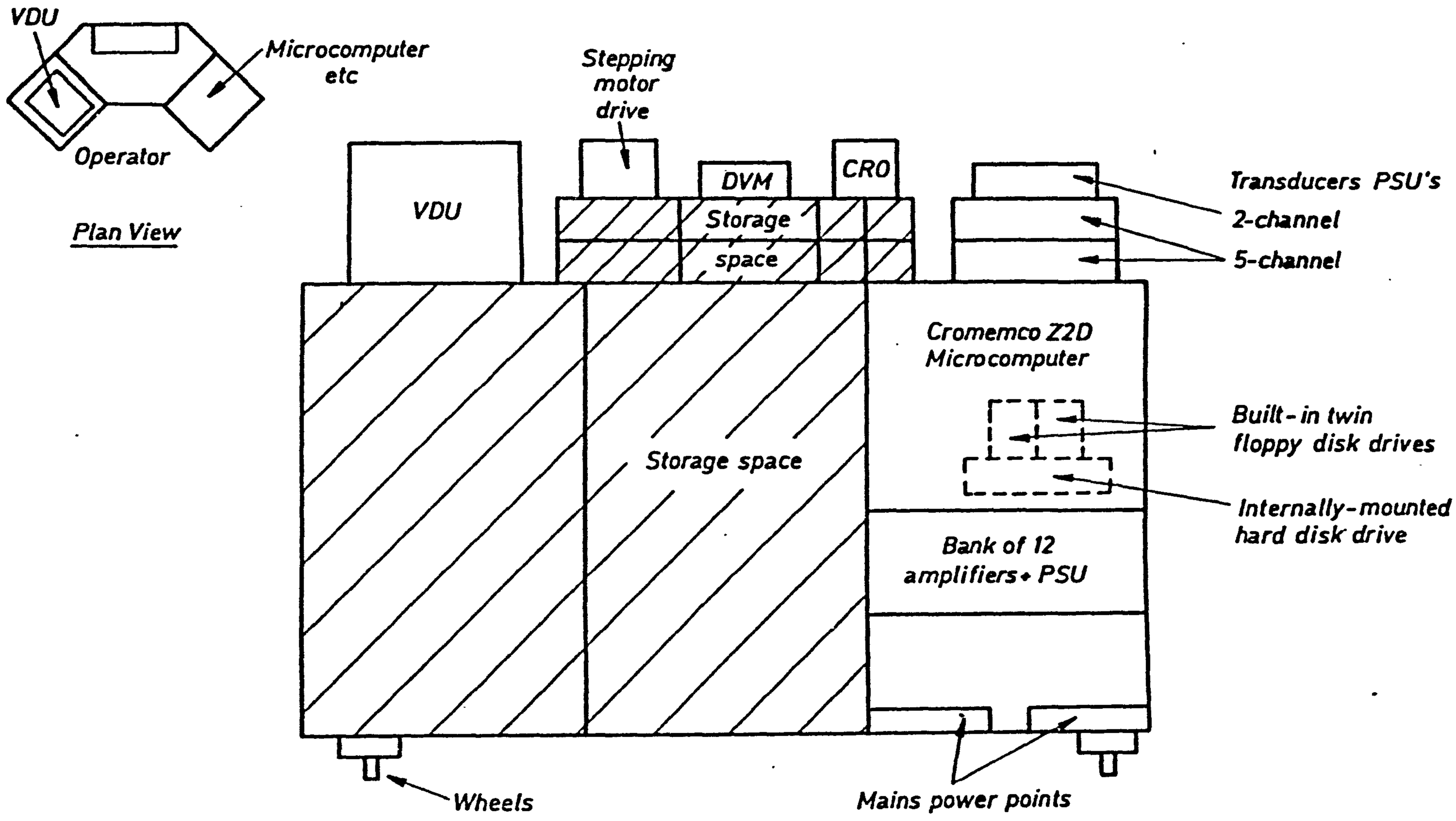

FIG. 3.5 INSTRUMENTATION CONSOLE UNIT

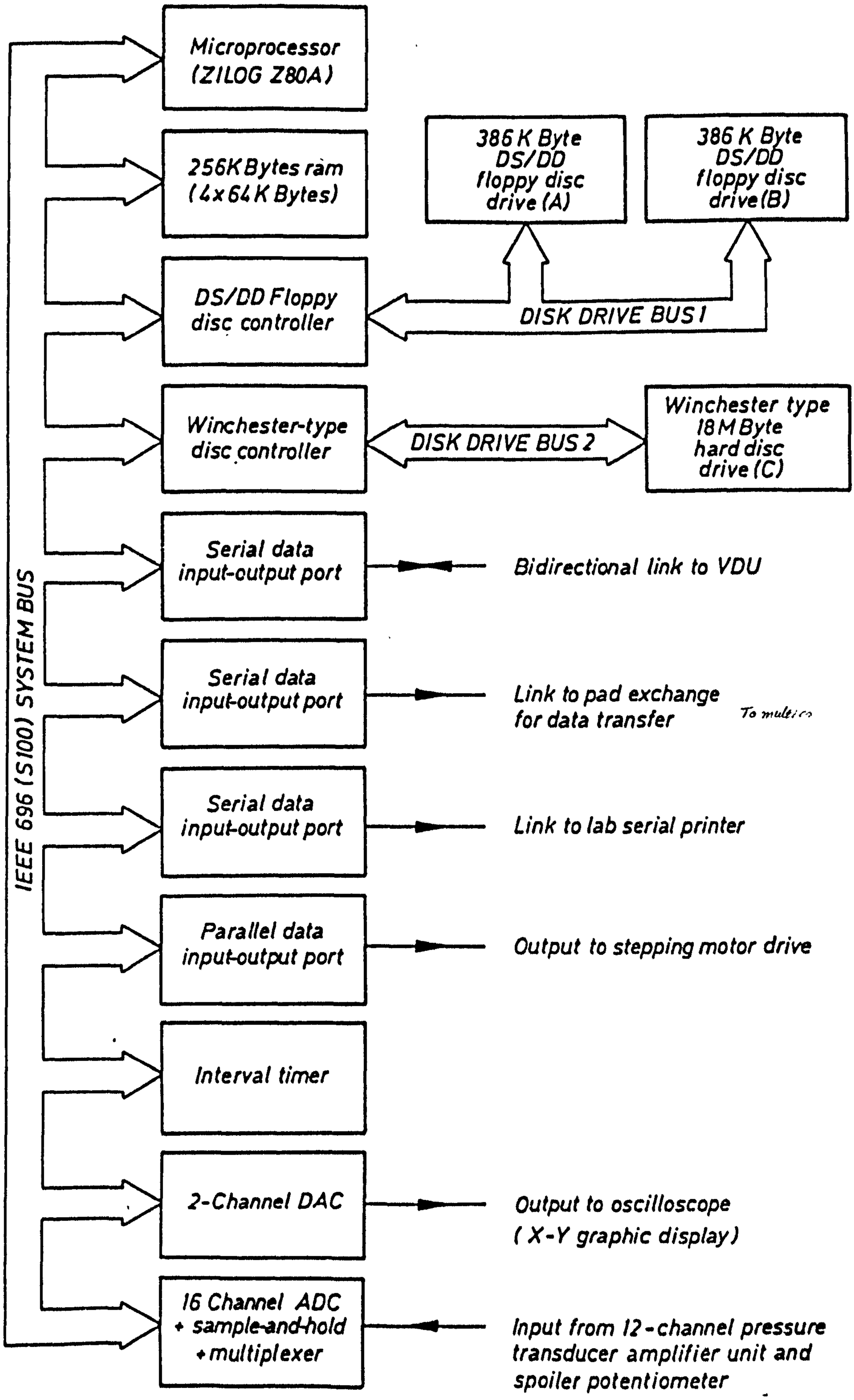

FIG. 3.6 SCHEMATIC DIAGRAM OF MICROCOMPUTER

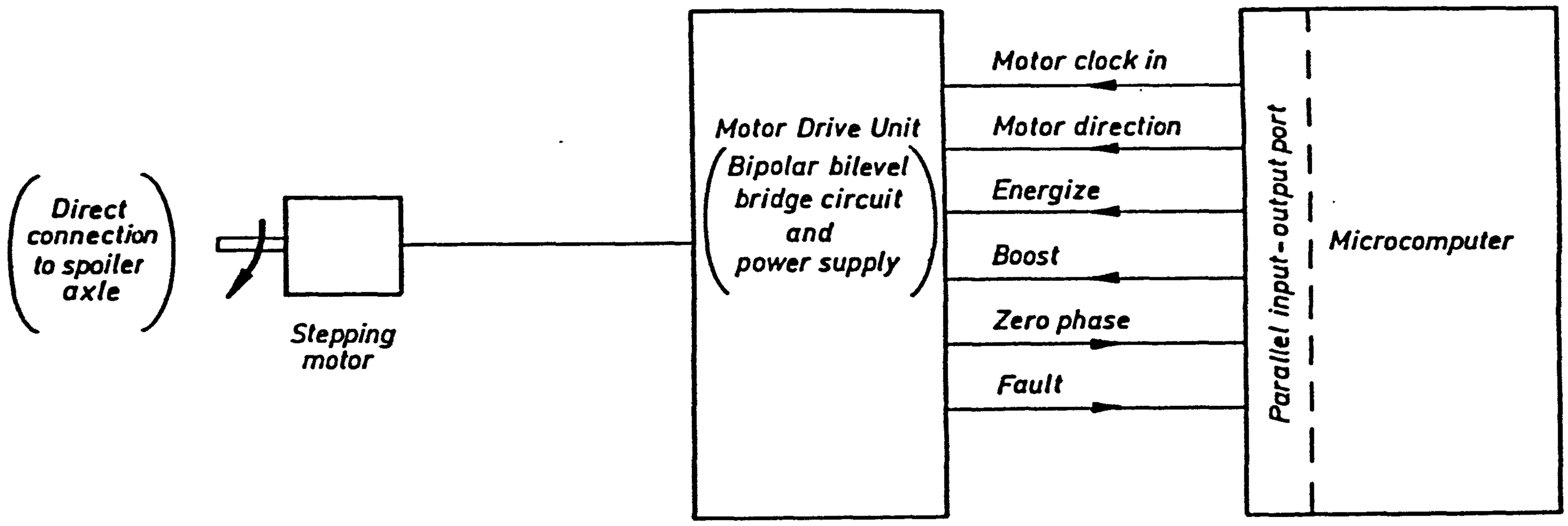

FIG. 3.7 SPOILER ACTUATION SUB-SYSTEM

FIG. 3.8 STEPPING MOTOR ATTACHMENT (STARBOARD ENDPLATE)

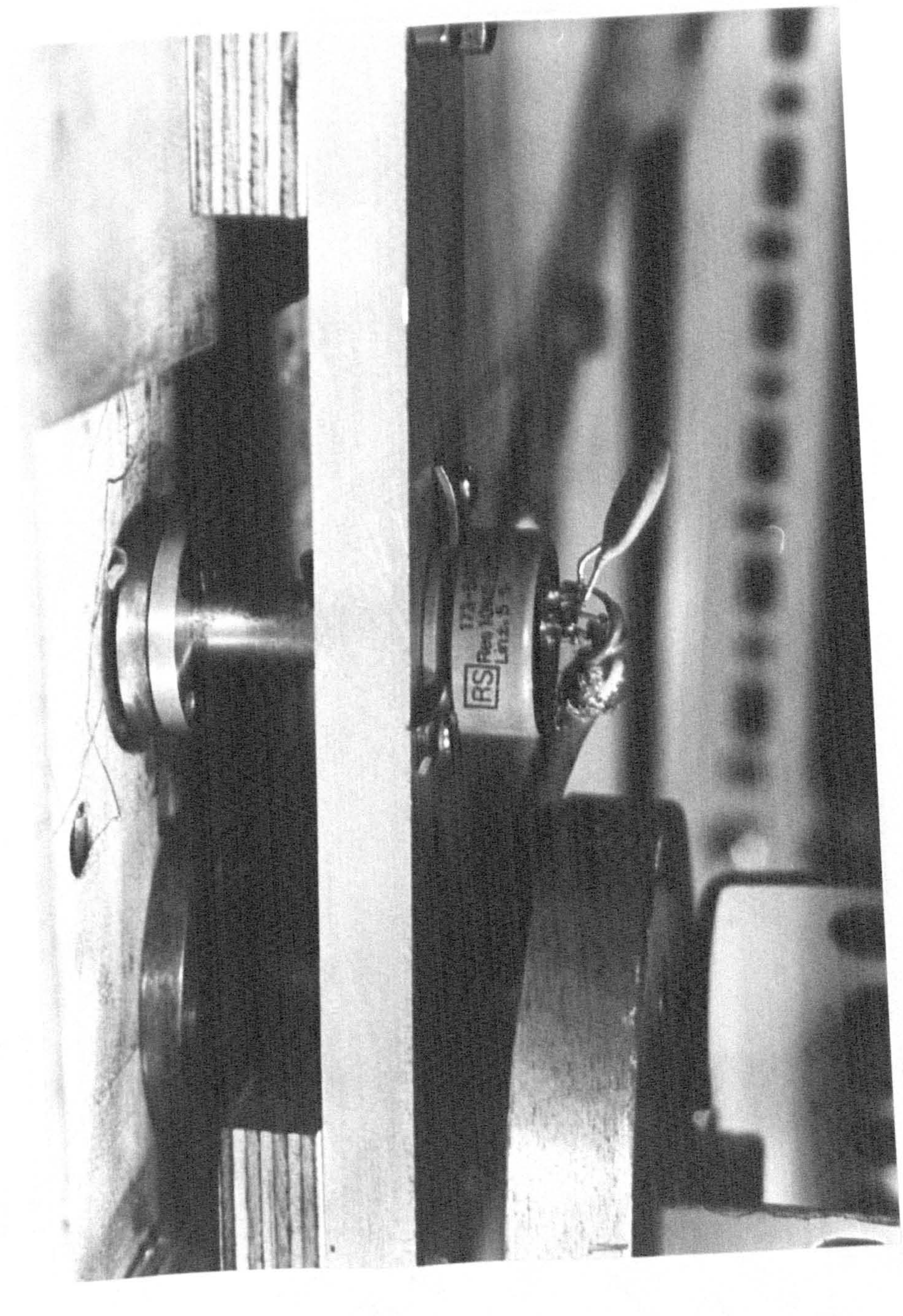

FIG. 3.9 SPOILER POSITION TRANSDUCER ATTACHMENT (PORT ENDPLATE)

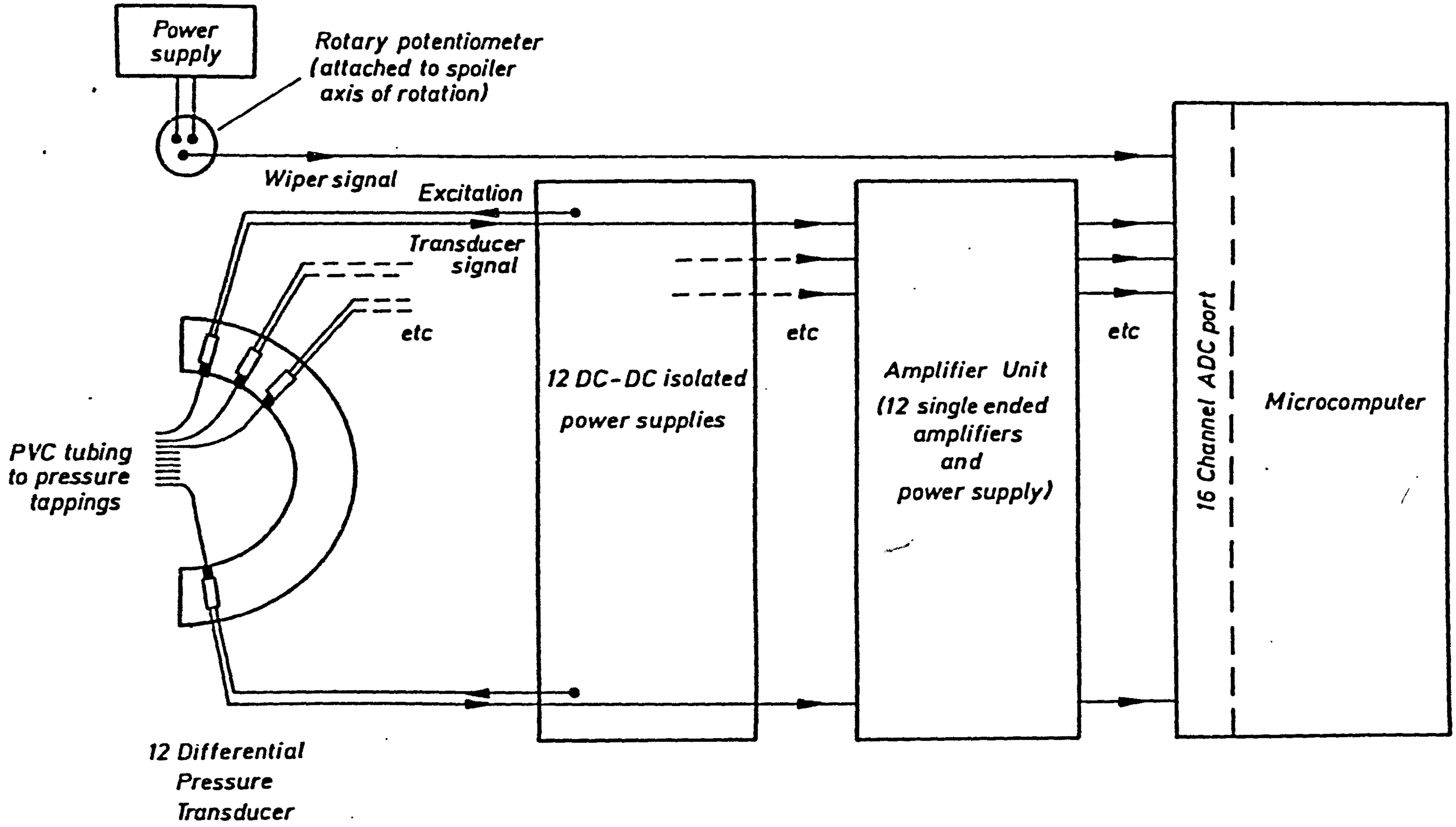

FIG. 3.10 DATA ACQUISITION SUB-SYSTEM

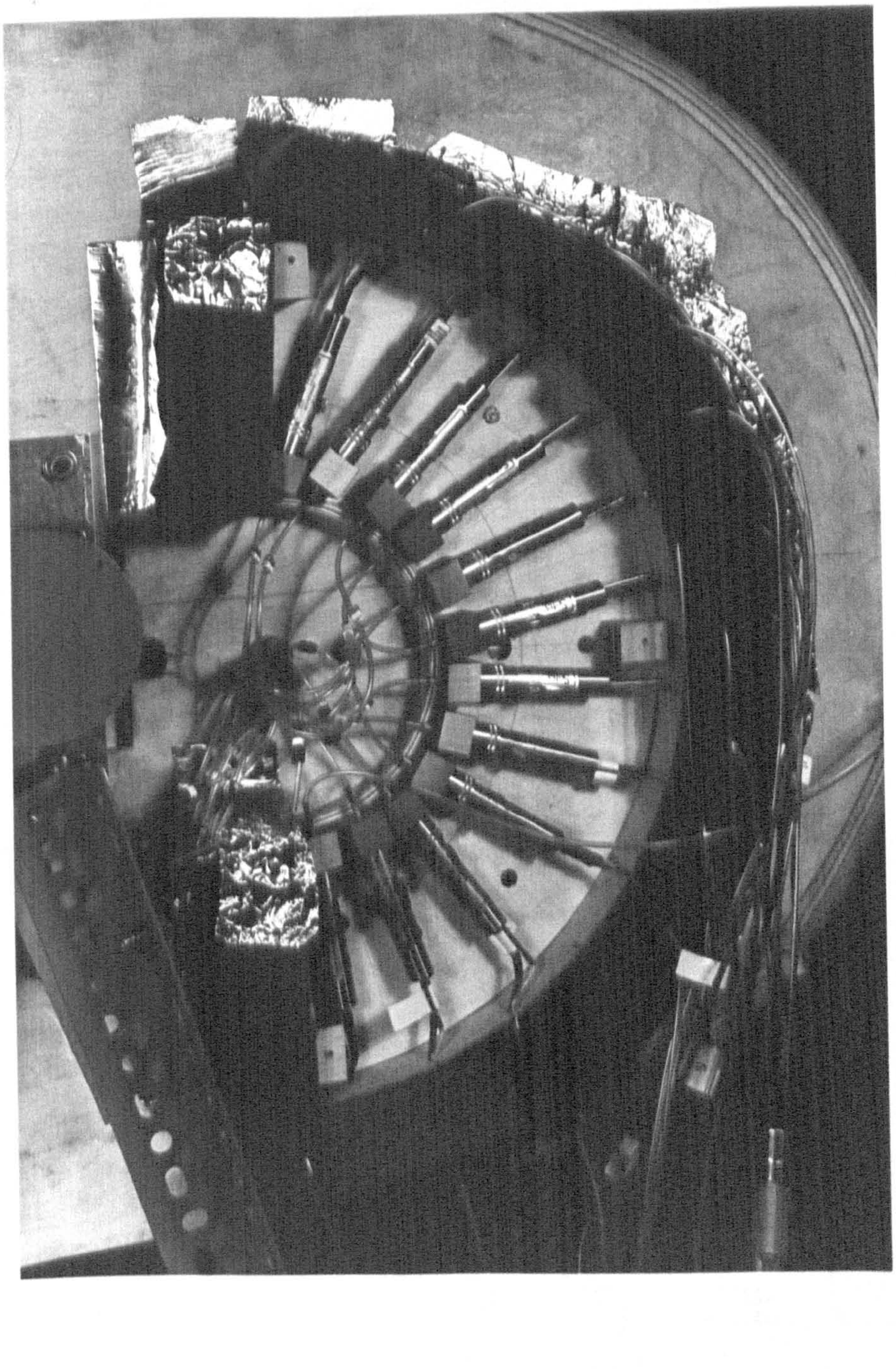

FIG. 3.11 PRESSURE TRANSDUCER ARRANGEMENT (NEXT TO STEPPING MOTOR)

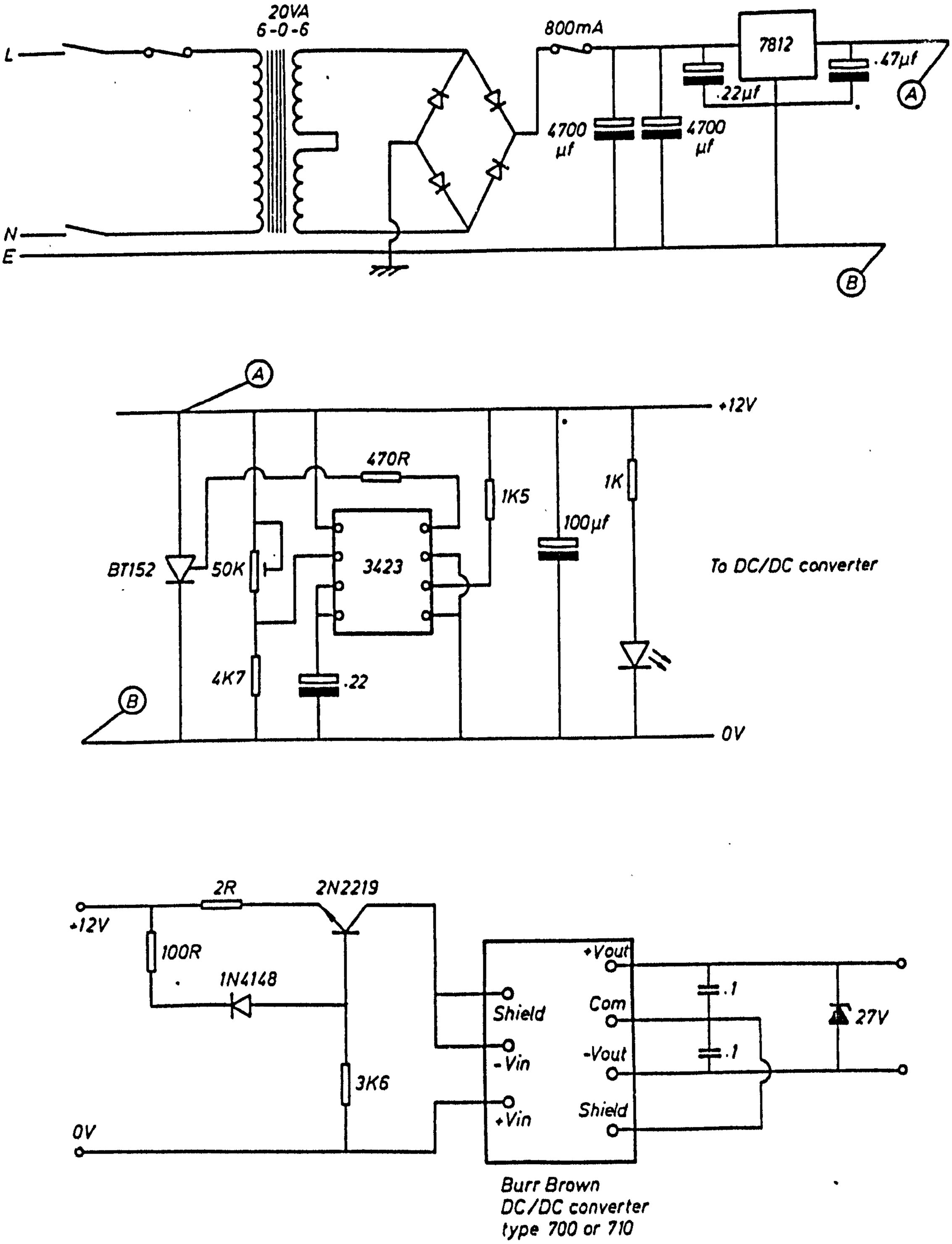

FIG. 3.12 SCHEMATIC CIRCUIT DIAGRAM OF A TRANSDUCER POWER SUPPLY

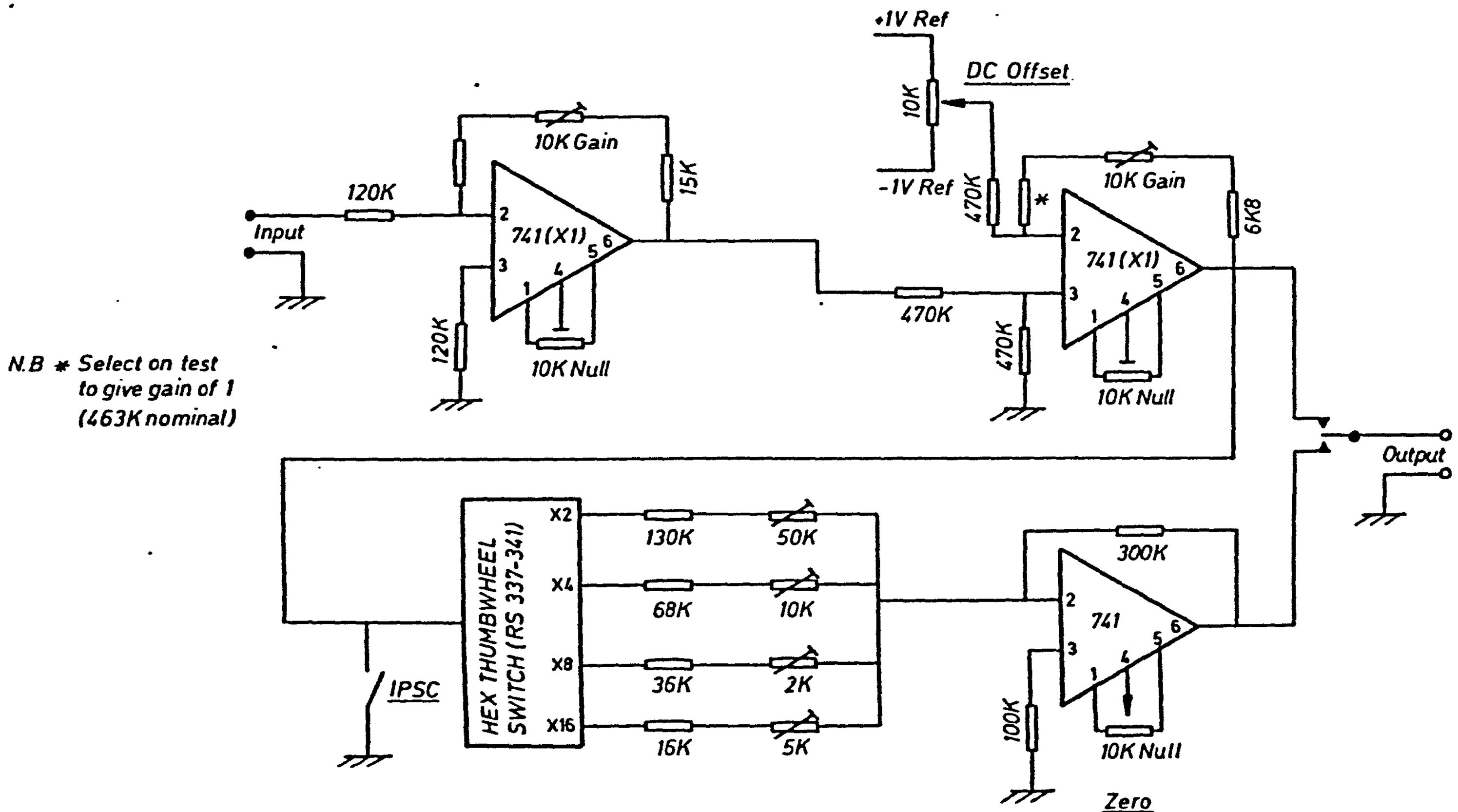

N.B * Select on test to give gain of 1 (463K nominal)

FIG. 3.13 SCHEMATIC CIRCUIT DIAGRAM OF A TRANSDUCER SIGNAL AMPLIFIER (SUPPLY OMITTED)

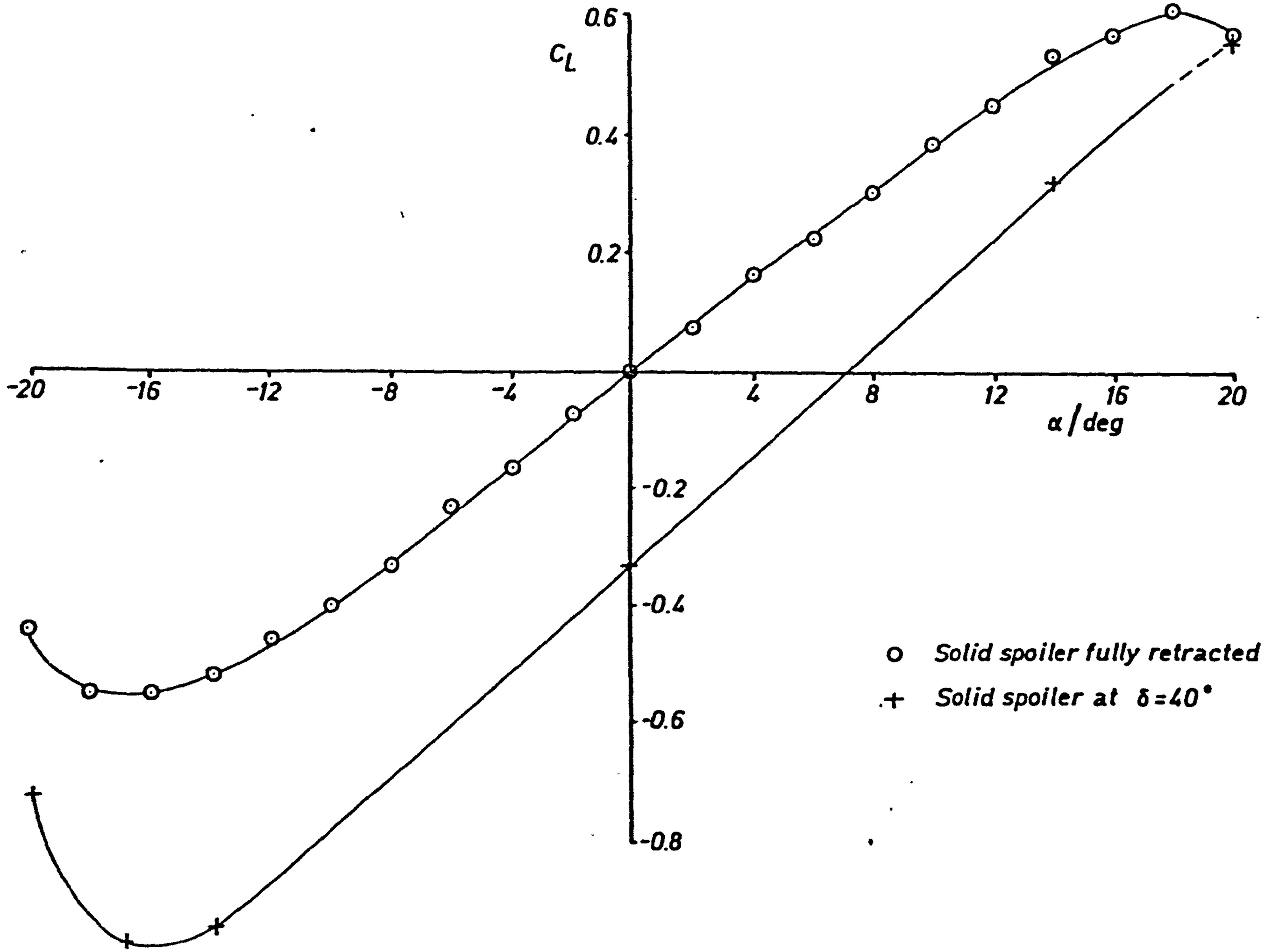

FIG. 5.1 LIFT VARIATION WITH ANGLE OF INCIDENCE

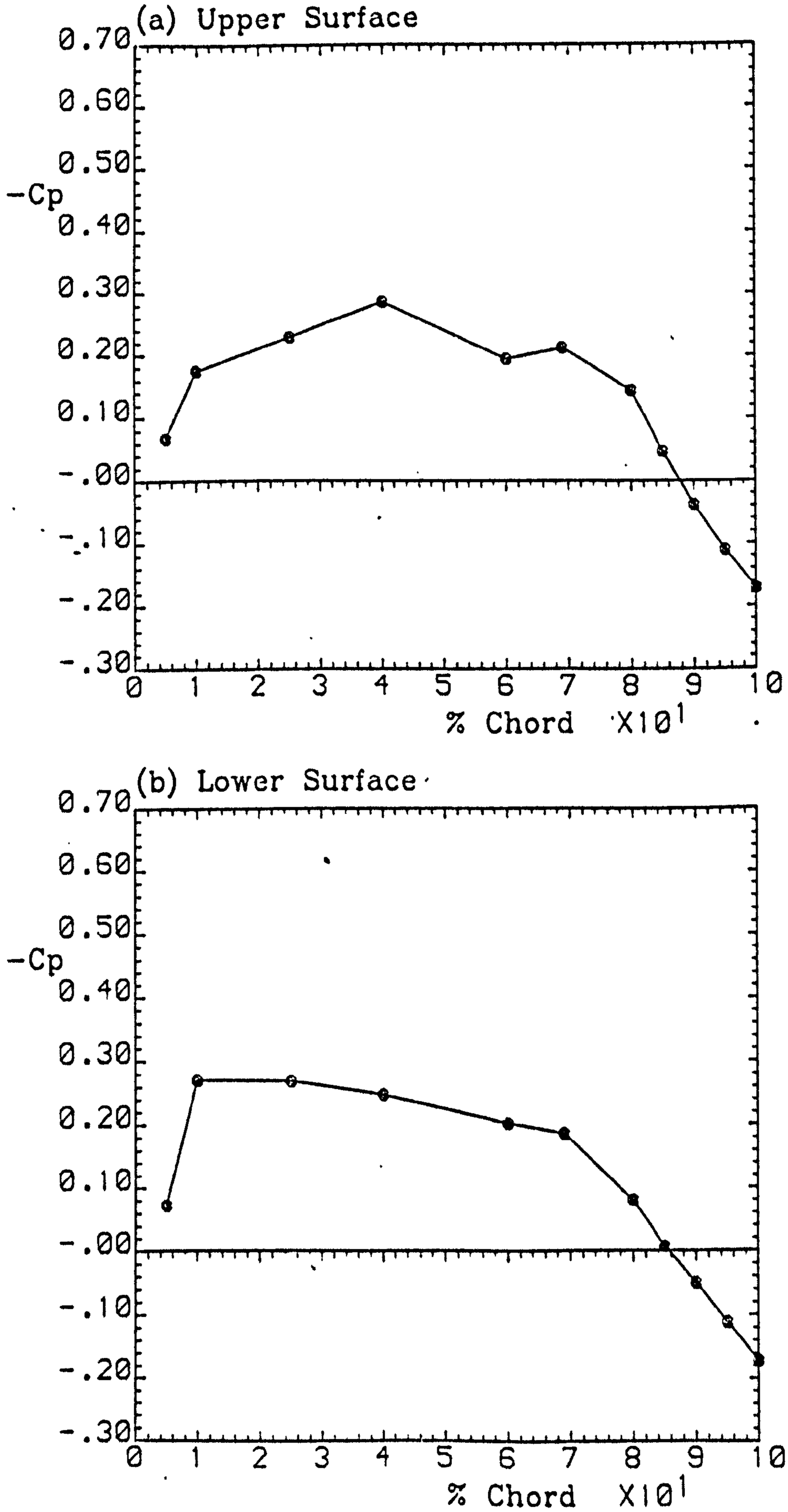

Fig. 5.2 Mean pressure distribution

Run 1111

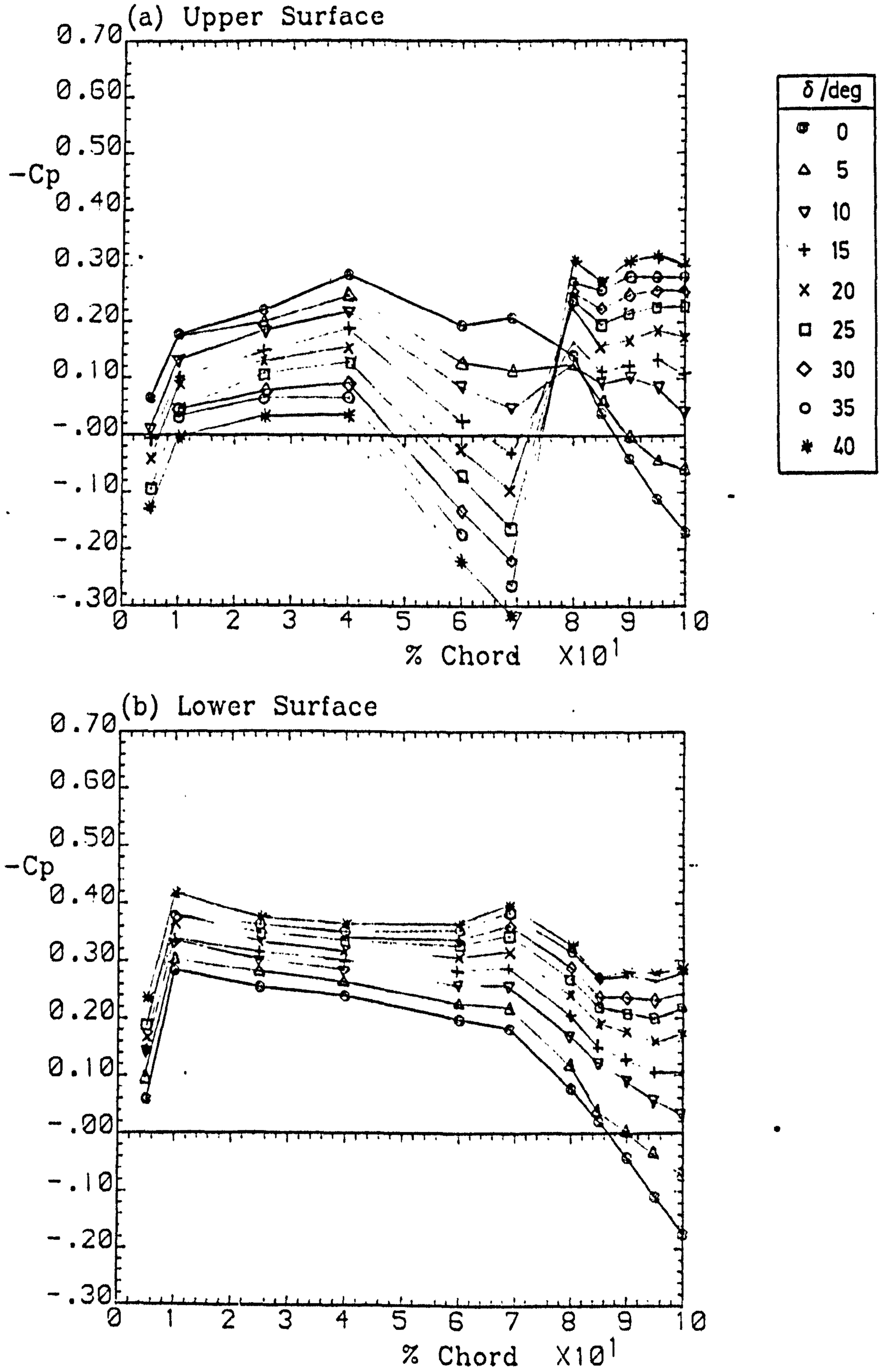

Fig. 5.3 Mean pressure distribution

Run 1301

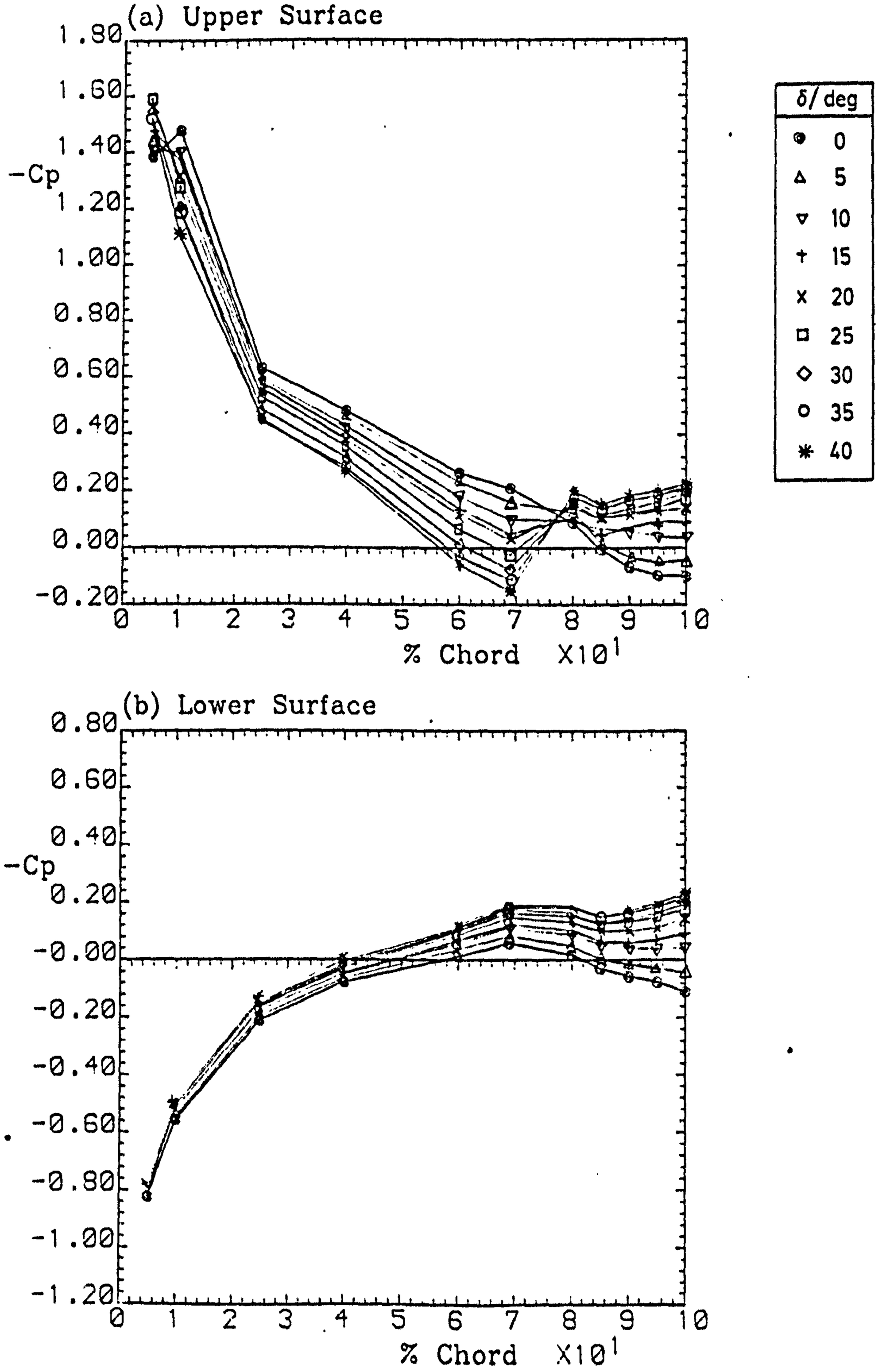

Fig. 5.4 Mean pressure distribution

Run 1311

SPOILER CONFIG.	Incidence/Deg.				
	20	14	0	-14	-20
SOLID	△	◇	□	○	▽
GAPPED		x	+		
PERFORATED		Y	⅄		

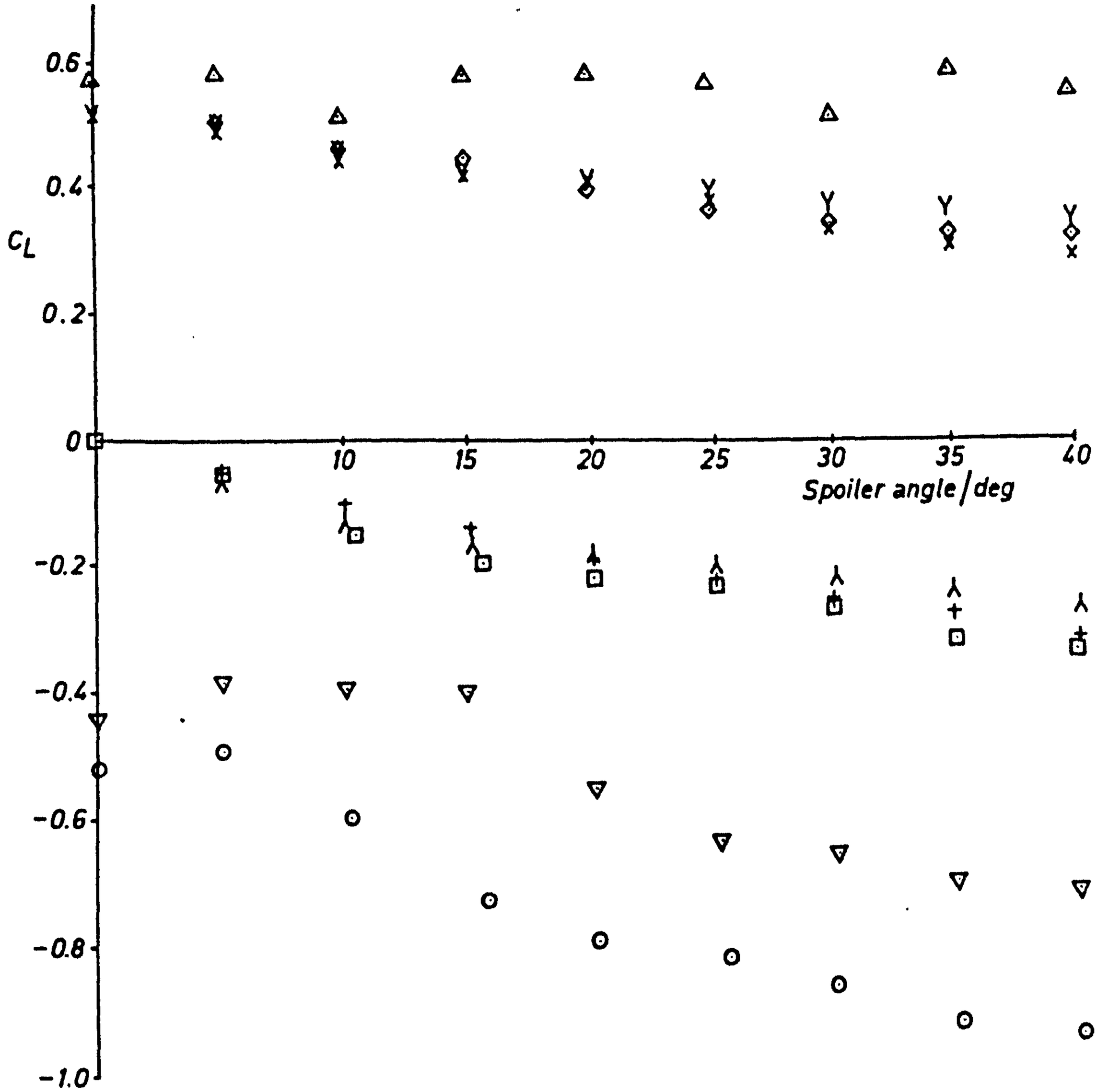

FIG. 5.5 LIFT VARIATION WITH STEADY SPOILER ANGLE

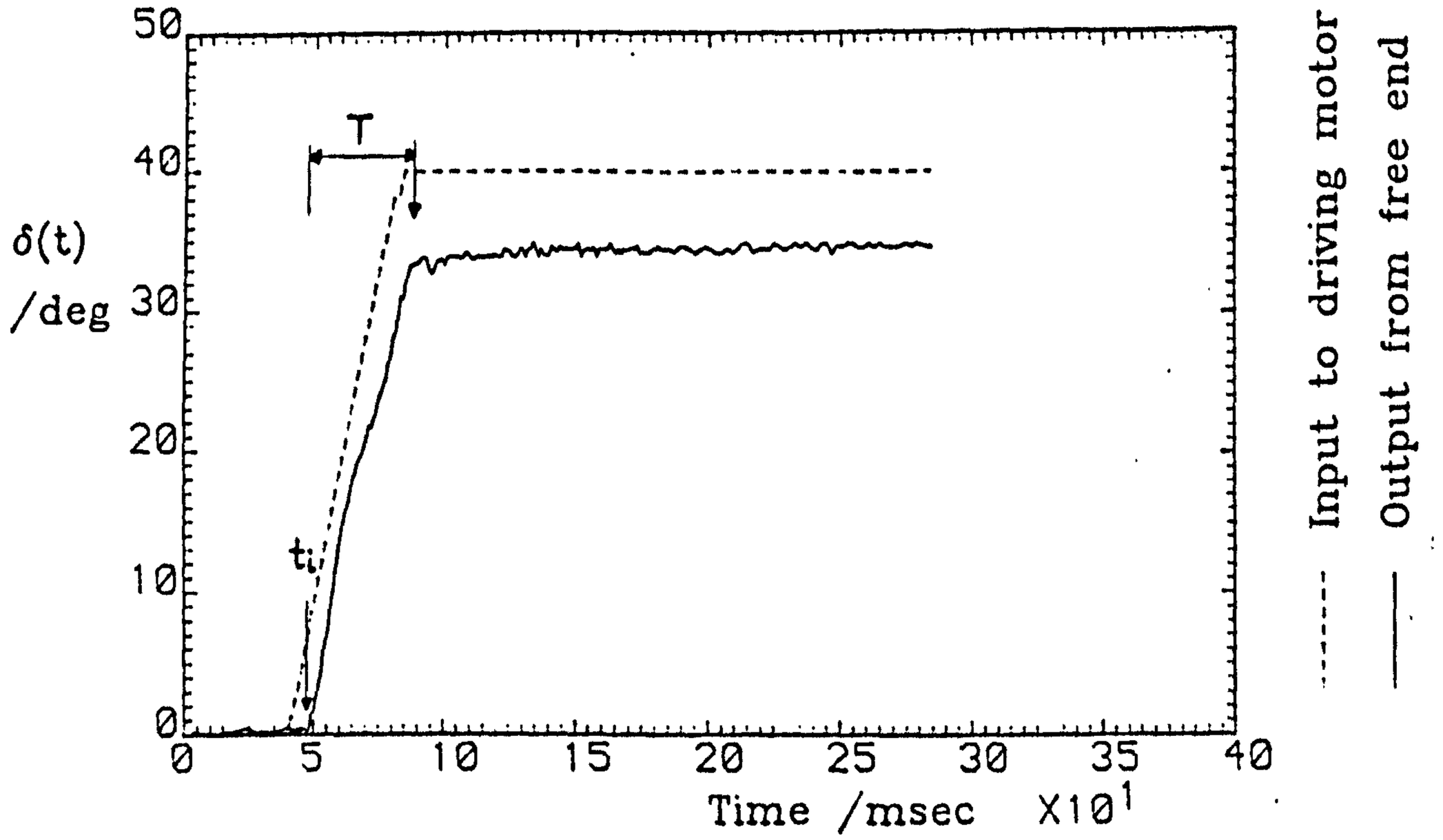

Fig. 5.6 (a) Spoiler displacement trace

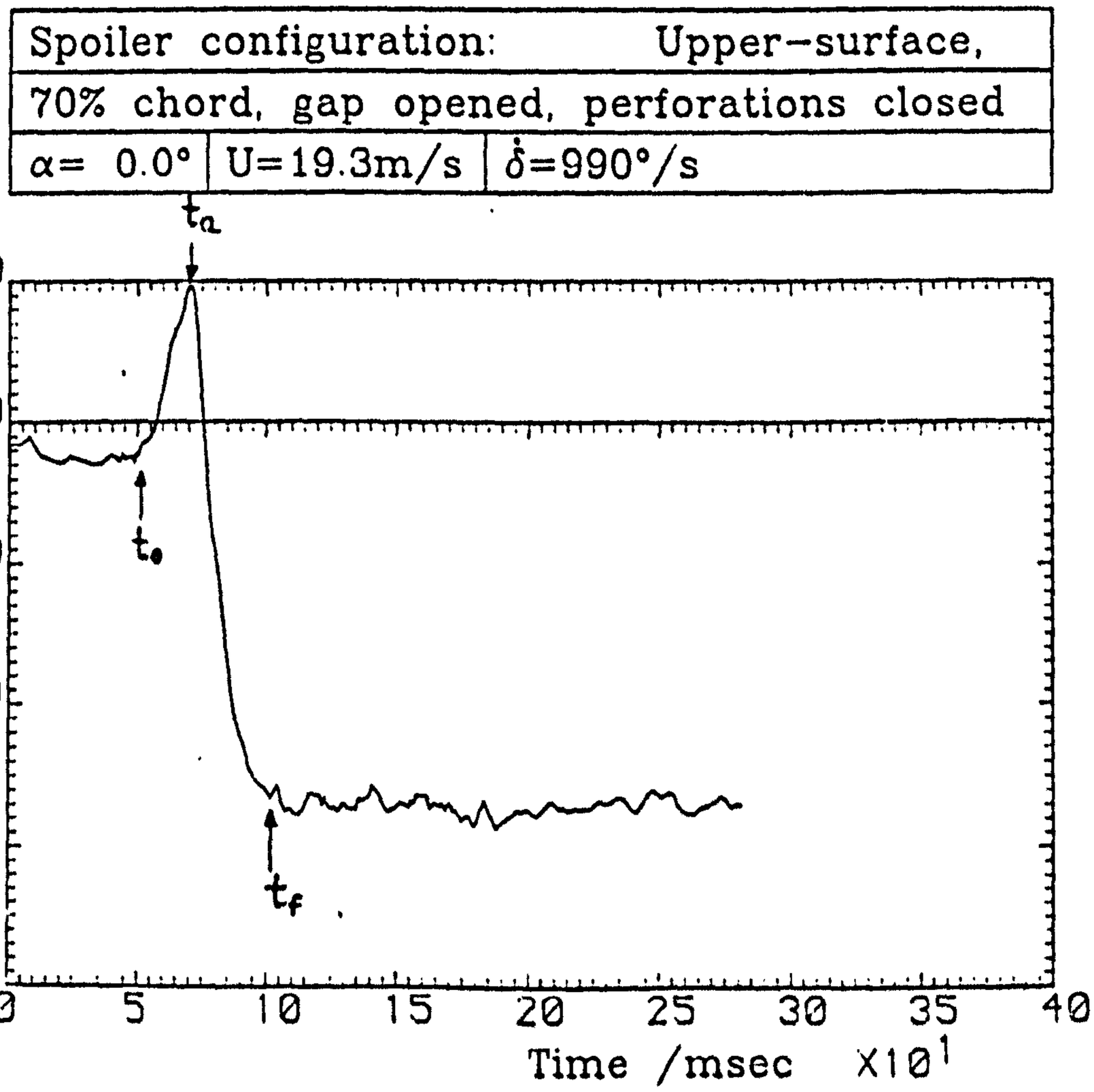

Fig. 5.6 (b) Aerofoil lift time history

Run 3001

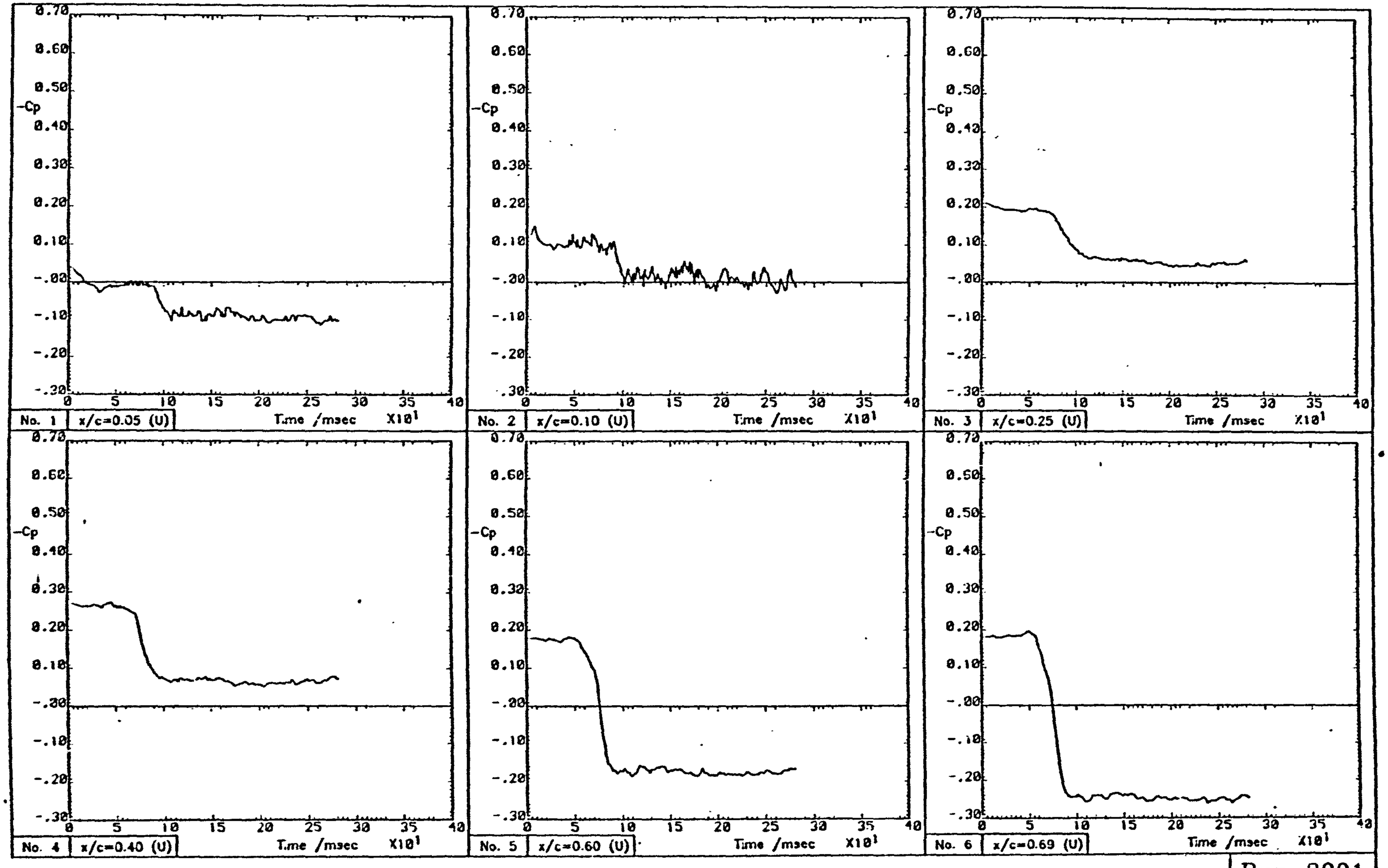

Fig. 5.7(a) Pressure signal time histories

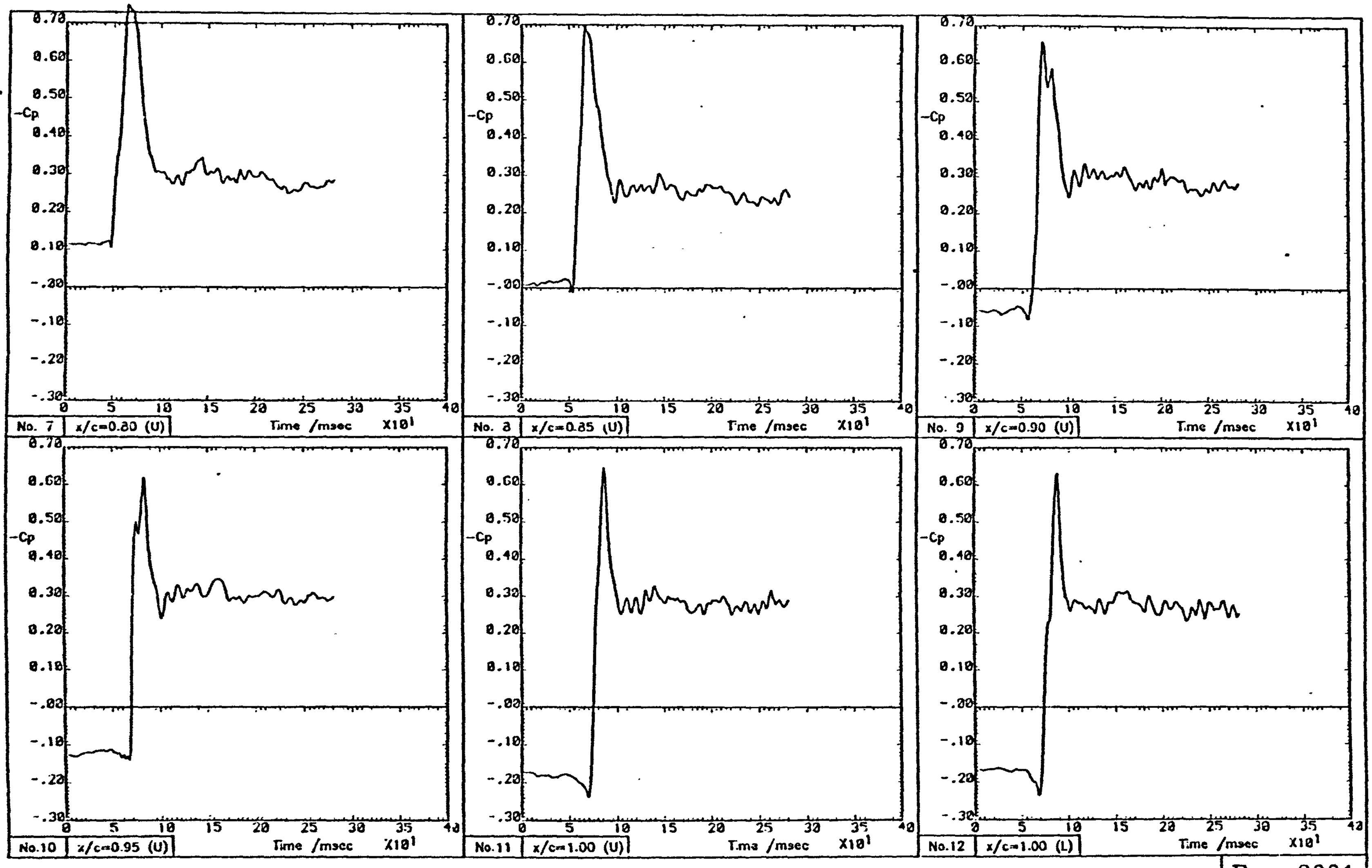

Run 3001

Fig. 5.7(b) Pressure signal time histories

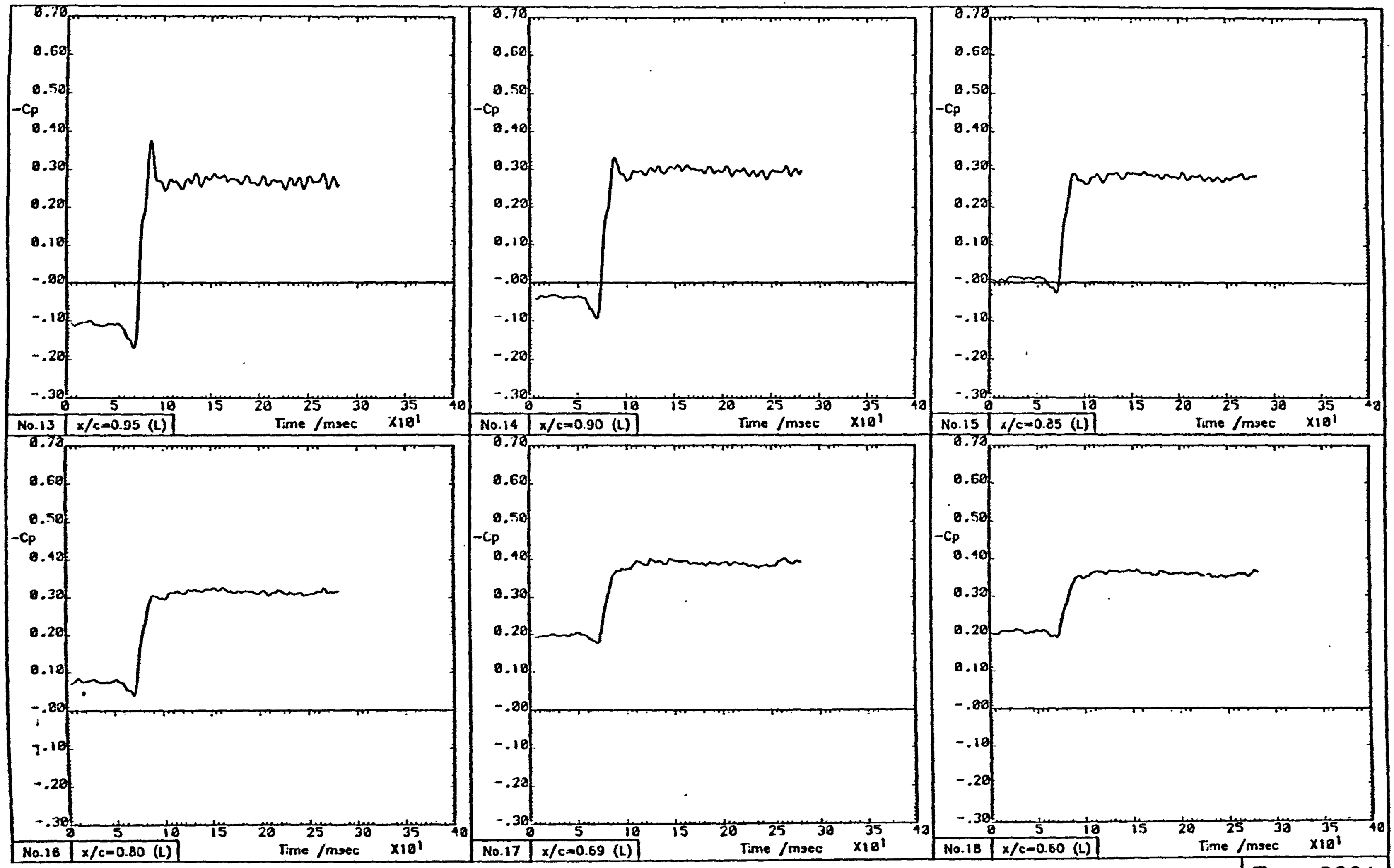

Fig. 5.7(c) Pressure signal time histories

Run 3001

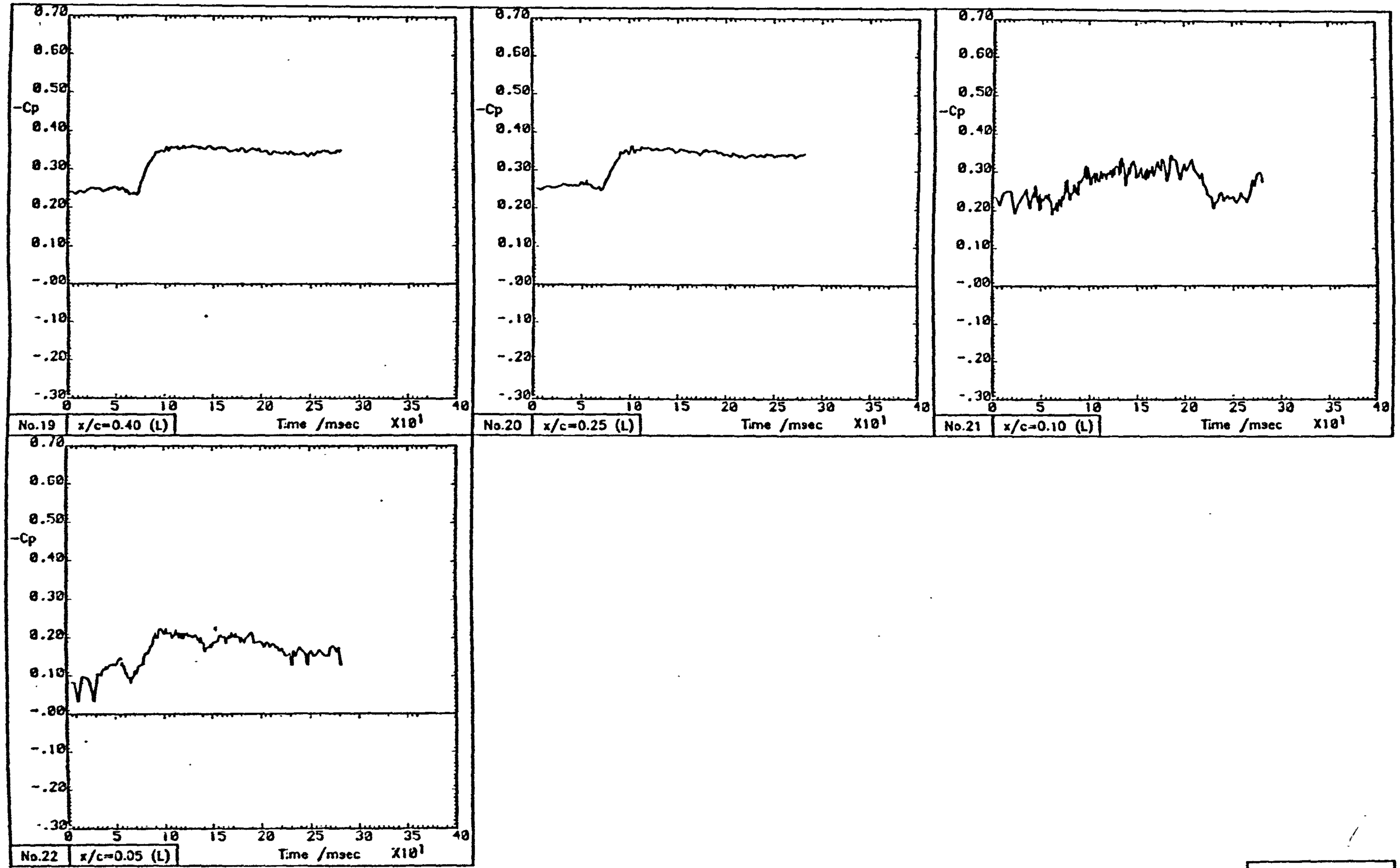

Fig. 5.7(d) Pressure signal time histories

Run 3001

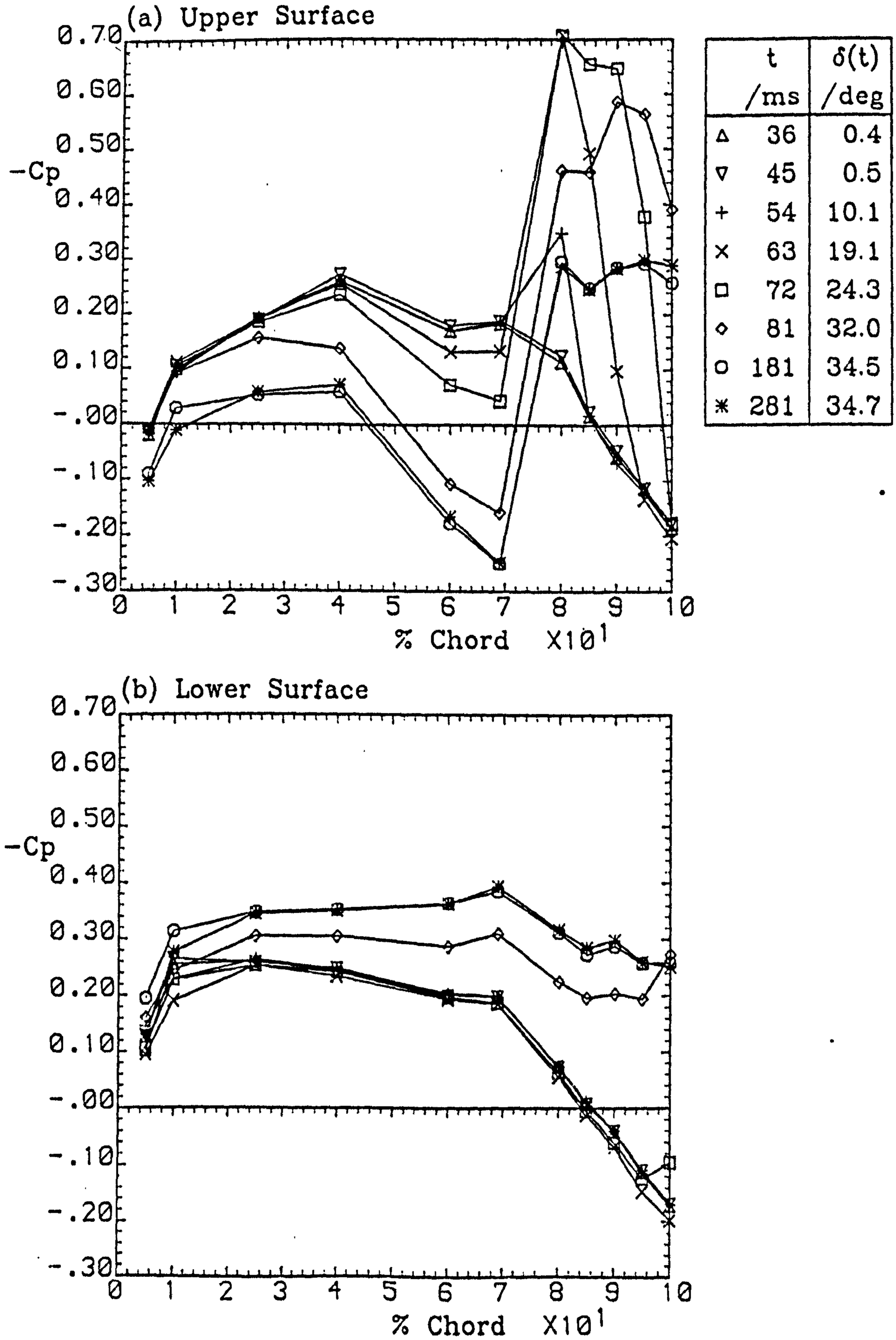

Fig. 5.8 Time-varying pressure distributions

Run 3001

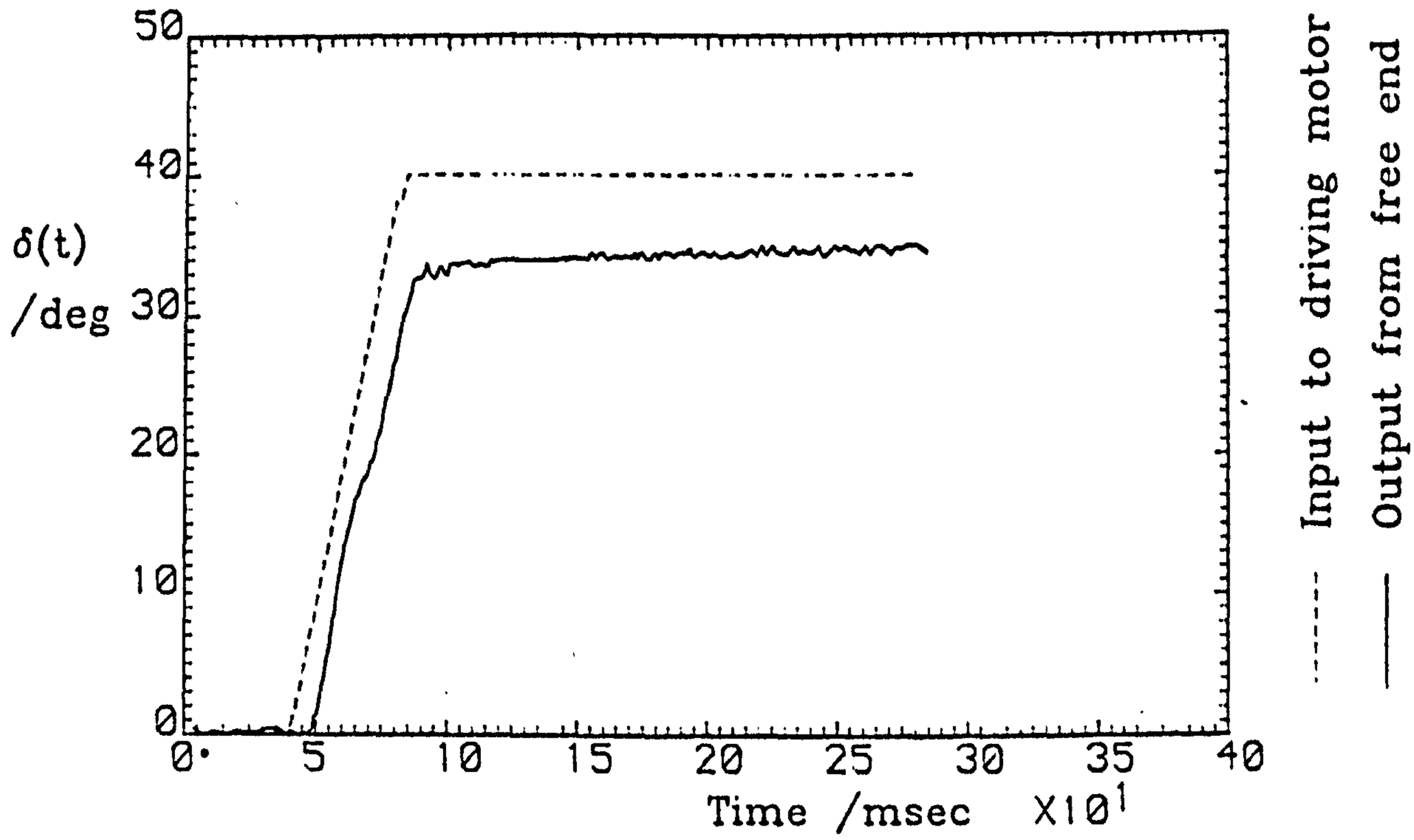

Fig. 5.9(a) Spoiler displacement trace

Spoiler configuration: Upper-surface,		
70% chord, gap opened, perforations closed		
α= 0.0°	U=10.0m/s	$\dot{\delta}$=990°/s

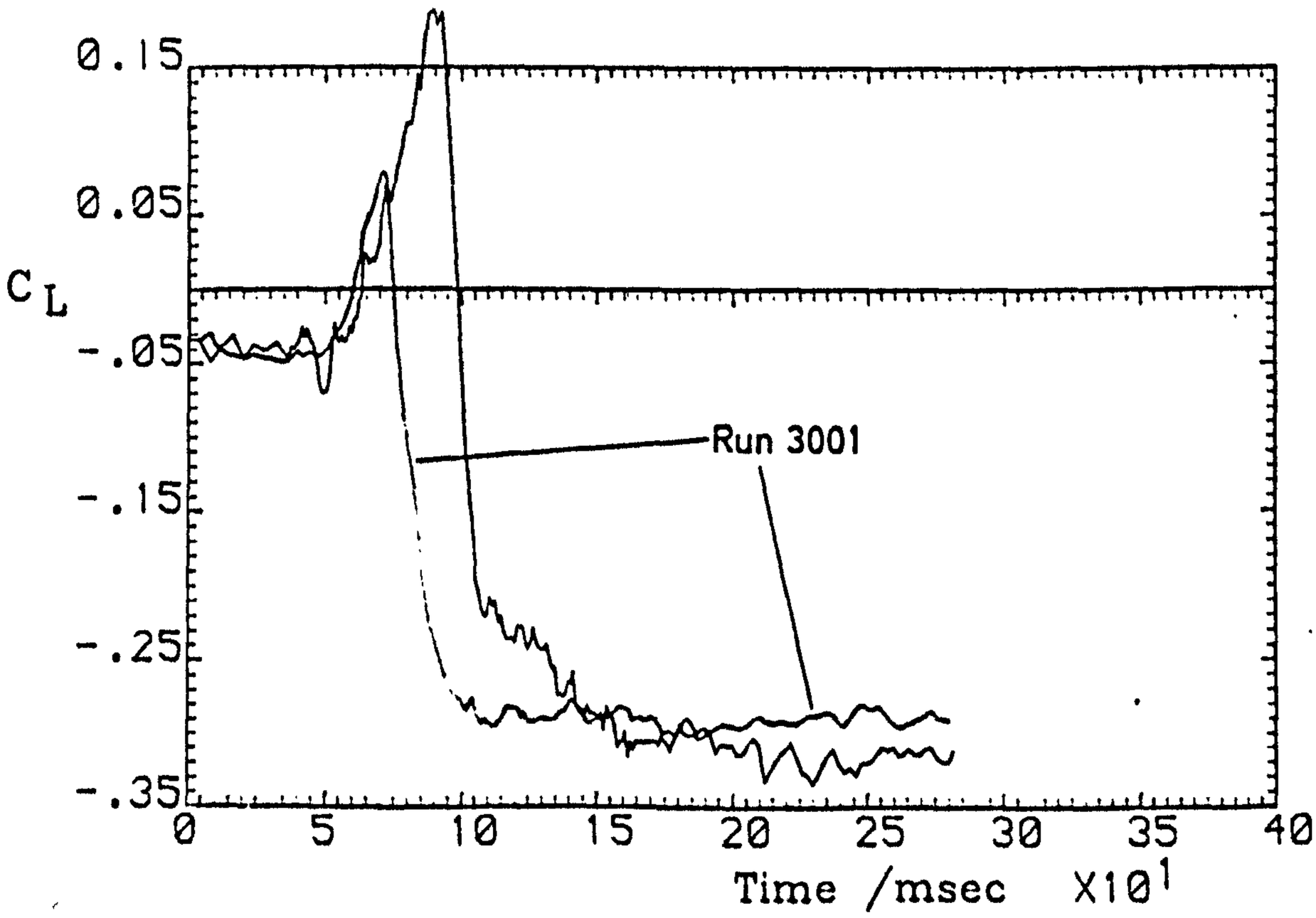

Fig. 5.9(b) Aerofoil lift time history

Run 3007

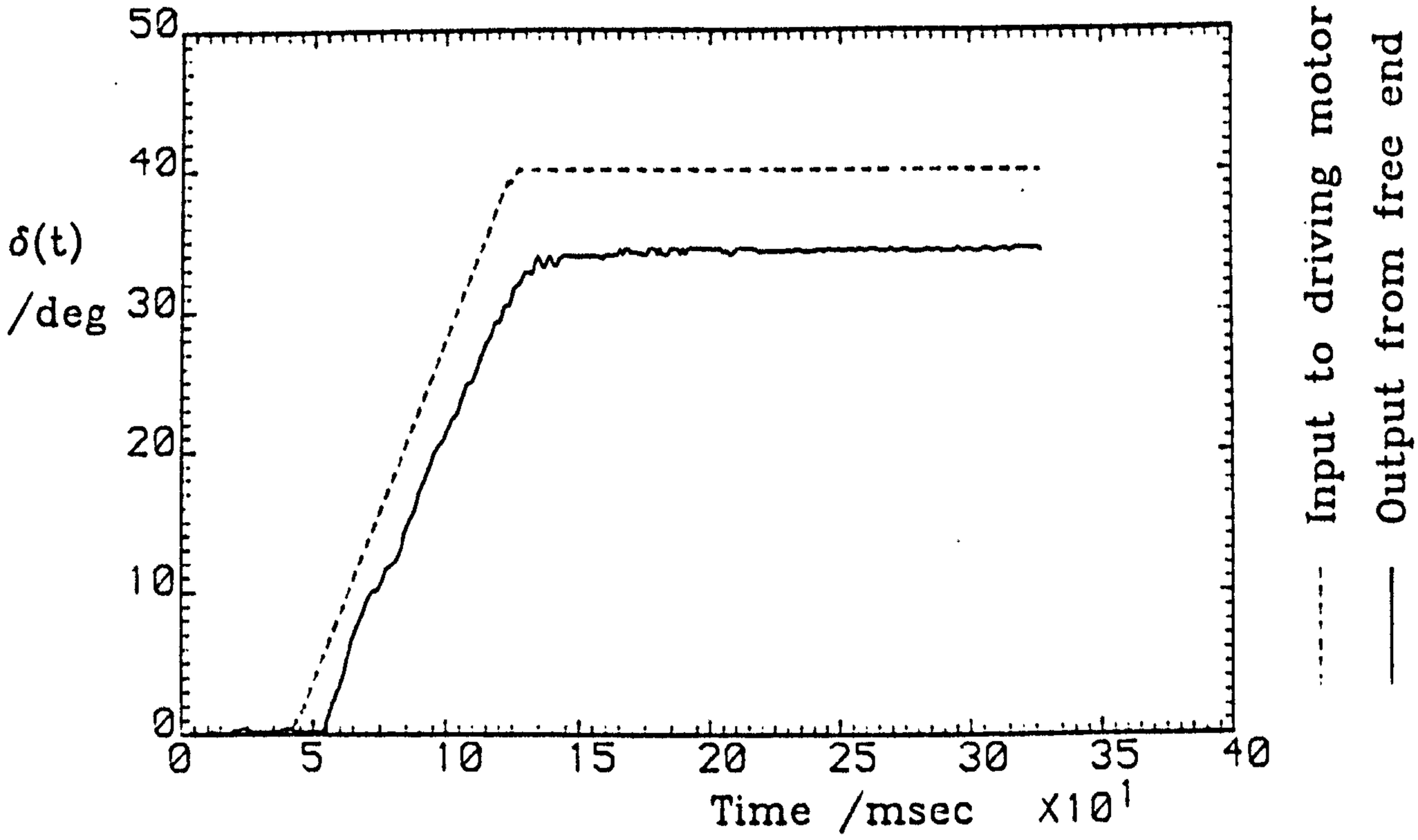

Fig. 5.10(a) Spoiler displacement trace

Spoiler configuration: Upper-surface,		
70% chord, gap opened, perforations closed		
α= 0.0°	U=19.3m/s	$\dot{\delta}$=500°/s

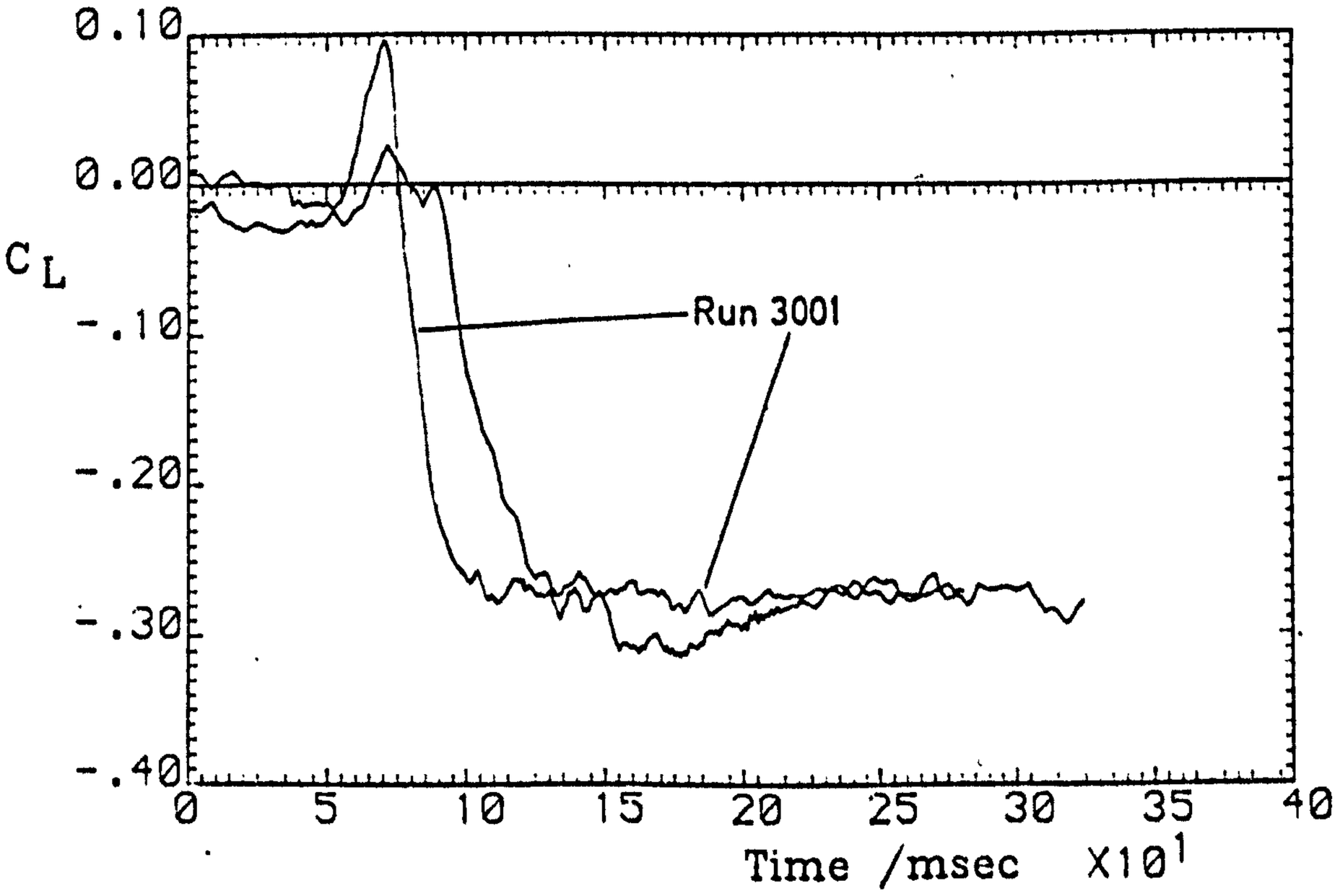

Fig. 5.10(b) Aerofoil lift time history

Run 3003

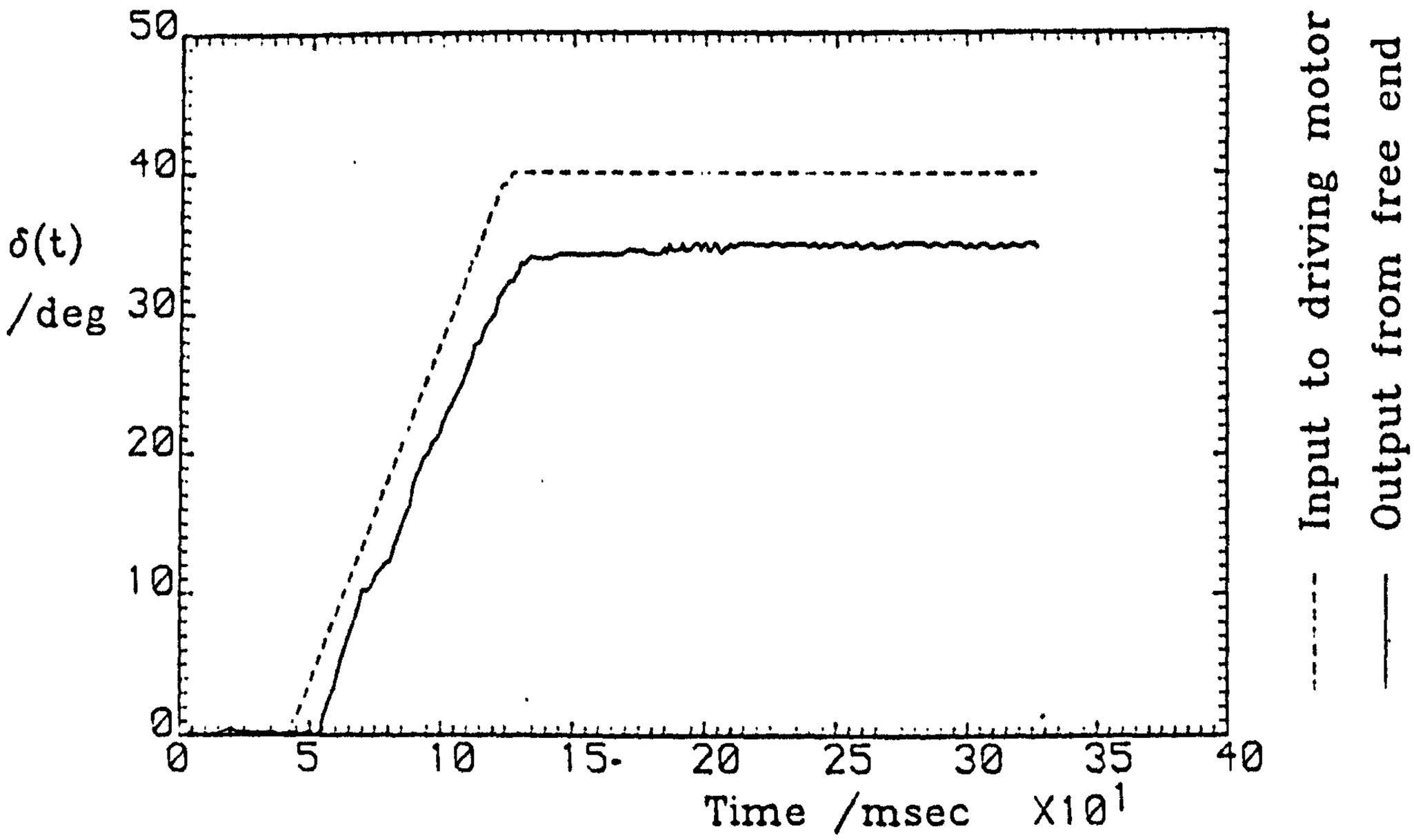

Fig. 5.11(a) Spoiler displacement trace

Spoiler configuration: Upper-surface,		
70% chord, gap opened, perforations closed		
α= 0.0°	U=10.0m/s	$\dot{\delta}$=500°/s

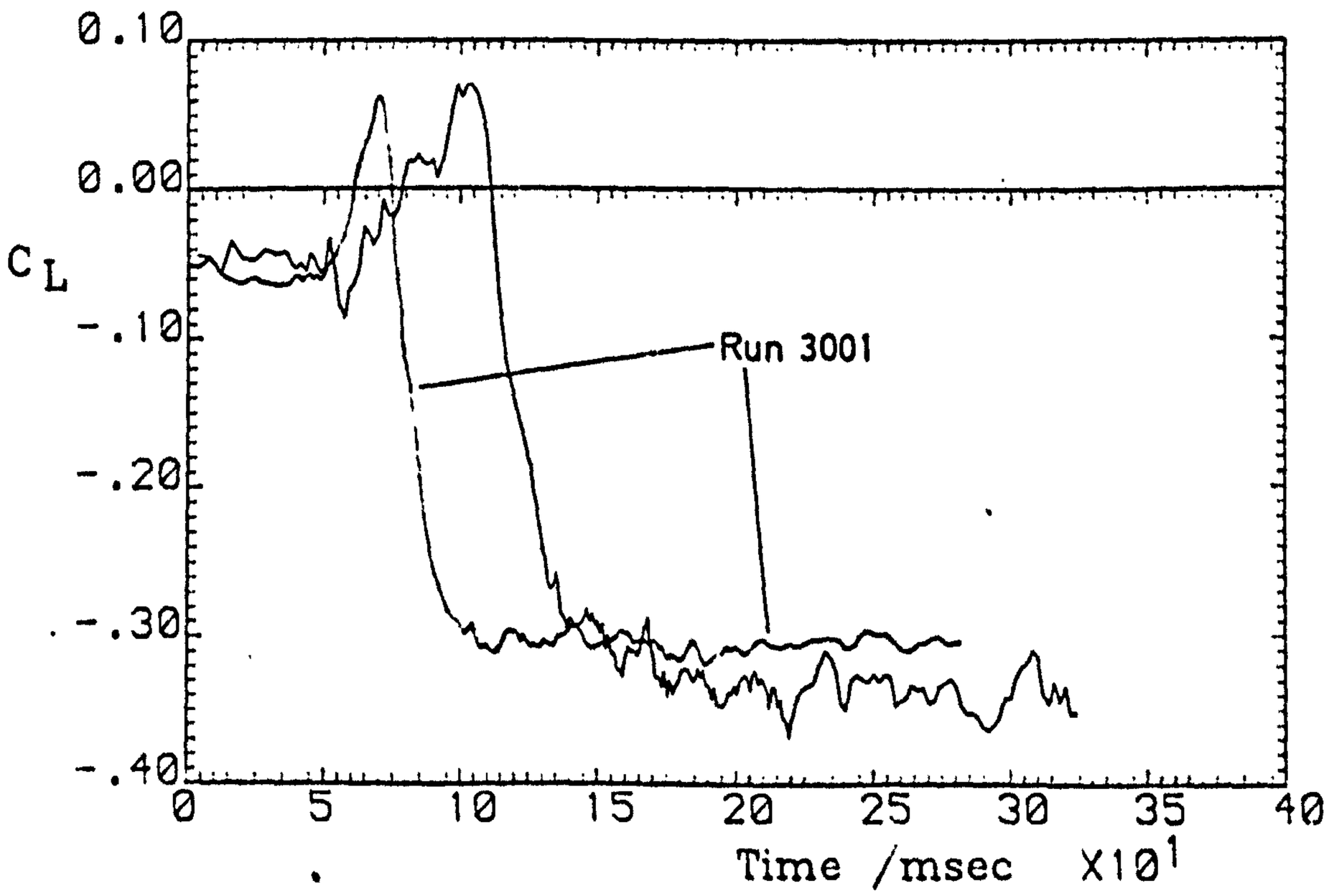

Fig. 5.11(b) Aerofoil lift time history

Run 3009

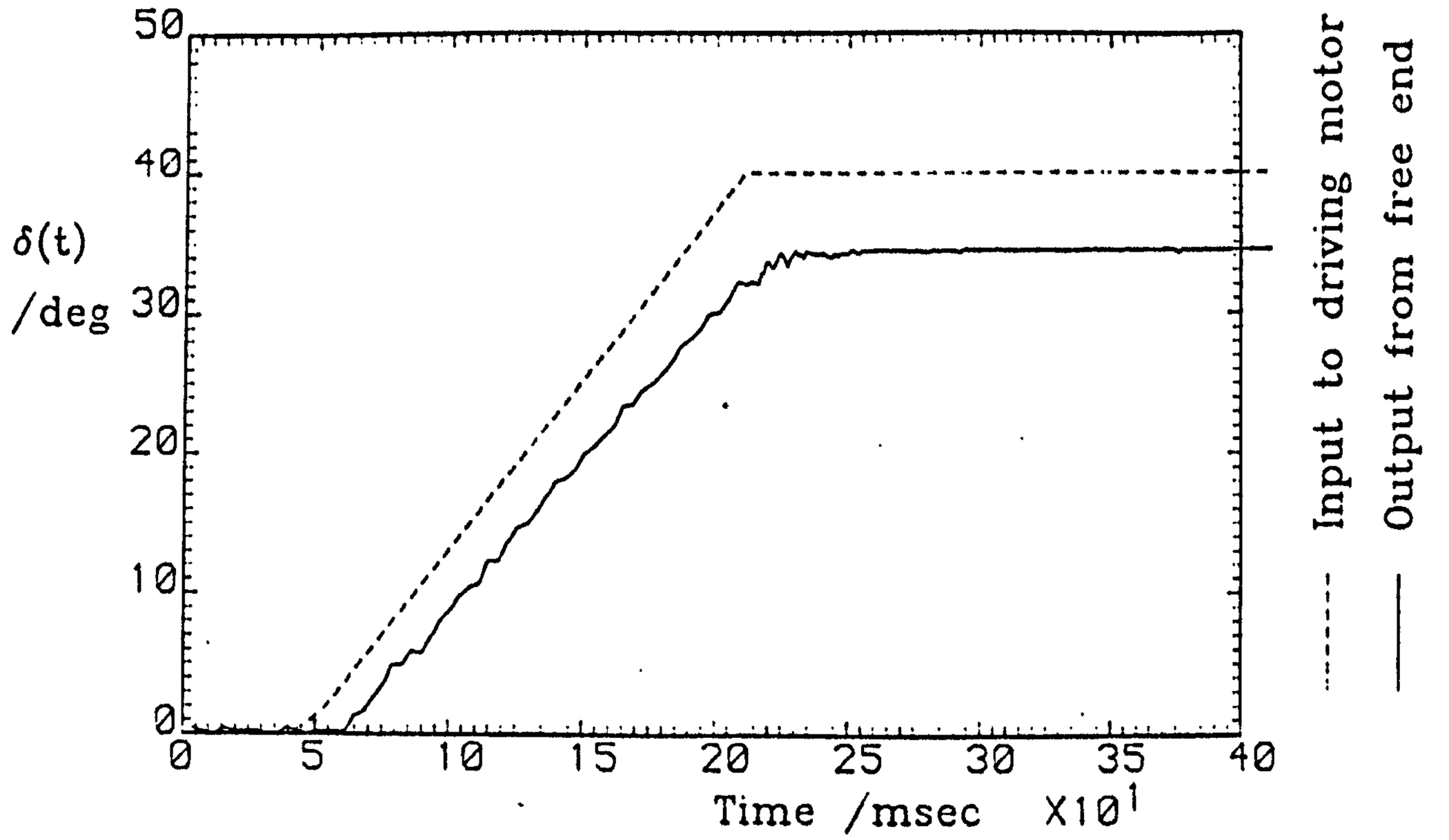

Fig. 5.12(a) Spoiler displacement trace

Spoiler configuration: Upper-surface,		
70% chord, gap opened, perforations closed		
α= 0.0°	U=20.0m/s	$\dot{\delta}$=250°/s

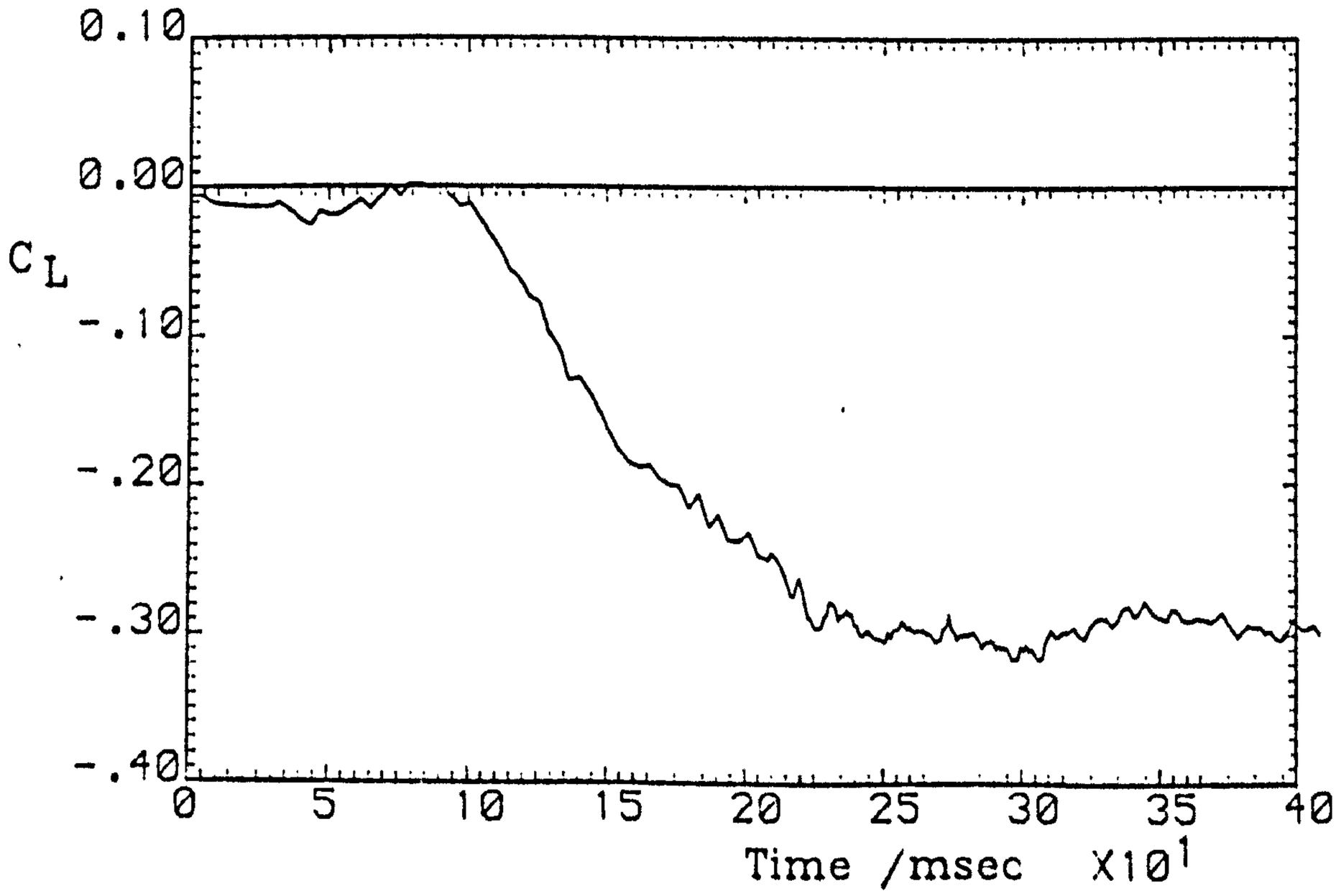

Fig. 5.12(b) Aerofoil lift time history

Run 3005

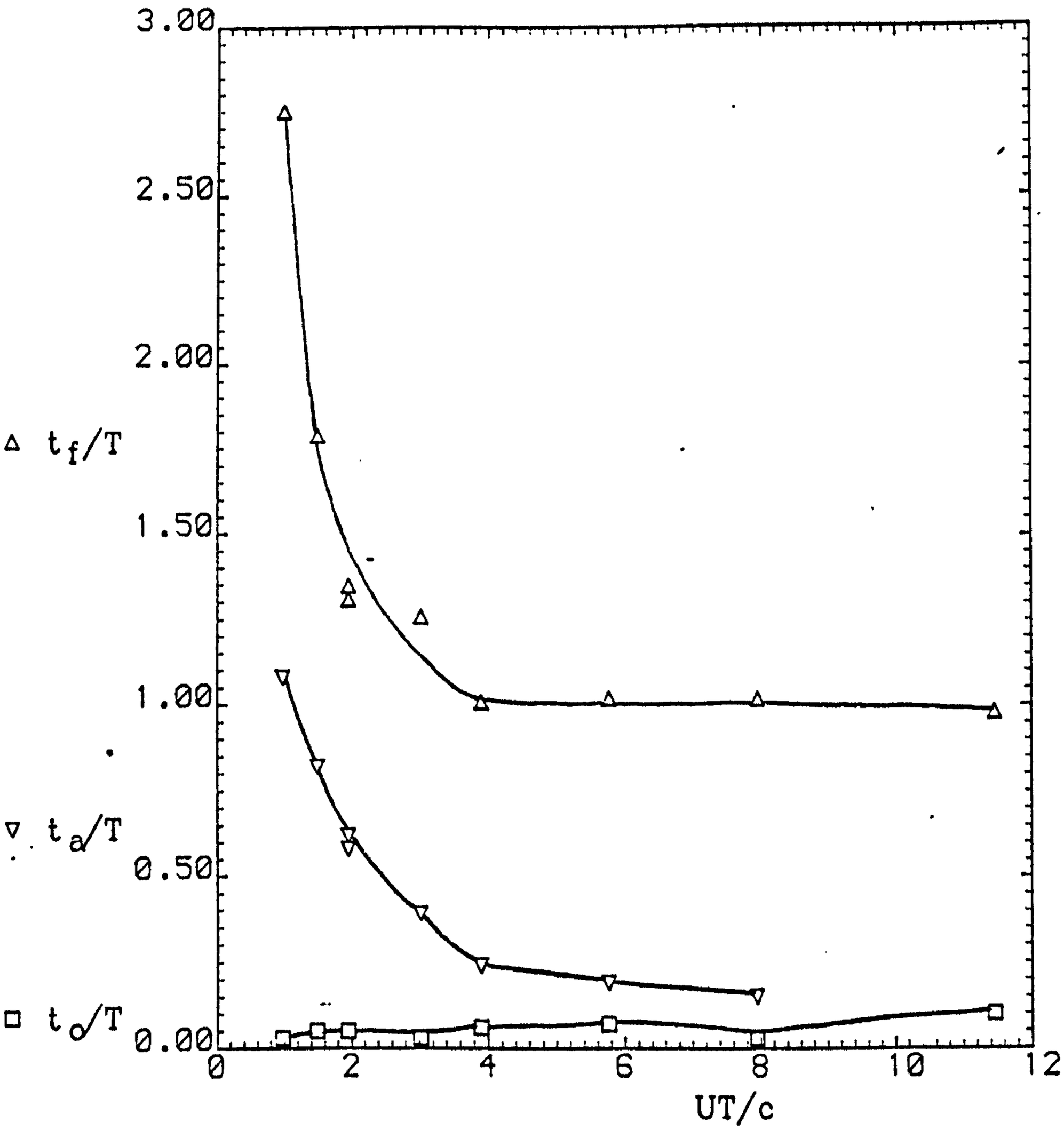

Spoiler configuration: Upper-surface,		
70% chord, gap opened, perforations closed		
α= 0.0°	U=10-20m/s	T=40-235msec
Data from run sequence 3001-3009		

Fig. 5.13 Correlation of delay times for spoiler extension

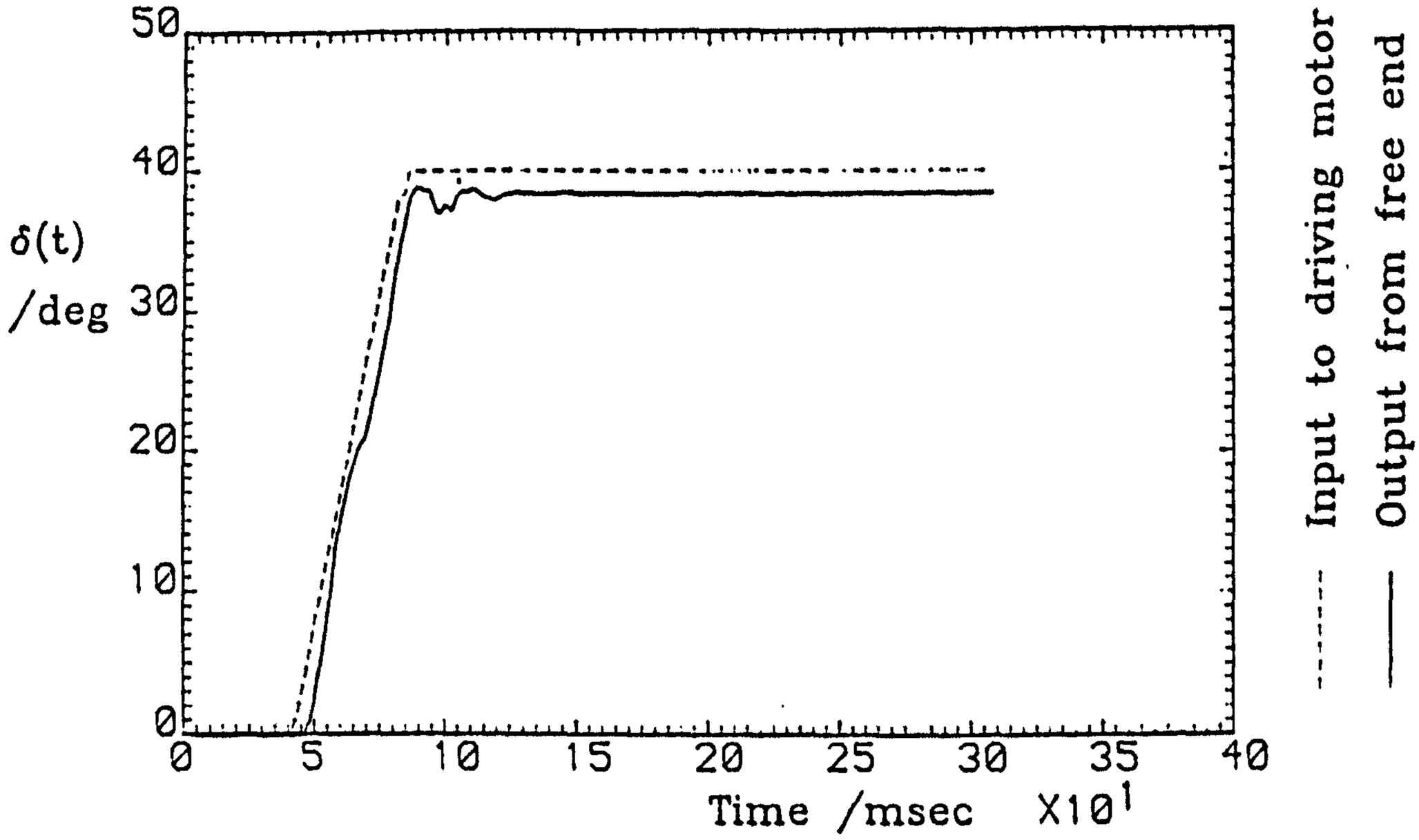

Fig. 5.14(a) Spoiler displacement trace

Spoiler configuration: Upper-surface,		
70% chord, gap closed, perforations closed		
α= 0.0°	U=20.0m/s	$\dot{\delta}$=990°/s

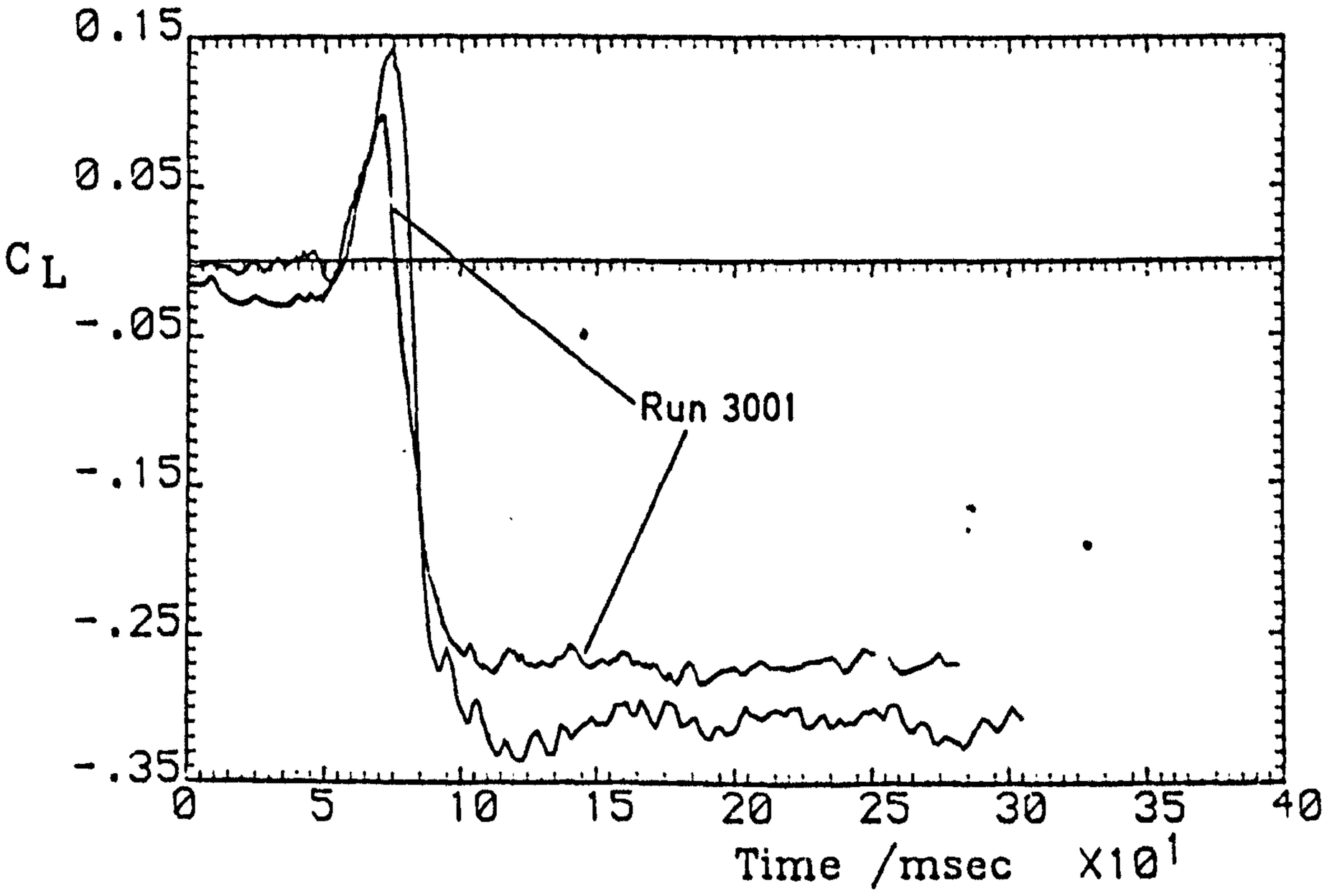

Fig. 5.14(b) Aerofoil lift time history

Run 3201

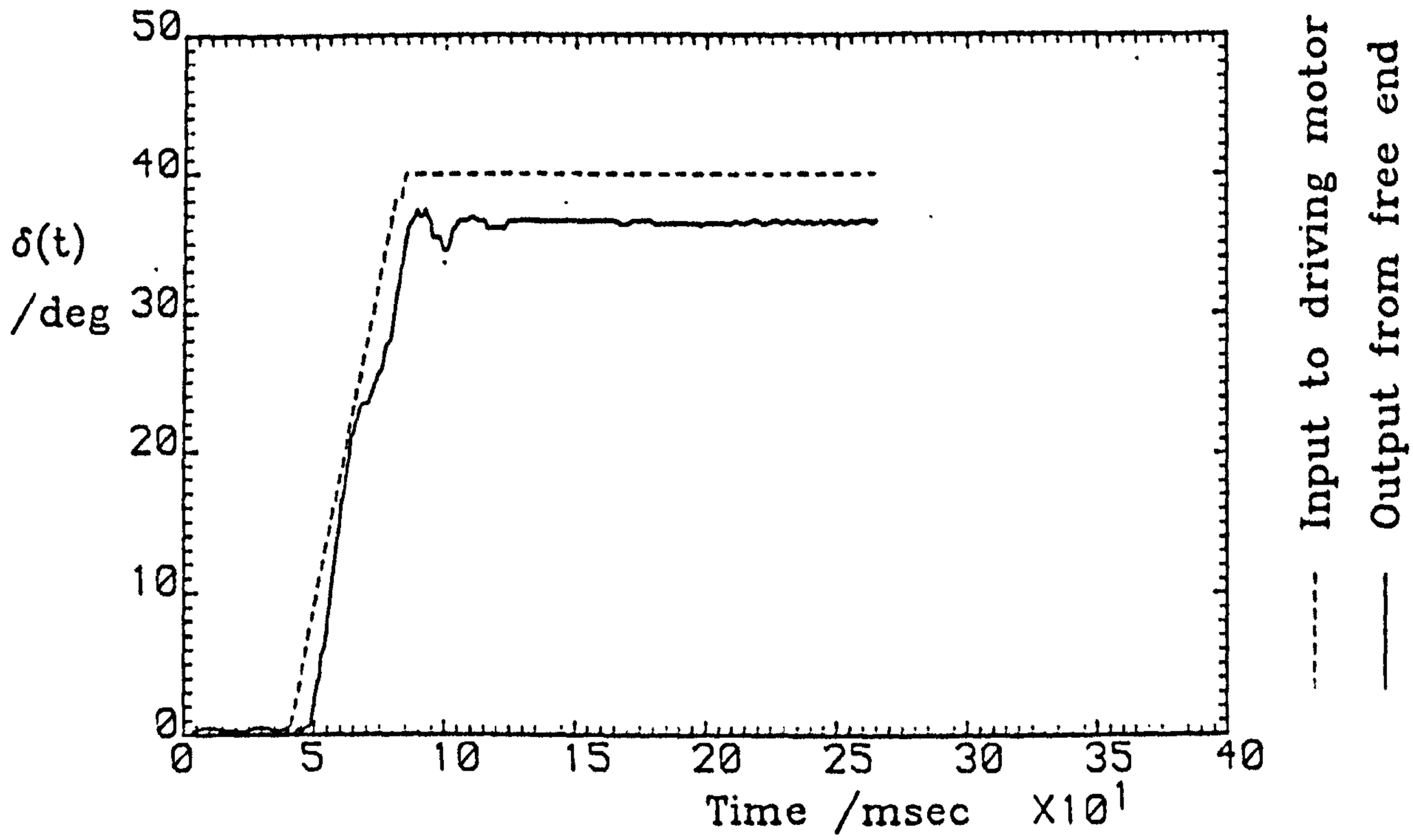

Fig. 5.15(a) Spoiler displacement trace

Spoiler configuration: Upper-surface,		
70% chord, gap opened, perforations opened		
α= 0.0°	U=20.0m/s	$\dot{\delta}$=990°/s

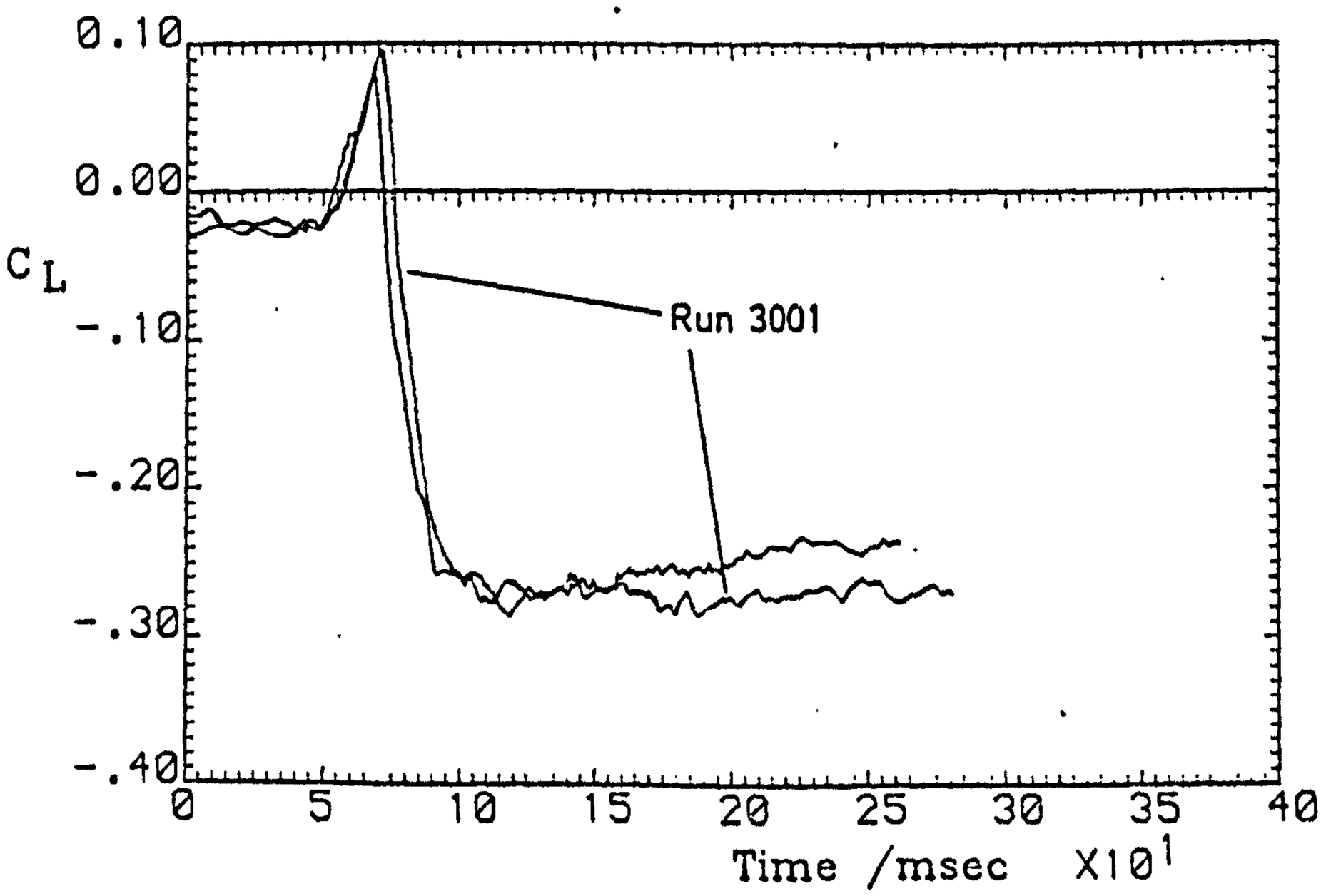

Fig. 5.15(b) Aerofoil lift time history

Run 2001

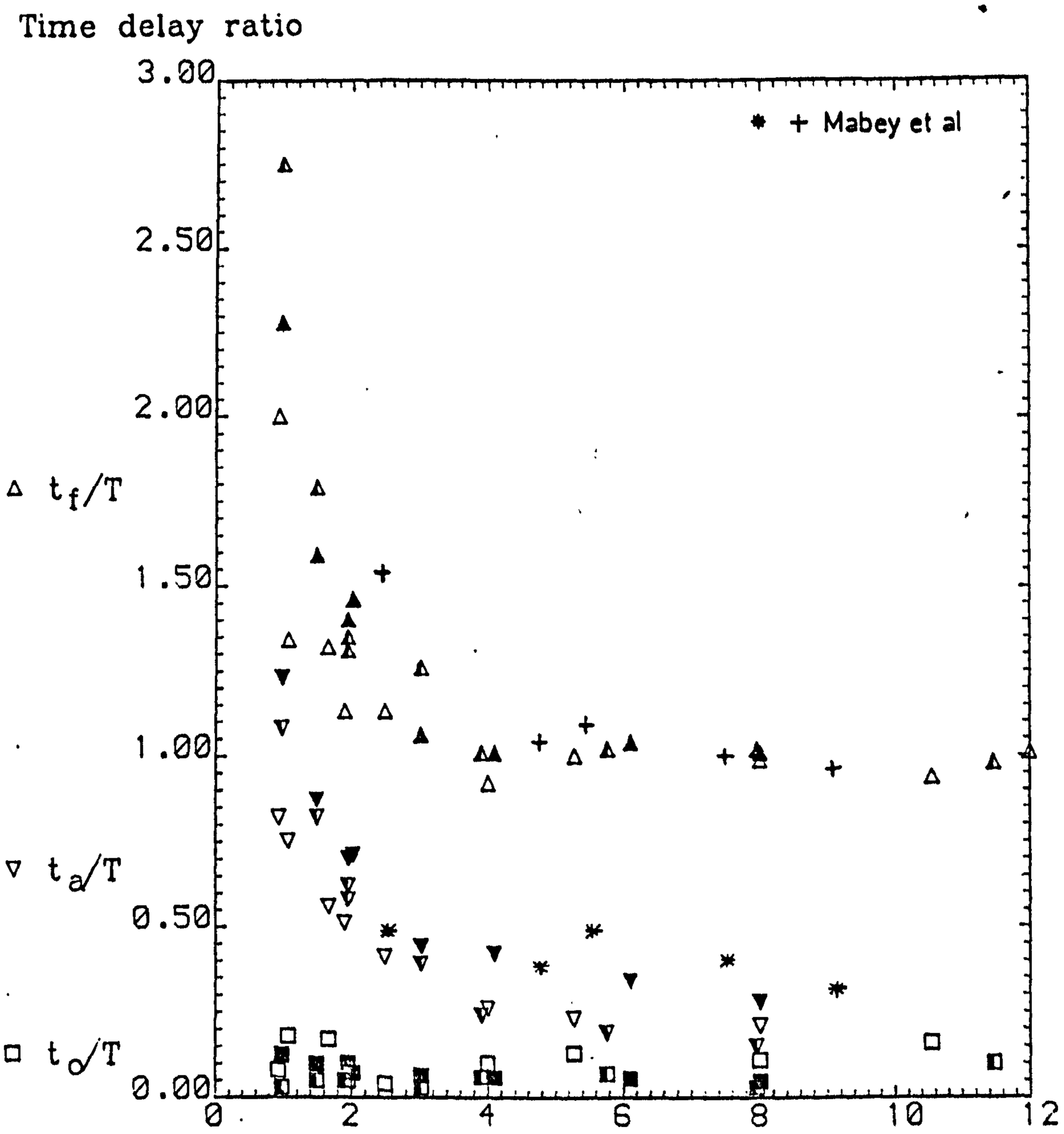

Spoiler geometry: "Solid"(filled symbols),		
"Gapped"(half-filled), "Perforated"(empty)		
α= 0.0°	U=10-20m/s	T=39-246msec
Data from Runs 300X,320X,200X (X=1-9)		

Fig. 5.16 Correlation of delay times for spoiler extension

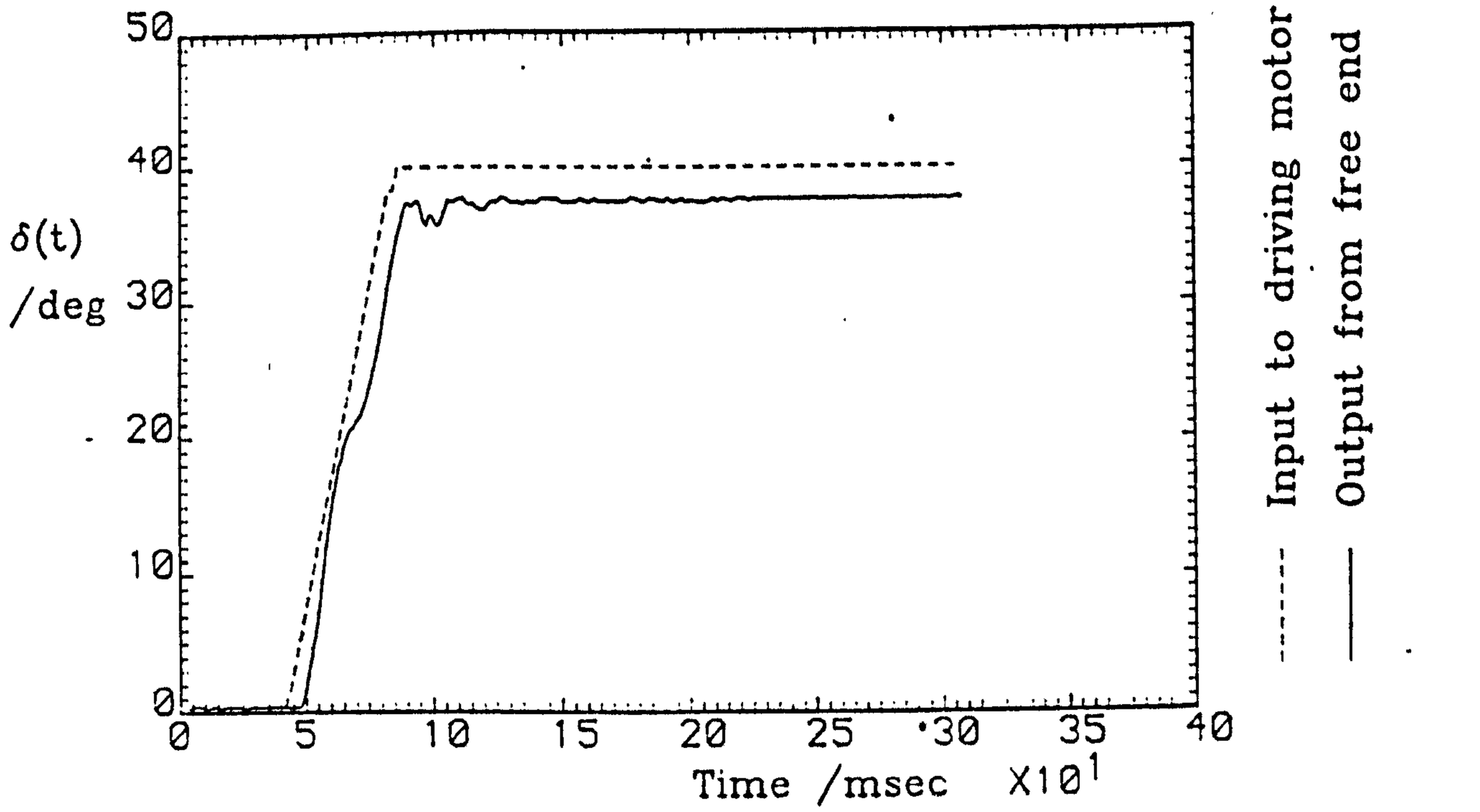

Fig. 5.17(a) Spoiler displacement trace

Spoiler configuration: Upper-surface,		
70% chord, gap opened, perforations closed		
α=14.0°	U=20.0m/s	$\dot{\delta}$=990°/s

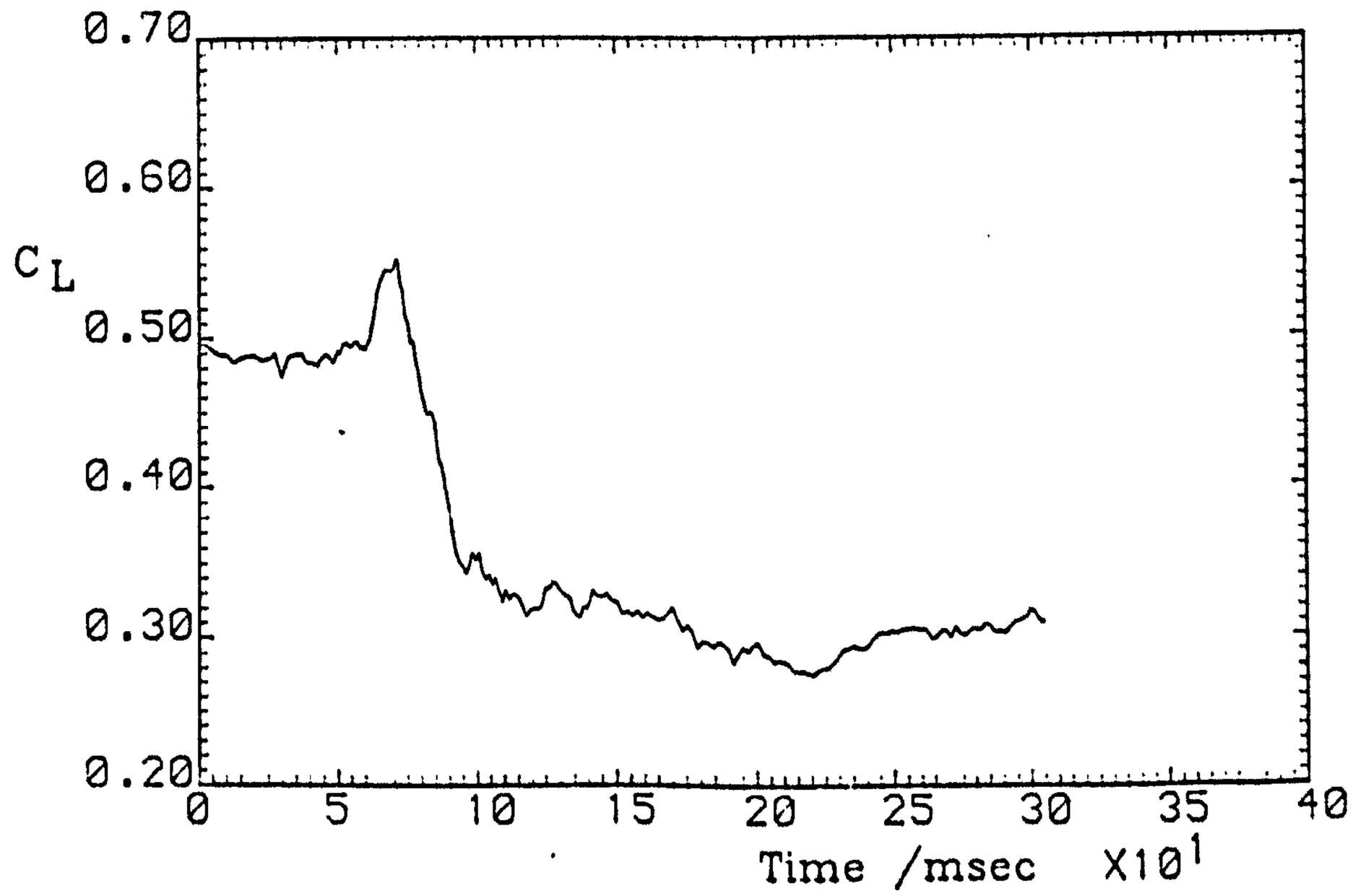

Fig. 5.17(b) Aerofoil lift time history

Run 5001

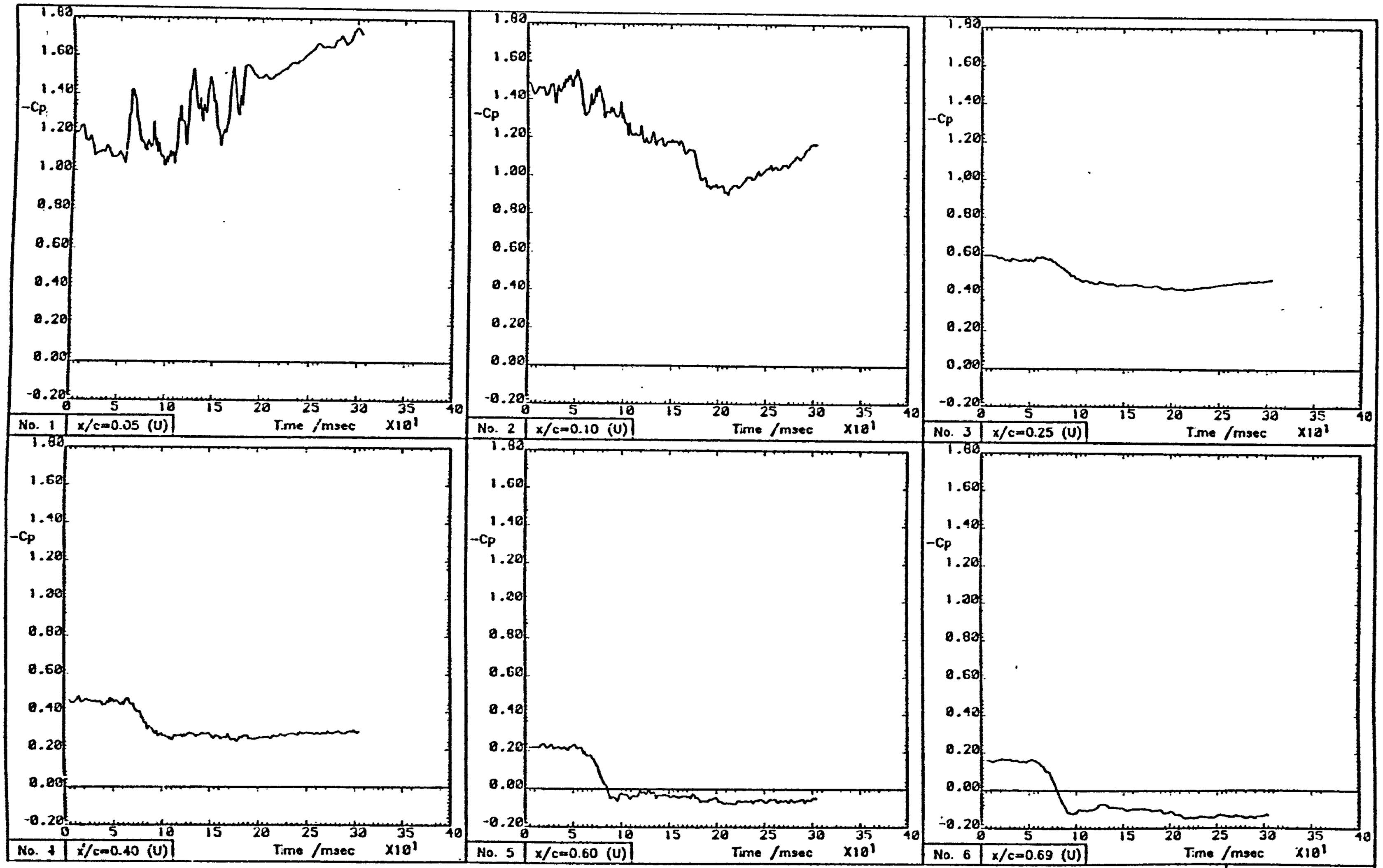

Fig. 5.18 (a) Pressure signal time histories

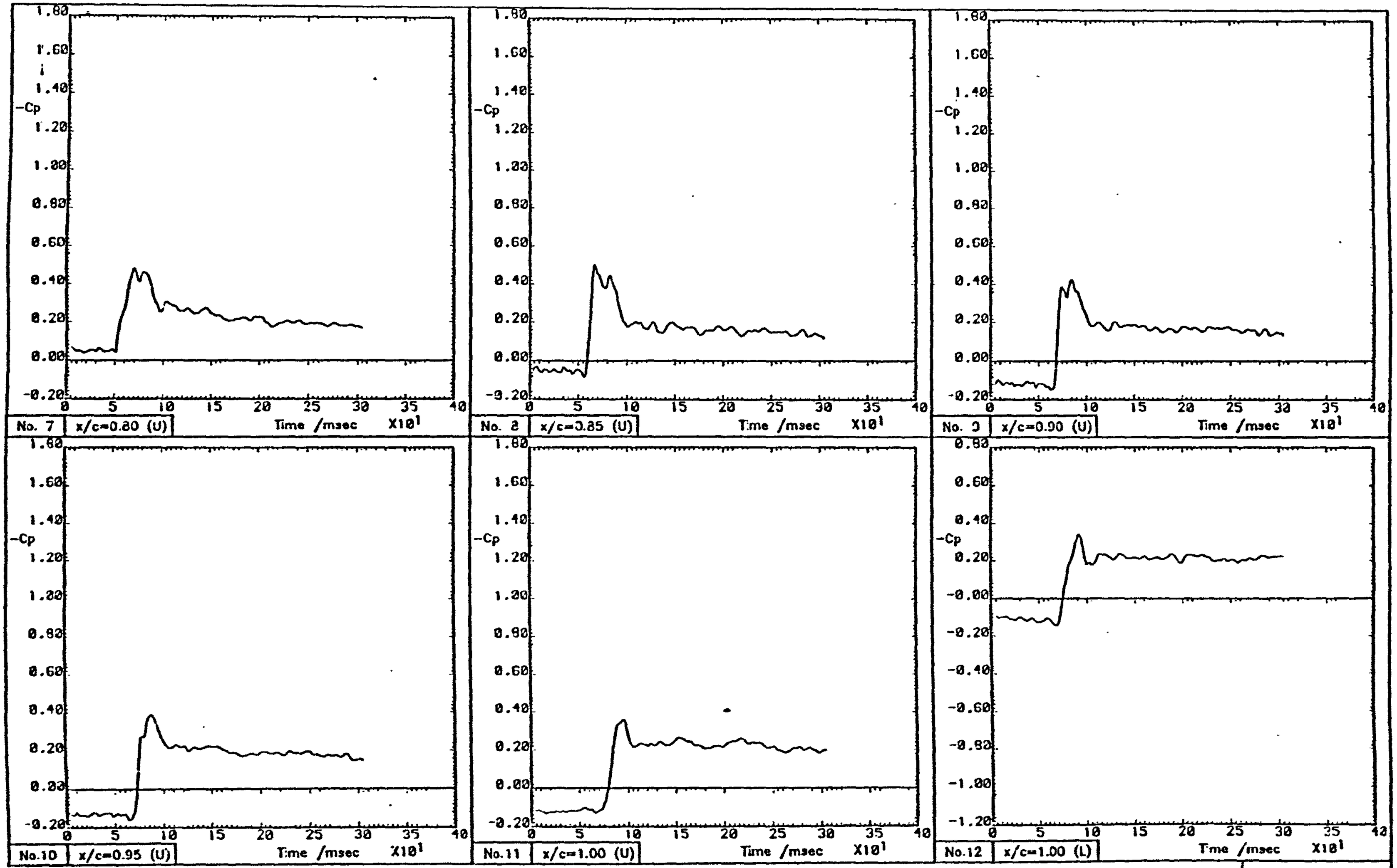

Fig. 5.18(b) Pressure signal time histories

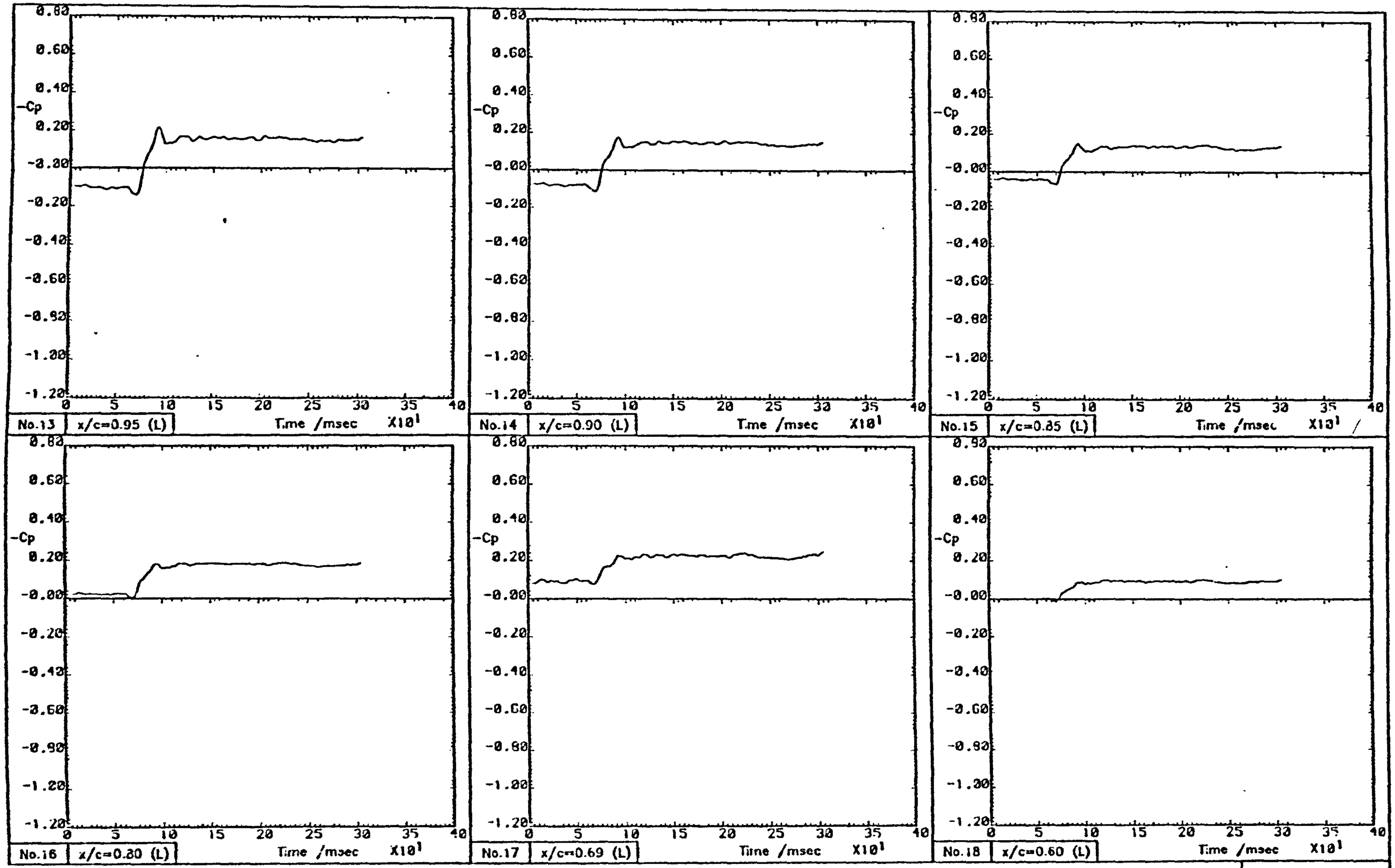

Run 5001

Fig. 5.18(c) Pressure signal time histories

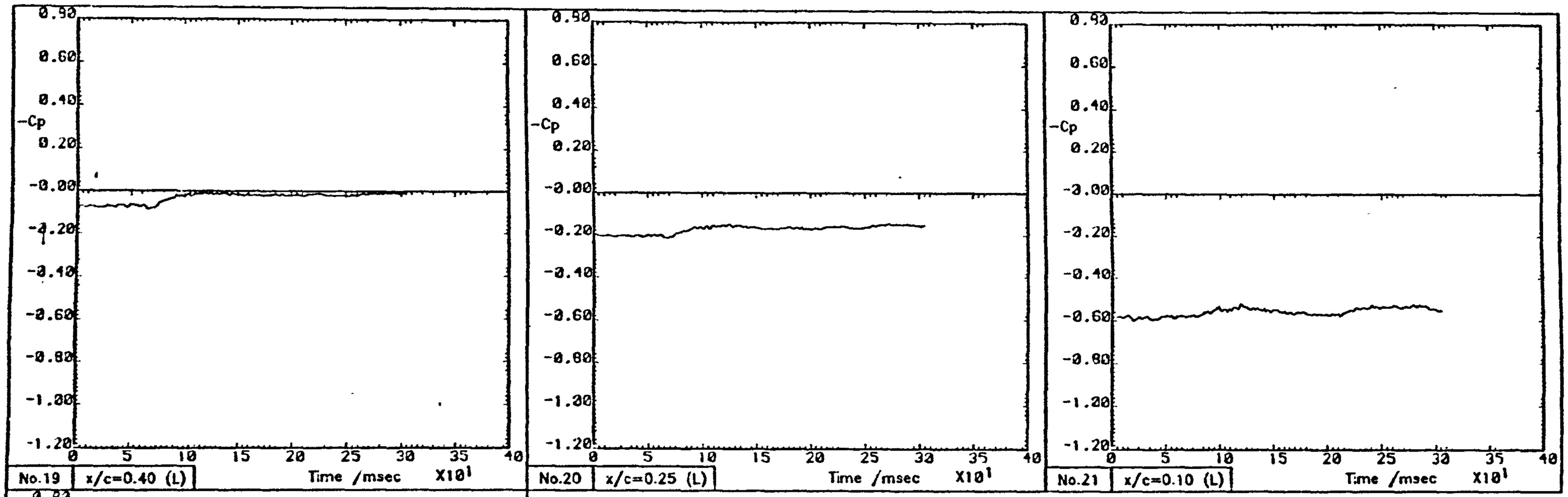

Fig. 5.18(d) Pressure signal time histories

Run 5001

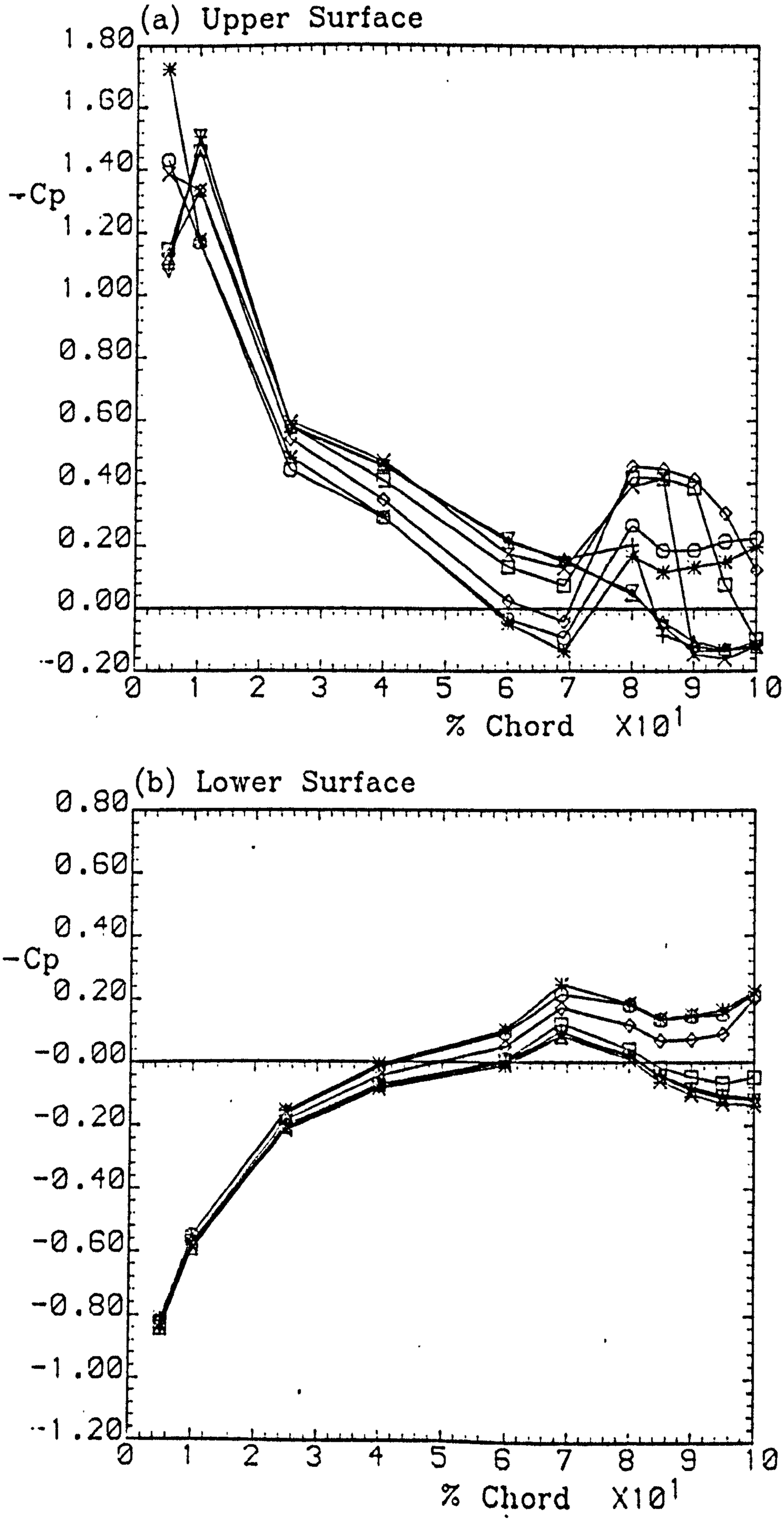

	t /ms	δ(t) /deg
△	37	0.4
▽	46	1.7
+	55	13.7
×	64	20.8
□	73	25.9
◇	82	35.5
○	142	37.6
✳	304	37.6

Fig 5.19 Time-varying pressure distributions

Run 5001

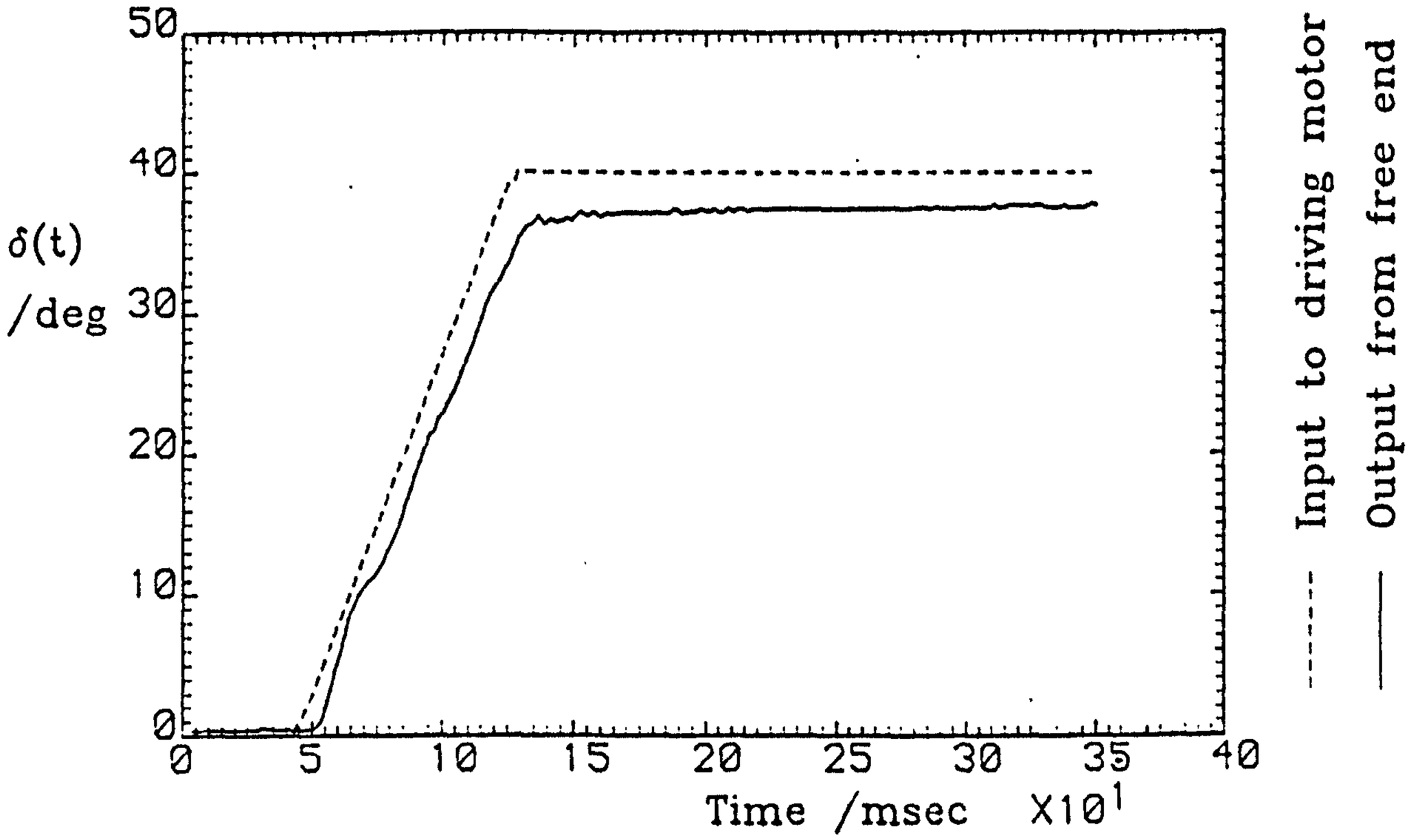

Fig. 5.20(a) Spoiler displacement trace

Spoiler configuration: Upper-surface,		
70% chord, gap opened, perforations closed		
α=14.0°	U=20.0m/s	$\dot{\delta}$=500°/s

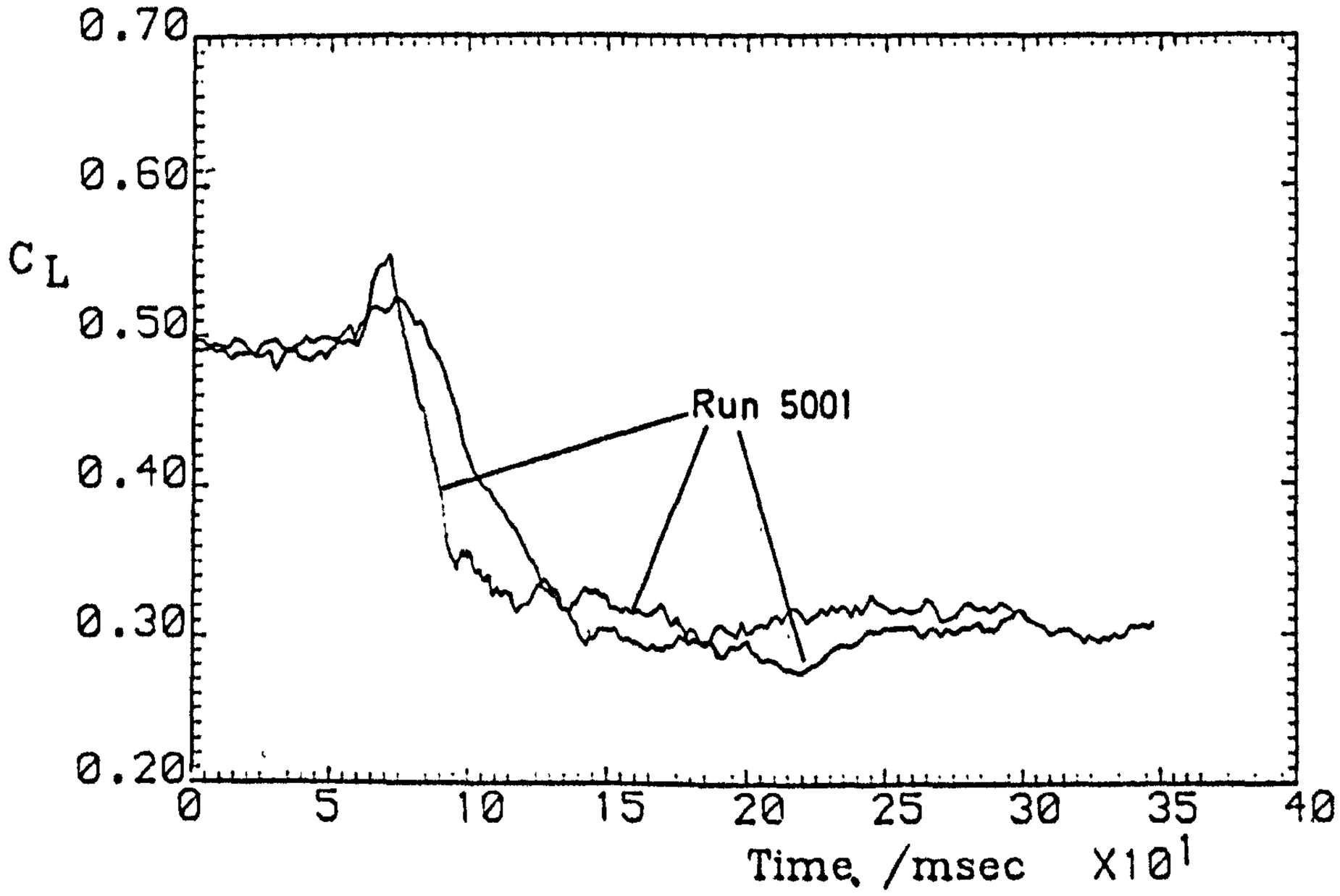

Fig. 5.20(b) Aerofoil lift time history

Run 5003

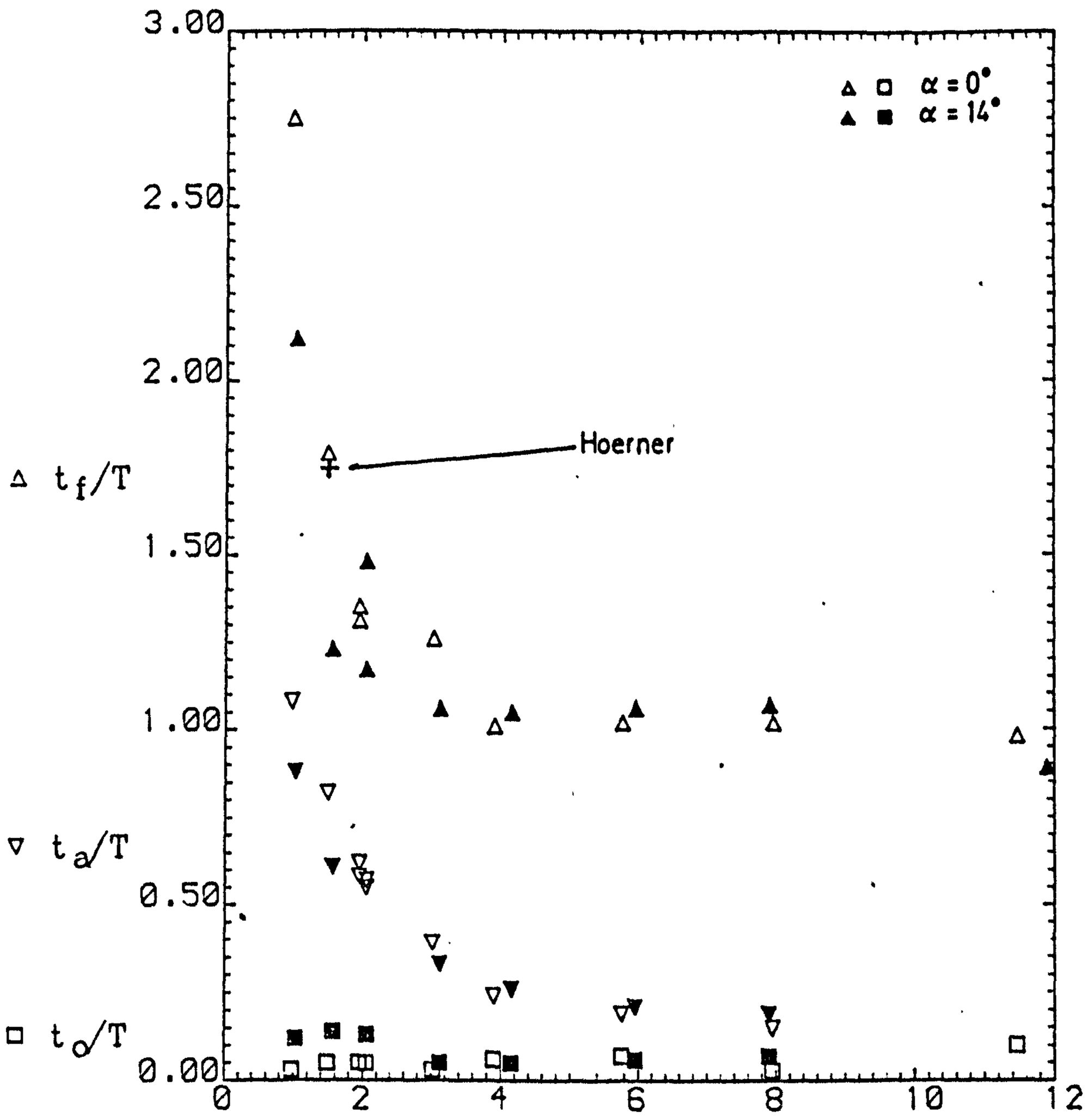

Spoiler configuration:		Upper-surface,
70% chord, gap opened, perforations closed		
α=0–14°	U=10–20m/s	T=40–235msec
Data from Runs 300X, 500X (X=1–9)		

Fig. 5.21 Correlation of delay times for spoiler extension

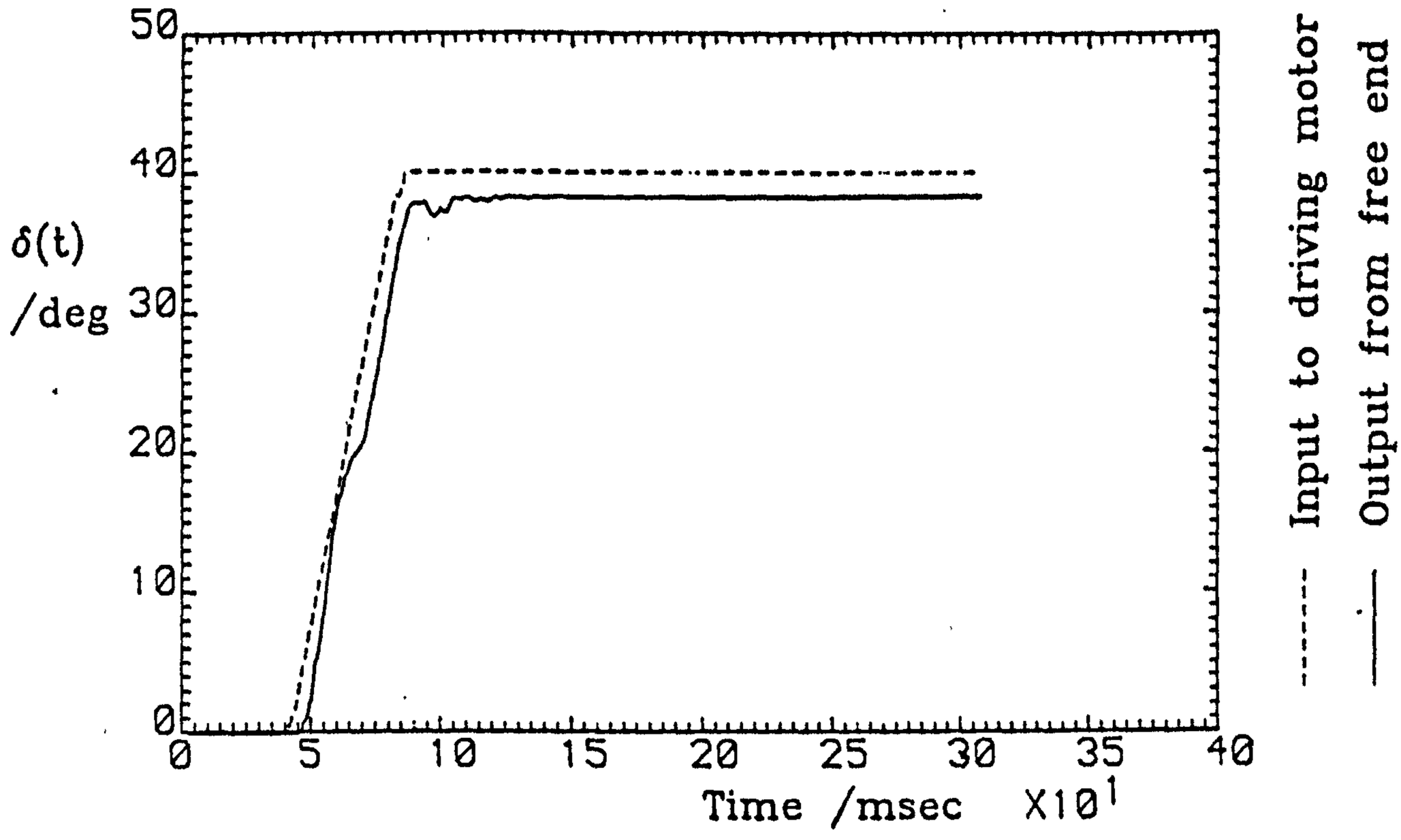

Fig.5.22(a) Spoiler displacement trace

Spoiler configuration: Upper-surface,		
70% chord, gap closed, perforations closed		
α=14.0°	U=20.0m/s	$\dot{\delta}$=990°/s

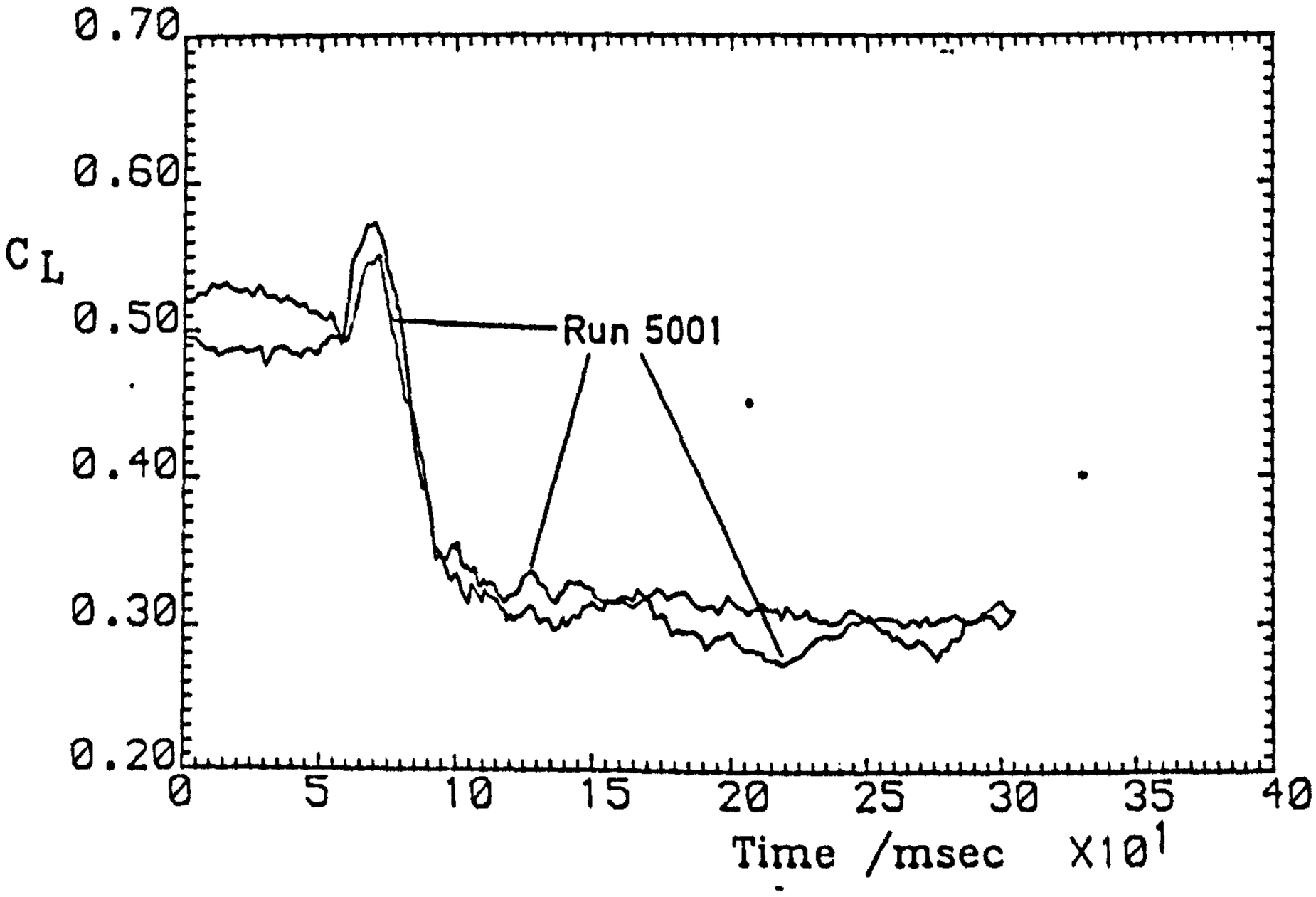

Fig. 5.22(b) Aerofoil lift time history

Run 5101

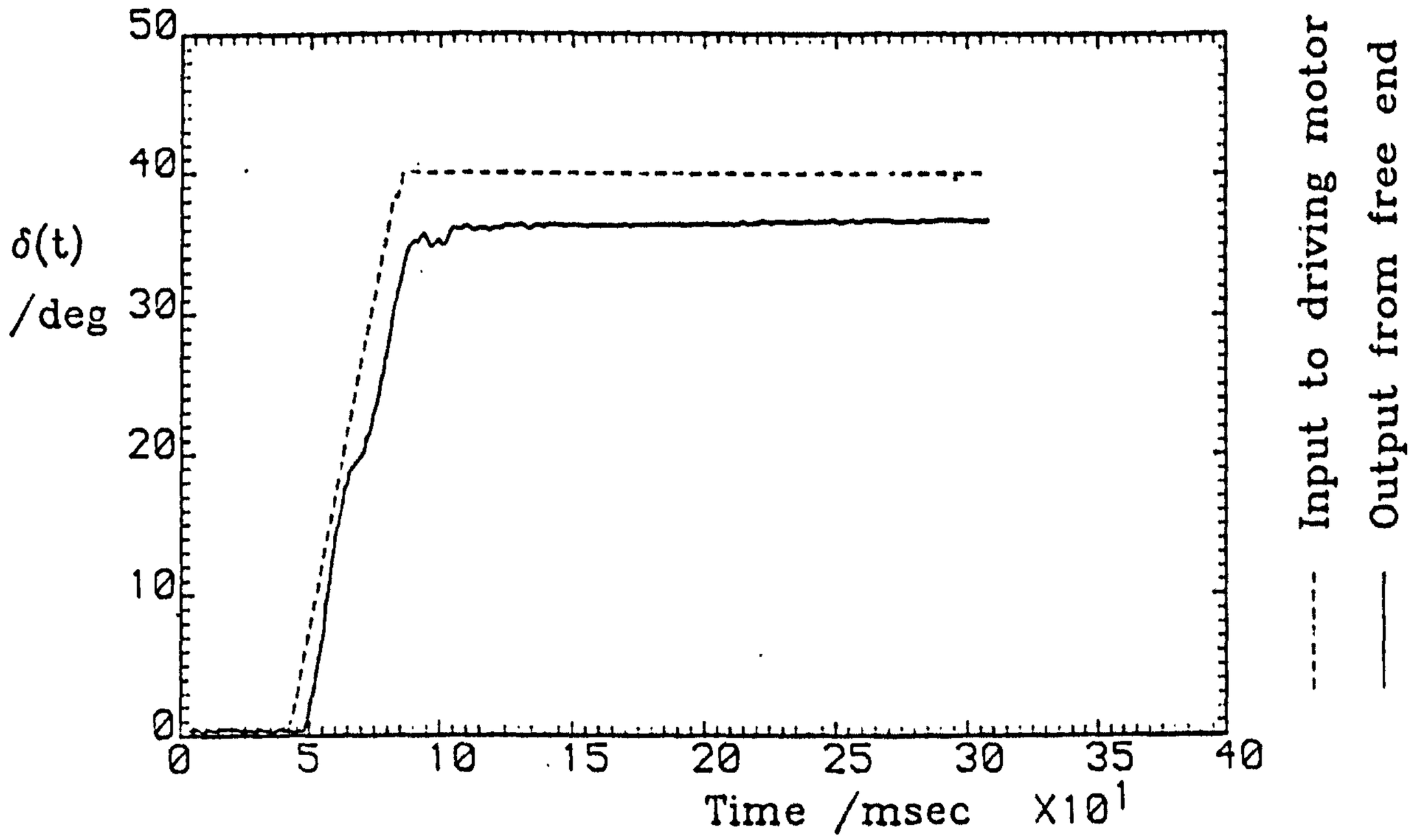

Fig. 5.23(a) Spoiler displacement trace

Spoiler configuration: Upper-surface,		
70% chord, gap opened, perforations opened		
α=14.0°	U=20.0m/s	$\dot{\delta}$=990°/s

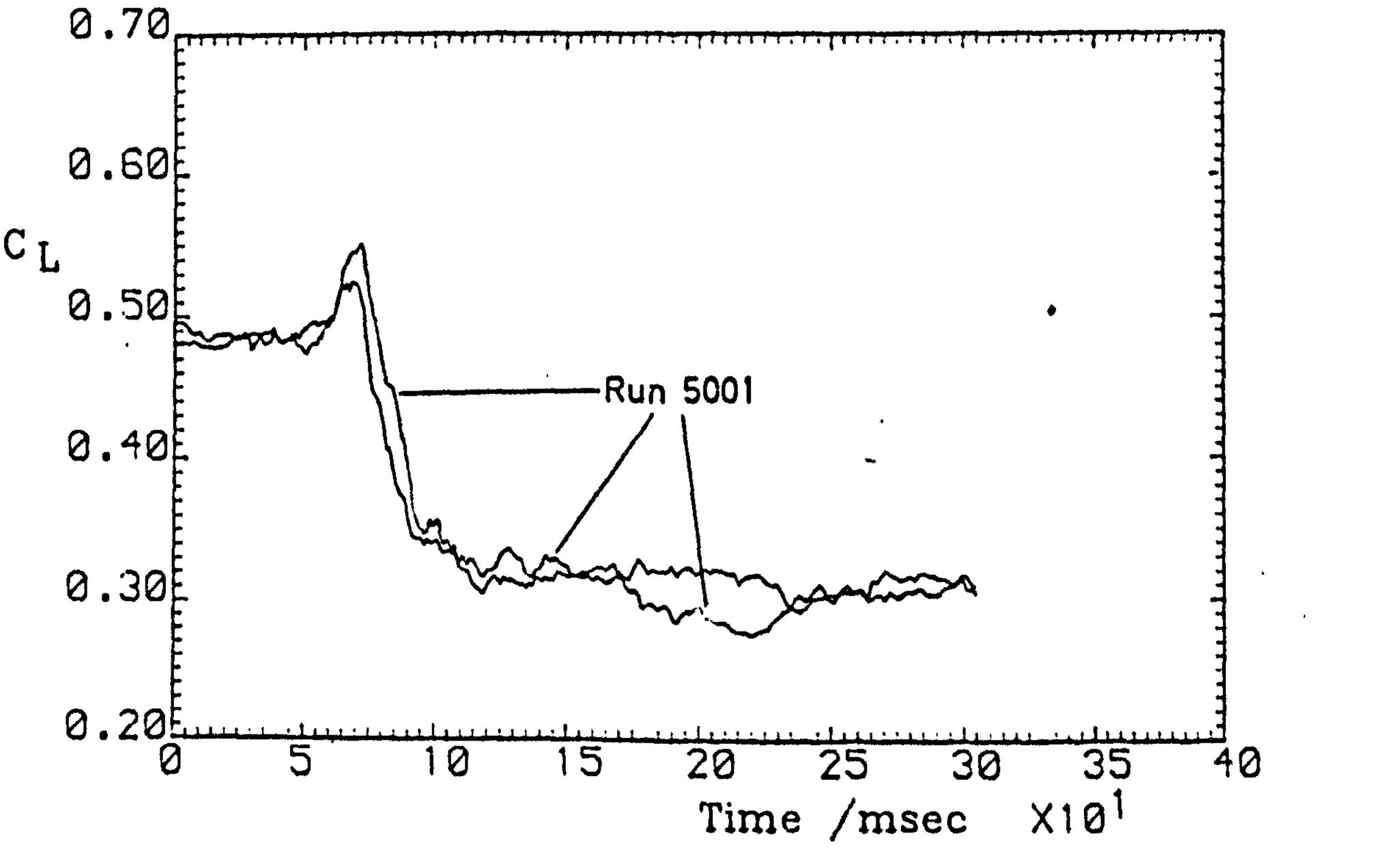

Fig. 5.23(b) Aerofoil lift time history

Run 4011

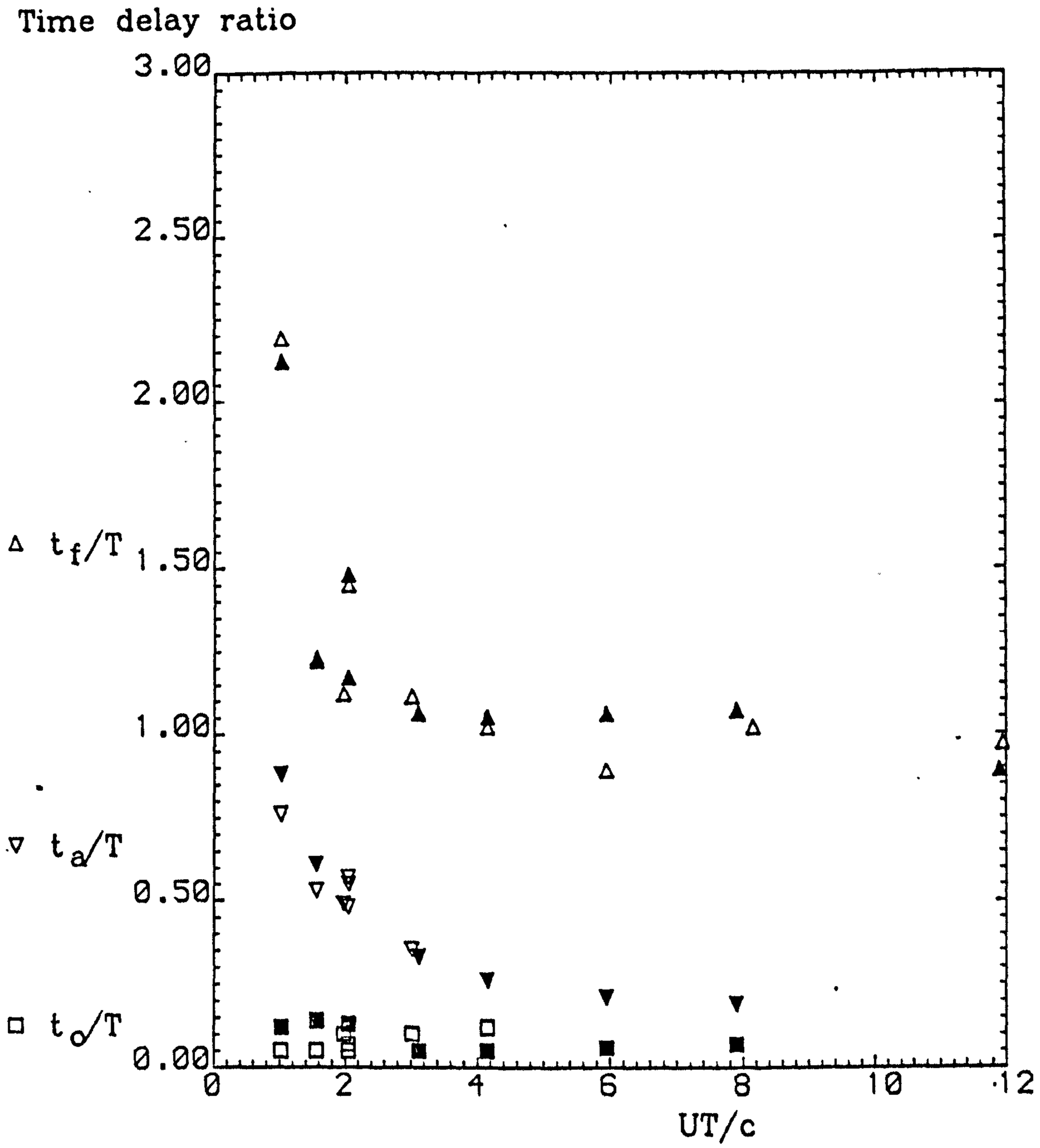

Spoiler geometry: "Gapped"(filled symbols),		
"Perforated"(empty symbols)		
α=14.0°	U=10–20m/s	T=42–245msec
Data from Runs 500X, 401X (X=1–9)		

Fig. 5.24 Correlation of delay times for spoiler extension

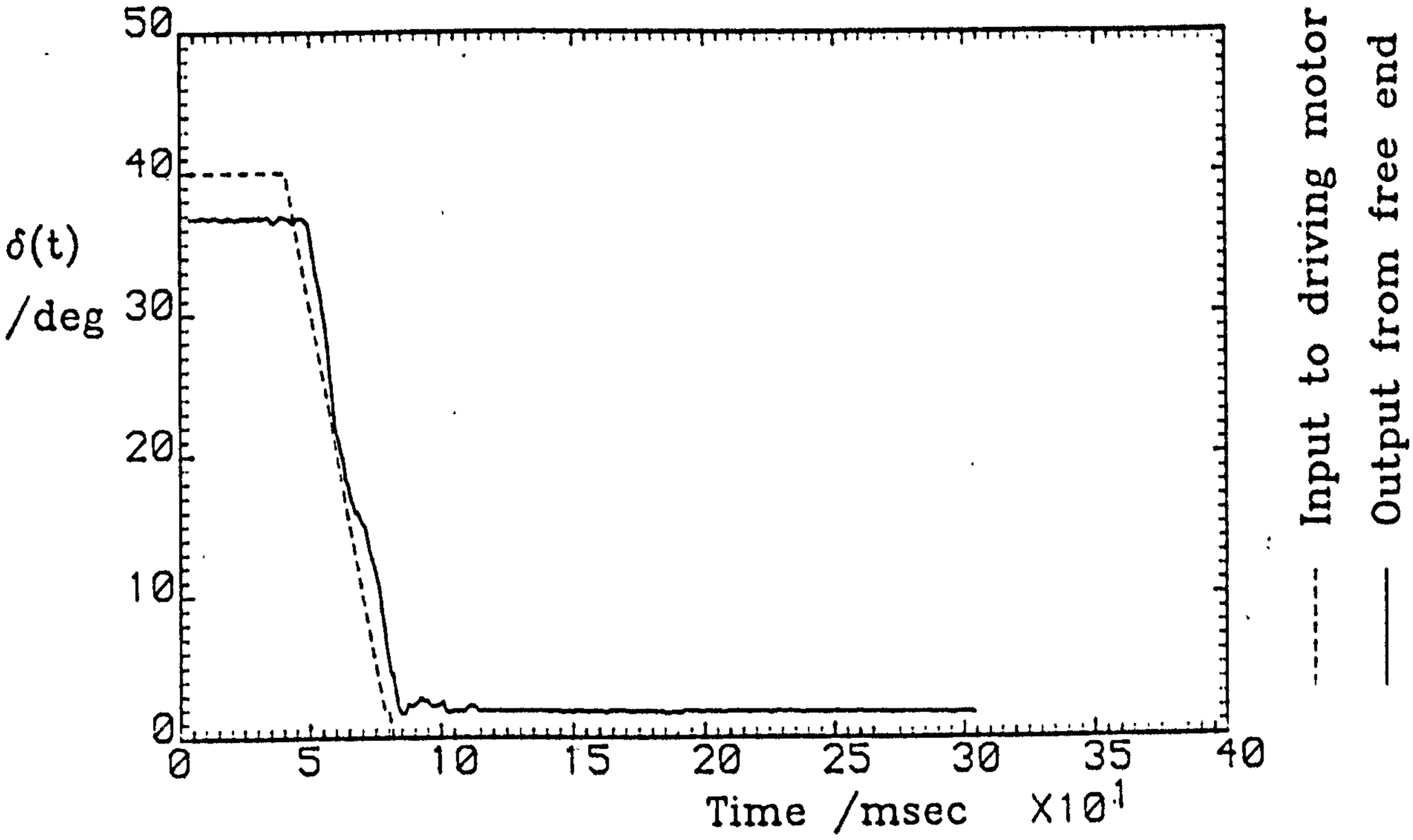

Fig. 5.25(a) Spoiler displacement trace

Spoiler configuration: Upper-surface,		
70% chord, gap opened, perforations closed		
α= 0.0°	U=20.0m/s	$\dot{\delta}$=990°/s

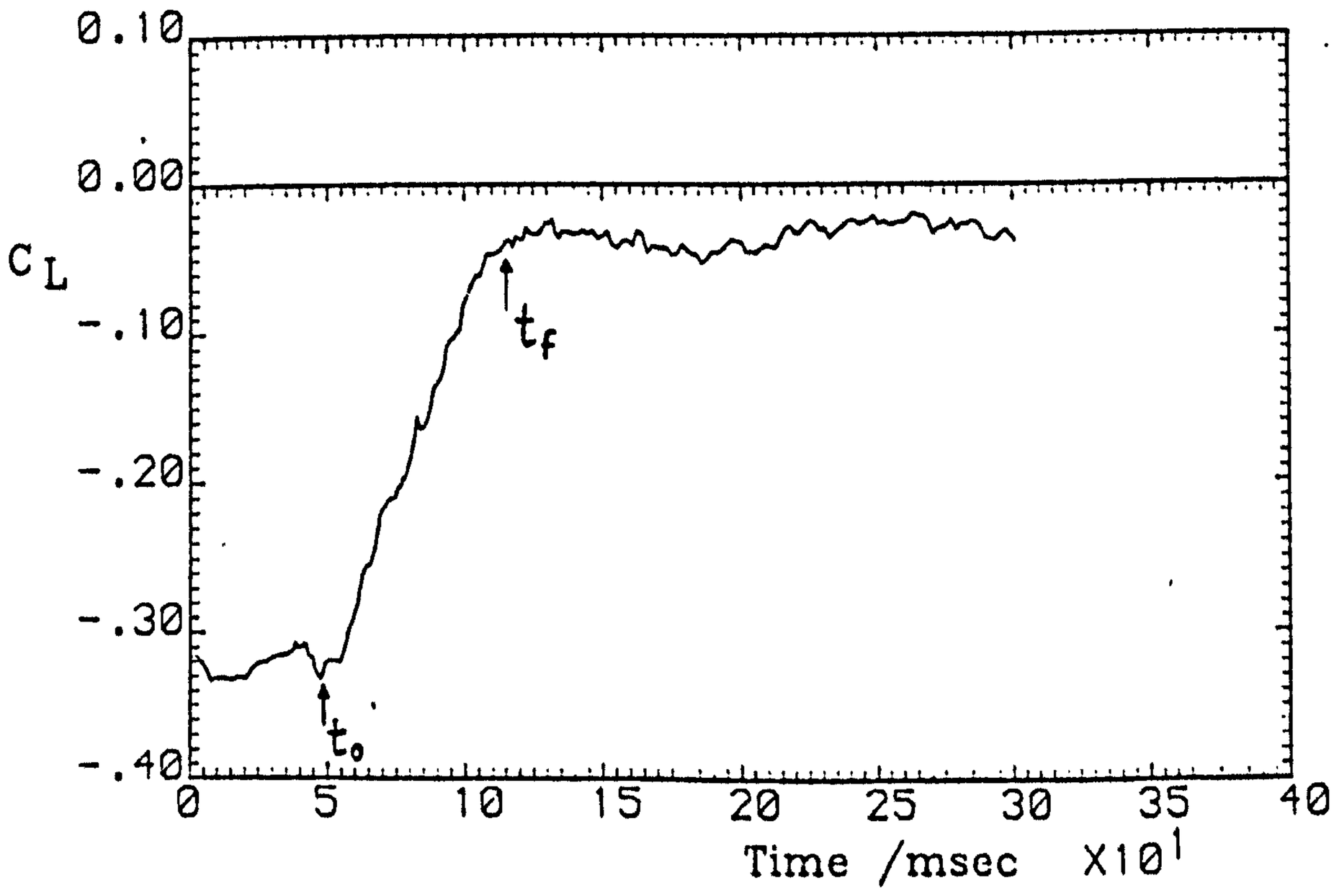

Fig. 5.25(b) Aerofoil lift time history

Run 3051

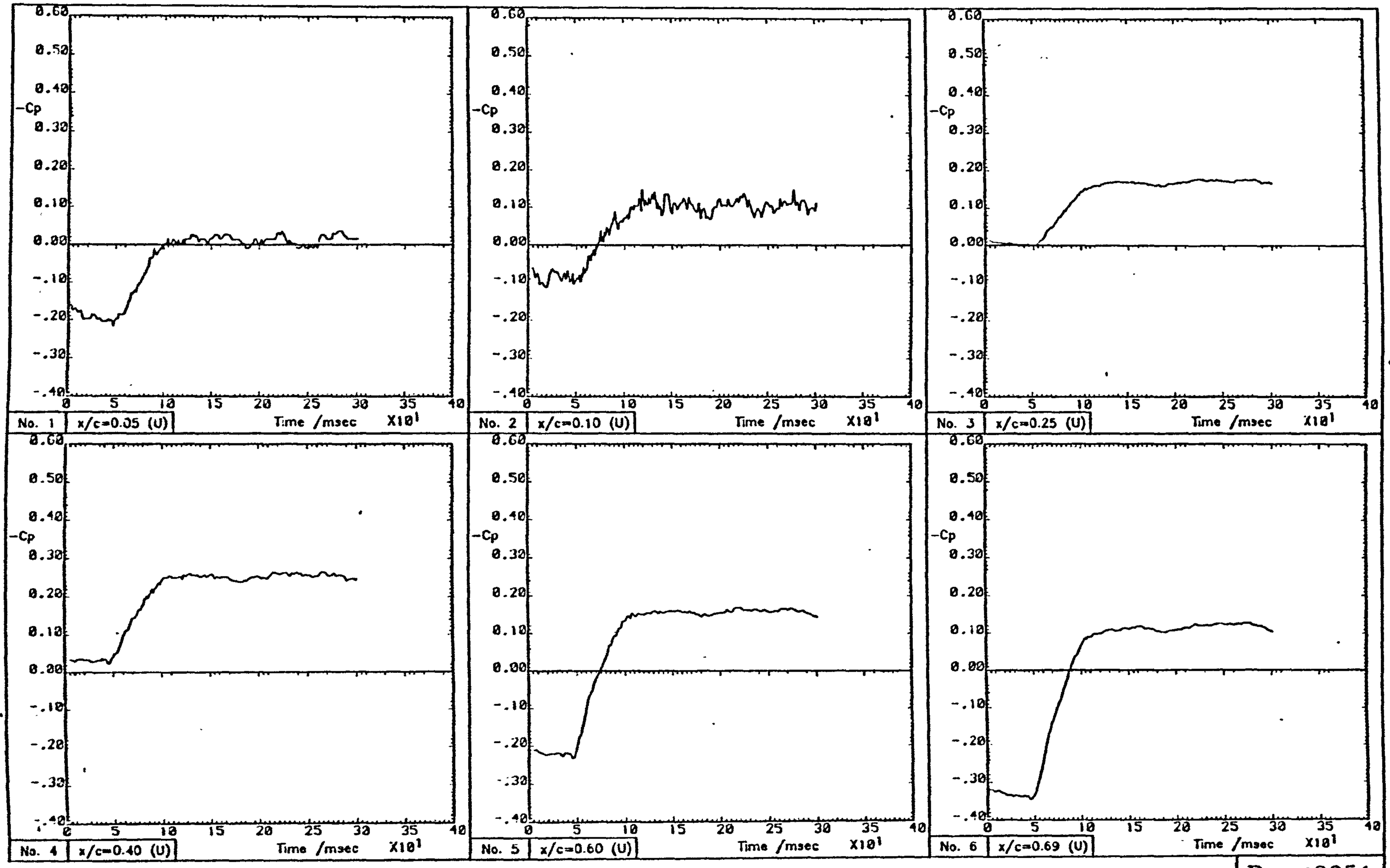

Fig. 5.26 (a) Pressure signal time histories

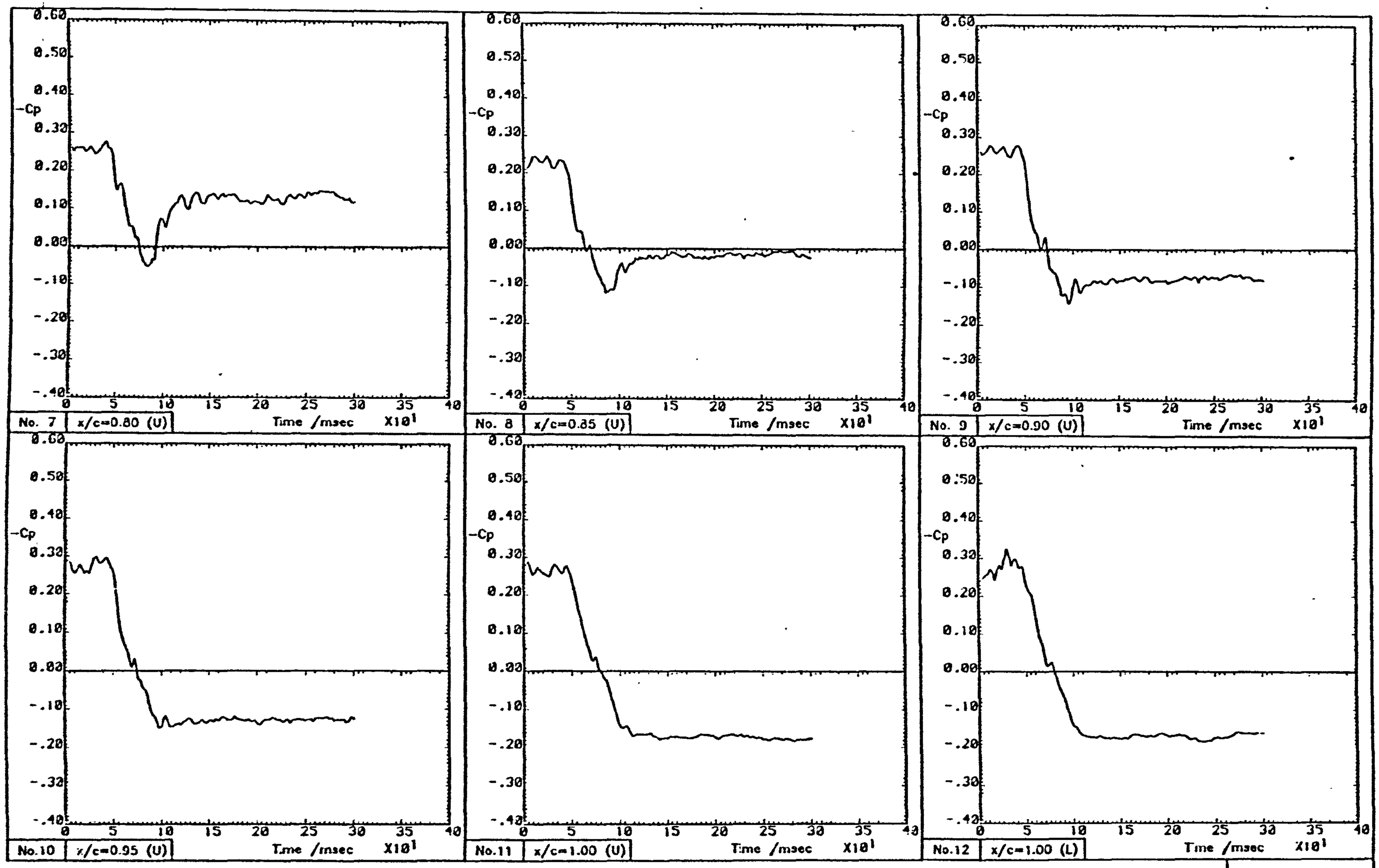

Fig. 5.26 (b) Pressure signal time histories

Run 3051

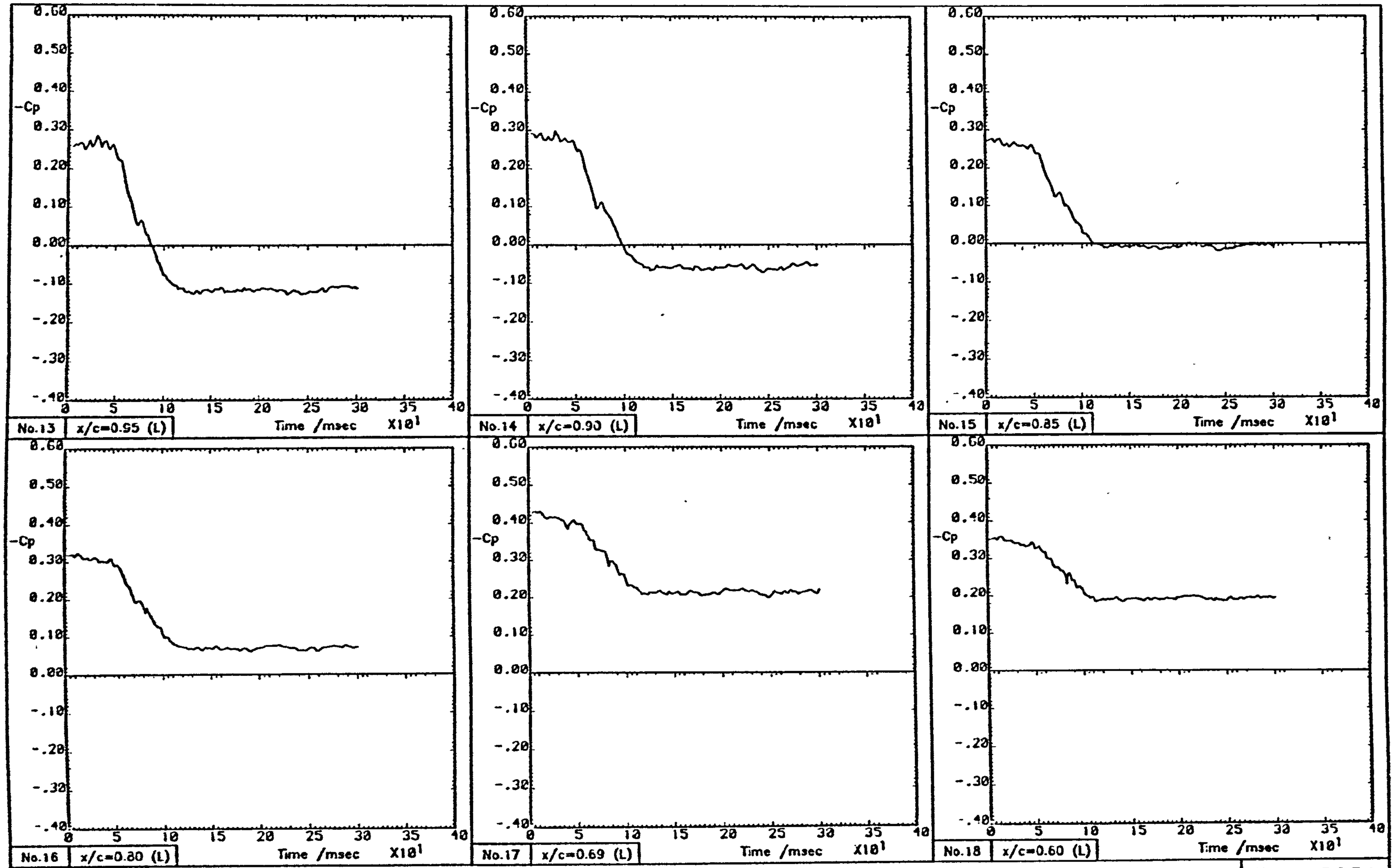

Fig. 5.26 (c) Pressure signal time histories

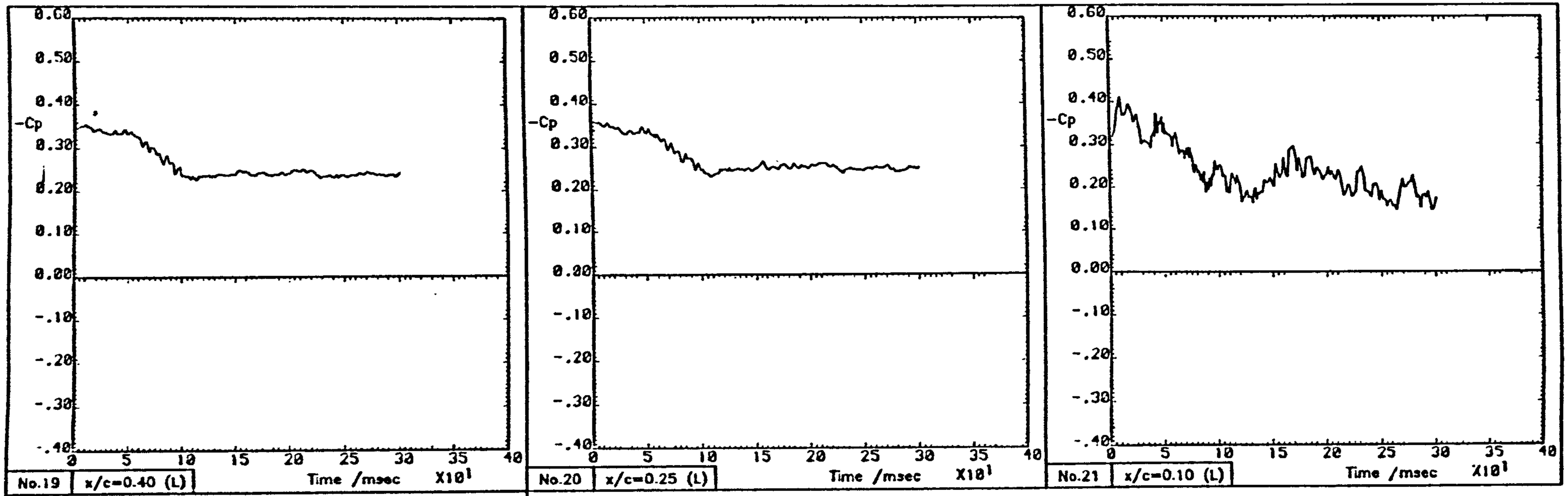

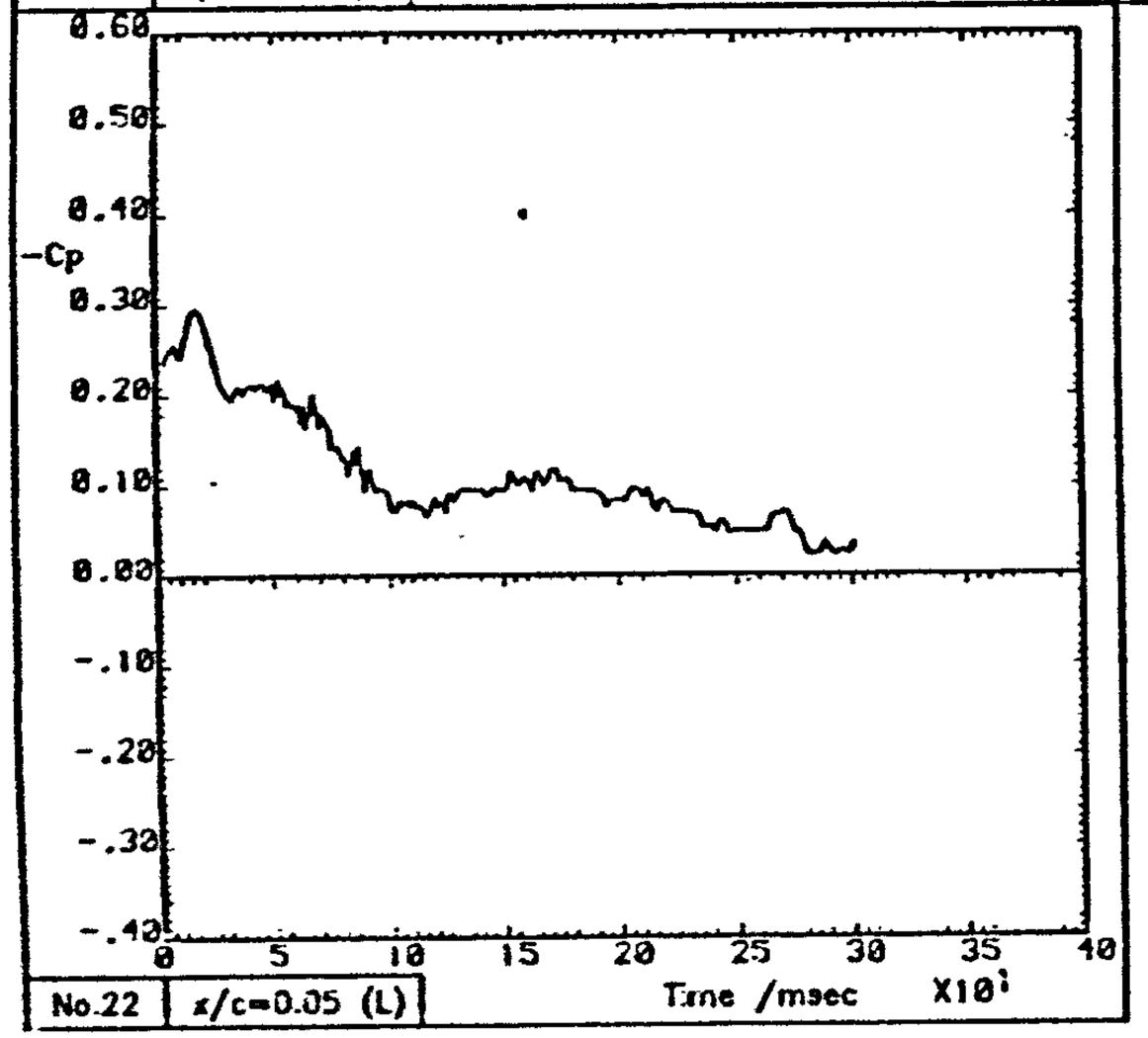

Fig. 5.26(d) Pressure signal time histories

Run 3051

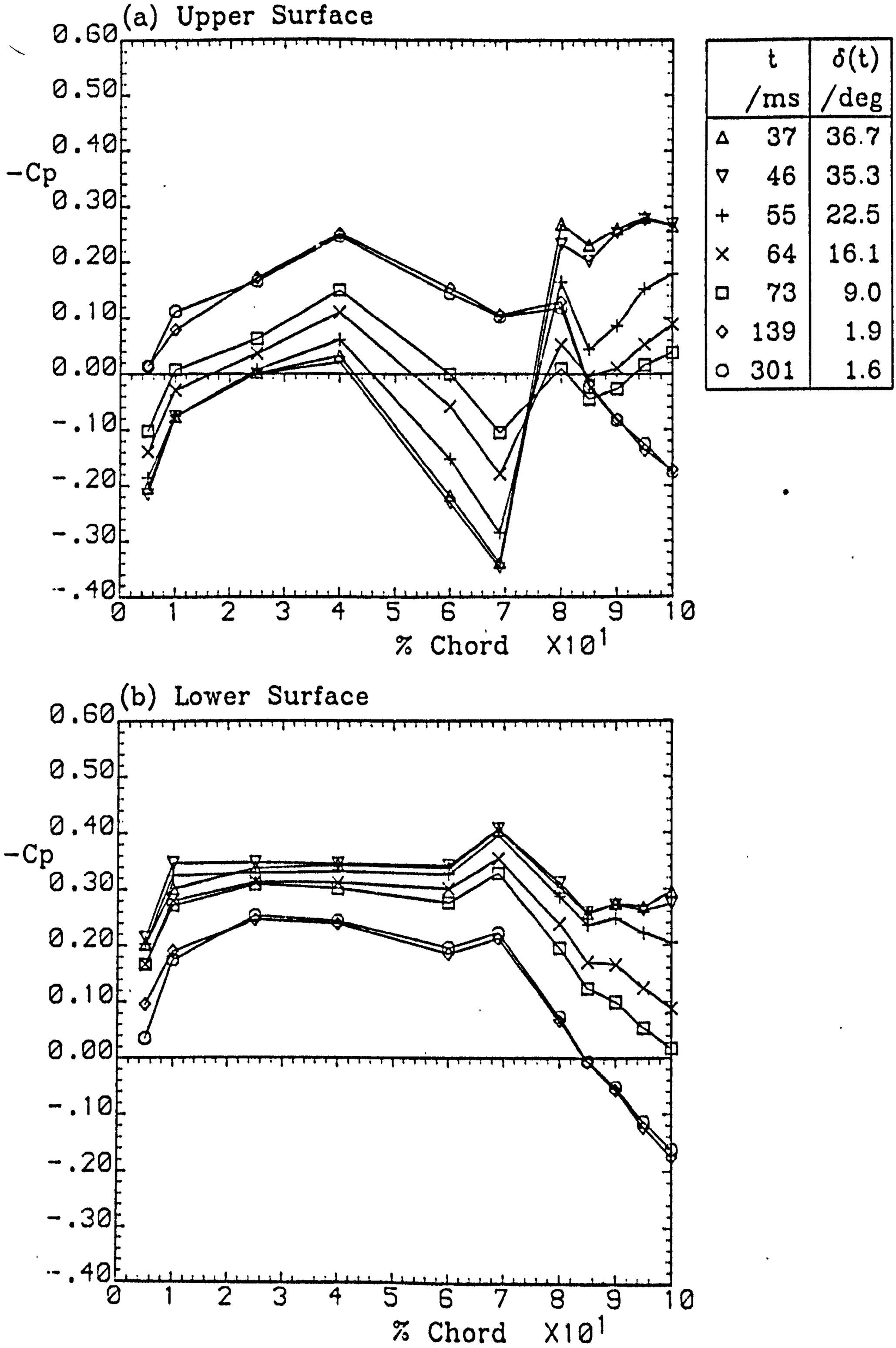

	t /ms	δ(t) /deg
△	37	36.7
▽	46	35.3
+	55	22.5
×	64	16.1
□	73	9.0
◇	139	1.9
○	301	1.6

Fig. 5.27 Time-varying pressure distributions

Run 3051

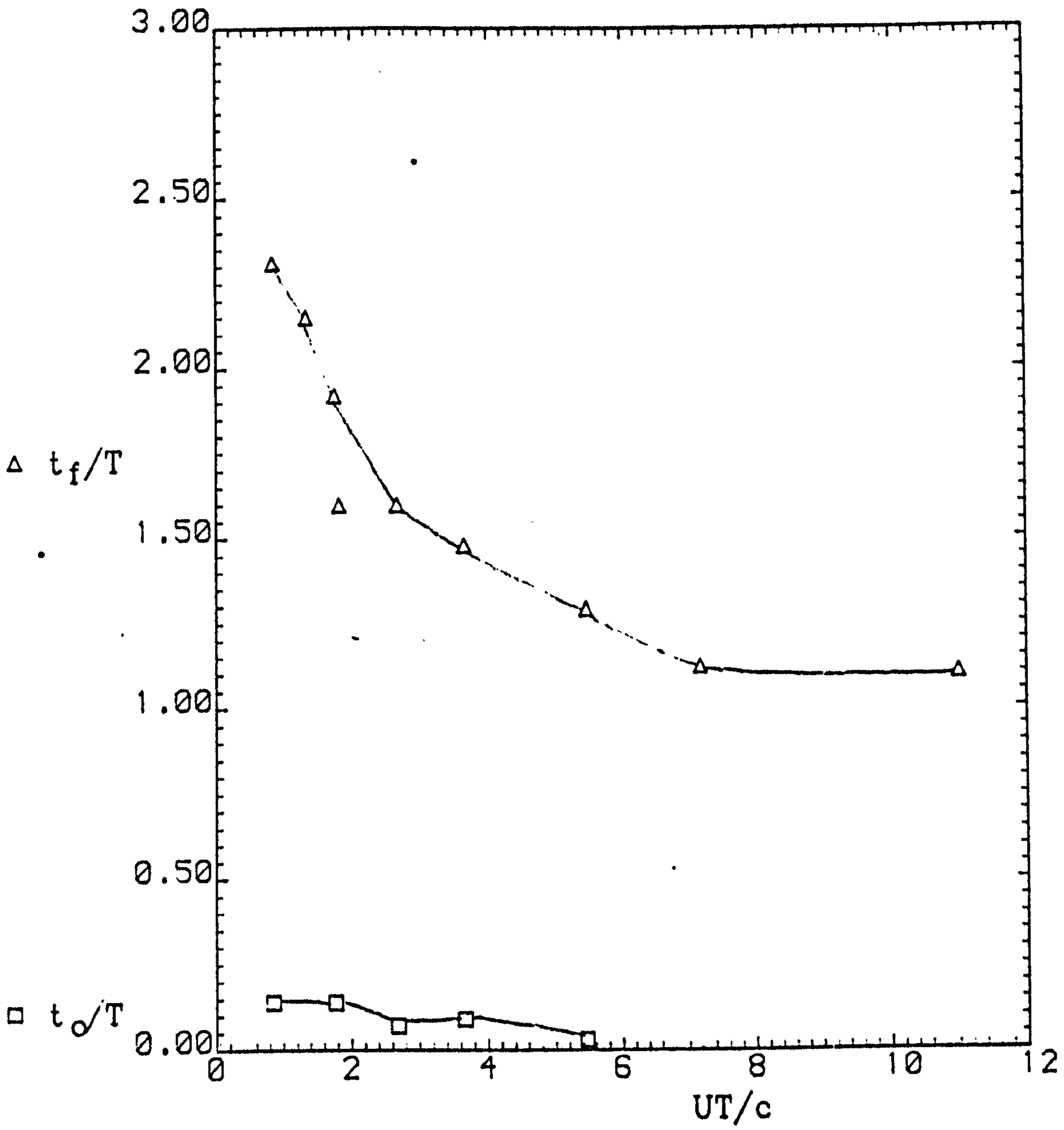

Spoiler configuration:		Upper-surface,
70% chord, gap opened, perforations closed		
α=. 0.0°	U=10-20m/s	T=35-226msec
Data from run sequence 3051-3059		

Fig. 5.28 Correlation of delay times for spoiler retraction

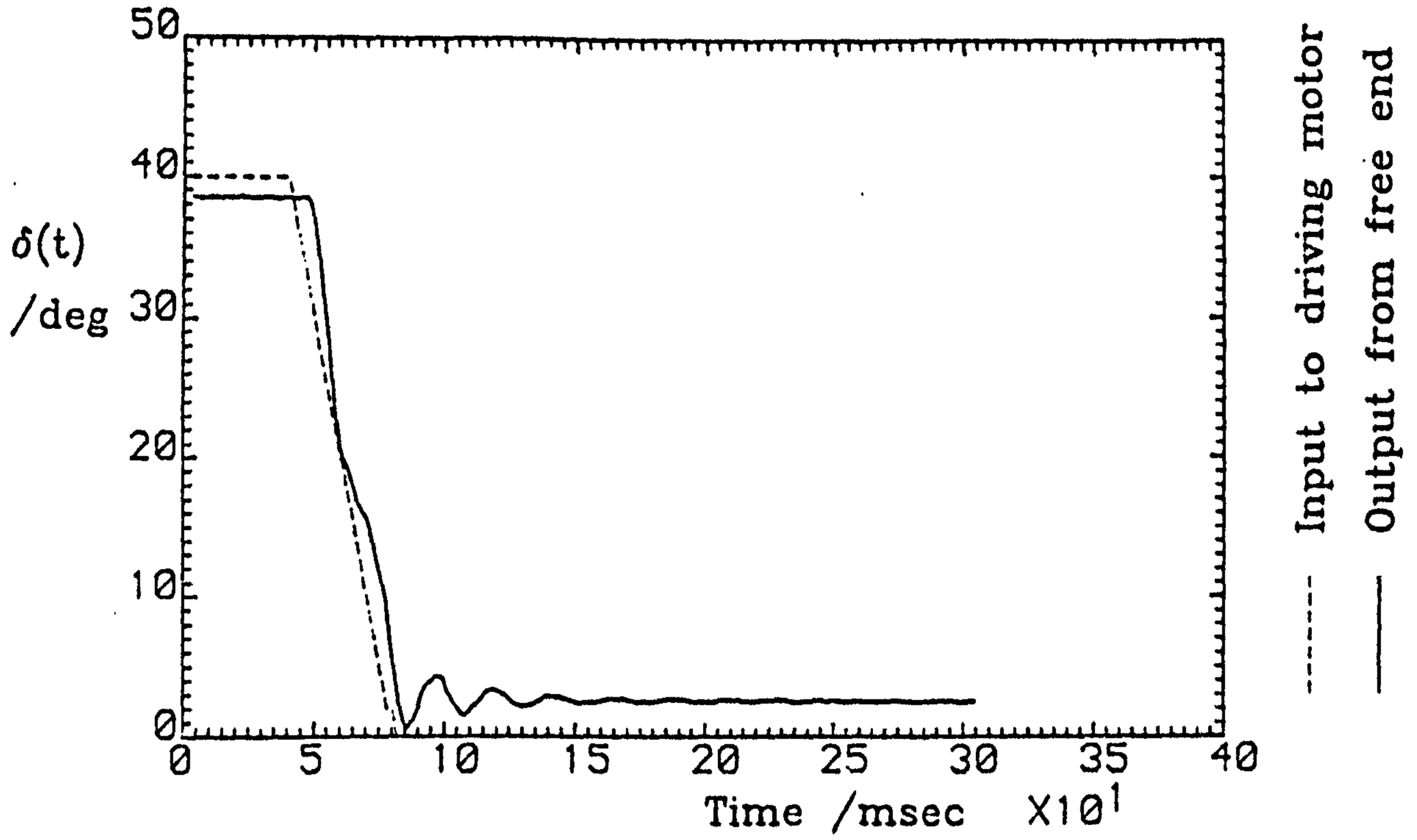

Fig. 5.29(a) Spoiler displacement trace

Spoiler configuration: Upper-surface,		
70% chord, gap closed, perforations closed		
α= 0.0°	U=20.0m/s	$\dot{\delta}$=990°/s

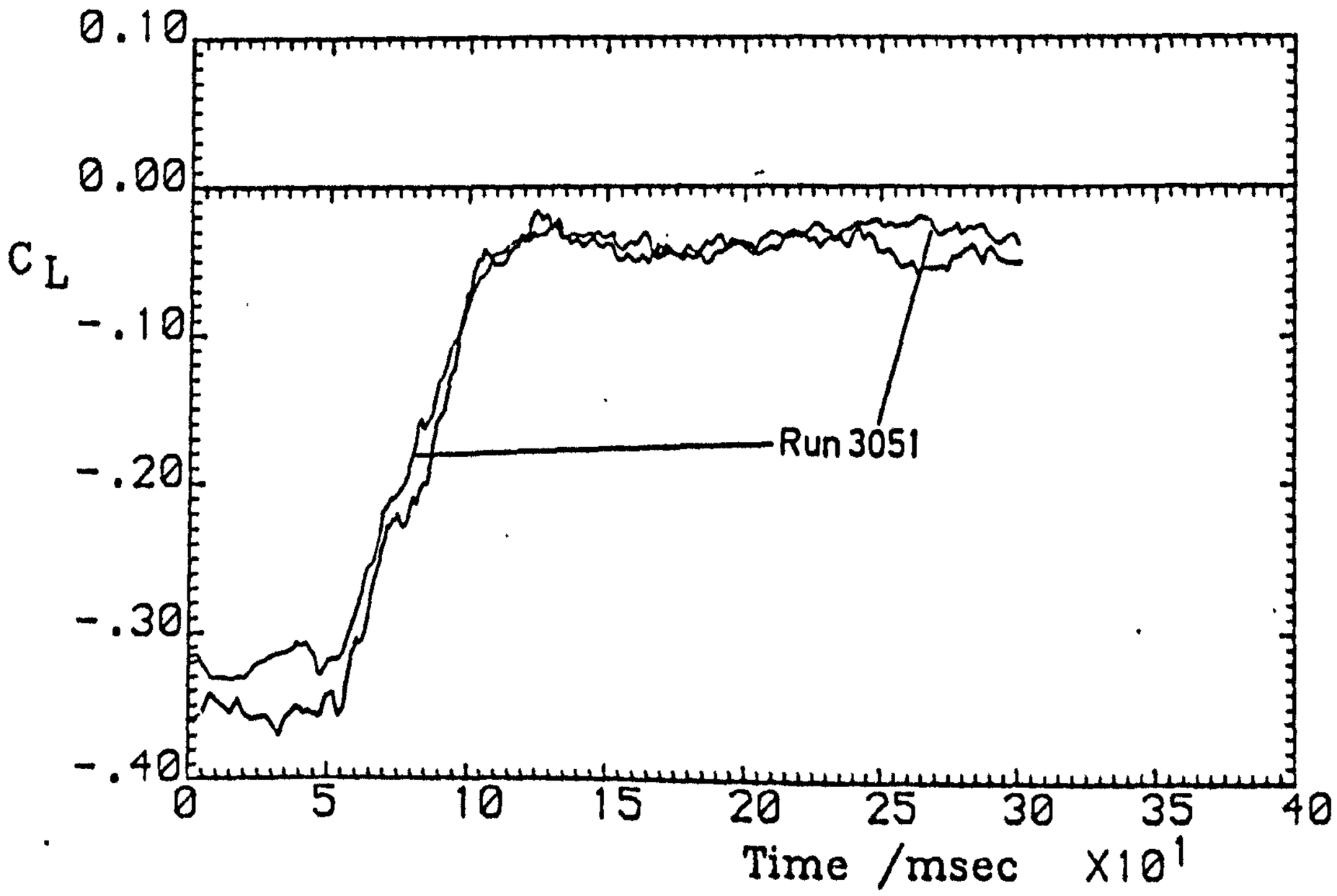

Fig. 5.29(b) Aerofoil lift time history

Run 3251

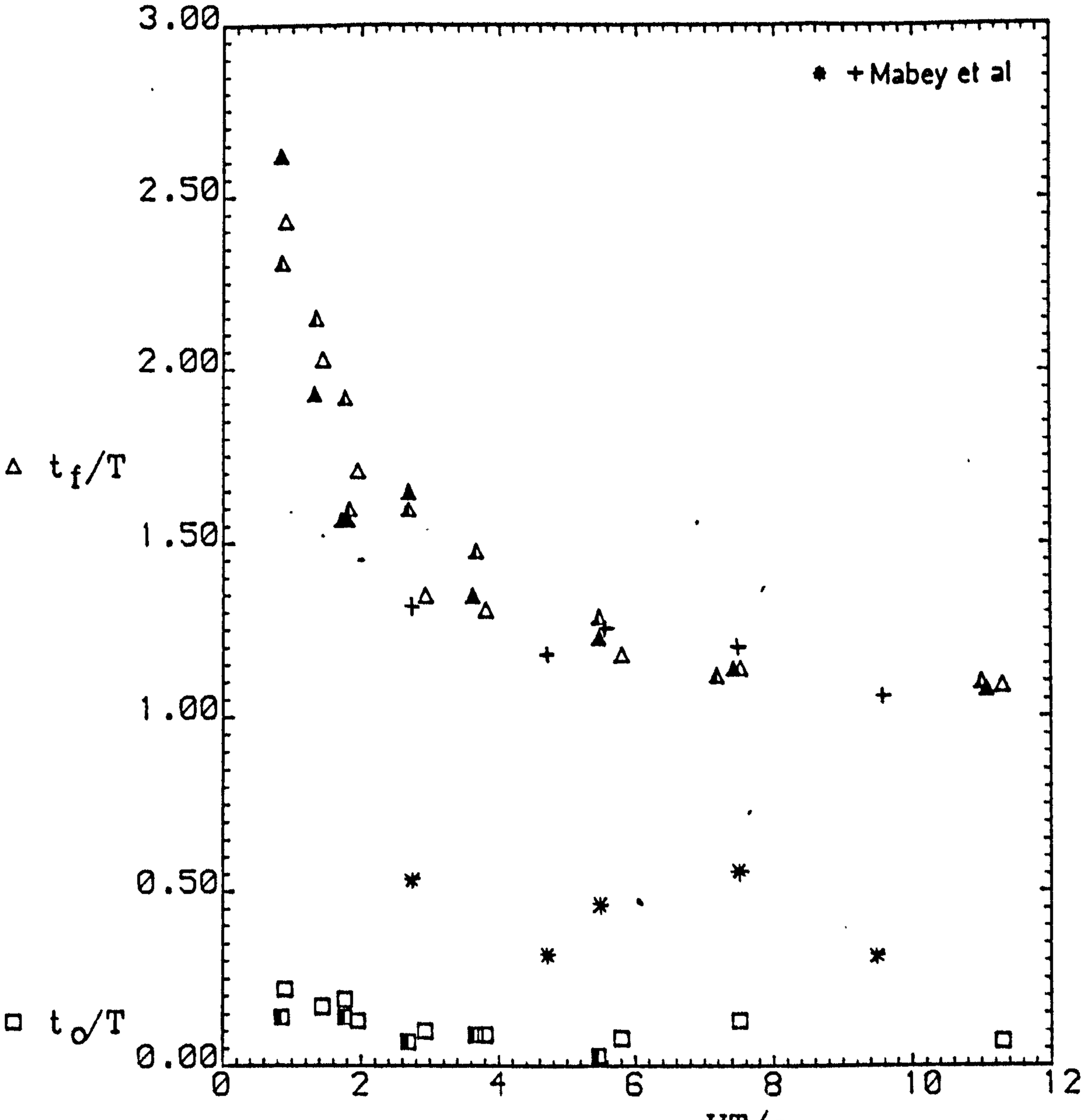

Spoiler geometry: "Solid"(filled symbols),		
"Gapped"(half-filled), "Perforated"(empty)		
α= 0.0°	U=10-20m/s	T=34-232msec
Data from Runs 305X,325X,205X (X=1-9)		

Fig. 5.30 Correlation of delay times for spoiler retraction

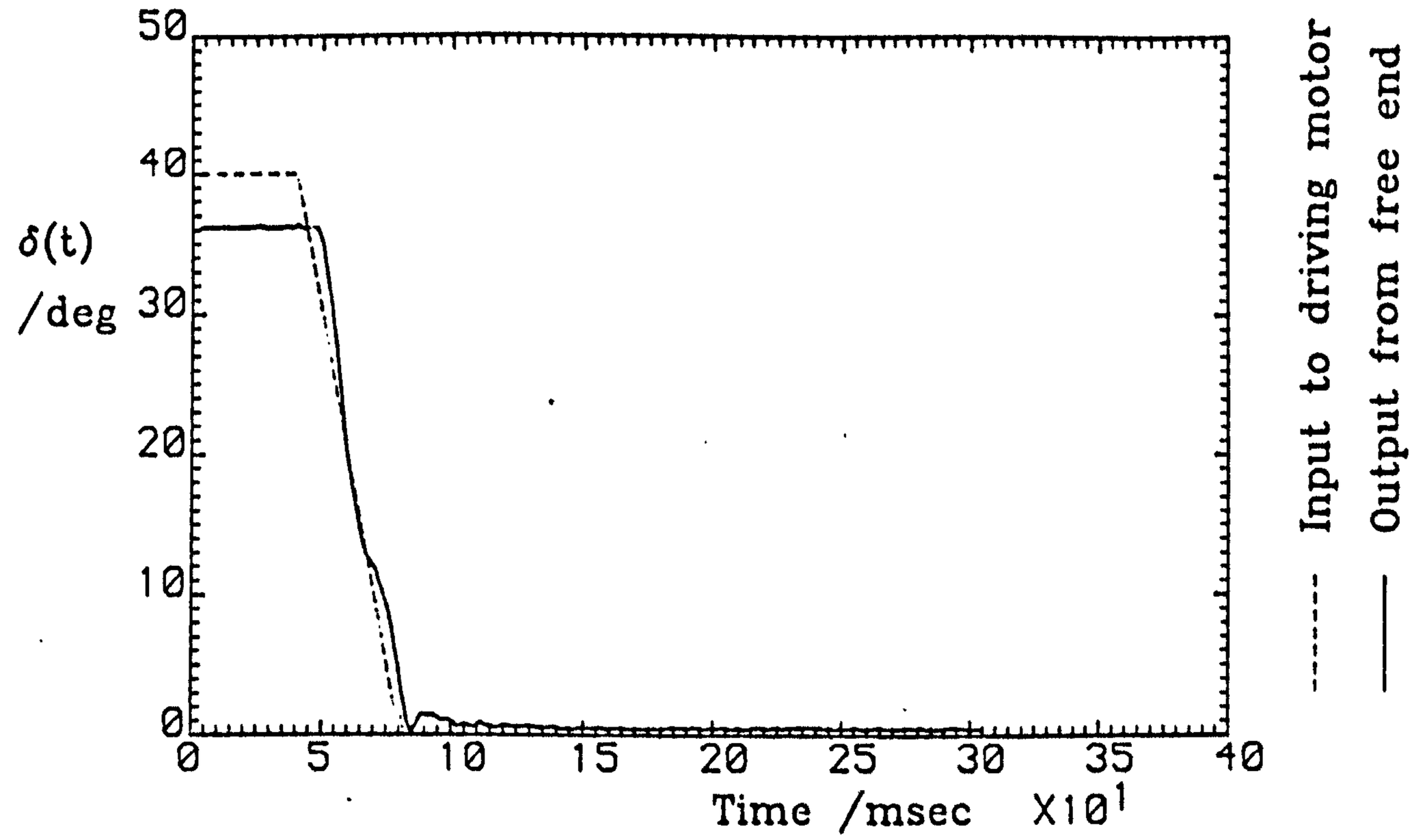

Fig. 5.31(a) Spoiler displacement trace

Spoiler configuration: Upper-surface,		
70% chord, gap opened, perforations closed		
α=14.0°	U=20.0m/s	$\dot{\delta}$=990°/s

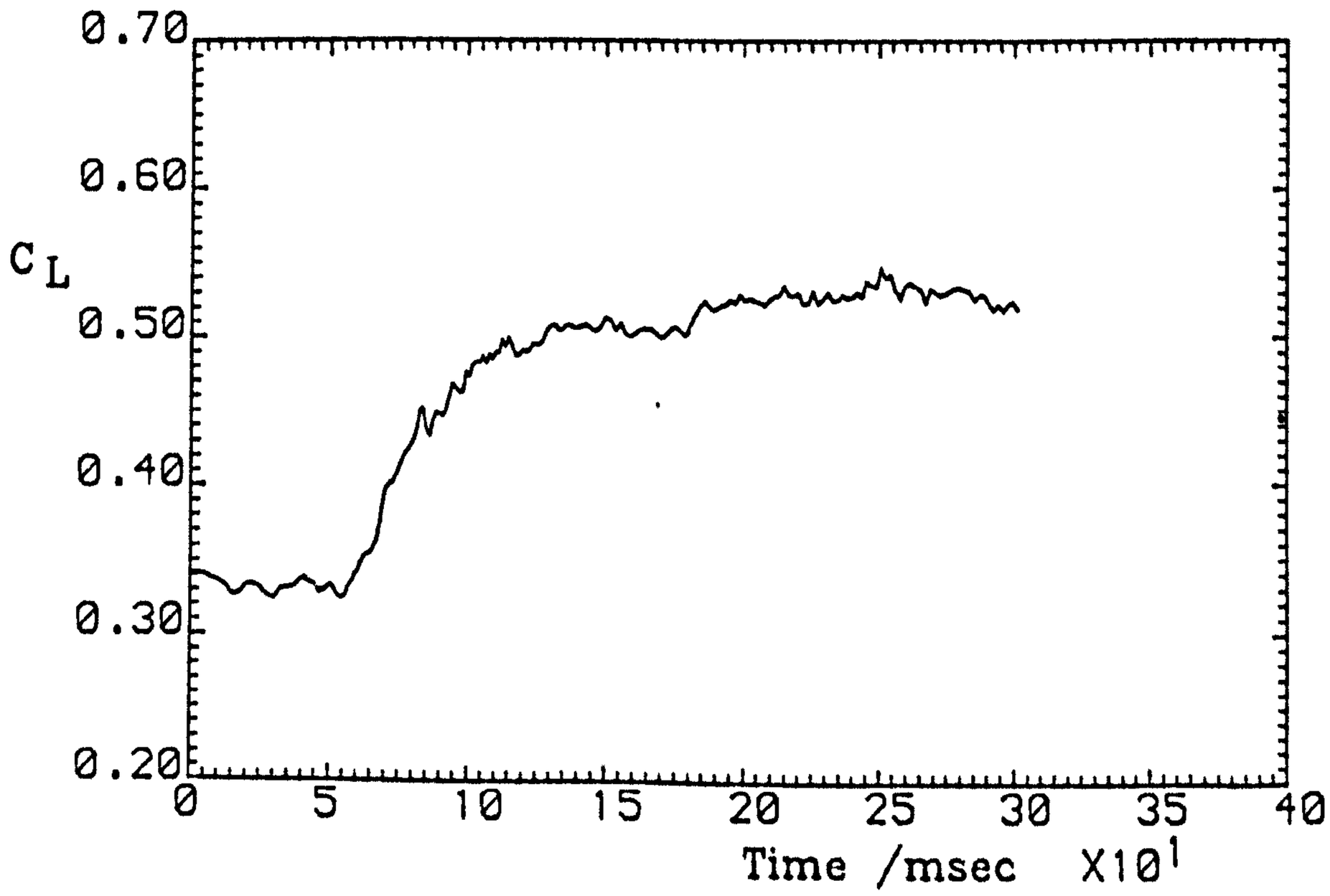

Fig. 5.31(b) Aerofoil lift time history

Run 5051

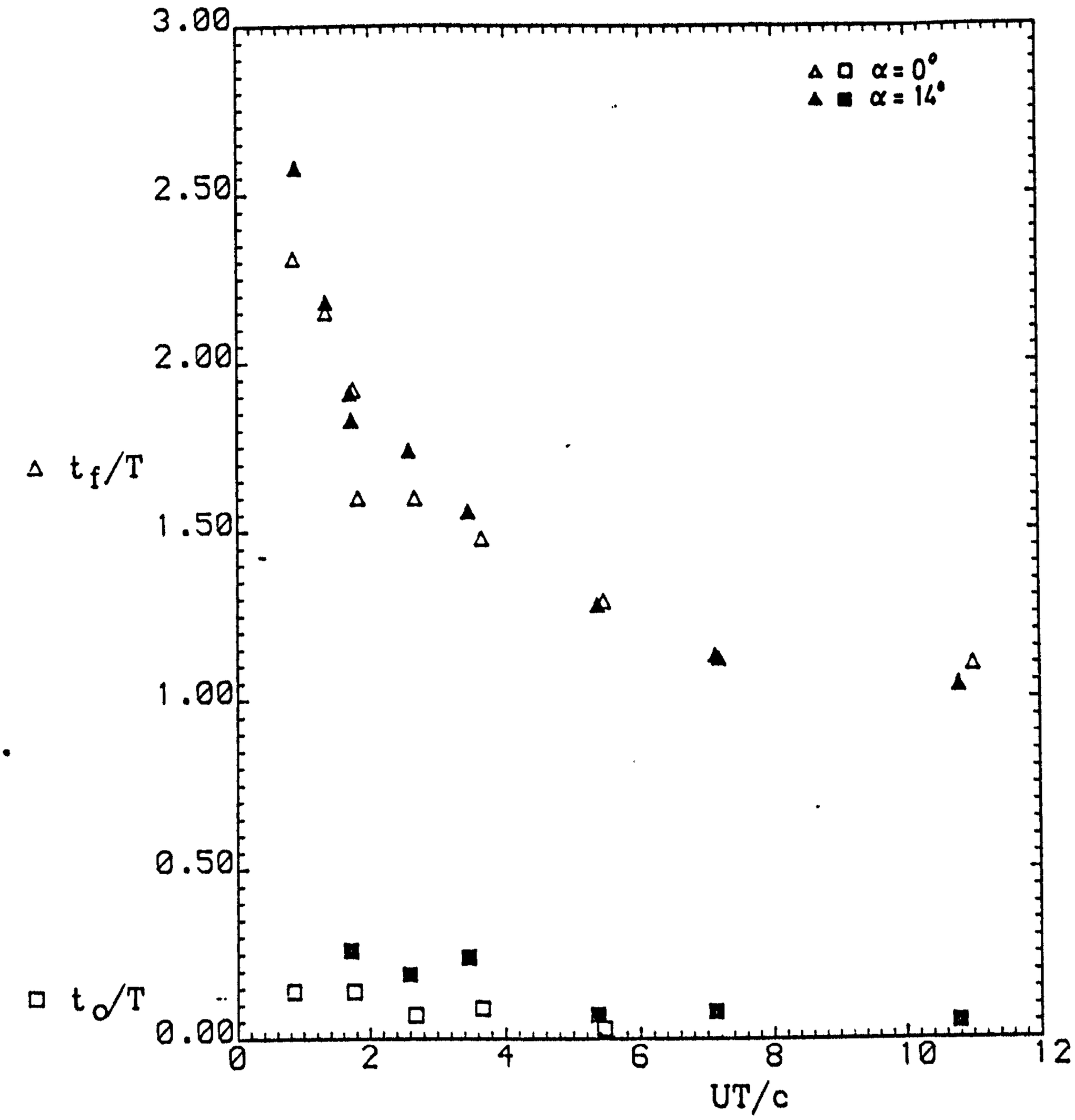

Spoiler configuration:		Upper-surface,
70% chord, gap opened, perforations closed		
α=0-14°	U=10-20m/s	T=35-226msec
Data from Runs 305X, 505X (X=1-9)		

Fig. 5.32 Correlation of delay times for spoiler retraction

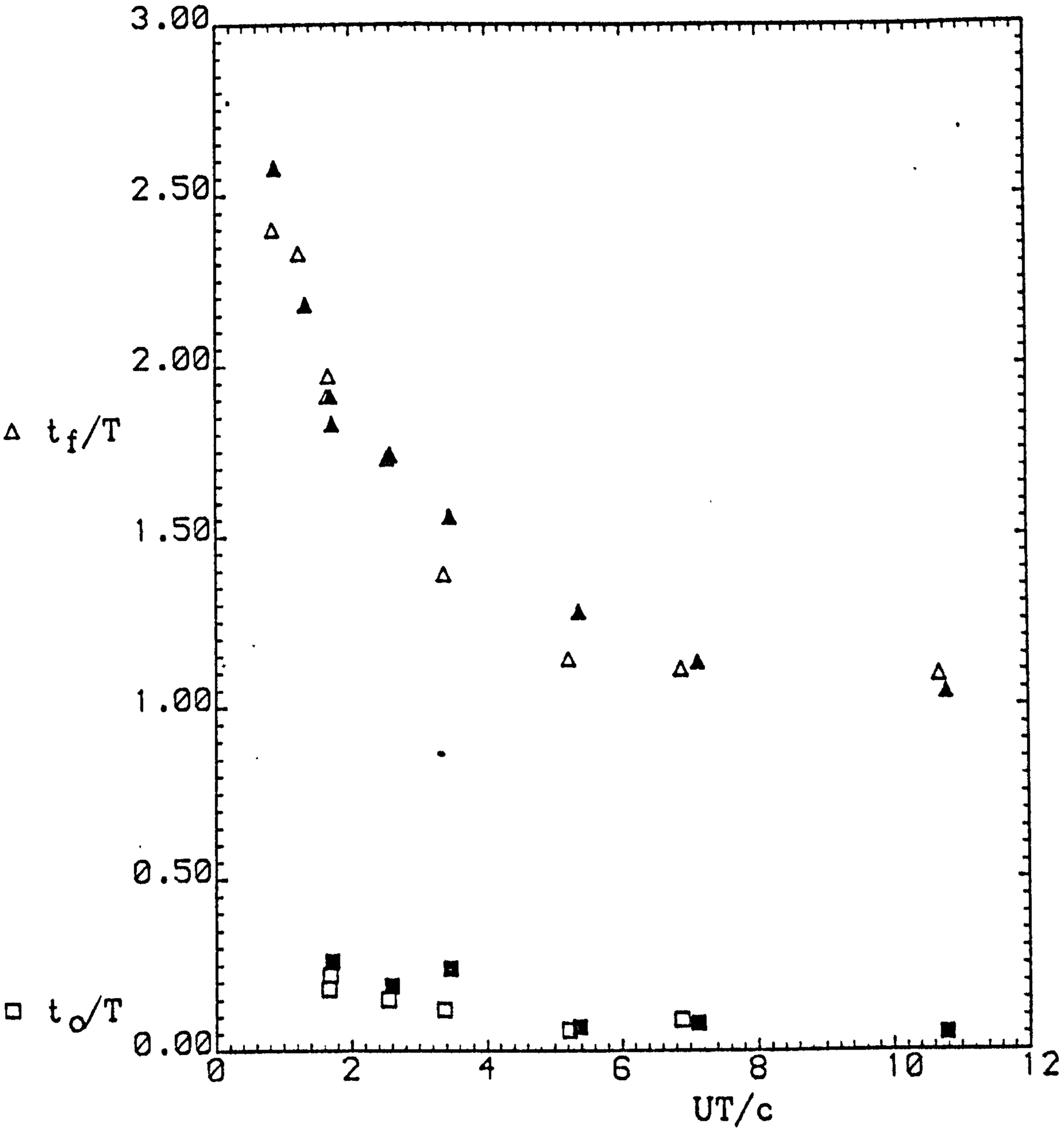

Spoiler geometry: "Gapped"(filled symbols),		
"Perforated"(empty symbols)		
α=14.0°	U=10–20m/s	T=35–221msec
Data from Runs 505X, 405X (X=1–9)		

Fig. 5.33 Correlation of delay times for spoiler retraction

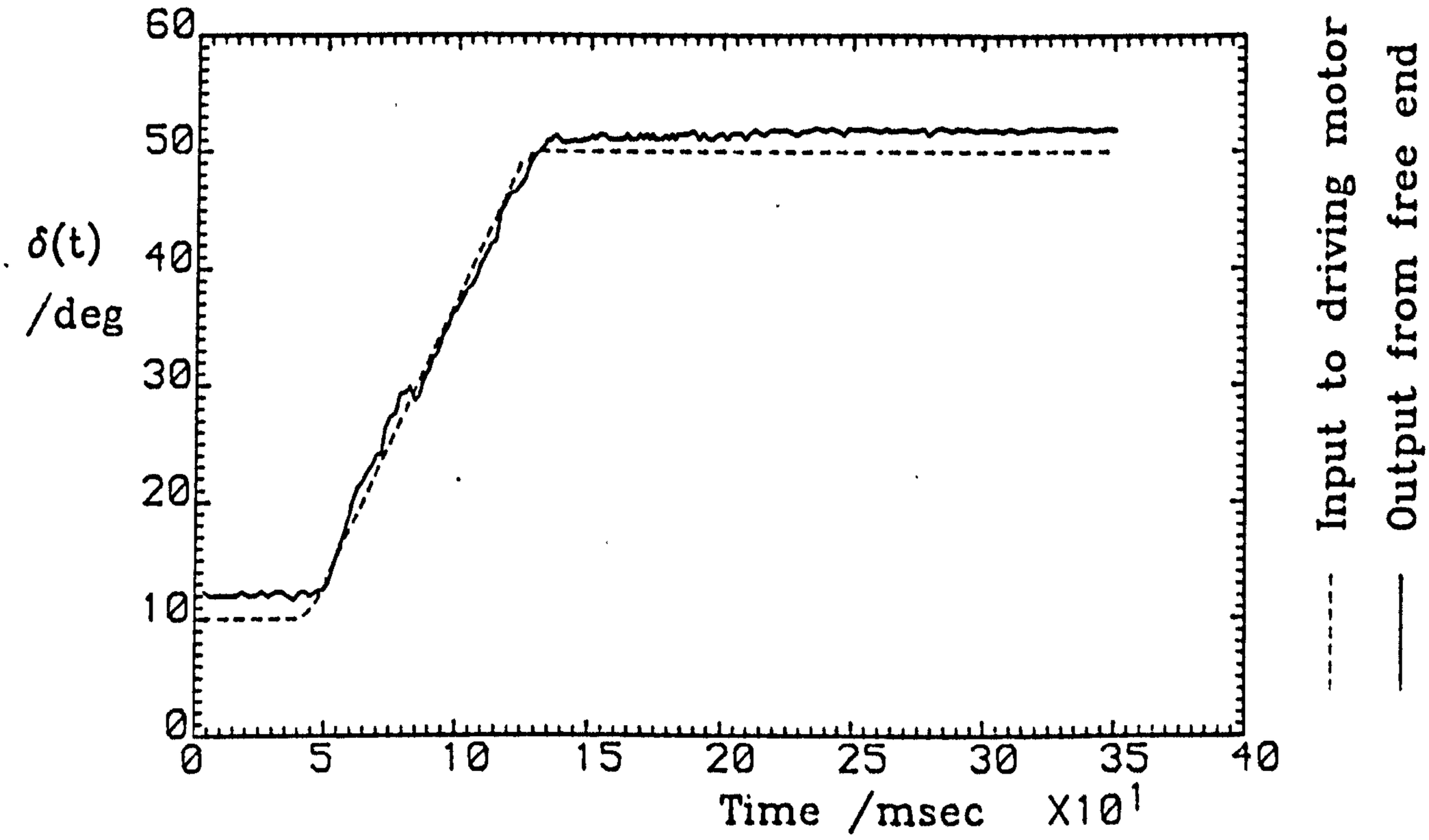

Fig. 5.34 (a) Spoiler displacement trace

Spoiler configuration: Upper-surface,		
70% chord, gap opened, perforations closed		
α= 0.0°	U=20.0m/s	$\dot{\delta}$=500°/s

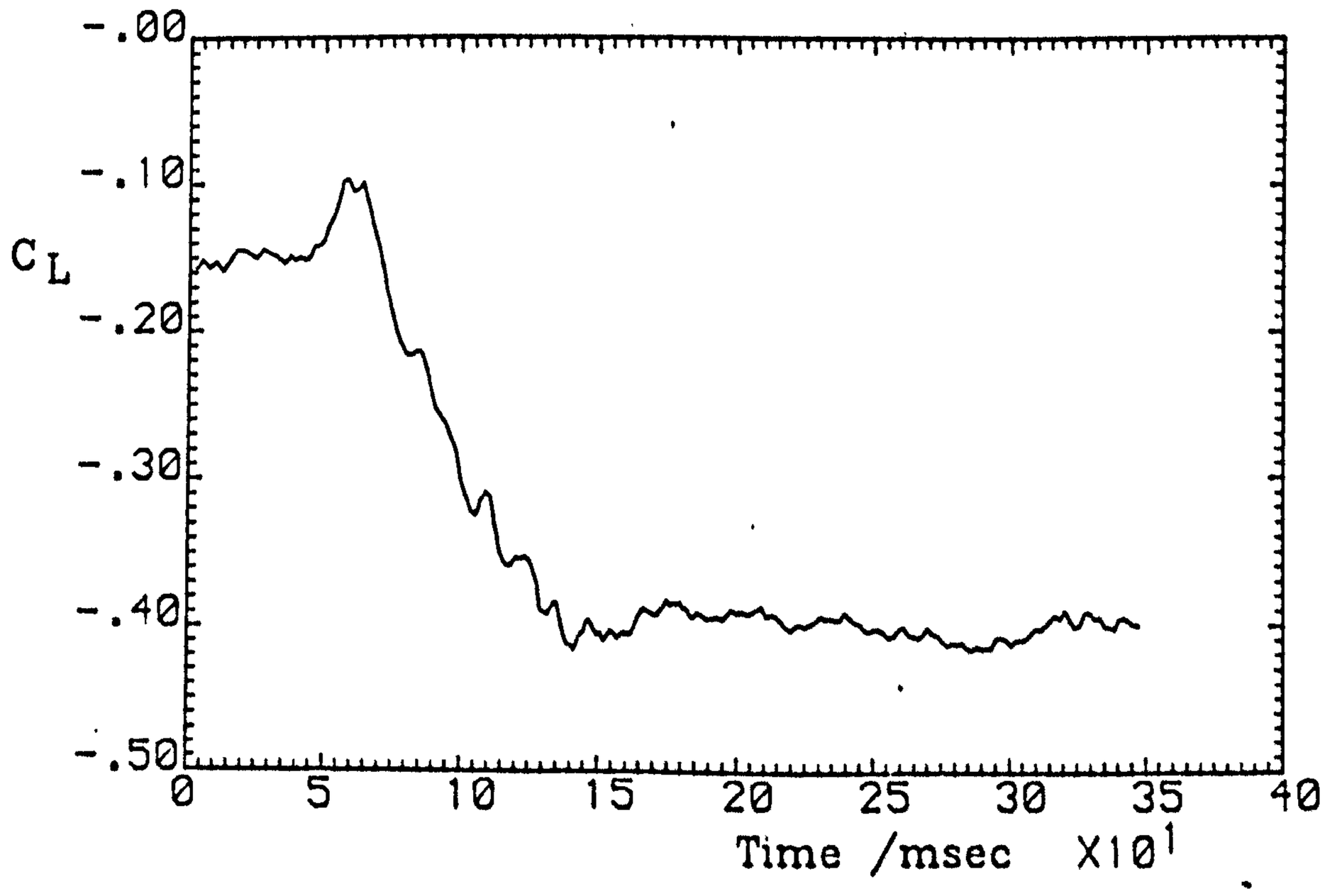

Fig. 5.34 (b) Aerofoil lift time history

Run 3103

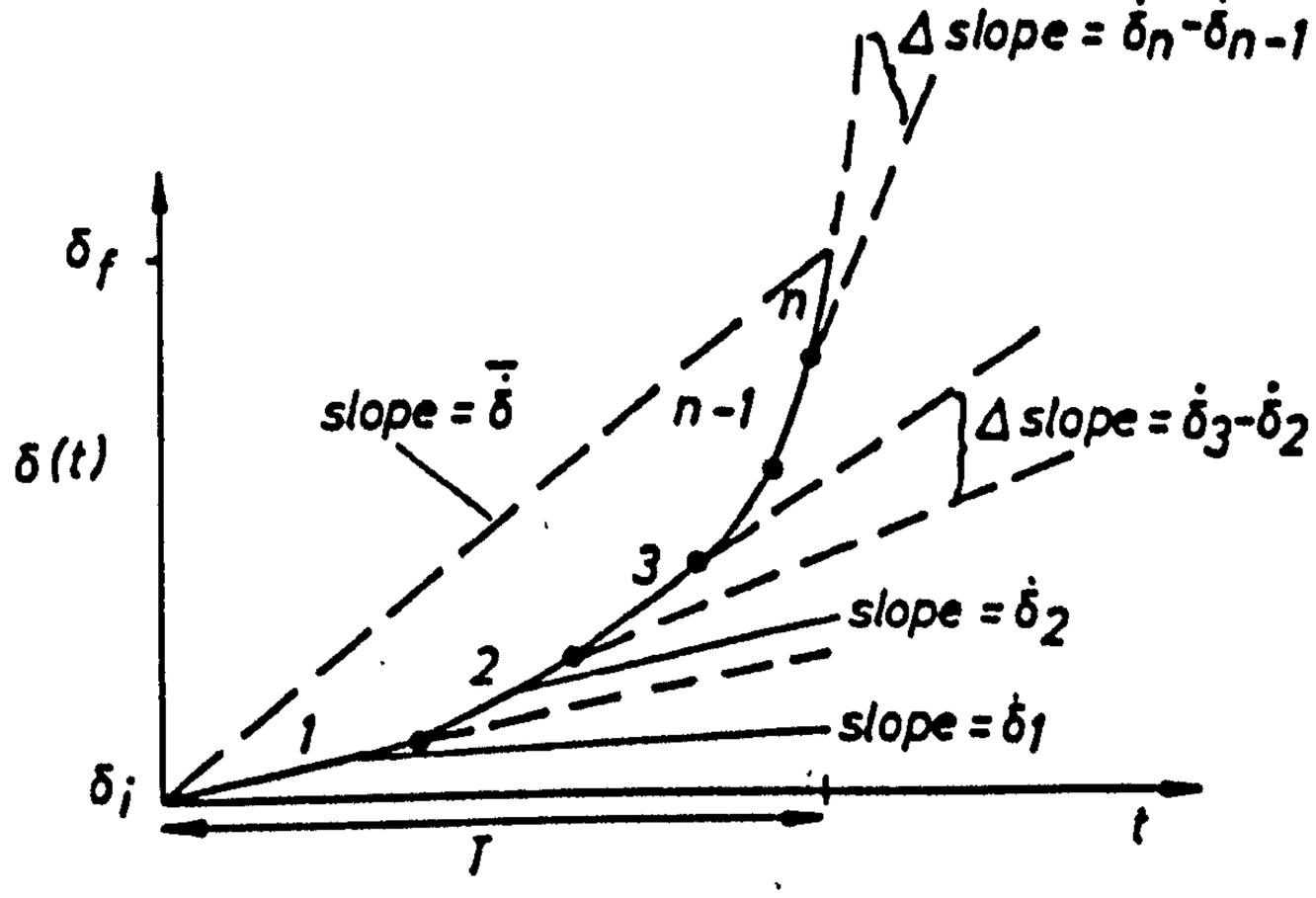

$\dot{\delta}_1 = \dot{\delta}_{qs} < \bar{\dot{\delta}}$

$(\dot{\delta}_i - \dot{\delta}_{i-1}) \leq \dot{\delta}_{qs}$ $(i = 2,3 \ldots n)$

$\dot{\delta}_n = \dot{\delta}_{max} > \bar{\dot{\delta}}$

(a) Minimised adverse lift for spoiler extension

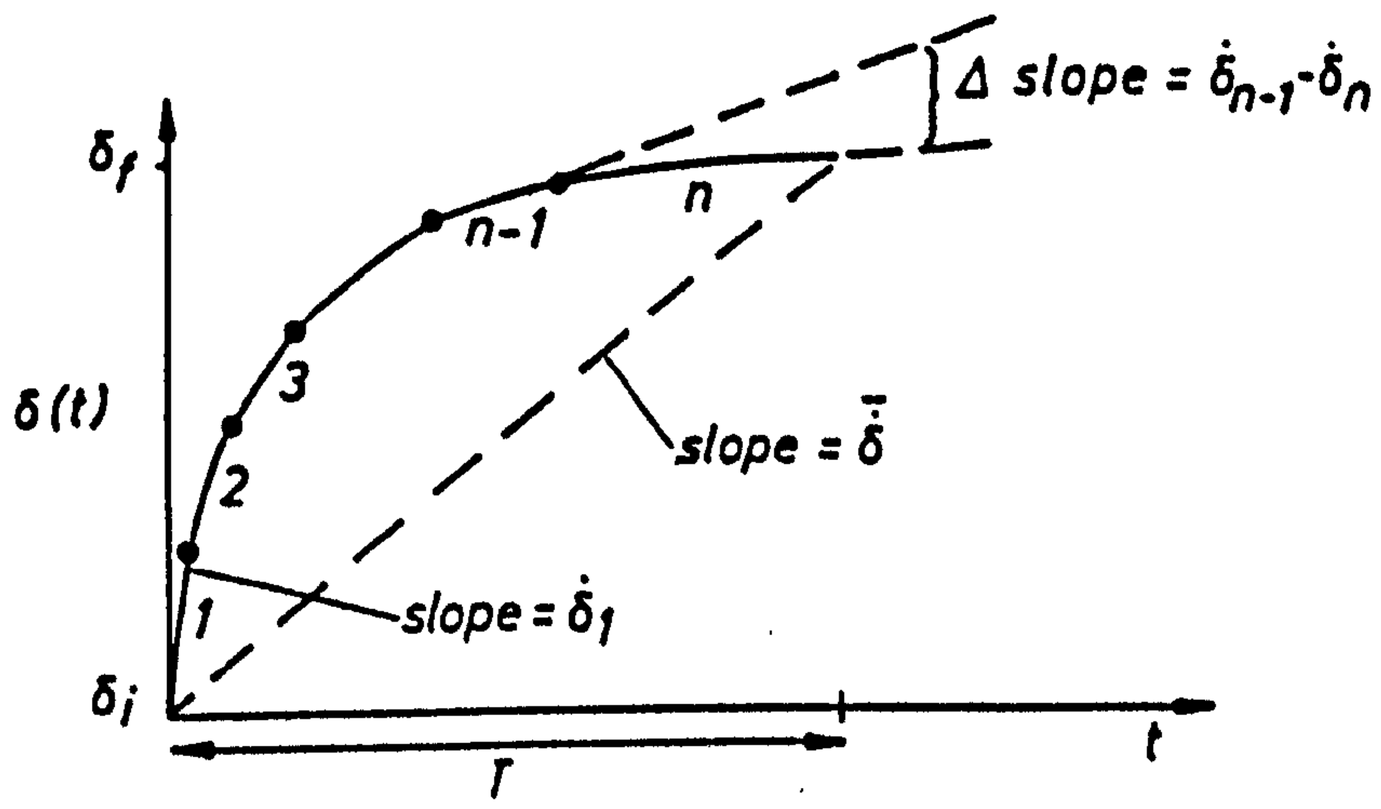

$\dot{\delta}_1 = \dot{\delta}_{max} > \bar{\dot{\delta}}$

$(\dot{\delta}_{i-1} - \dot{\delta}_i) << \bar{\dot{\delta}}$ $(i = 2,3 \ldots n)$

$\dot{\delta}_n << \bar{\dot{\delta}}$

(b) Maximised adverse lift for spoiler extension

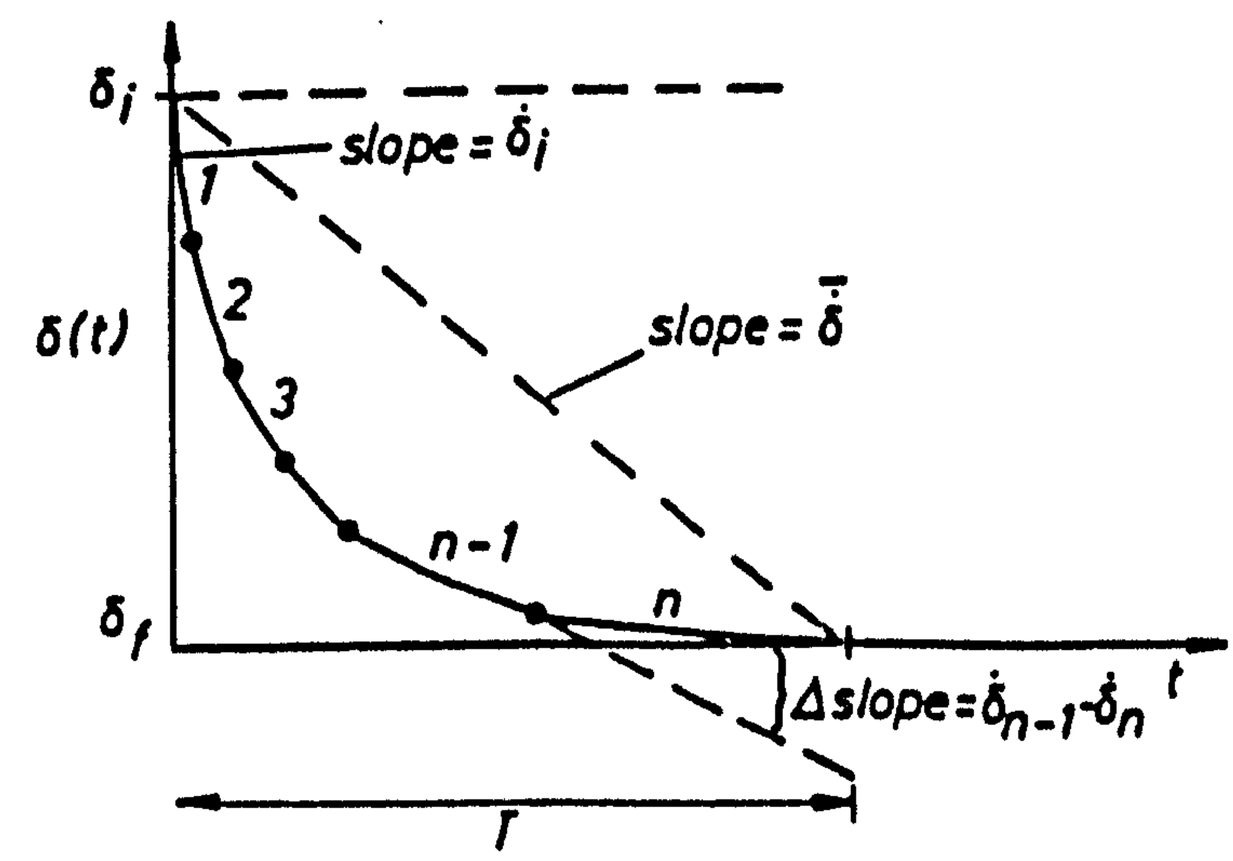

$\dot{\delta}_1 = \dot{\delta}_{max} > \bar{\dot{\delta}}$

$(\dot{\delta}_{i-1} - \dot{\delta}_i) << \bar{\dot{\delta}}$ $(i = 2,3 \ldots, n)$

$\dot{\delta}_n << \bar{\dot{\delta}}$

(c) Optimised lift response for spoiler retraction

FIG. 5.35 OPTIMISATION OF SPOILER DISPLACEMENT PROFILE

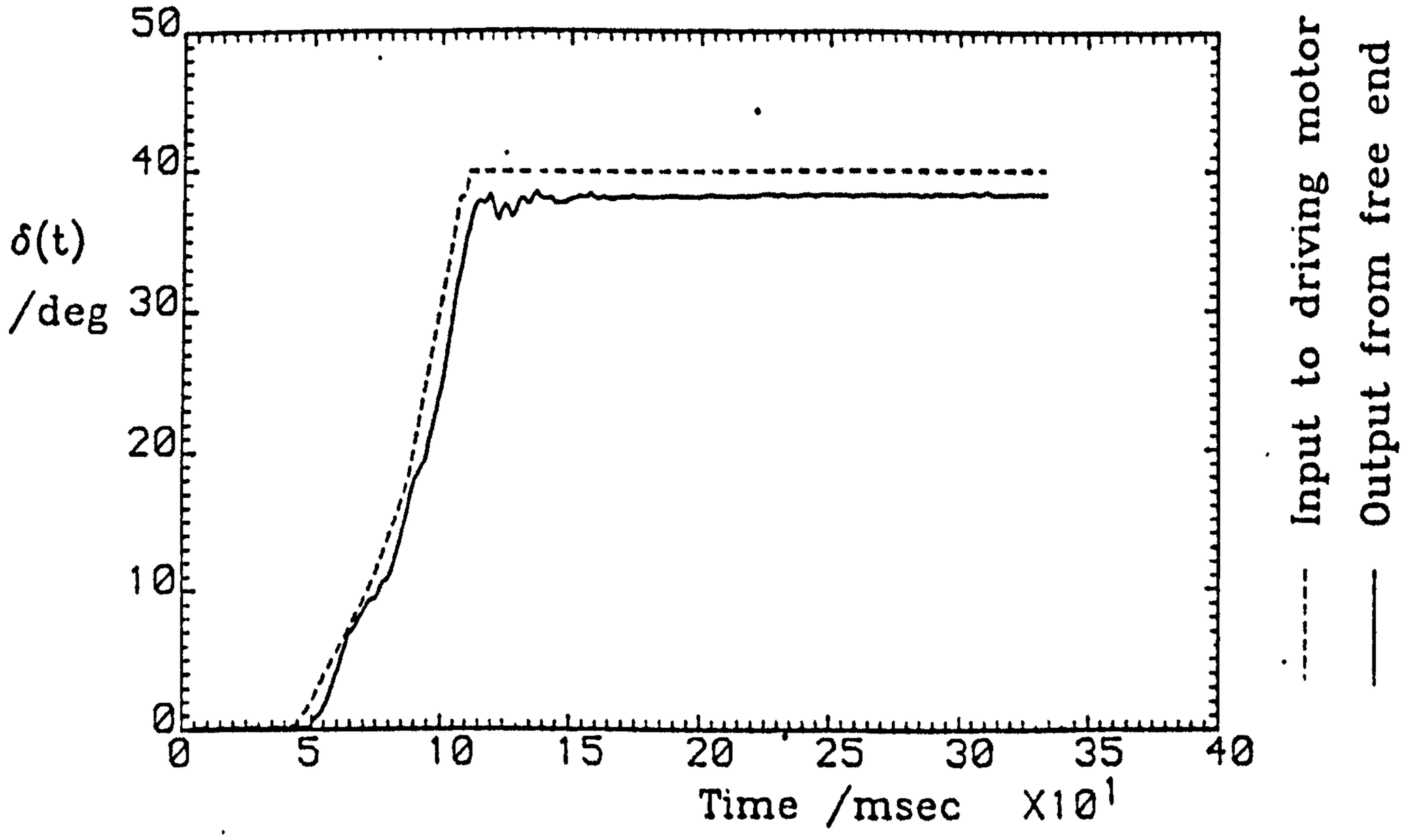

Fig. 5.36(a) Spoiler displacement trace

Spoiler configuration: Upper-surface,		
70% chord, gap opened, perforations closed		
α= 0.0°	U=20.0m/s	$\dot{\delta}$=425-593-990°/s

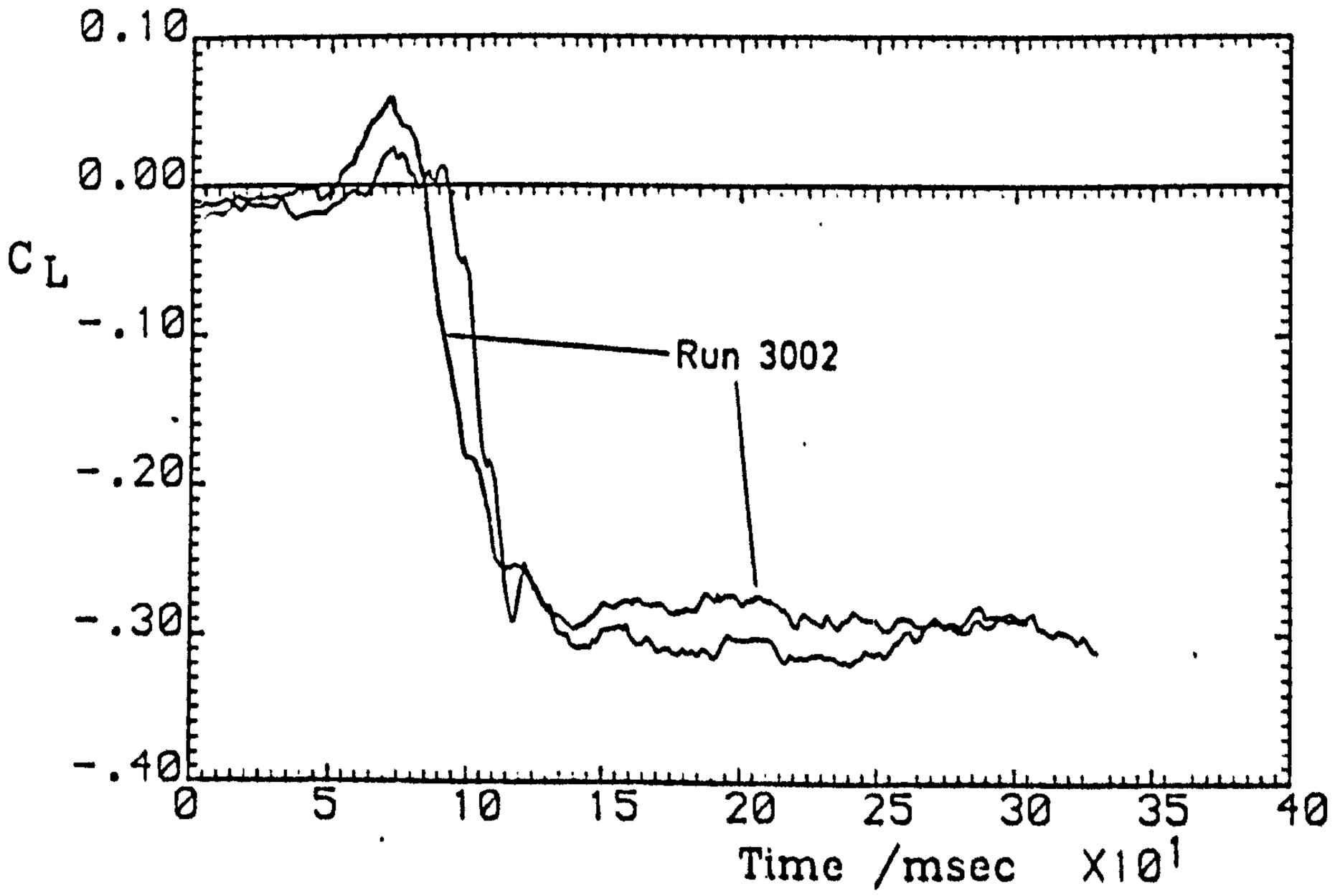

Fig. 5.36(b) Aerofoil lift time history

Run 3611

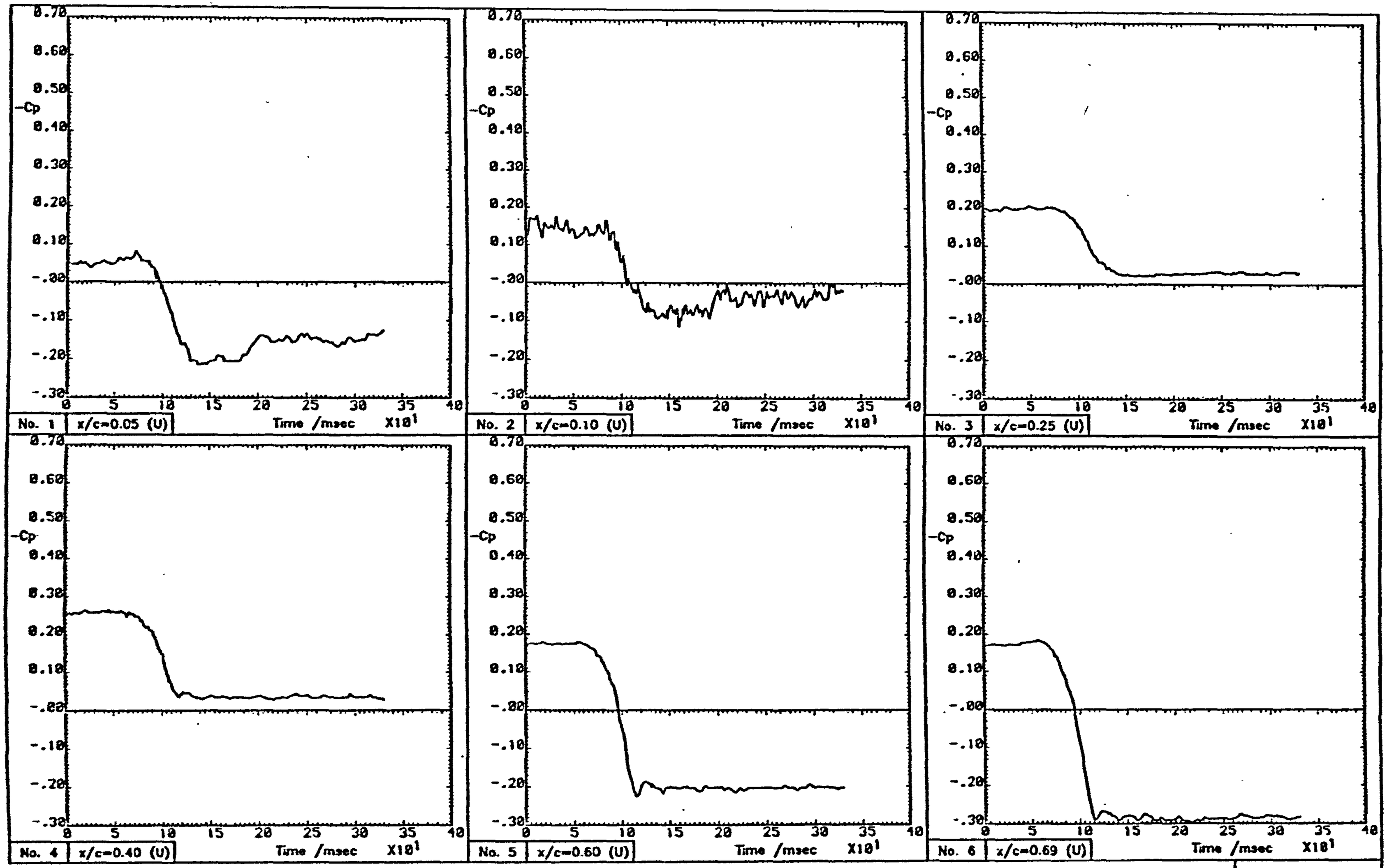

Fig. 5.37(a) Pressure signal time histories

Run 3611

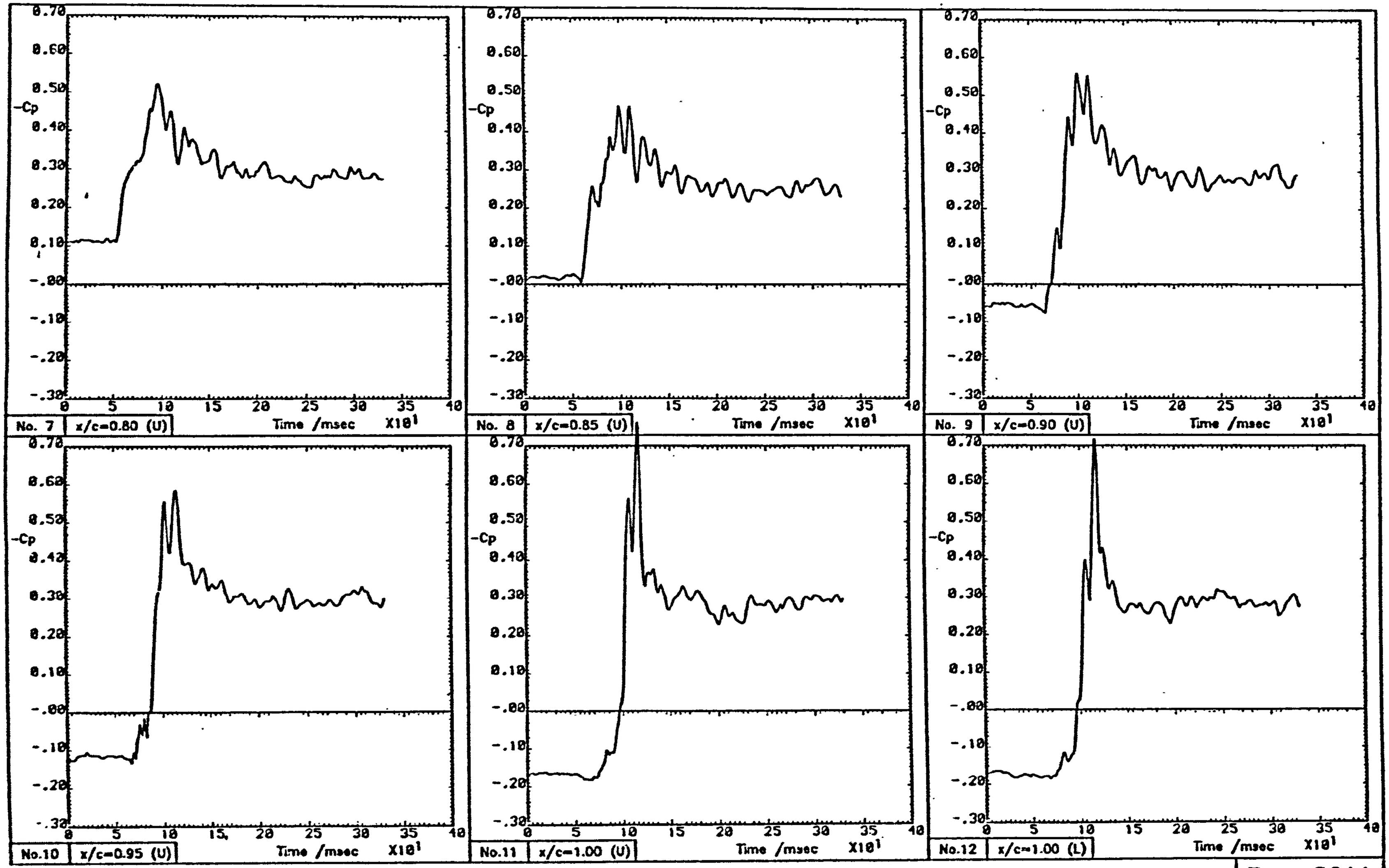

Fig. 5.37(b) Pressure signal time histories

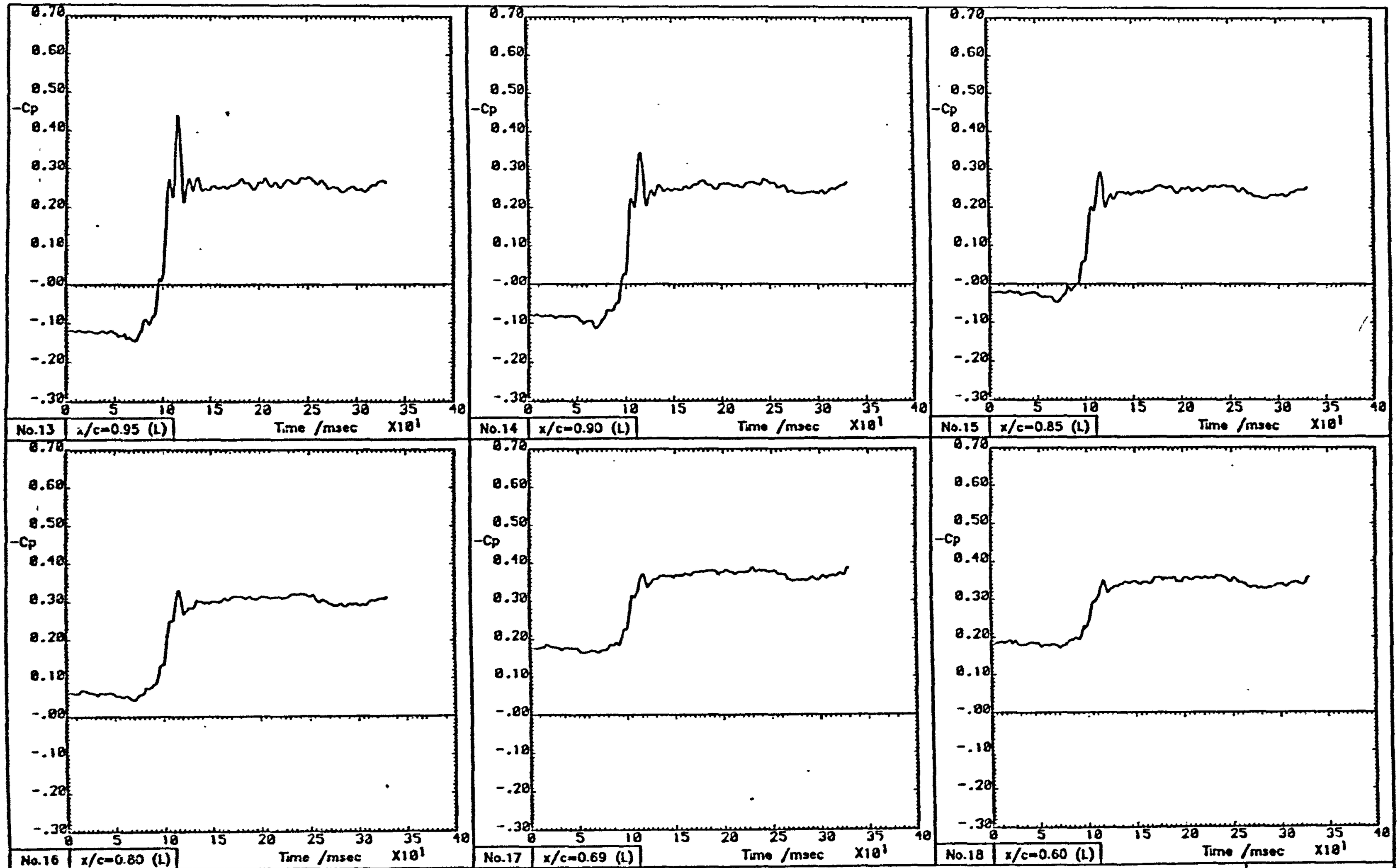

Fig. 5.37(c) Pressure signal time histories

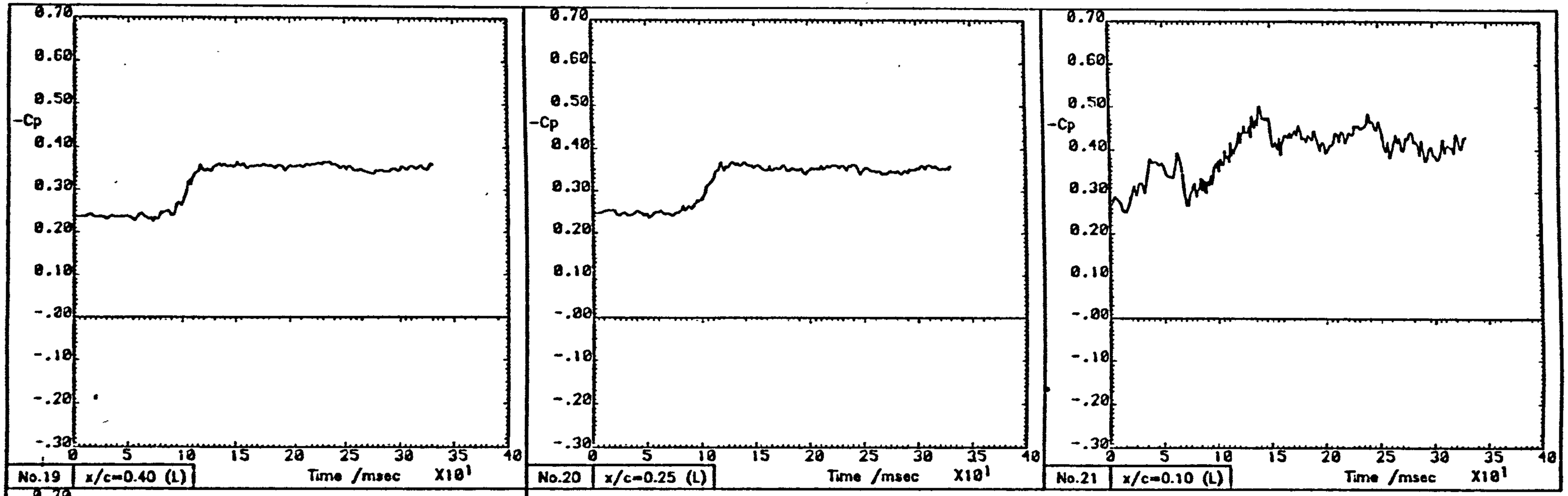

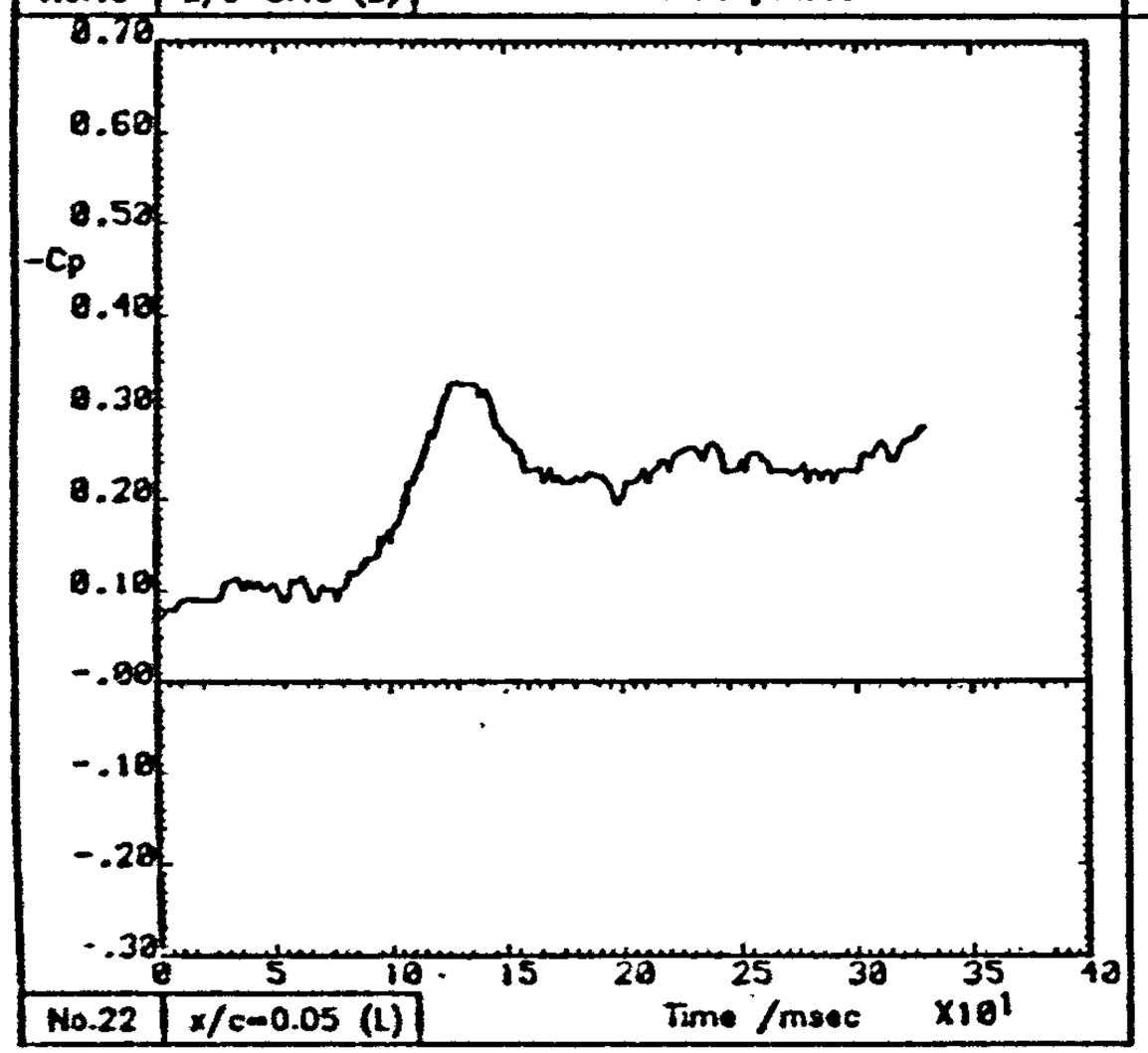

Fig. 5.37 (d) Pressure signal time histories

Run 3611

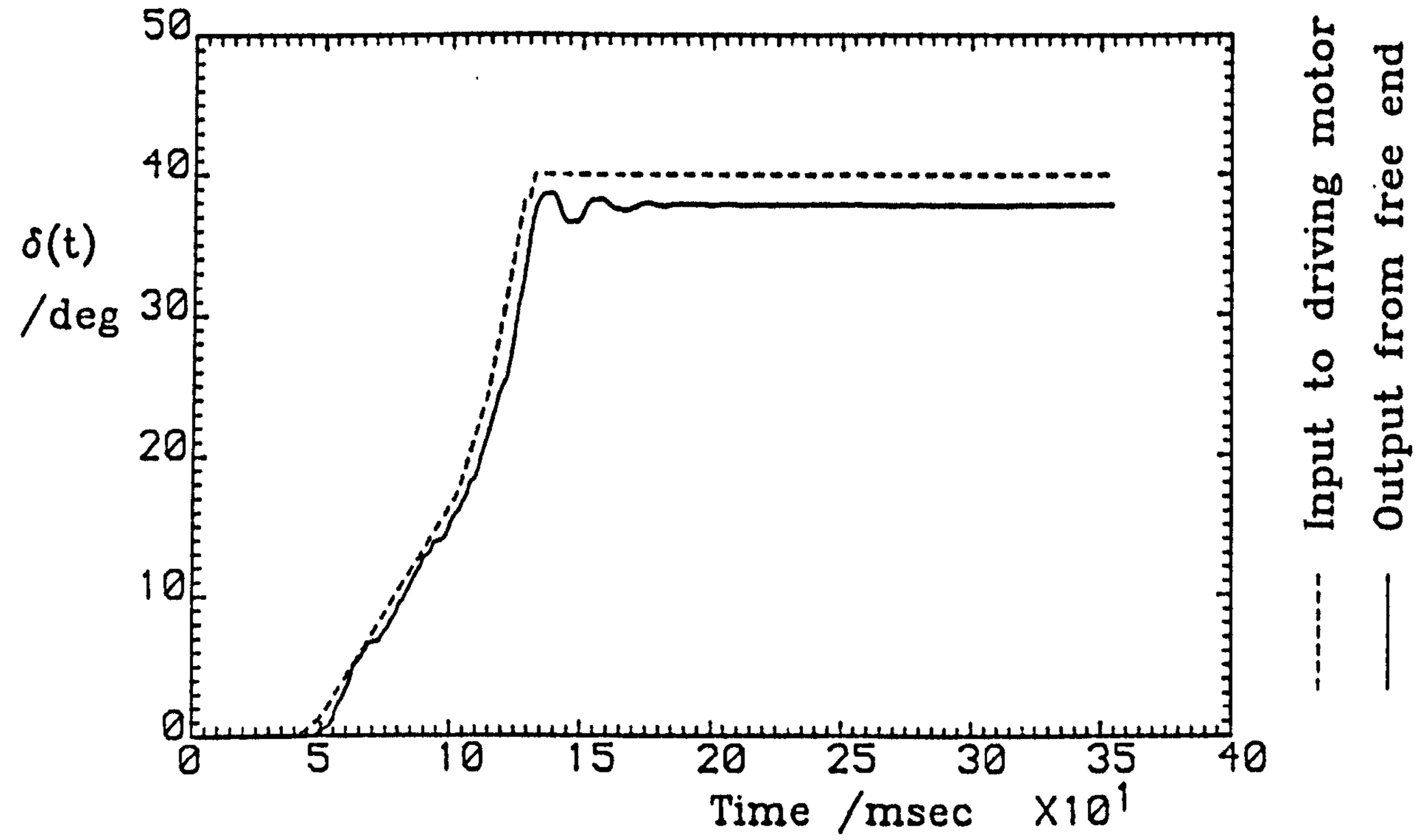

Fig. 5.38(a) Spoiler displacement trace

Spoiler configuration: Upper-surface,		
70% chord, gap closed, perforations closed		
α= 0.0°	U=20.0m/s	$\dot{\delta}$=330-600-990°/s

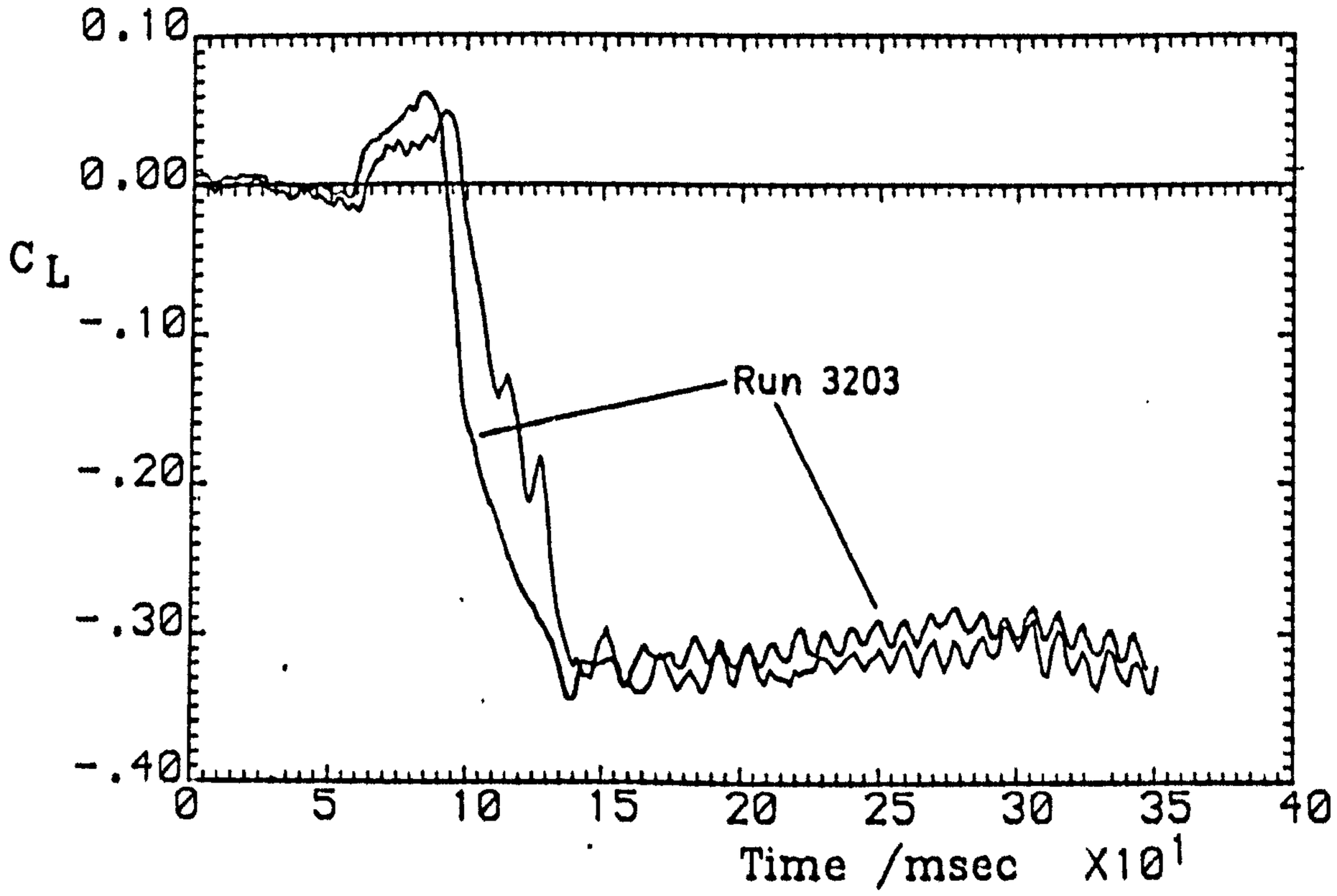

Fig. 5.38(b) Aerofoil lift time history

Run 3652

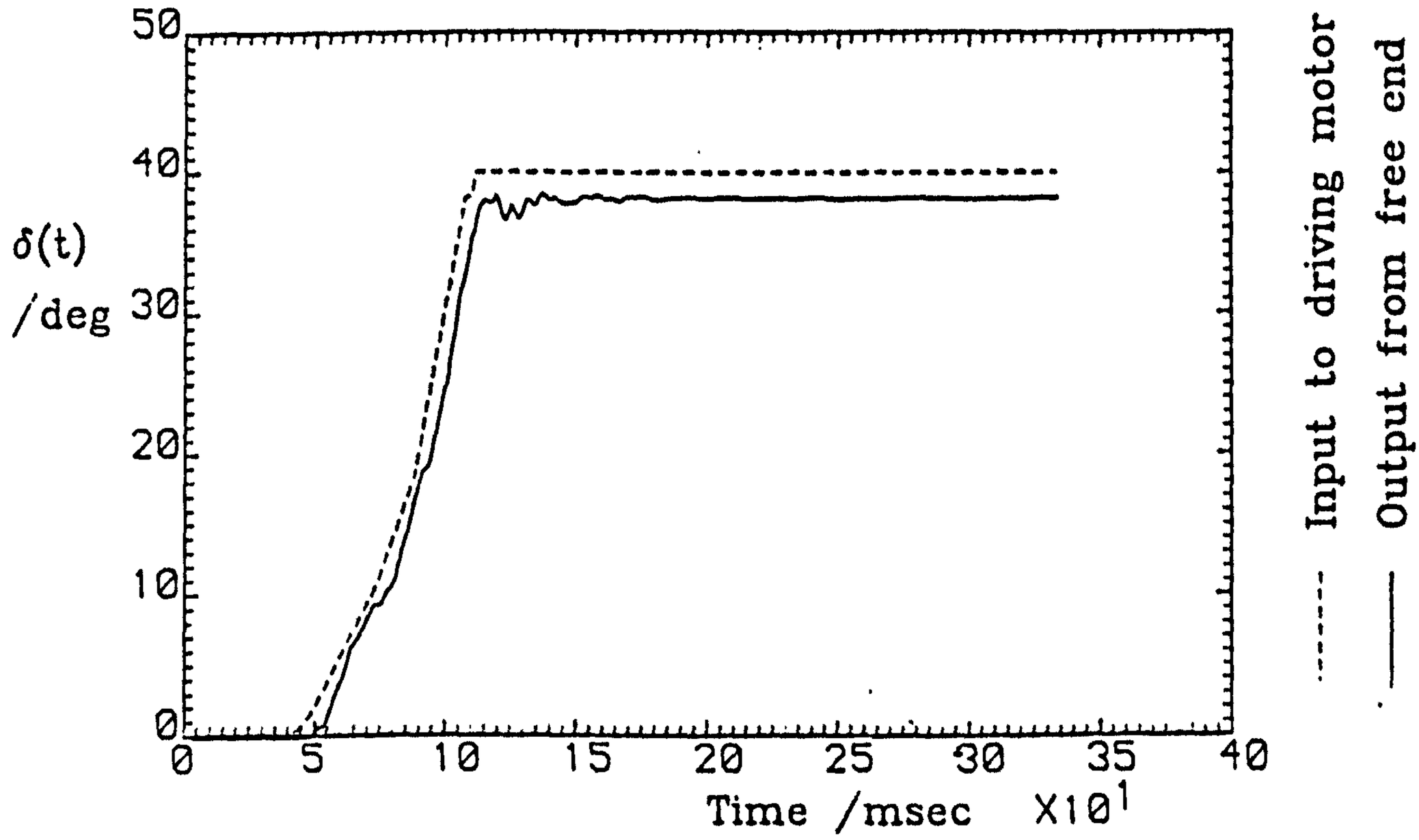

Fig. 5.39(a) Spoiler displacement trace

Spoiler configuration: Upper-surface,		
70% chord, gap opened, perforations closed		
α= 14.0°	U=20.0m/s	$\dot{\delta}$=425-593-990°/s

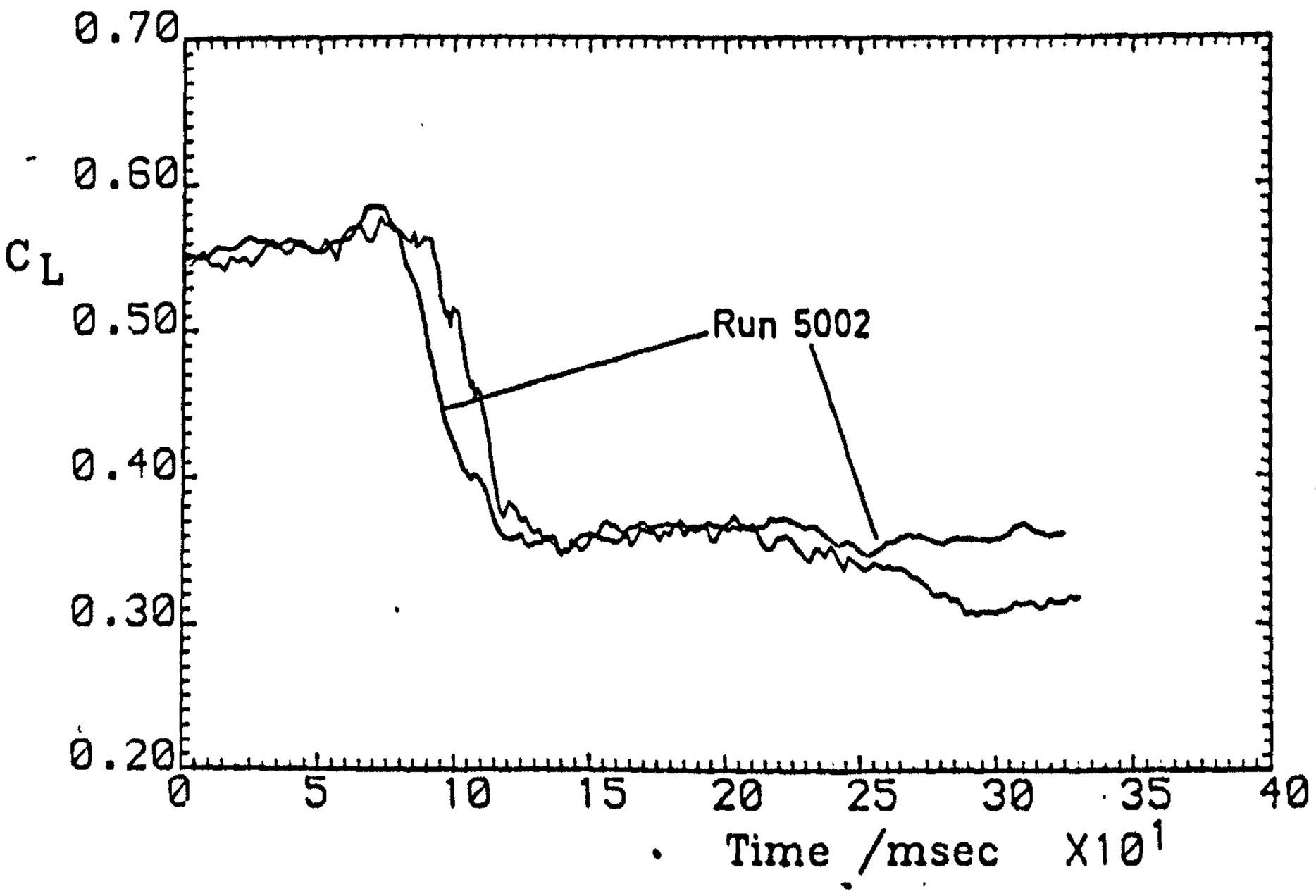

Fig. 5.39(b) Aerofoil lift time history

Run 5631

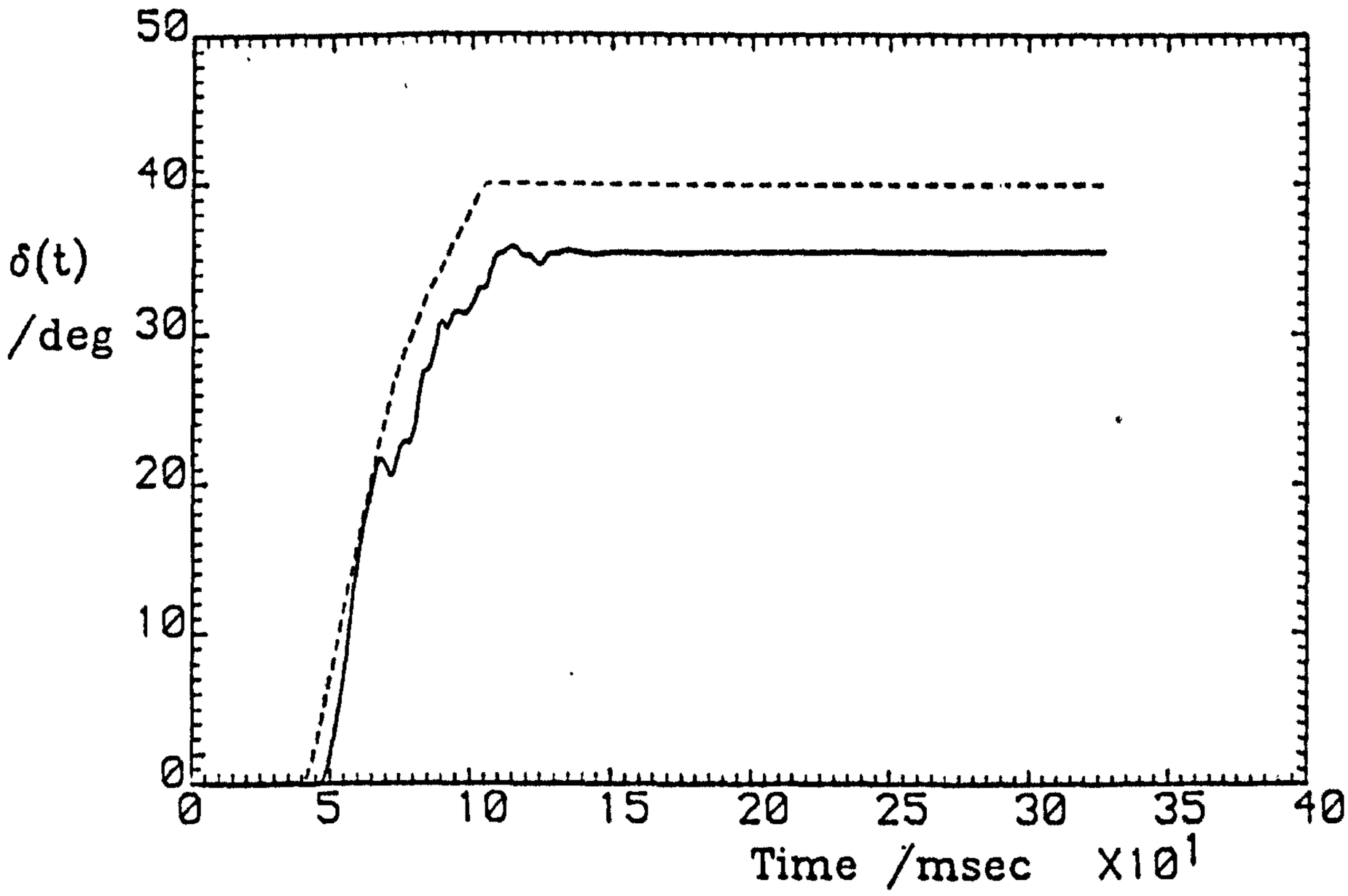

Fig. 5.40(a) Spoiler displacement trace

Spoiler configuration: Upper-surface,		
70% chord, gap opened, perforations closed		
α= 0.0°	U=20.0m/s	$\dot{\delta}$=990-778-560-344°/s

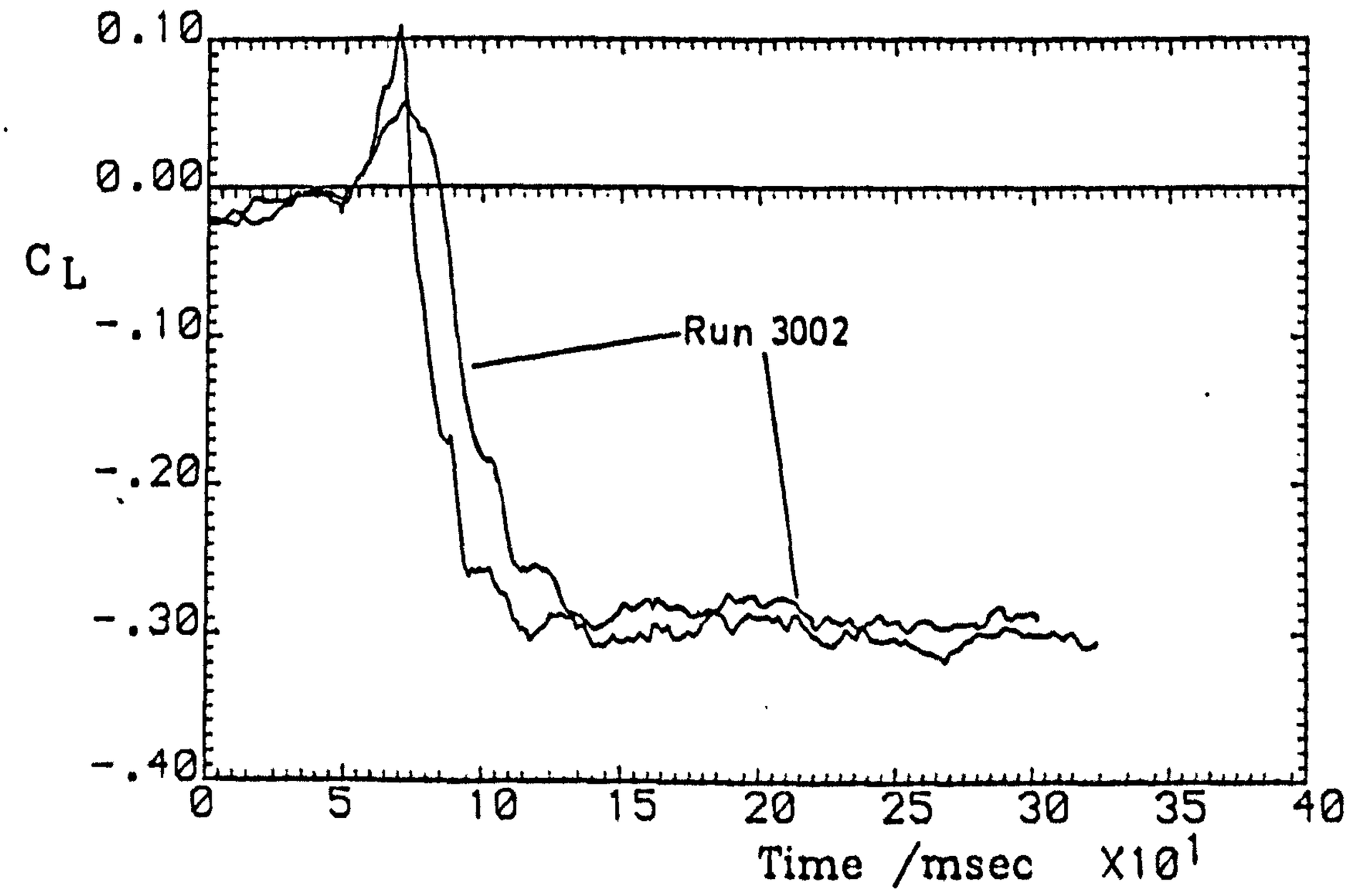

Fig. 5.40(b) Aerofoil lift time history

Run 3631

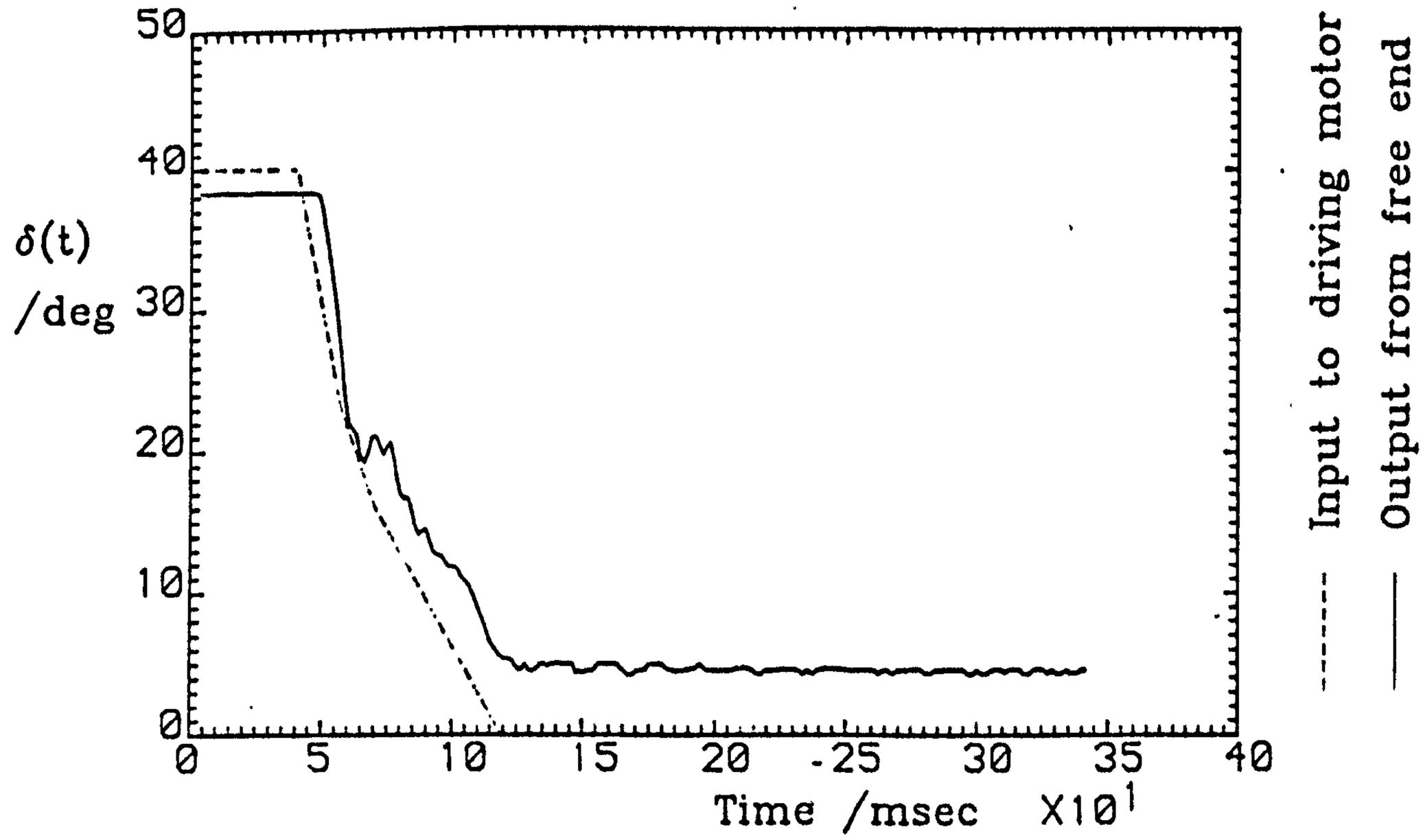

Fig. 5.41(a) Spoiler displacement trace

Spoiler configuration: Upper-surface,		
70% chord, gap opened, perforations closed		
α= 0.0°	U=20.0m/s	$\dot{\delta}$=990-600-330°/s

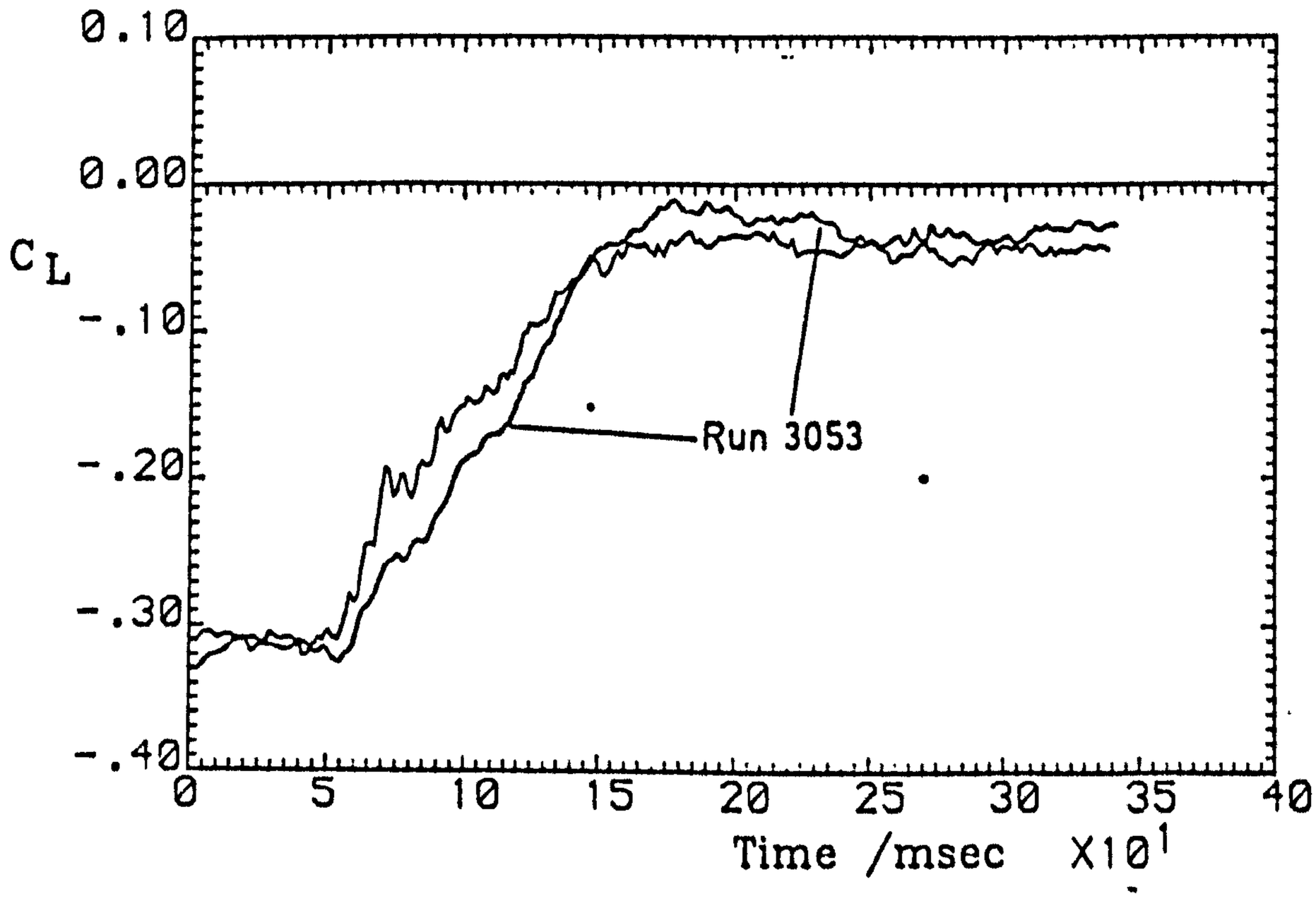

Fig. 5.41(b) Aerofoil lift time history

Run 3561

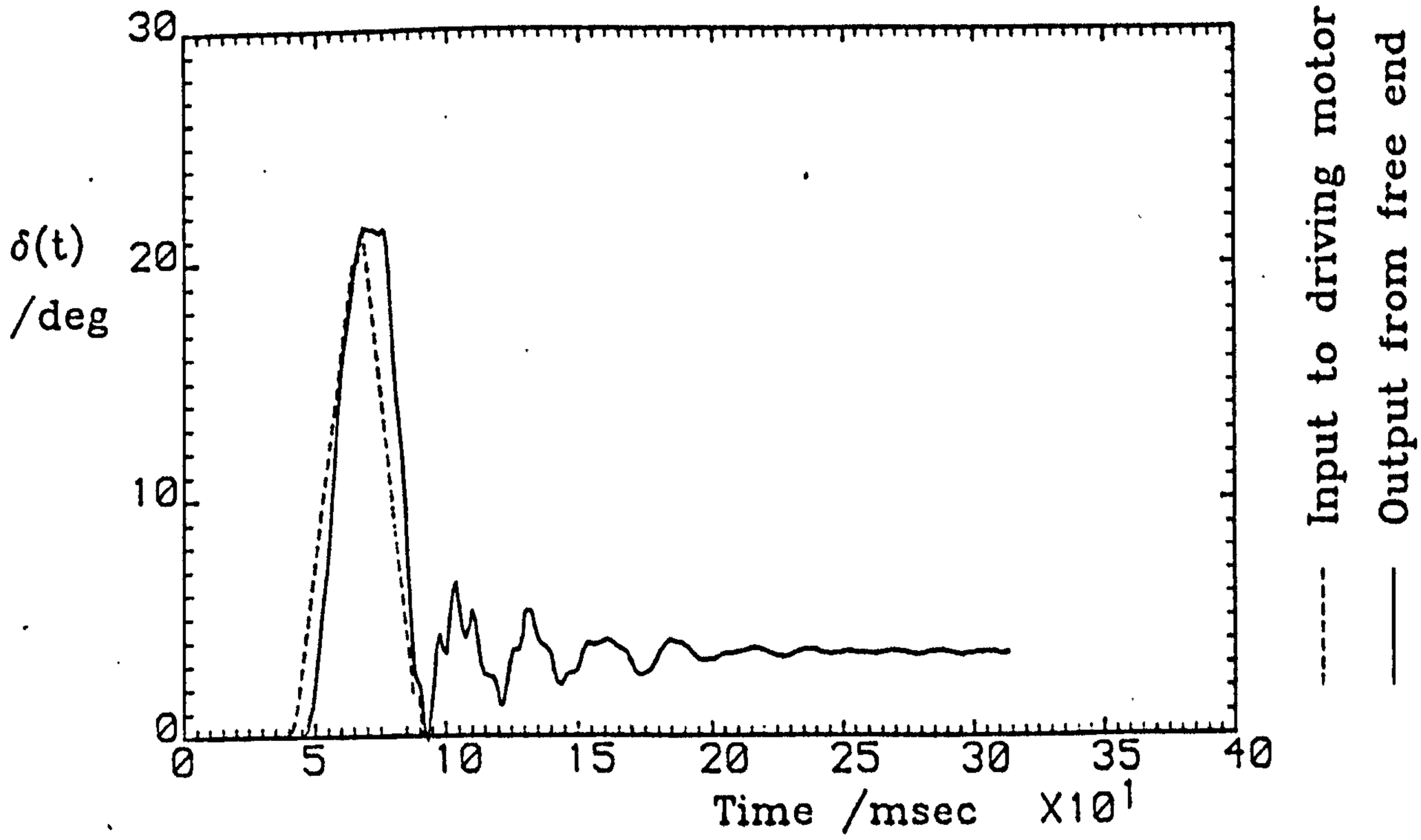

Fig. 5.42 (a) Spoiler displacement trace

Spoiler configuration: Upper-surface,		
70% chord, gap opened, perforations closed		
α= 0.0°	U=20.0m/s	$\dot{\delta}$=990-990°/s

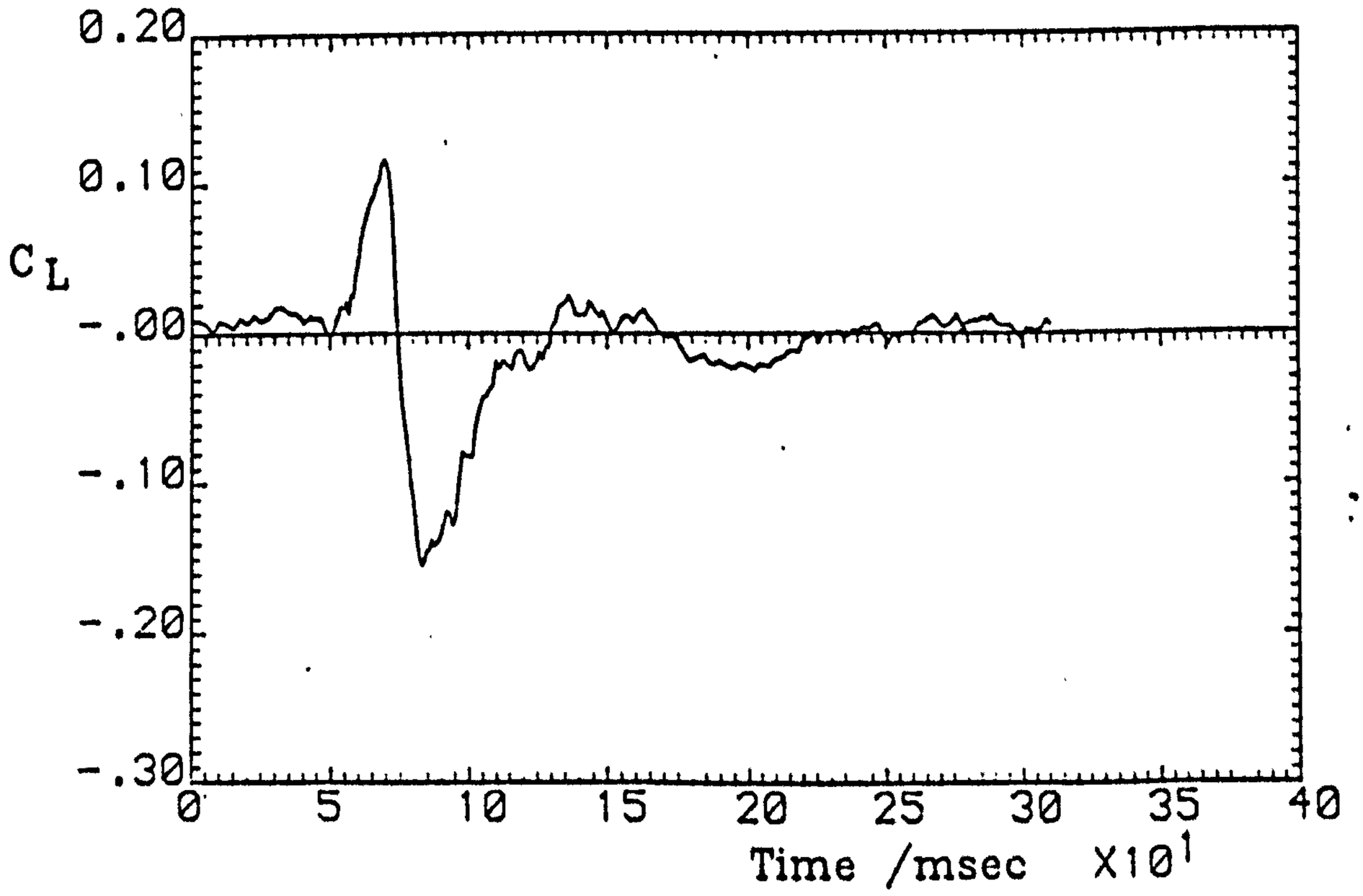

Fig. 5.42 (b) Aerofoil lift time history

Run 3901

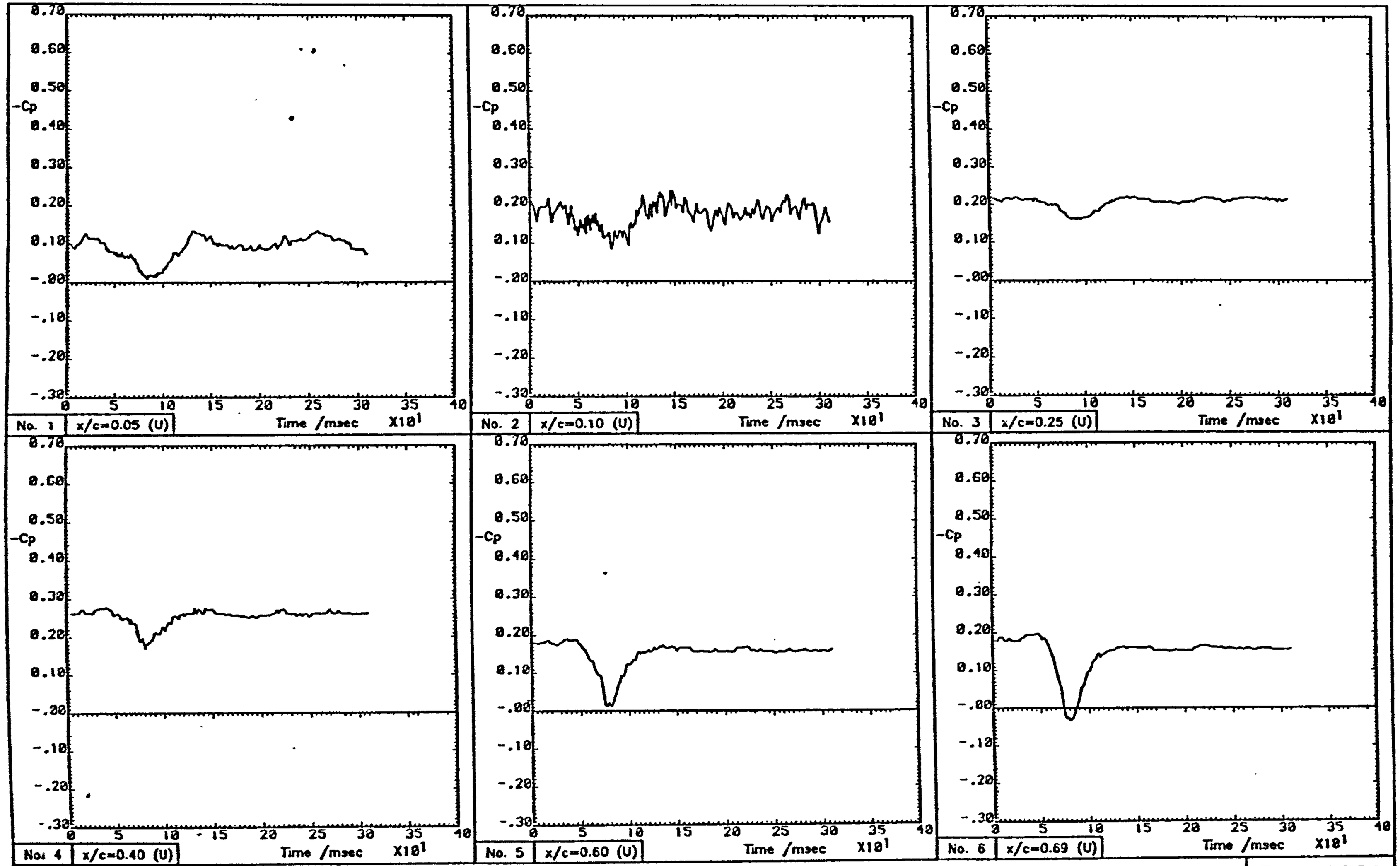

Fig. 5.43(a) Pressure signal time histories

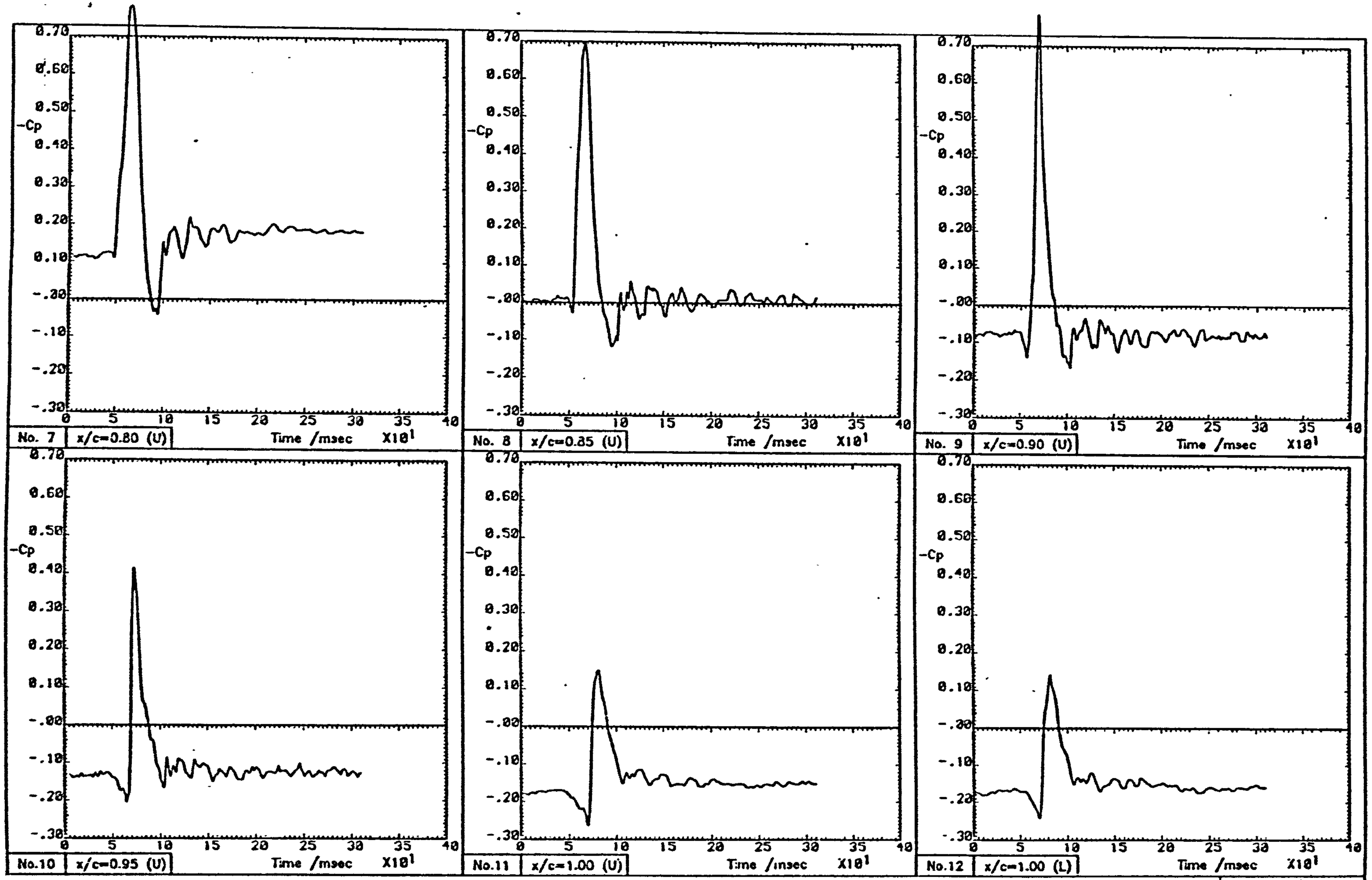

Fig. 5.43(b) Pressure signal time histories

Run 3901

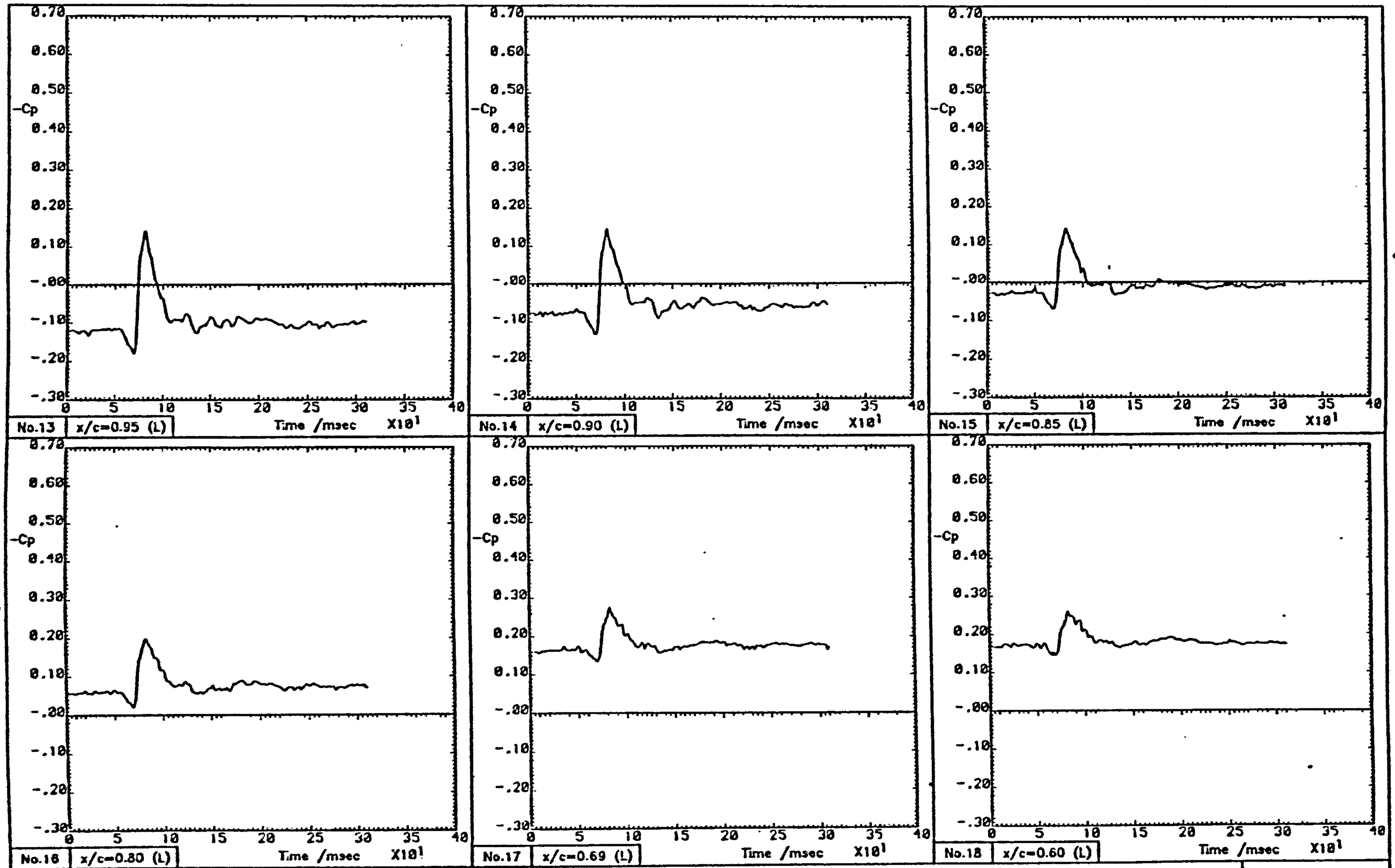

Fig. 5.43(c) Pressure signal time histories

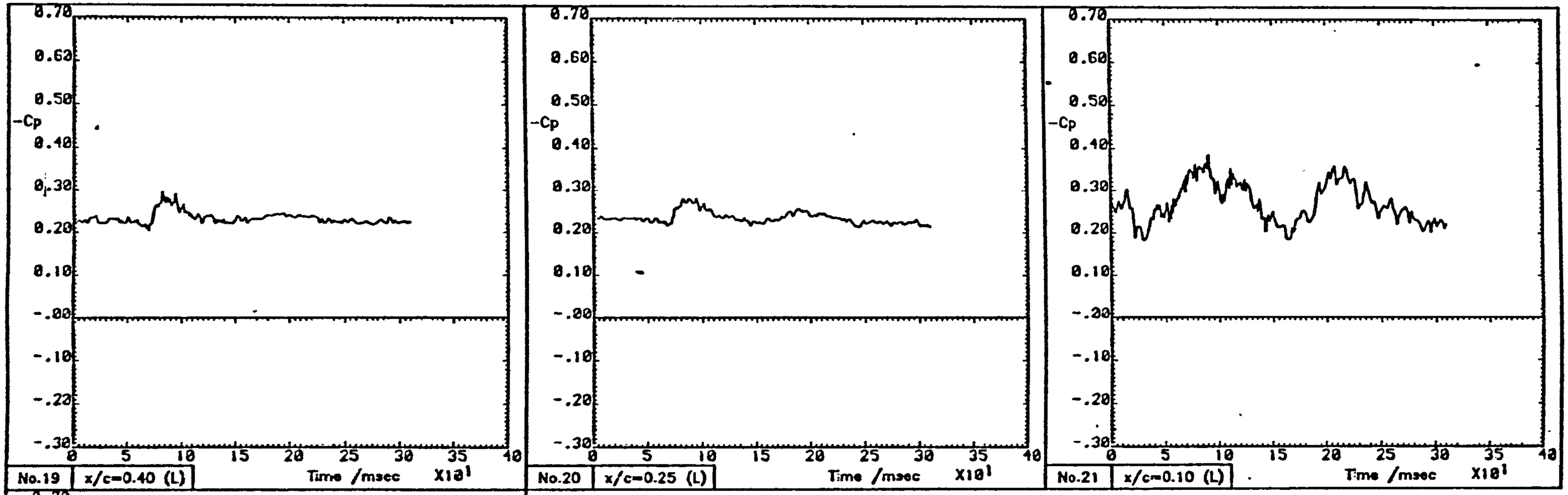

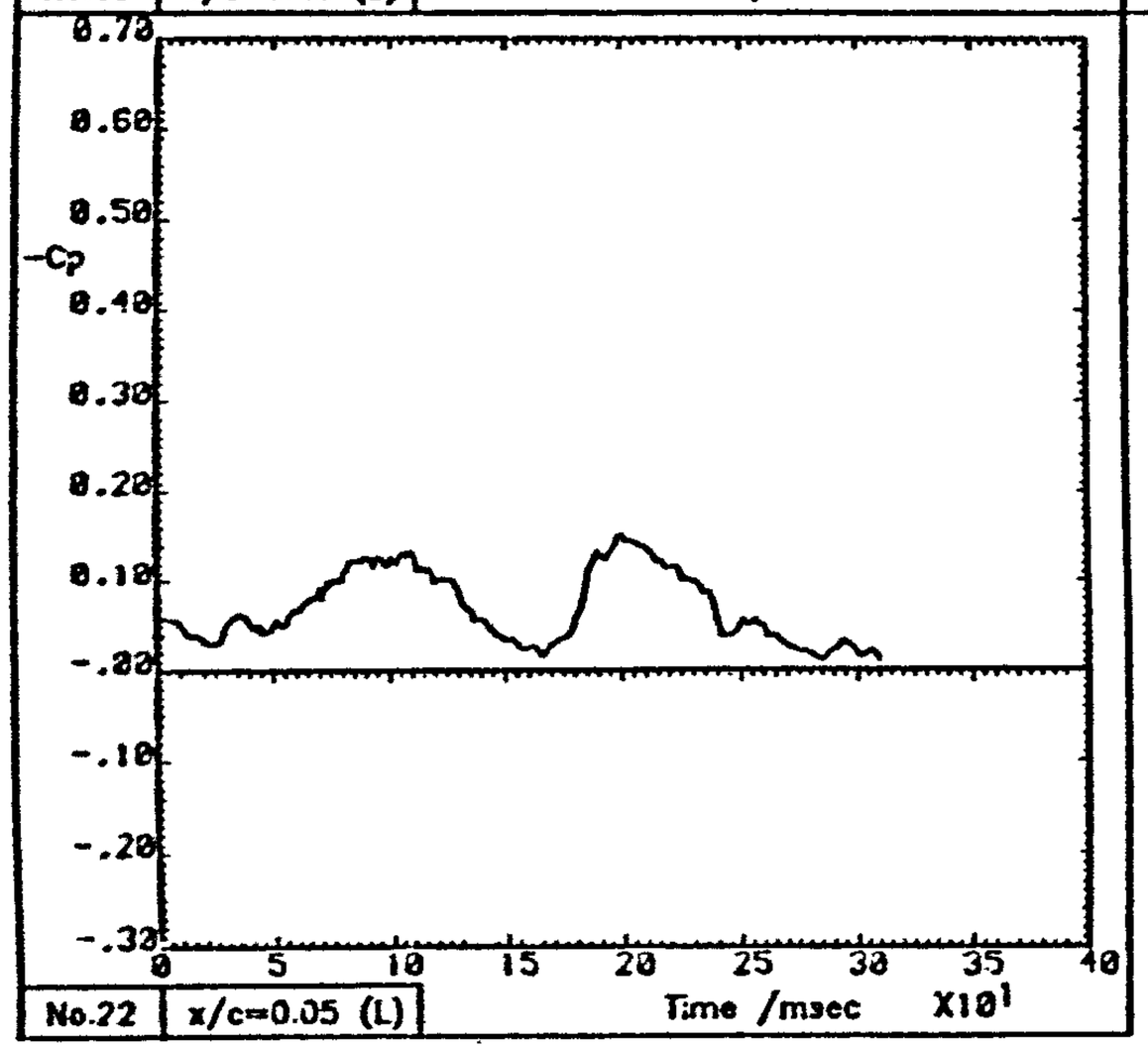

Fig. 5.43(d) Pressure signal time histories

Run 3901

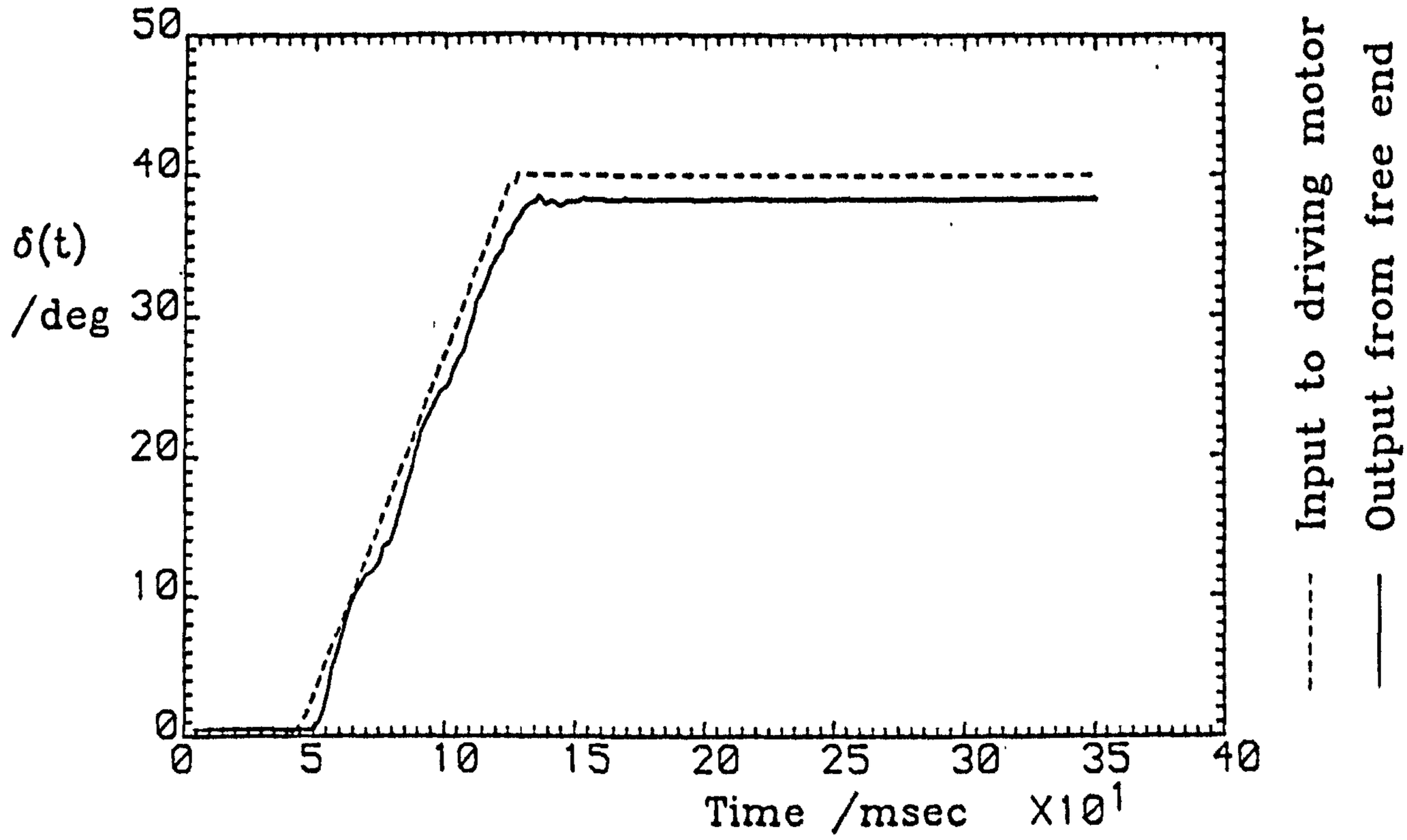

Fig. 5.44(a) Spoiler displacement trace

Spoiler configuration: Lower surface,		
70% chord, gap opened, perforations closed		
α=15.0°	U=20.0m/s	$\dot{\delta}$=500°/s

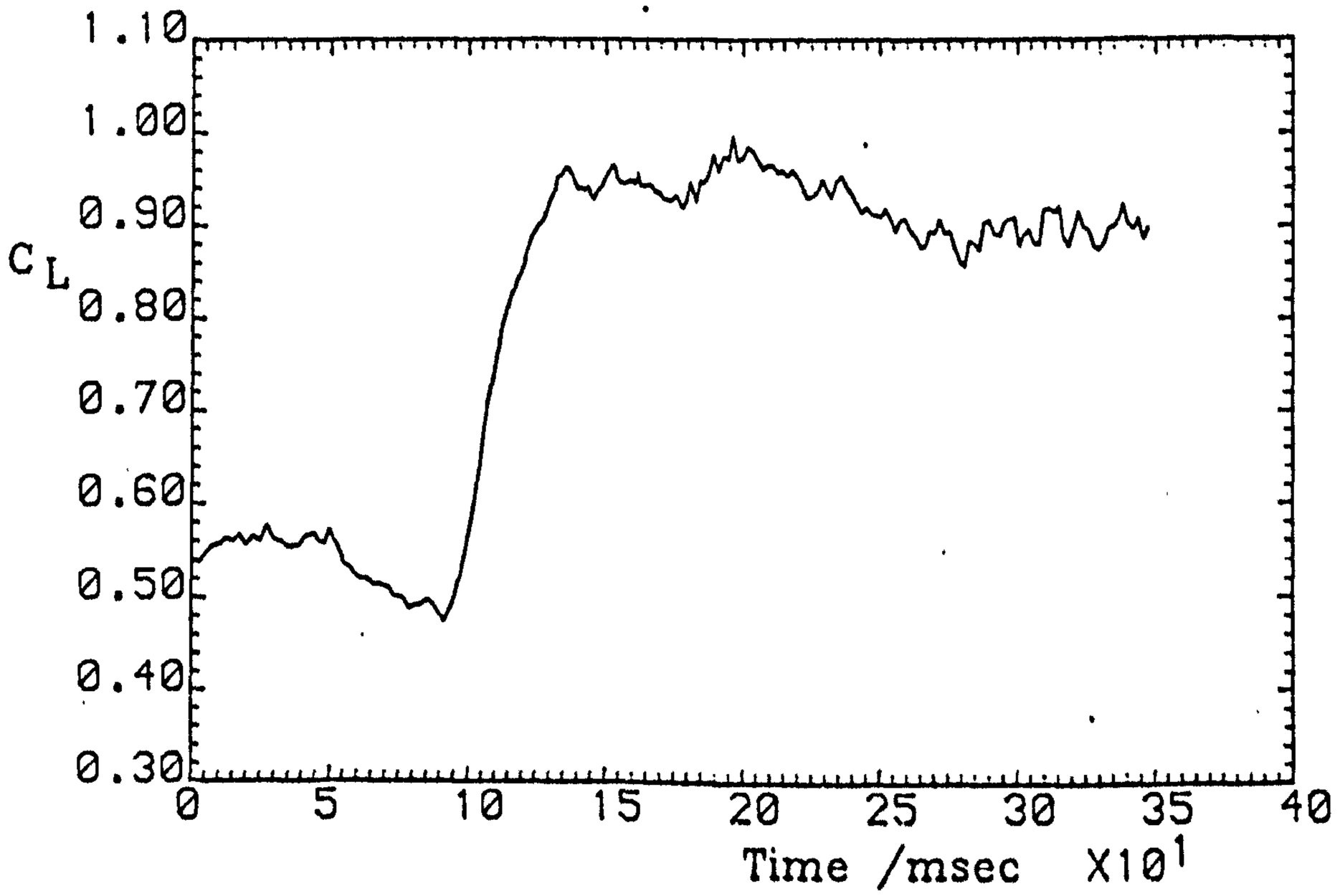

Fig. 5.44(b) Aerofoil lift time history

Run 9202

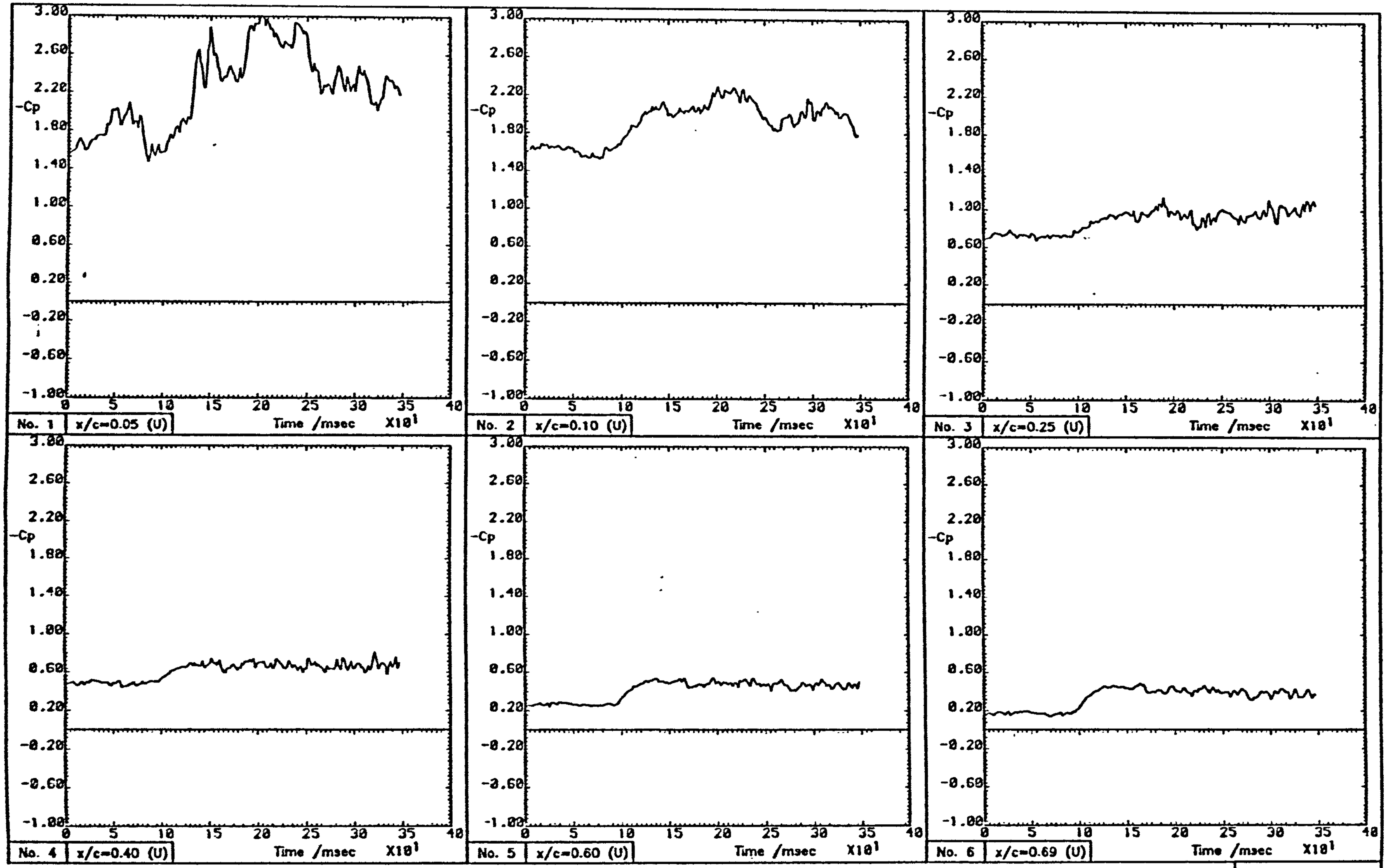

Fig. 5.45 (a) Pressure signal time histories

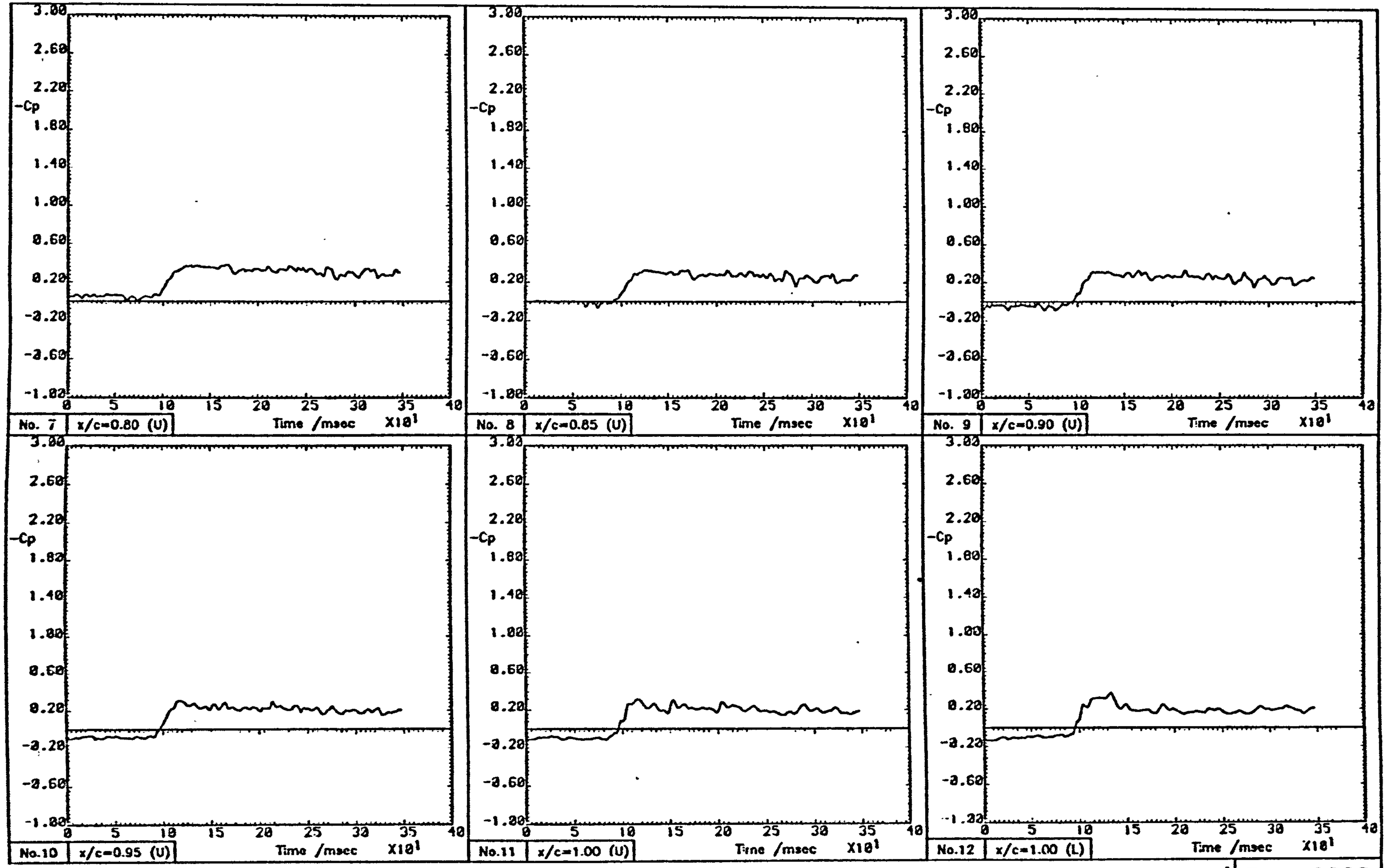

Fig. 5.45 (b) Pressure signal time histories

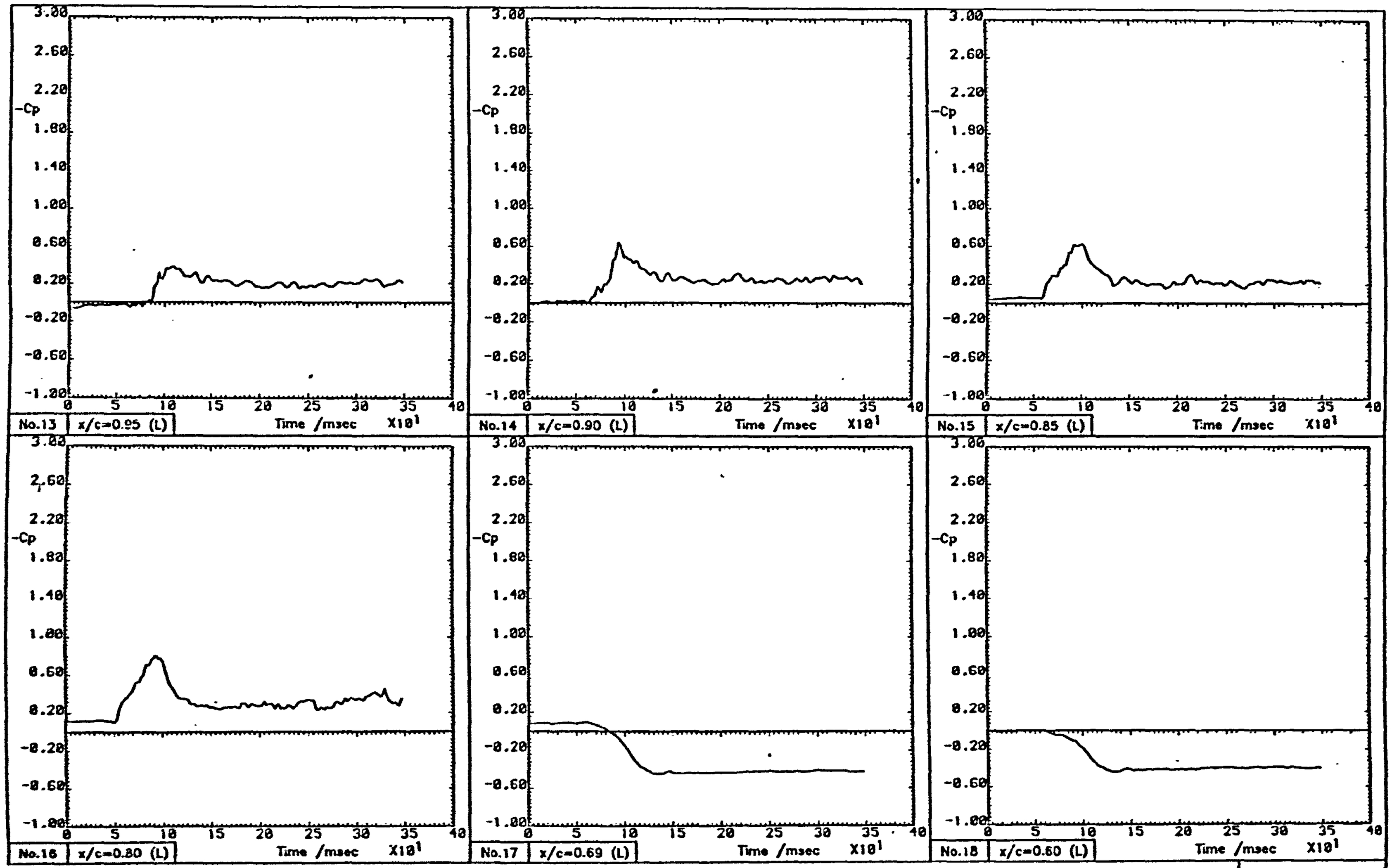

Fig. 5.45 (c) Pressure signal time histories

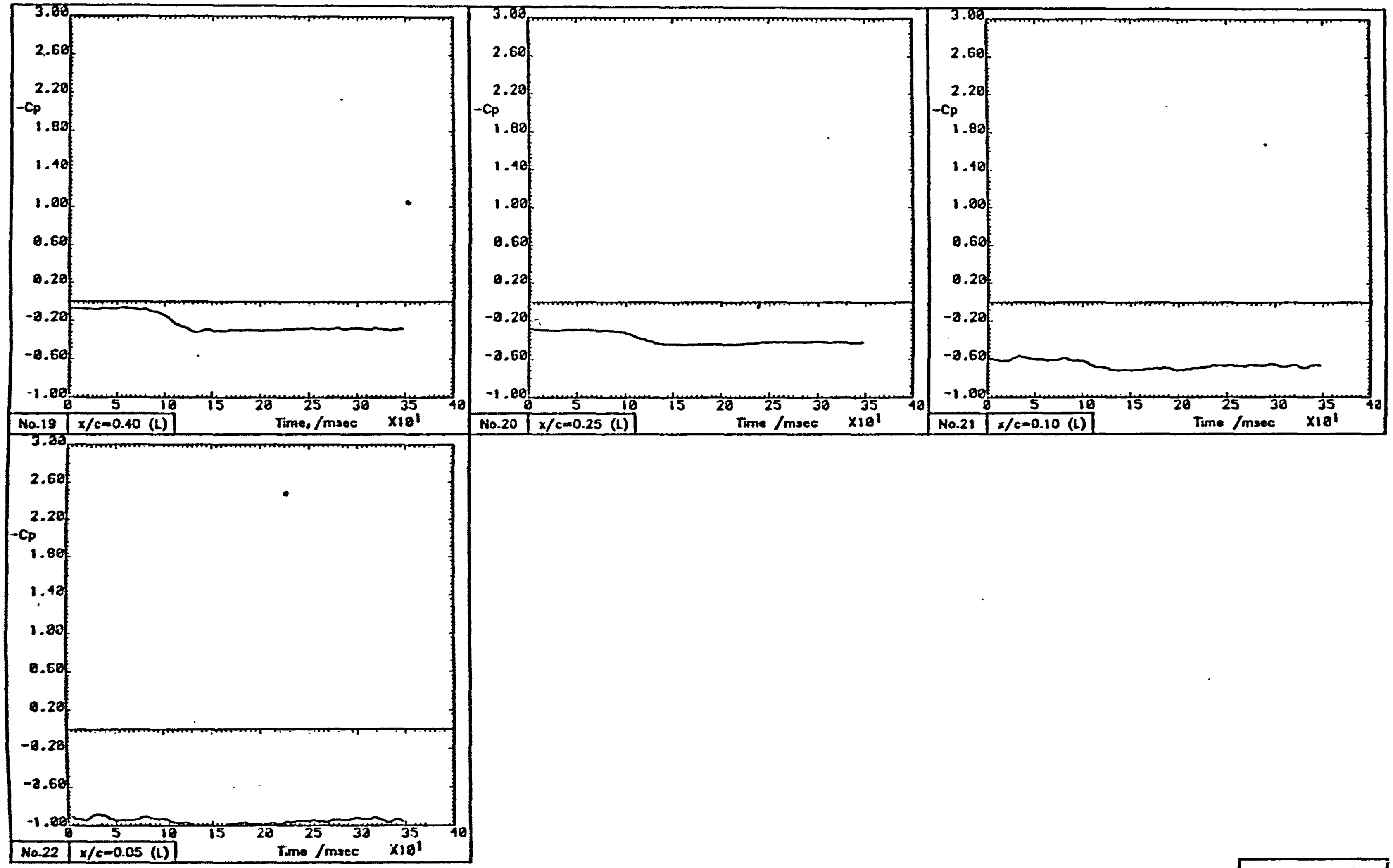

Fig. 5.45 (d) Pressure signal time histories

Run 9202

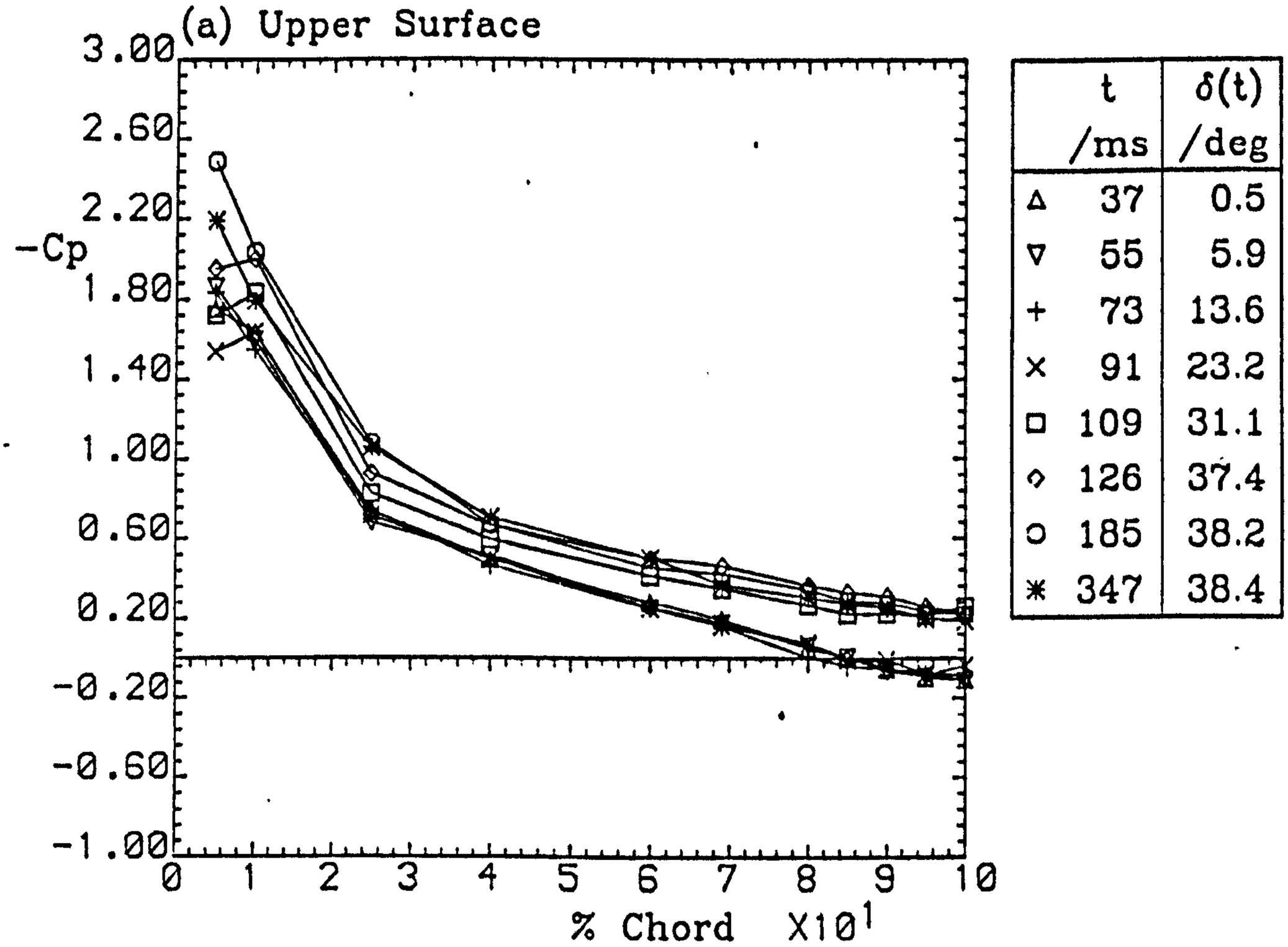

	t /ms	δ(t) /deg
△	37	0.5
▽	55	5.9
+	73	13.6
×	91	23.2
□	109	31.1
◇	126	37.4
○	185	38.2
✳	347	38.4

Fig. 5.46 Time-varying pressure distributions

Run 9202

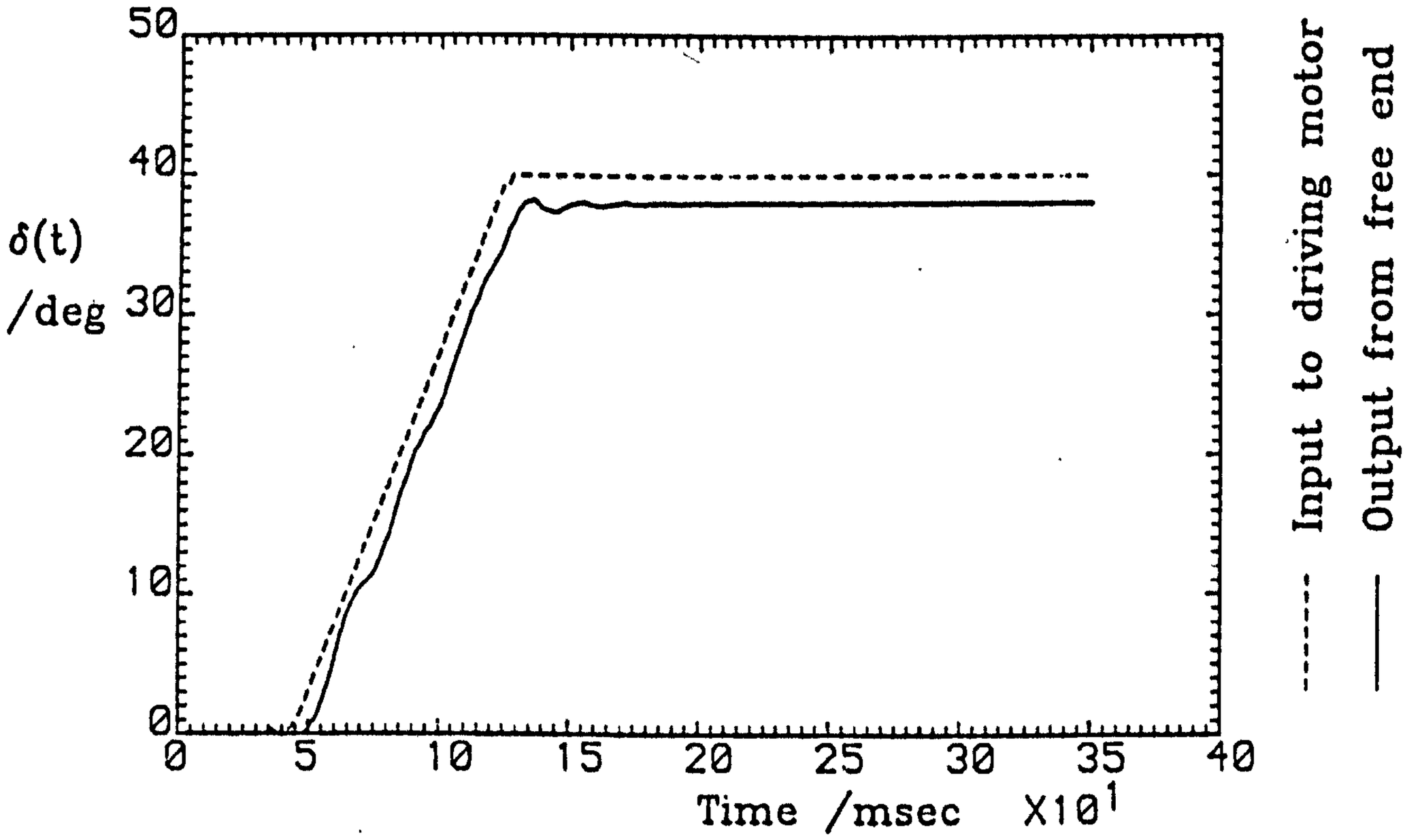

Fig. 5.47(a) Spoiler displacement trace

Spoiler configuration: Lower-surface,		
70% chord, gap closed, perforations closed		
α=15.0°	U=20.0m/s	$\dot{\phi}$=500°/s

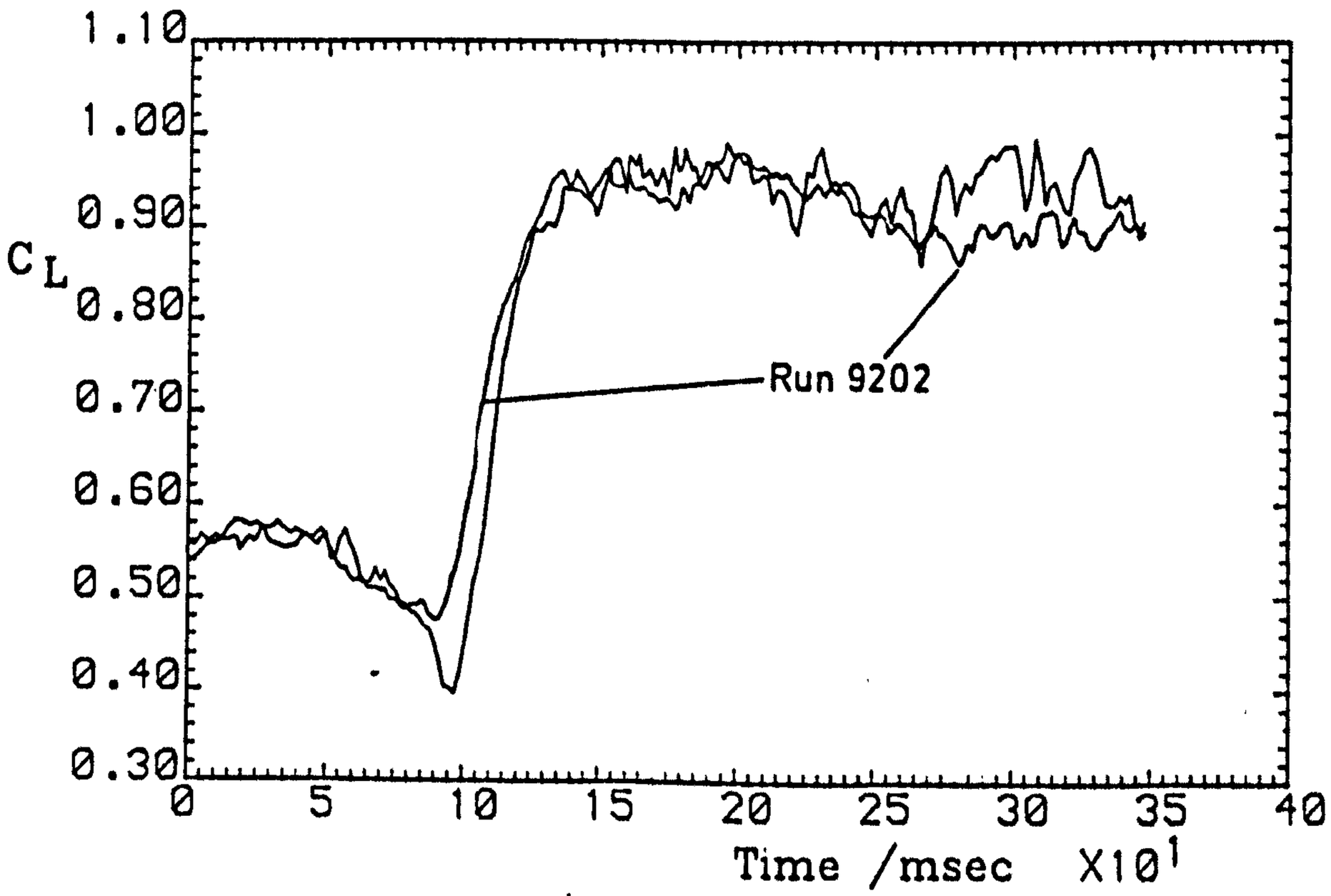

Fig. 5.47(b) Aerofoil lift time history

Run 9002

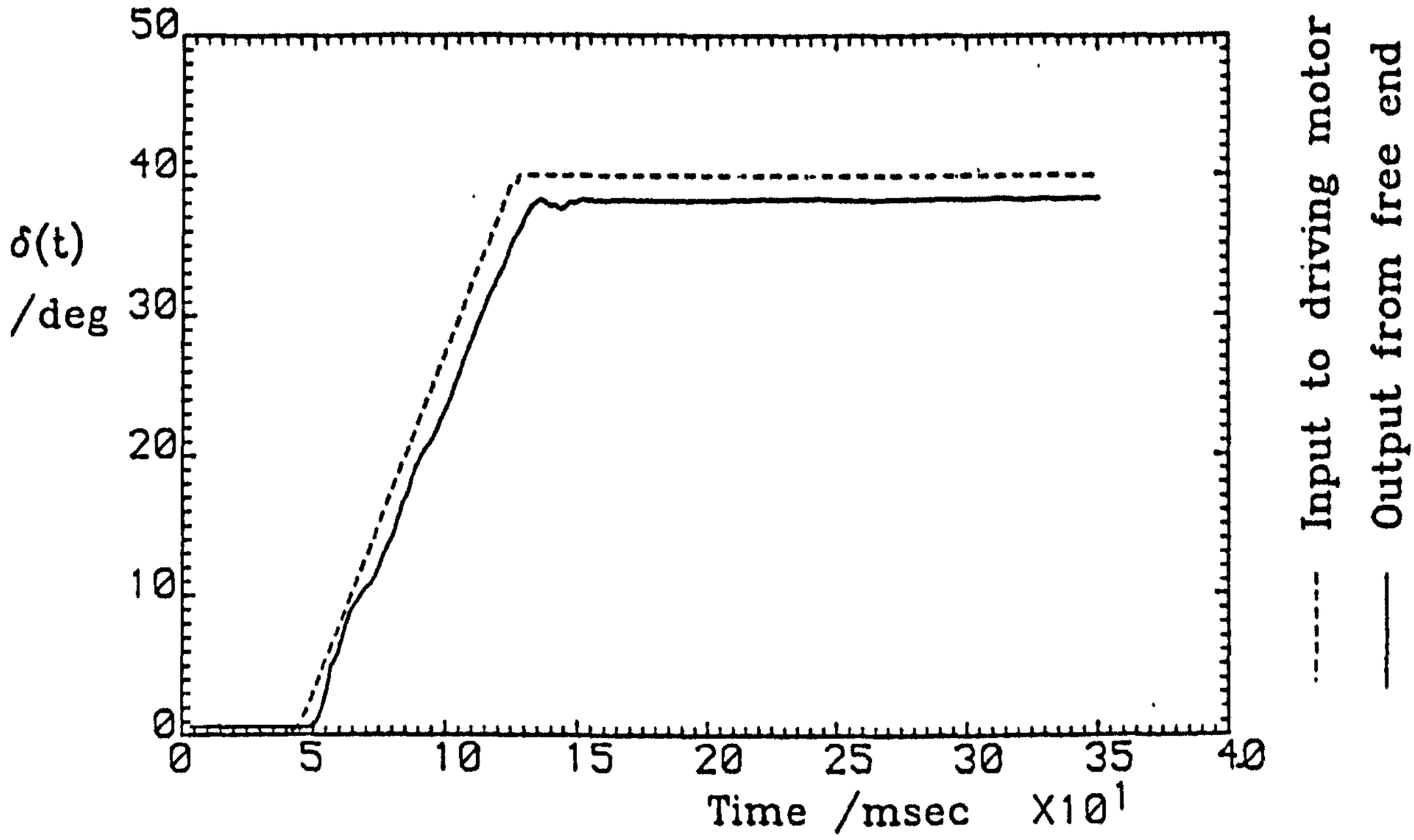

Fig. 5.48(a) Spoiler displacement trace

Spoiler configuration: Lower-surface,		
70% chord, gap closed, perforations closed		
α=20.0°	U=20.0m/s	$\dot{\delta}$=500°/s

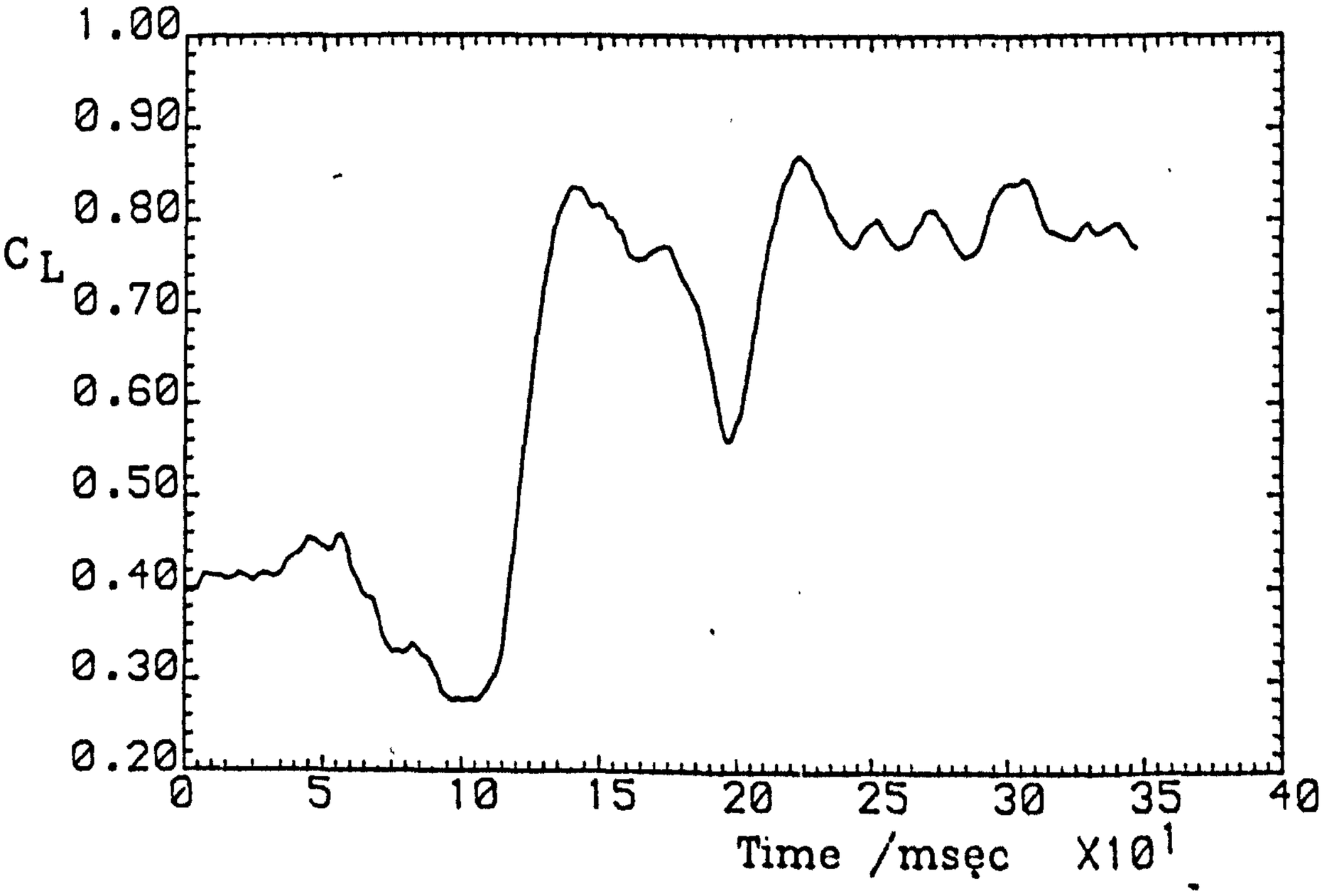

Fig. 5.48(b) Aerofoil lift time history

Run 7102

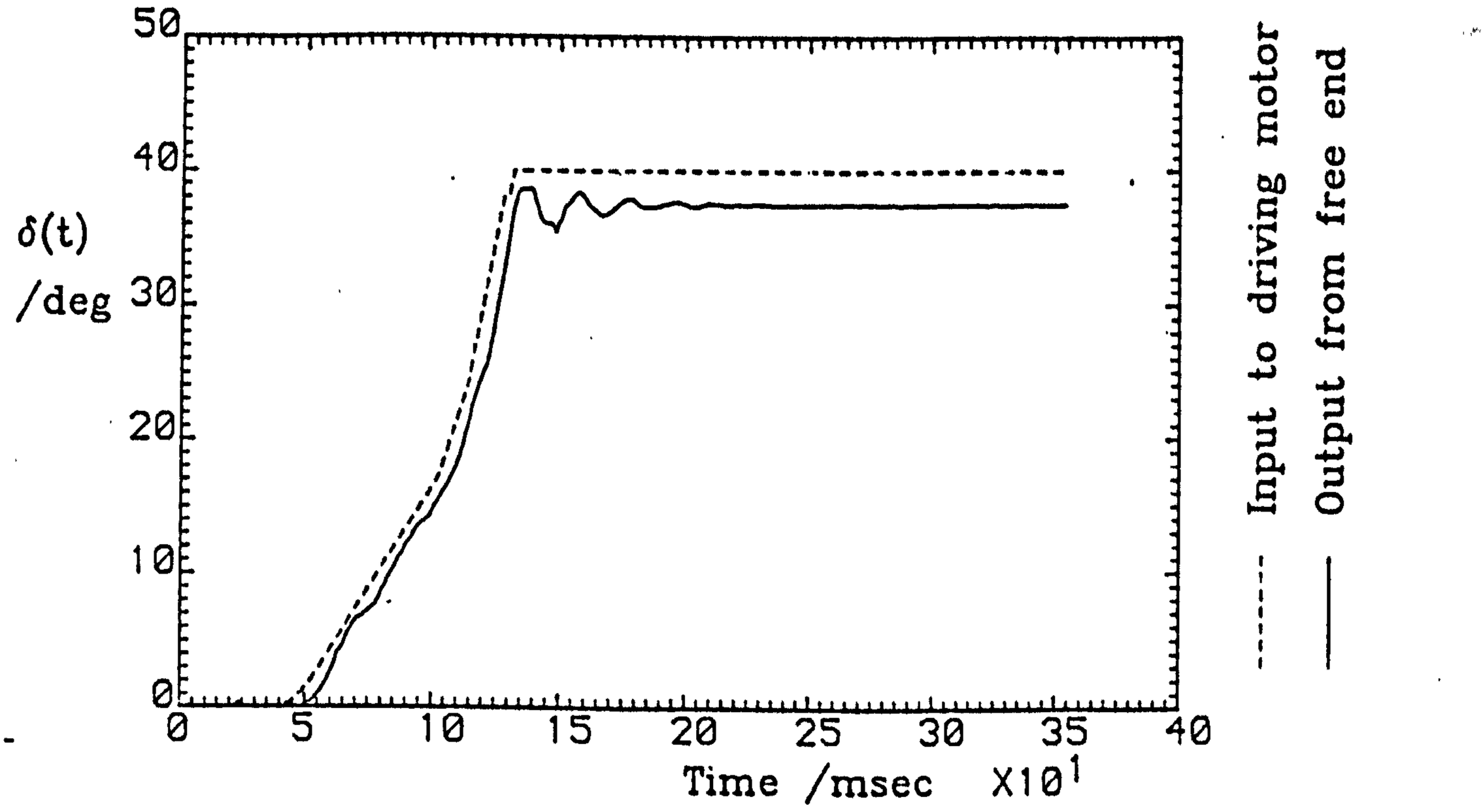

Fig. 5.49(a) Spoiler displacement trace

Spoiler configuration: Lower-surface,		
70% chord, gap closed, perforations closed		
α=15.0°	U=20.0m/s	$\dot{\delta}$=330-600-990°/s

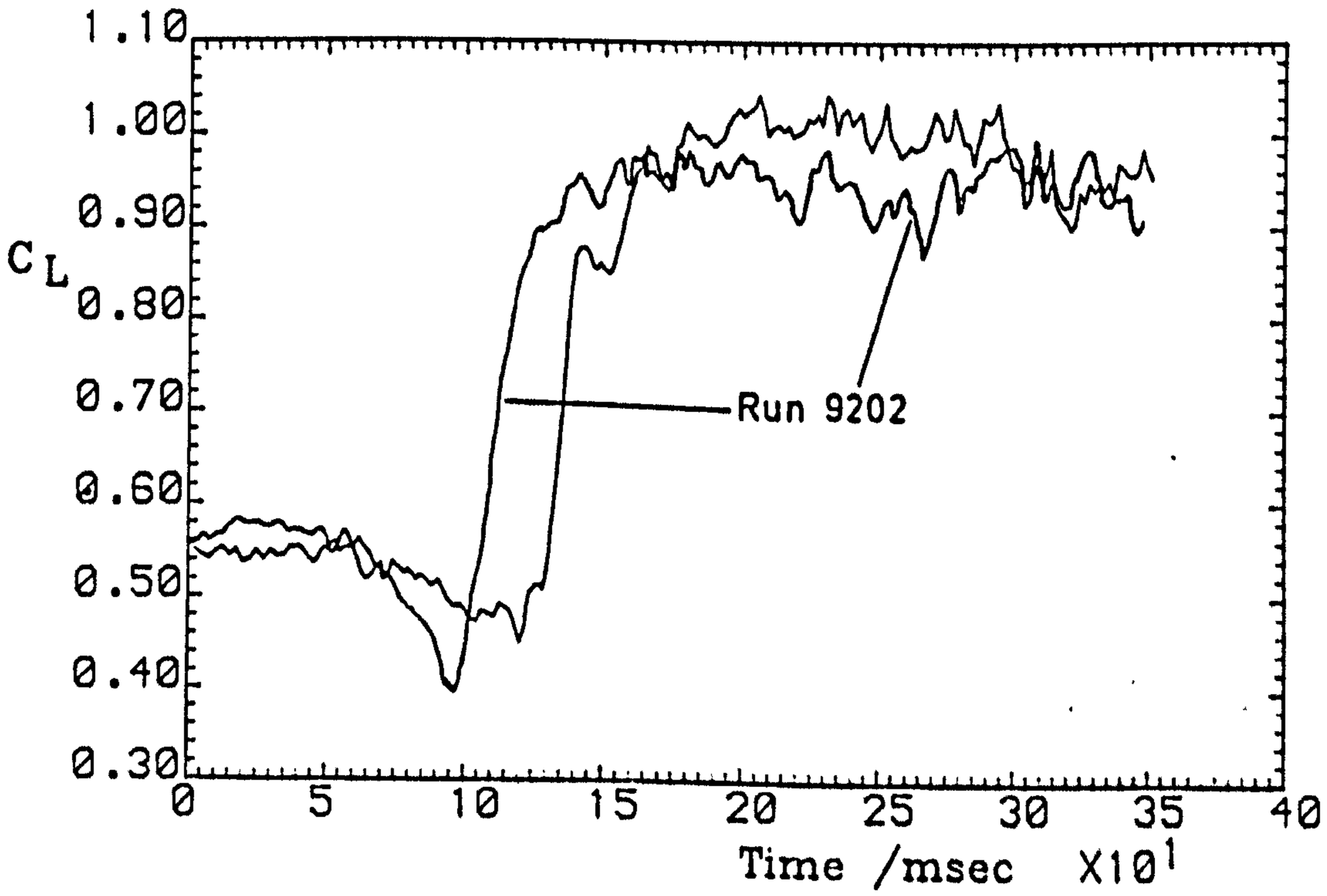

Fig. 5.49(b) Aerofoil lift time history

Run 9502

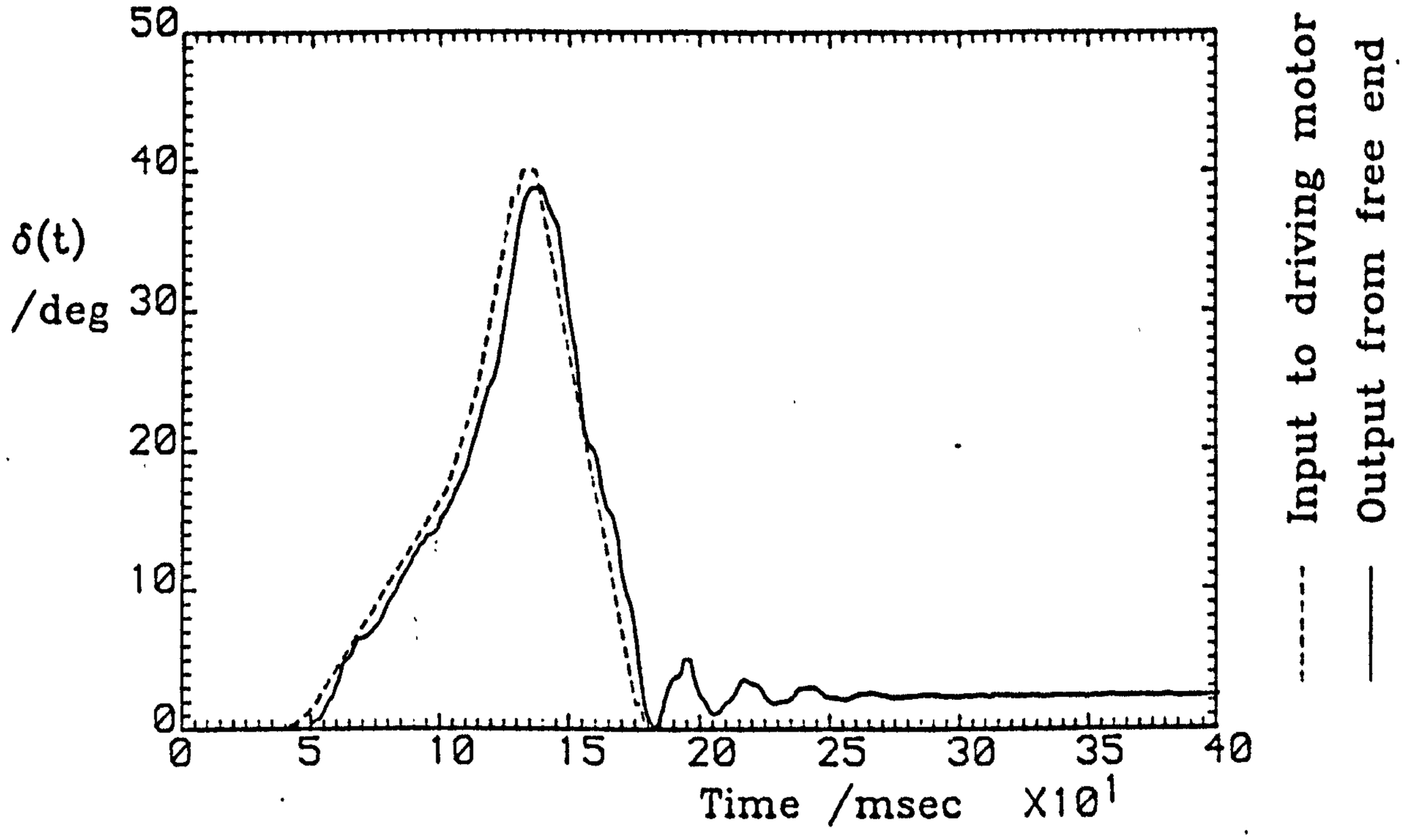

Fig. 5.50(a) Spoiler displacement trace

Spoiler configuration: Lower-surface,		
70% chord, gap closed, perforations closed		
α=15.0°	U=20.0m/s	$\dot{\delta}$=330-600-990-990°/s

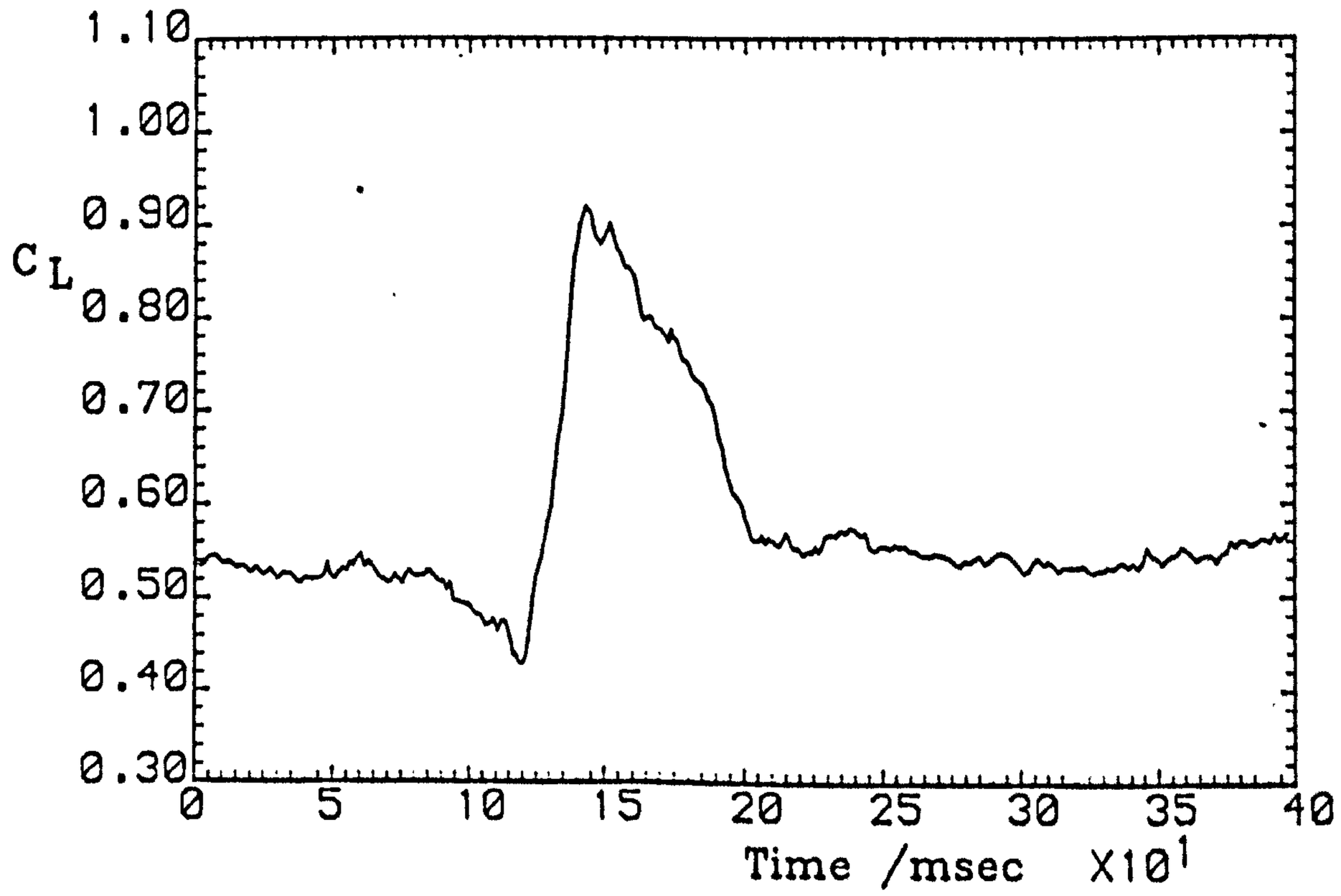

Fig. 5.50(b) Aerofoil lift time history

Run 9504

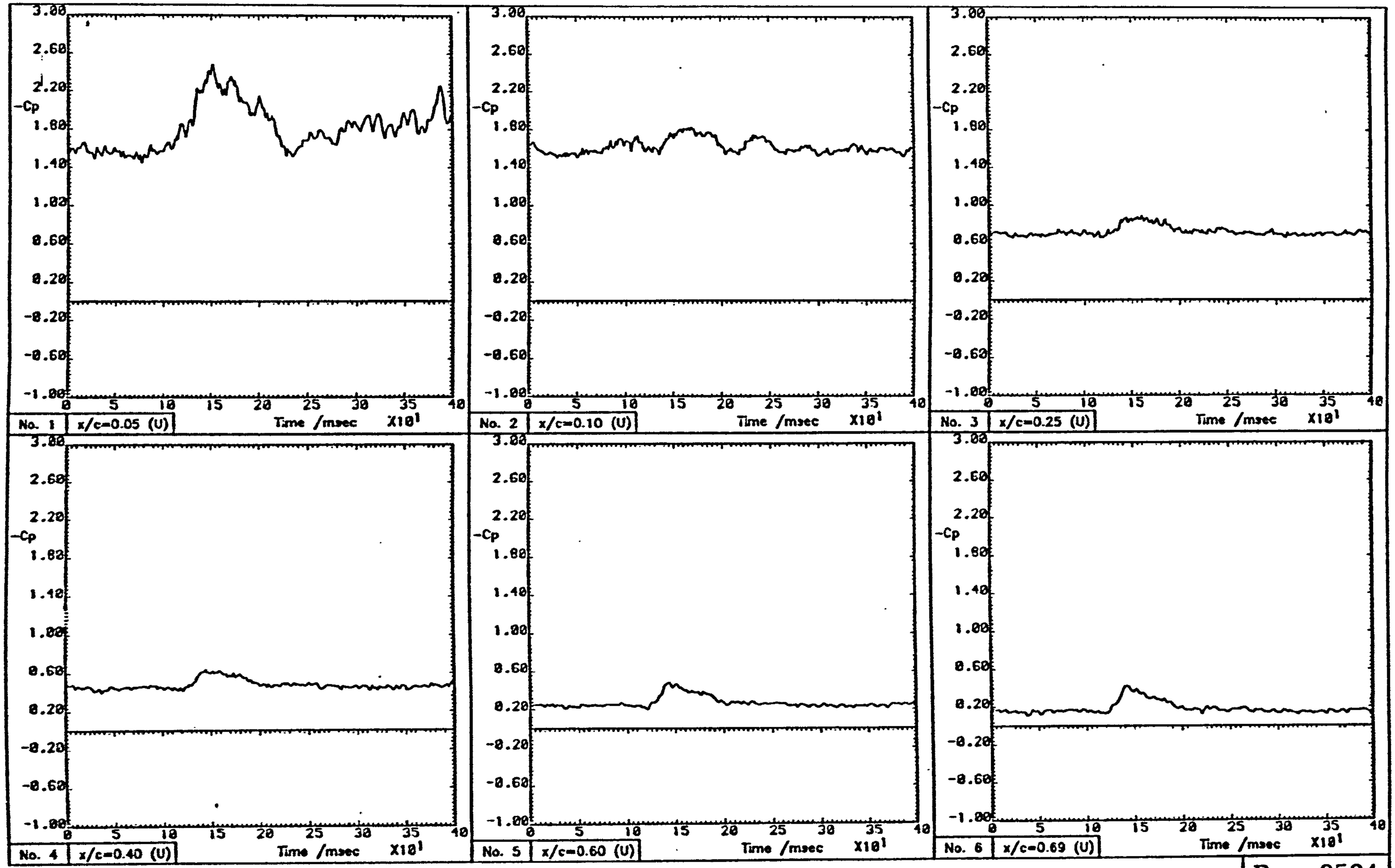

Fig. 5.51(a) Pressure signal time histories

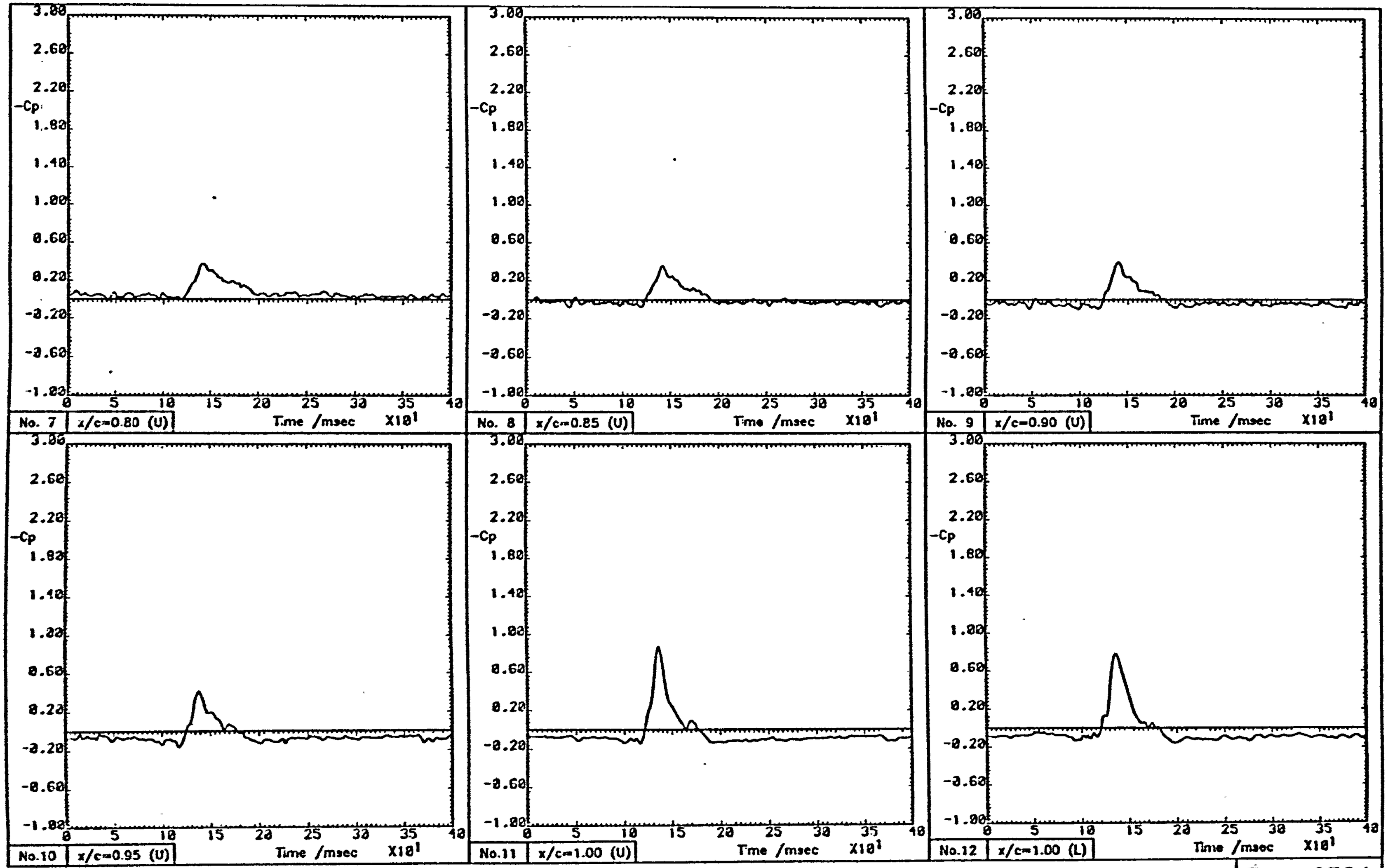

Fig. 5.51(b) Pressure signal time histories

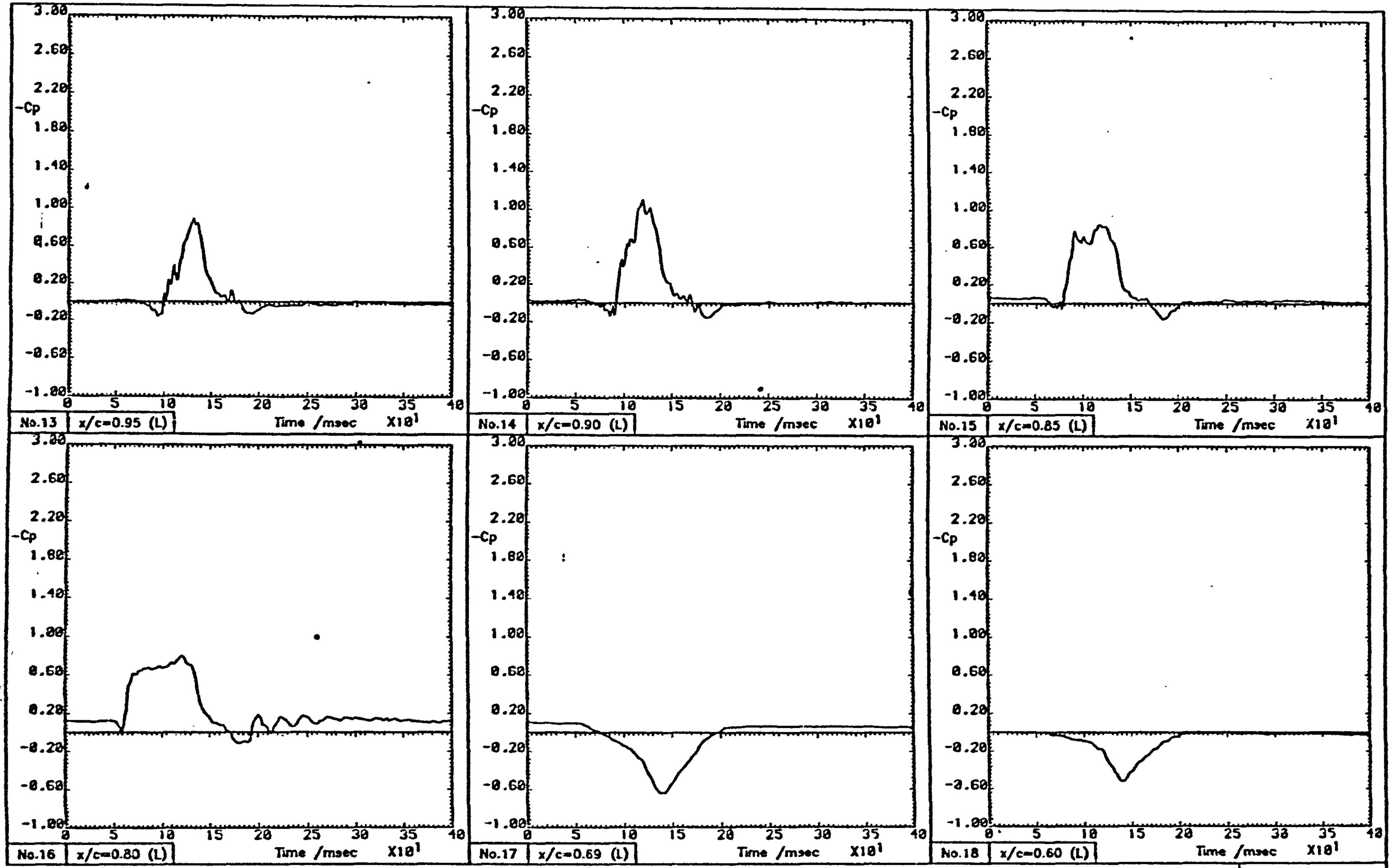

Fig. 5.51 (c) Pressure signal time histories

Run 9504

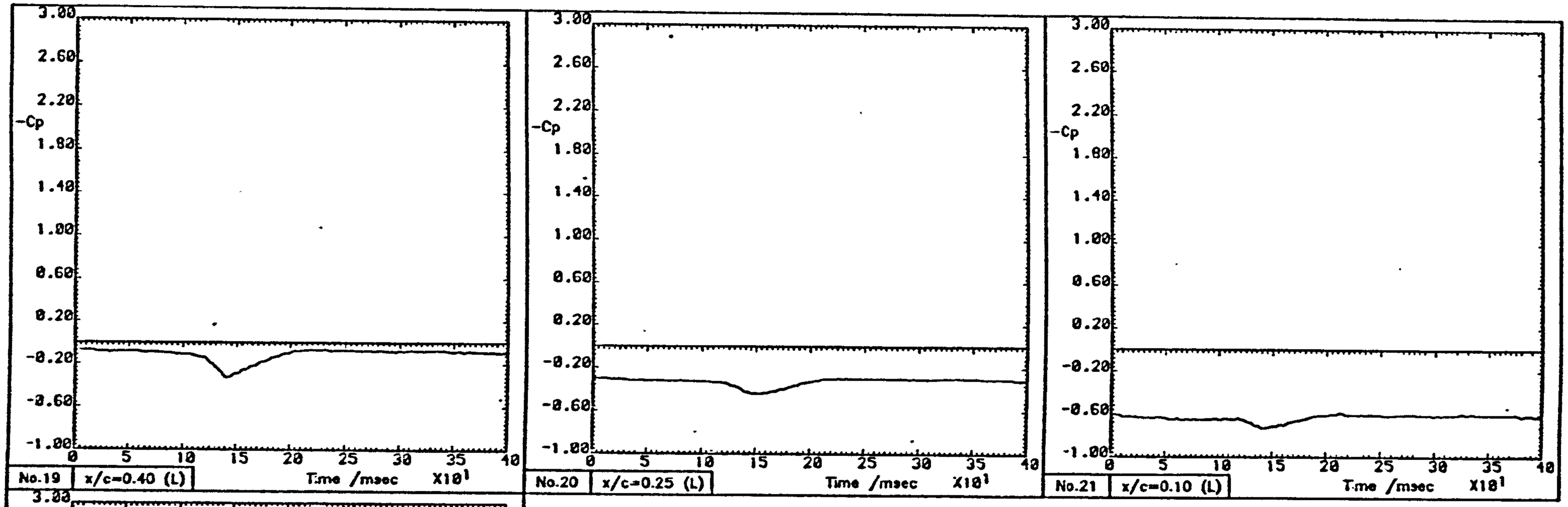

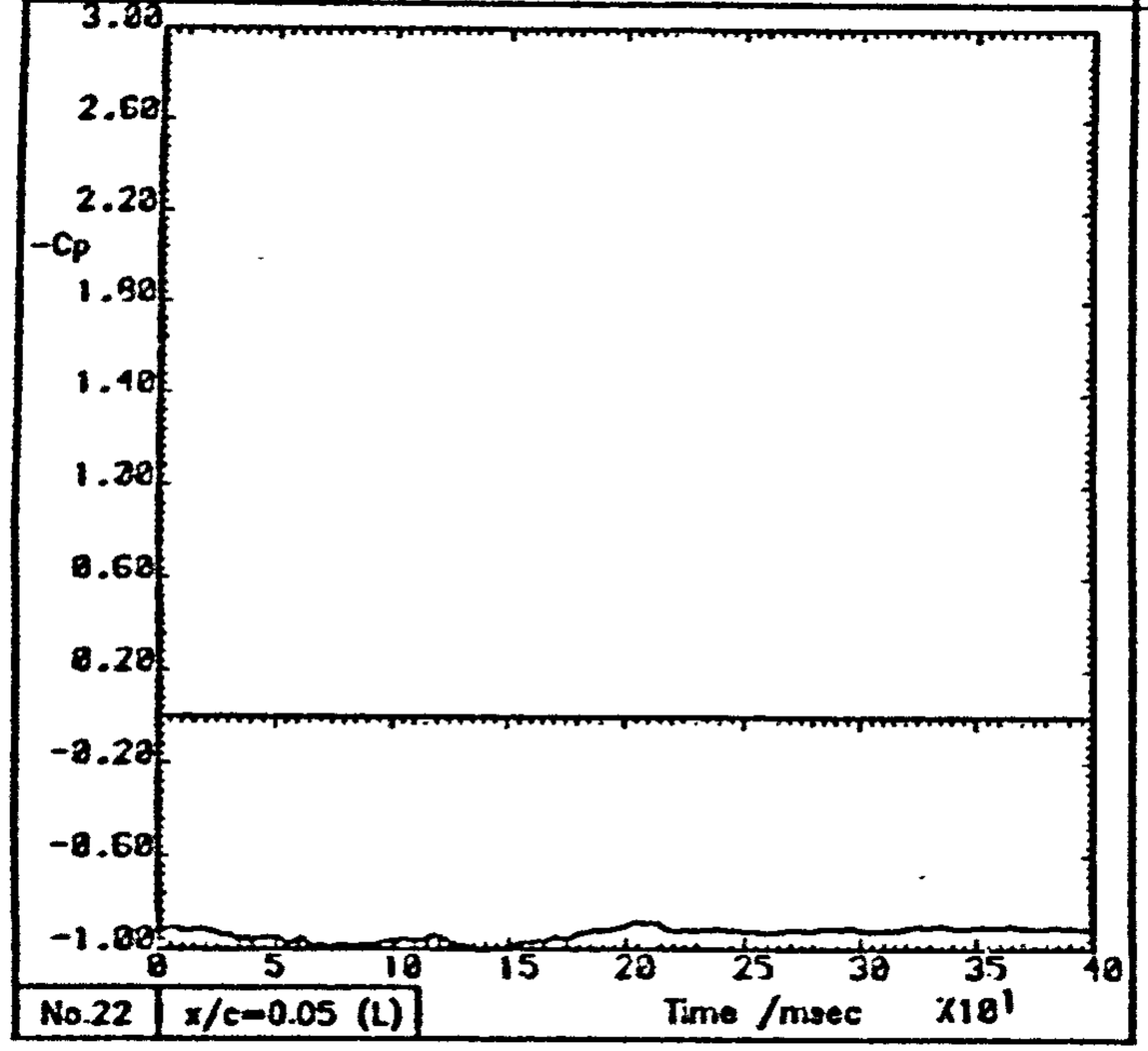

Fig. 5.51(d) Pressure signal time histories

Run 9504

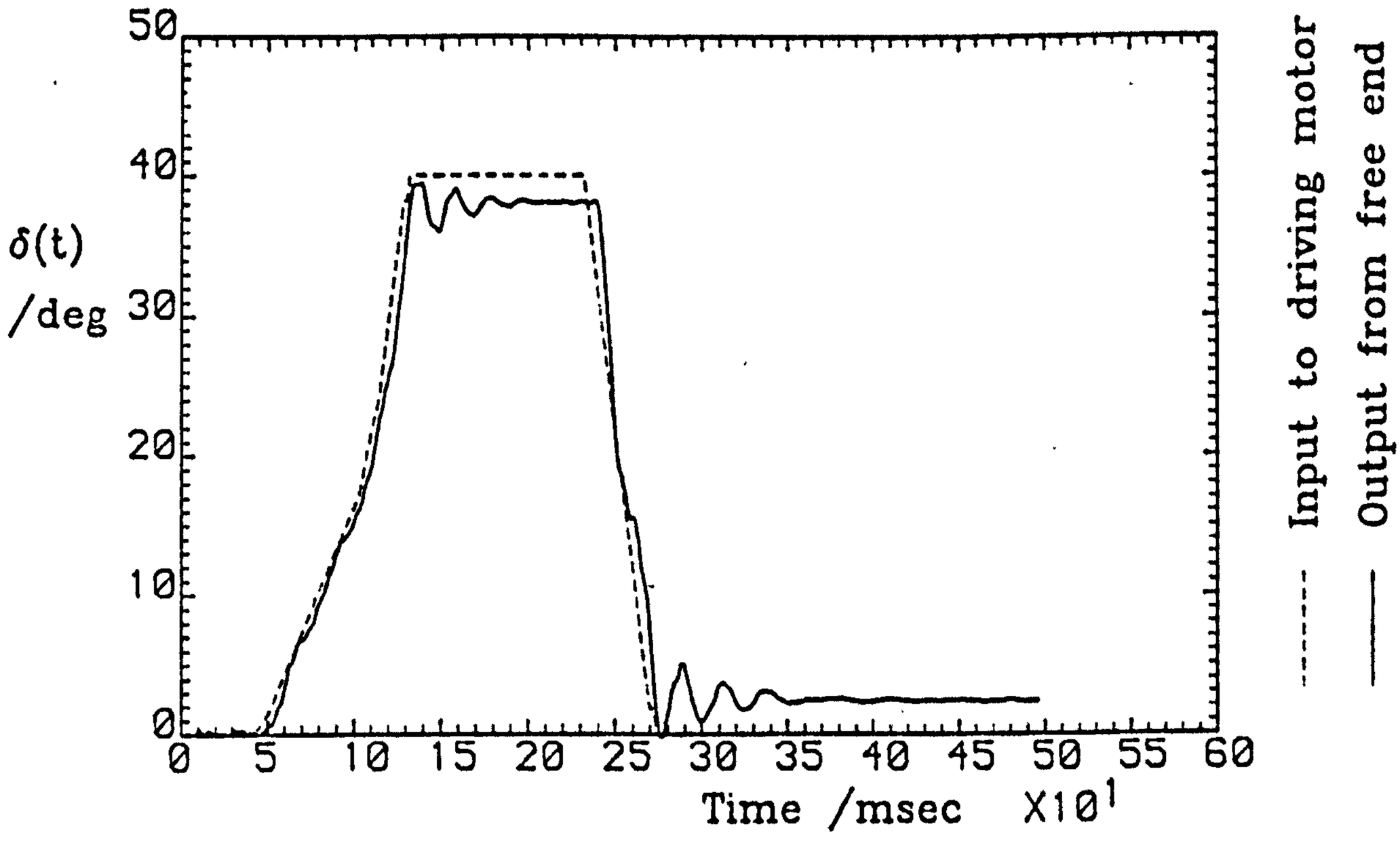

Fig. 5.52(a) Spoiler displacement trace

Spoiler configuration: Lower-surface,		
70% chord, gap closed, perforations closed		
α=15.0°	U=20.0m/s	$\dot{\delta}$=330-600-990-990°/s

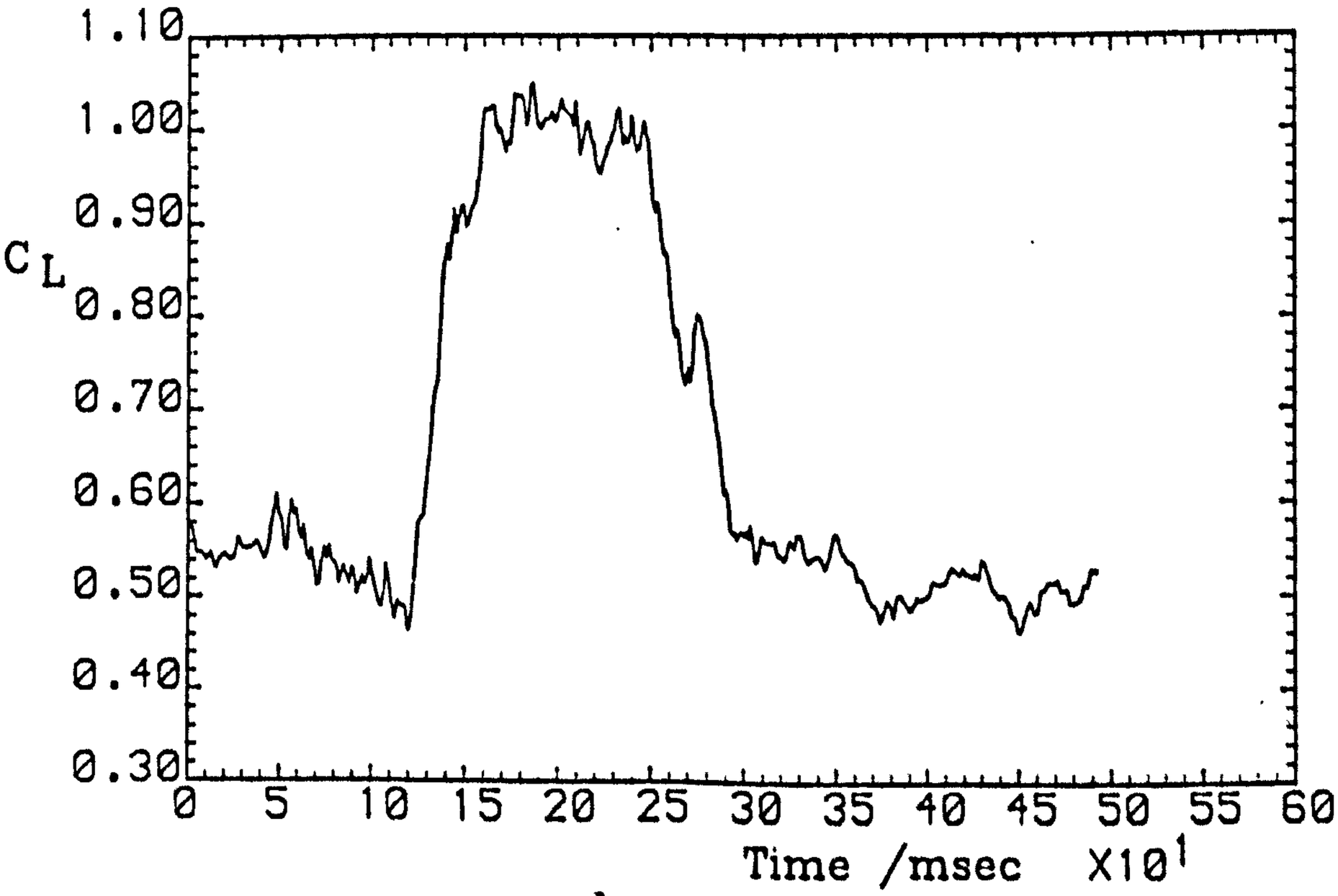

Fig. 5.52(b) Aerofoil lift time history

Run 9505

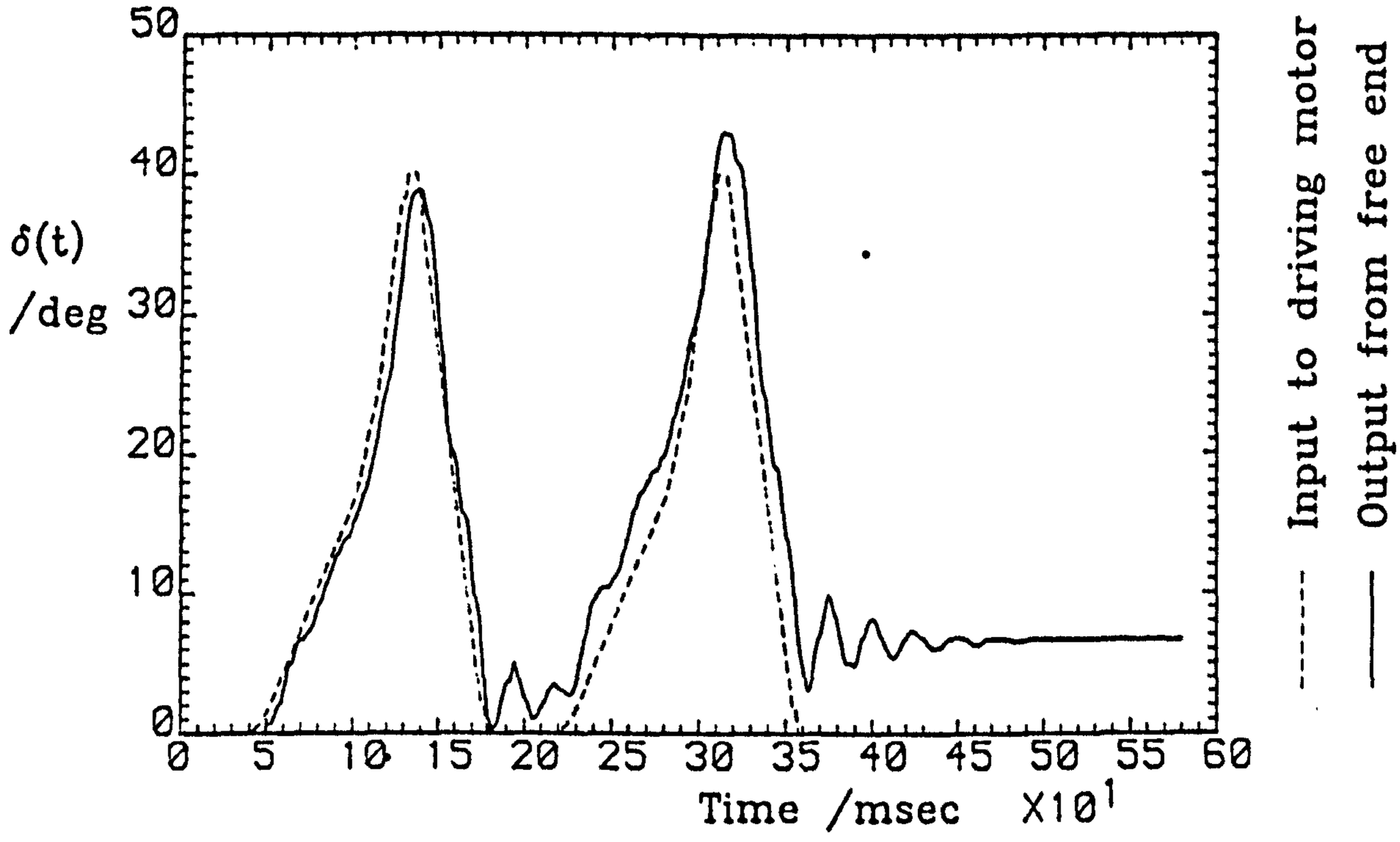

Fig. 5.53(a) Spoiler displacement trace

Spoiler configuration: Lower-surface,		
70% chord, gap closed, perforations closed		
α=15.0°	U=20.0m/s	$\dot{\delta}$=330-600-990-990°/s

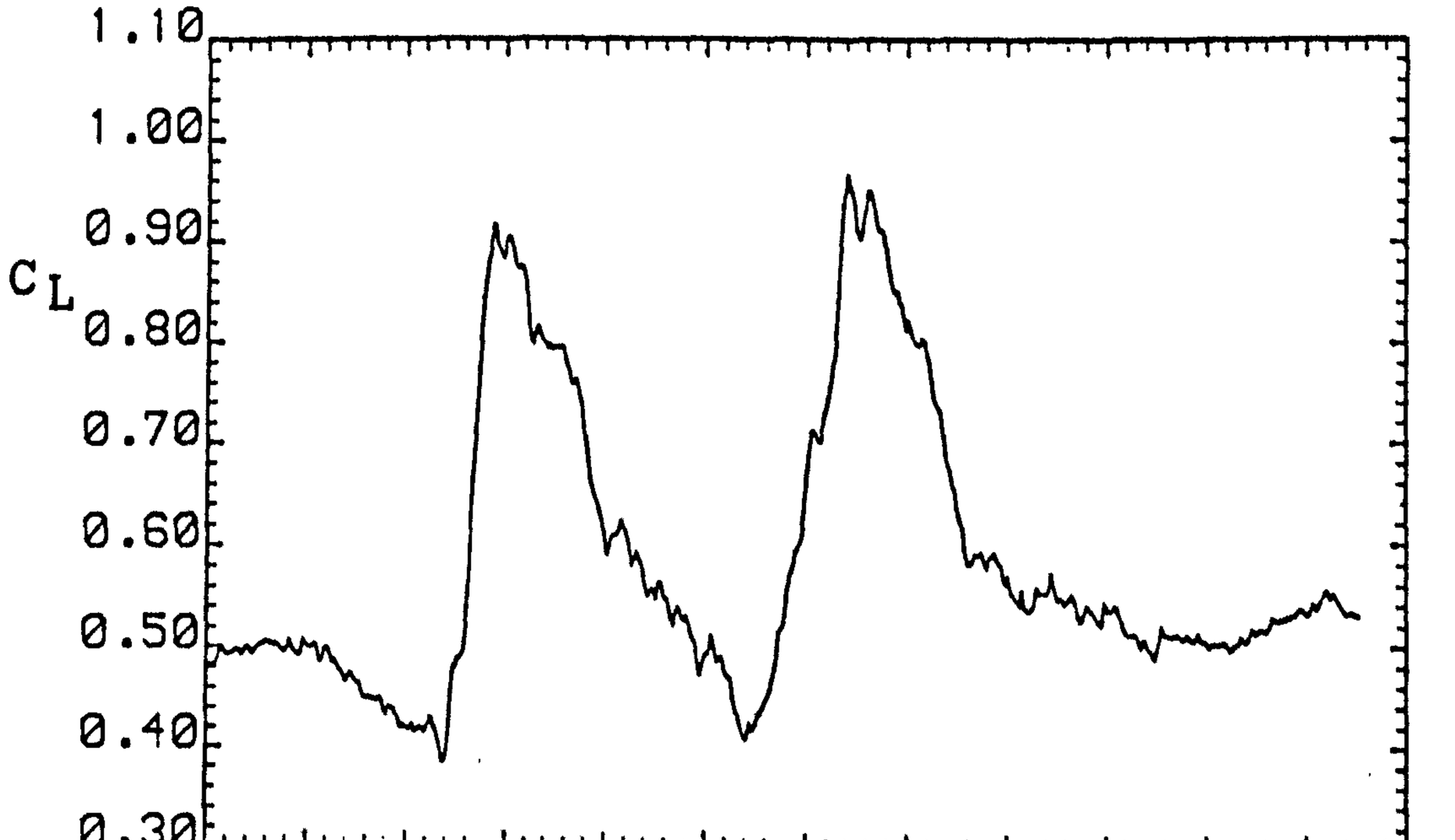

Fig. 5.53(b) Aerofoil lift time history

Run 9506

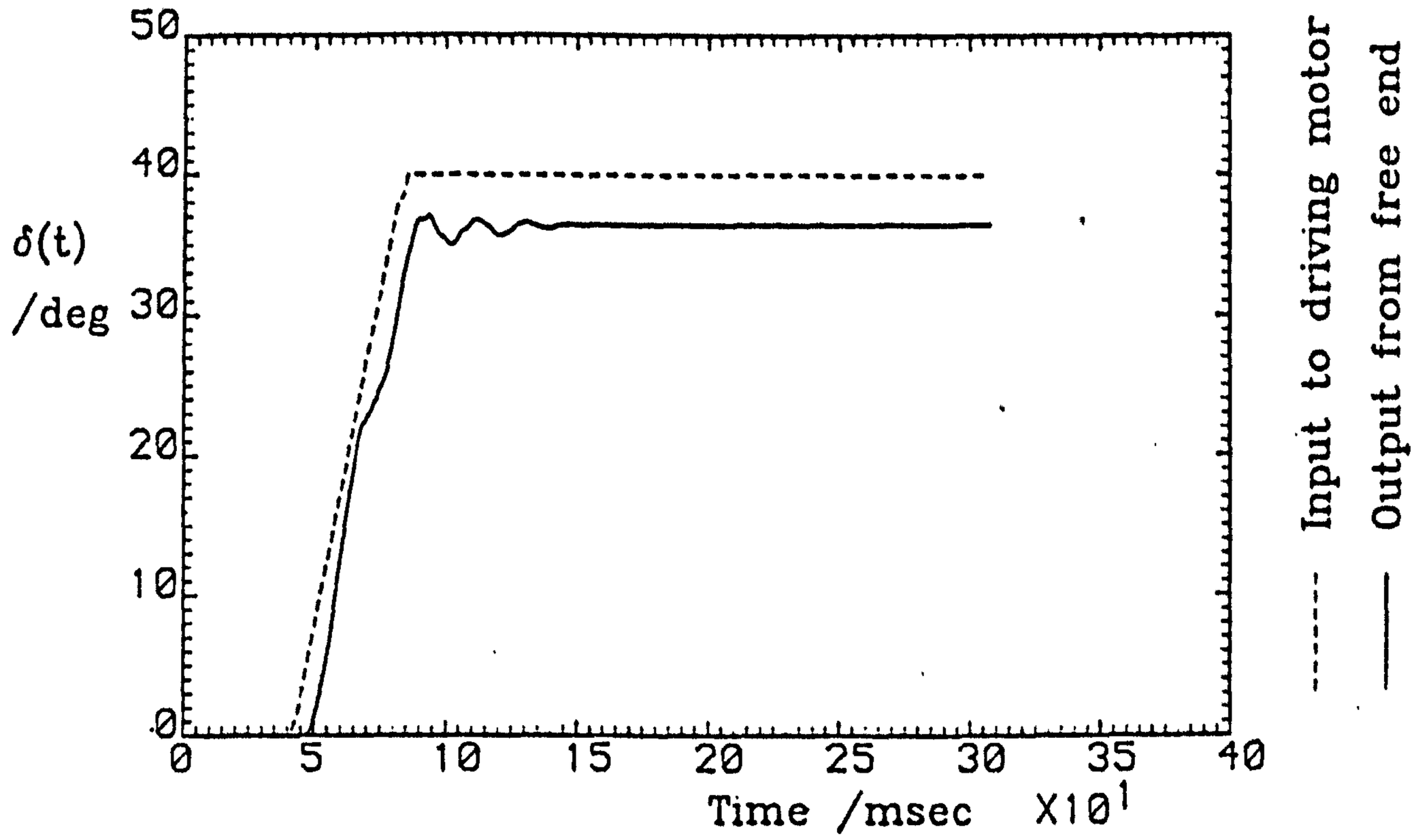

Fig. 5.54(a) Spoiler displacement trace

Spoiler configuration: Upper-surface,		
13% chord, gap opened, perforations closed		
α= 0.0°	U=20.0m/s	$\dot{\delta}$=990°/s

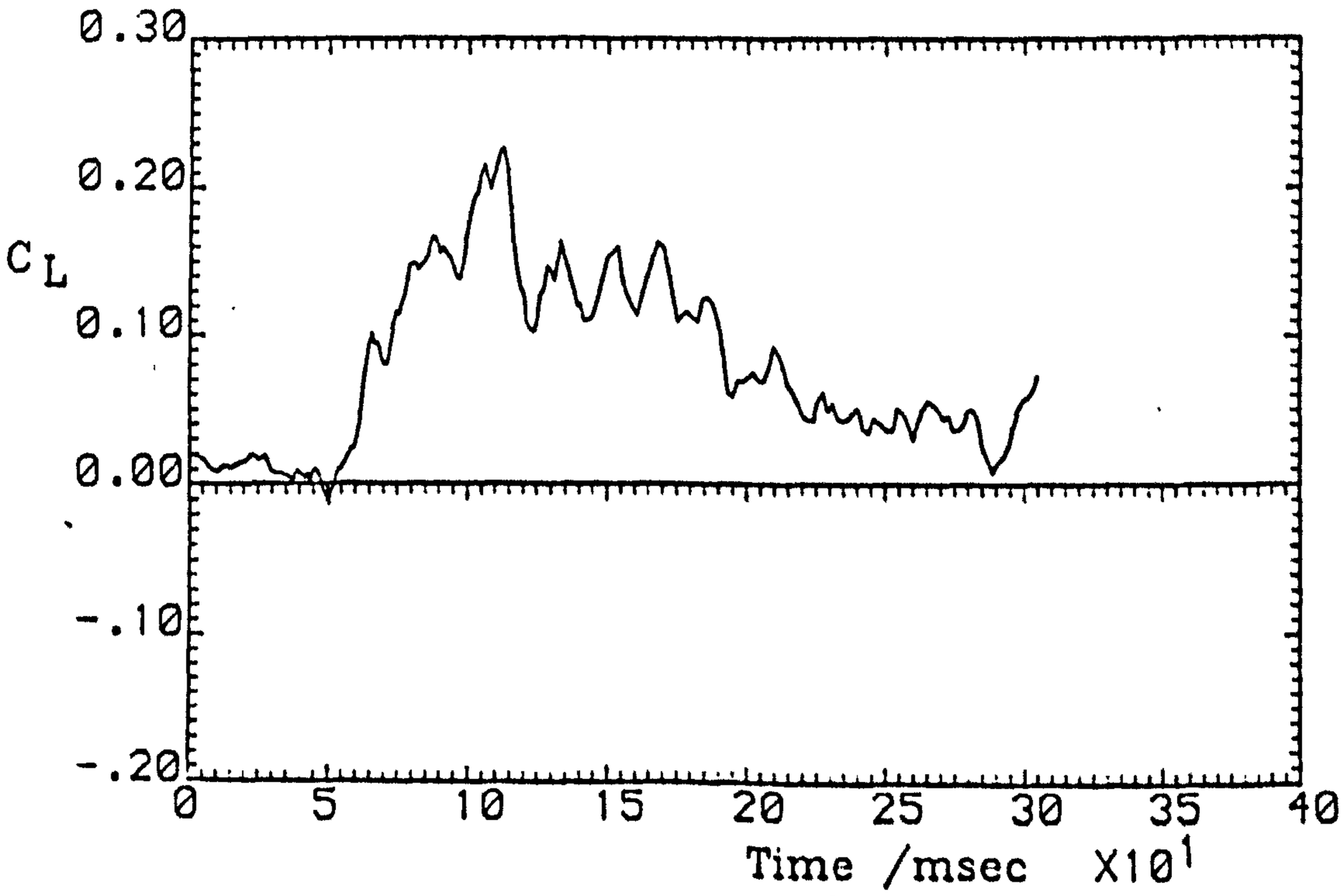

Fig. 5.54(b) Aerofoil lift time history

Run 3401

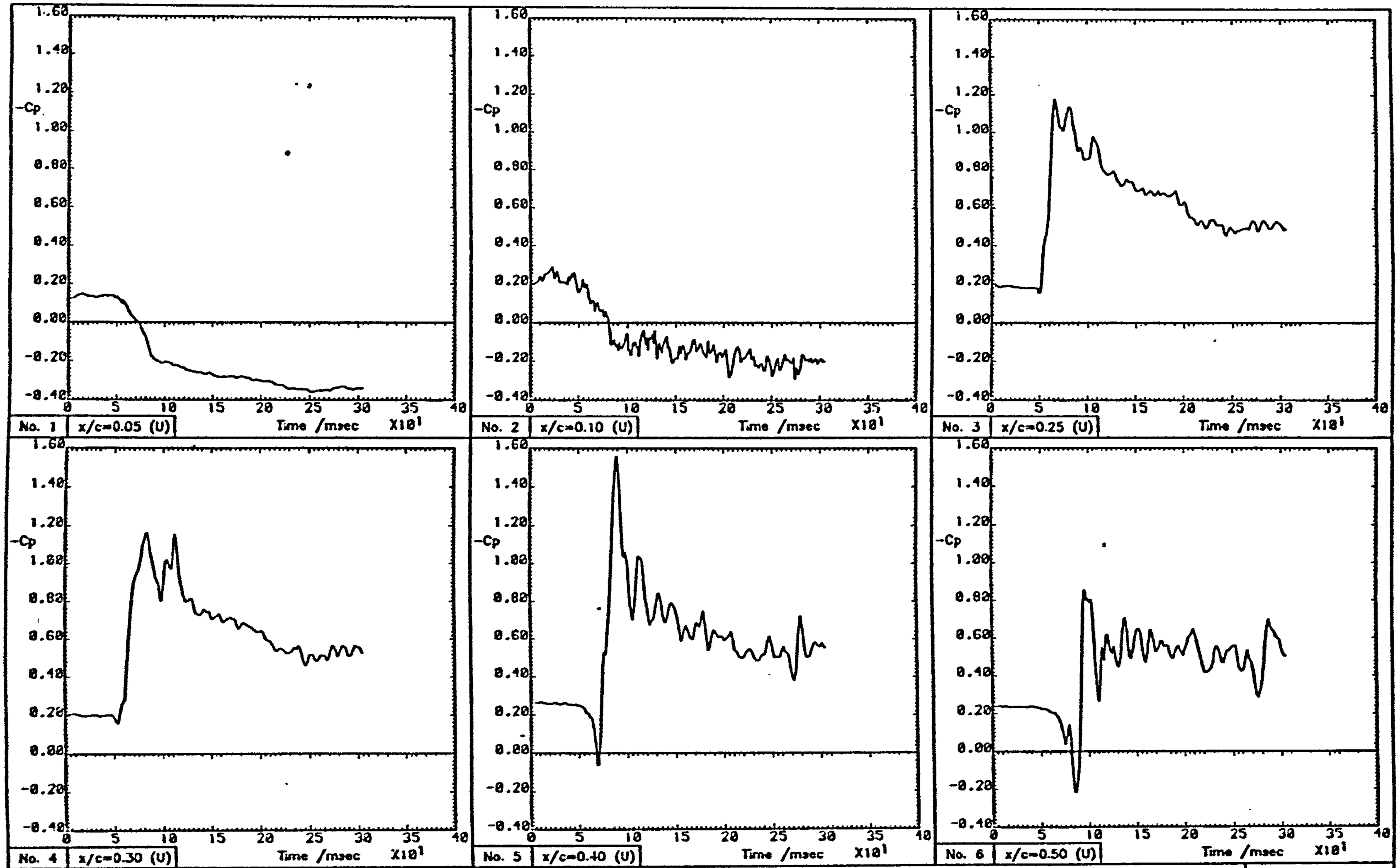

Fig. 5.55(a) Pressure signal time histories

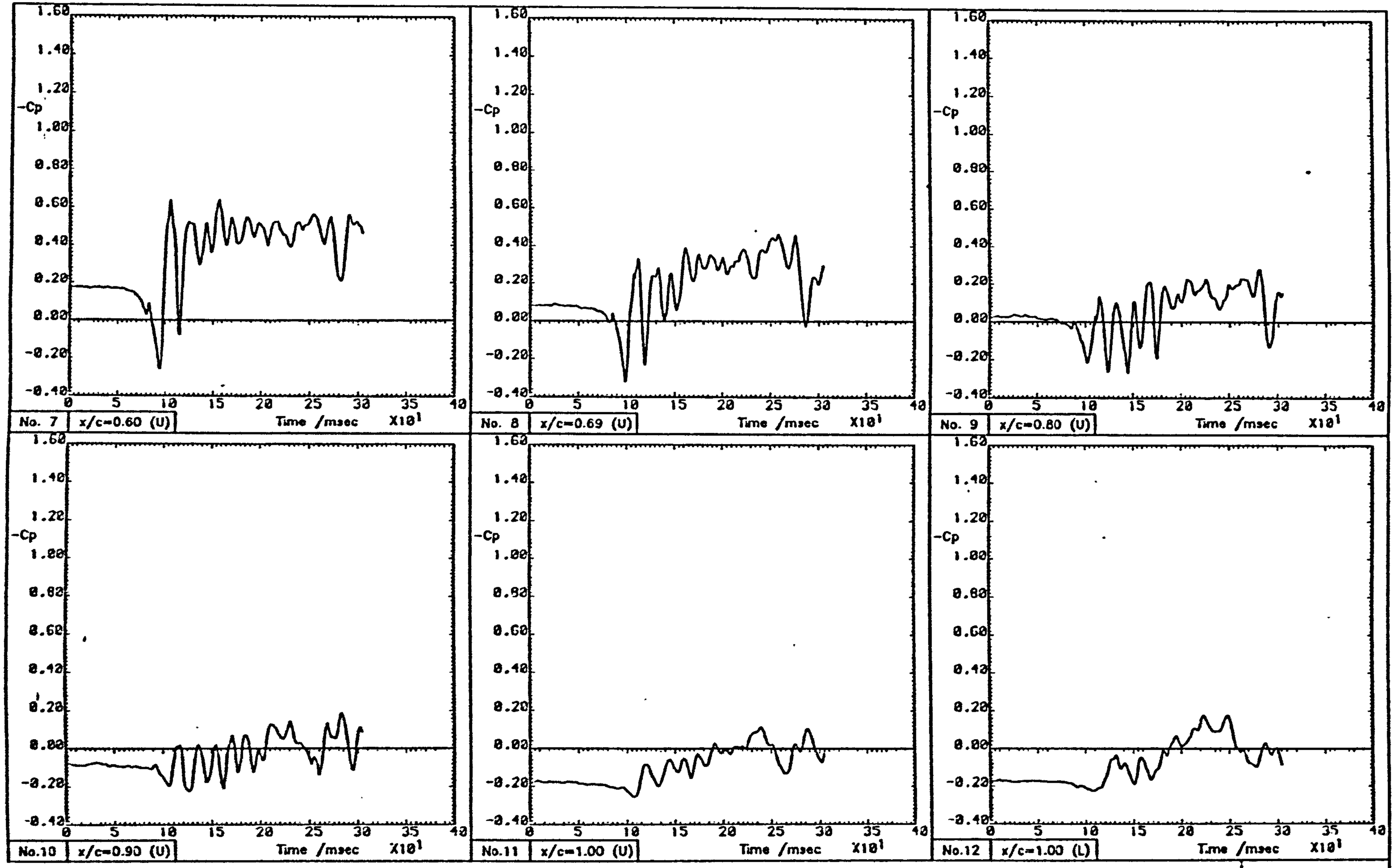

Fig. 5.55(b) Pressure signal time histories

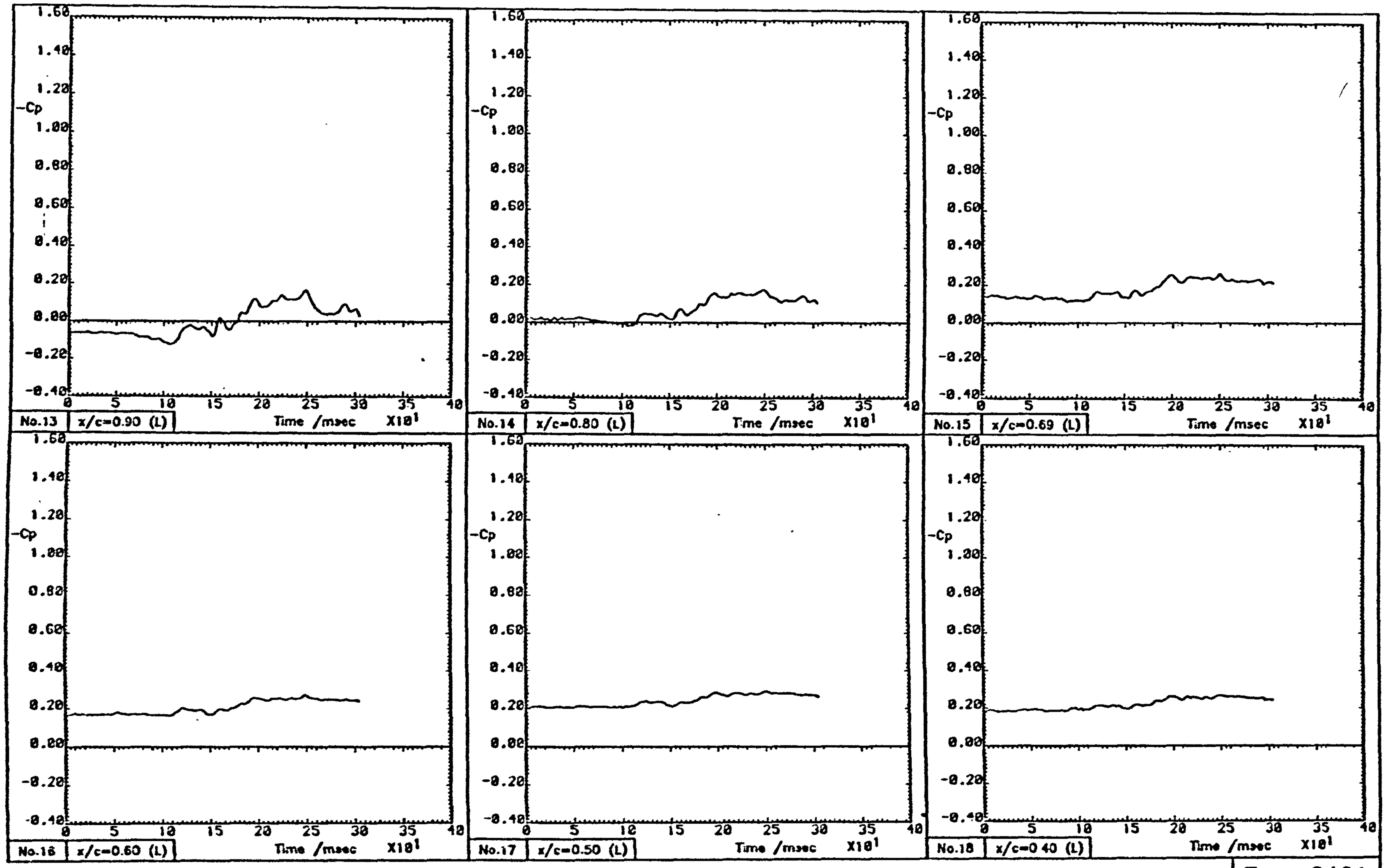

Fig. 5.55 (c) Pressure signal time histories

Run 3401

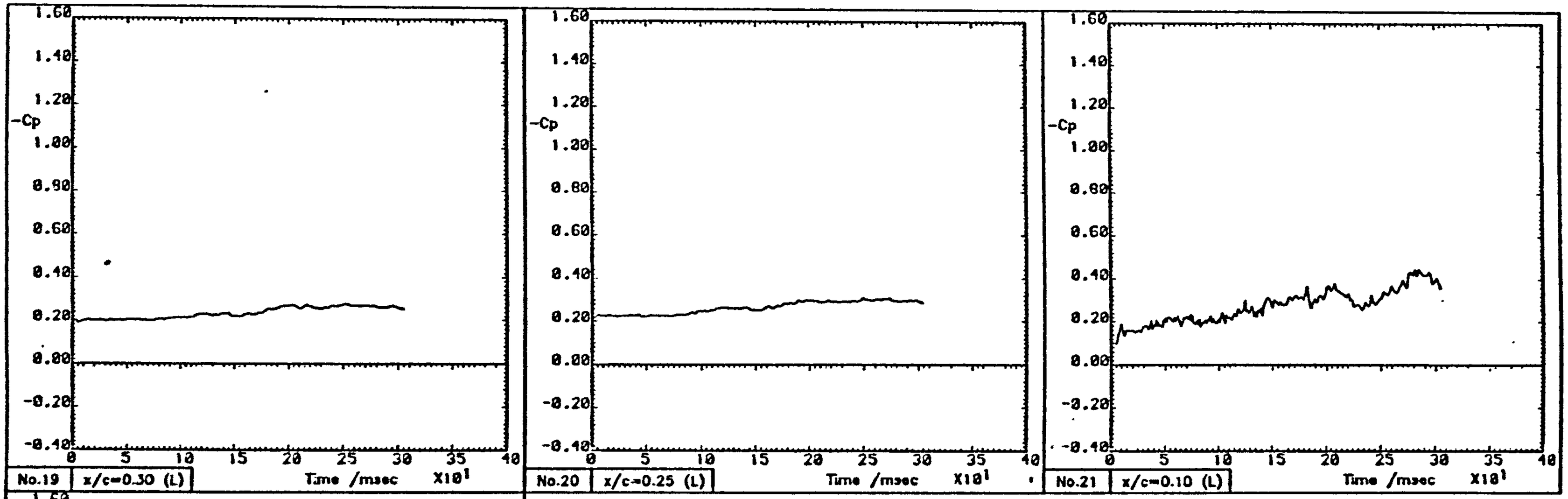

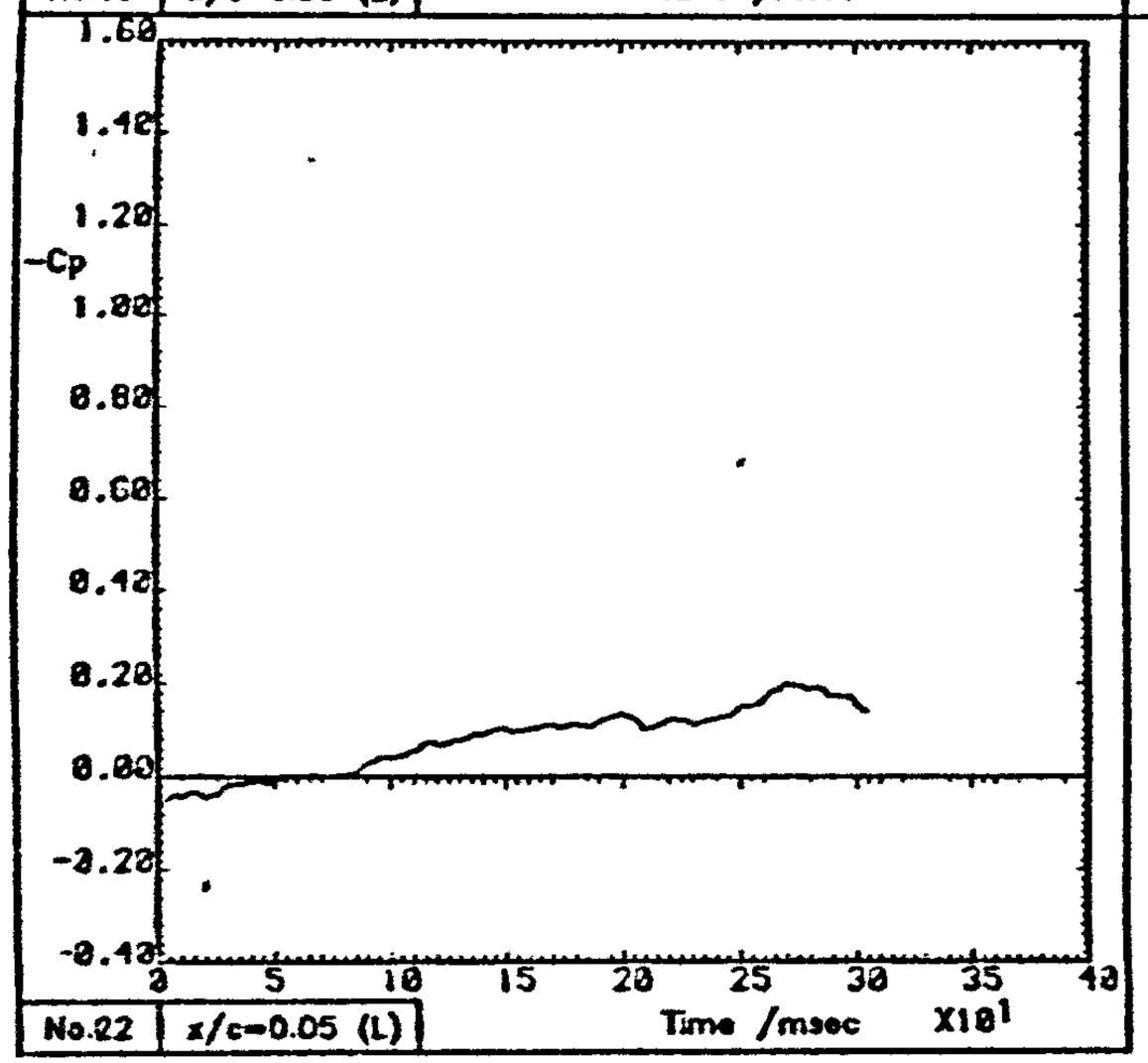

Fig. 5.55(d) Pressure signal time histories

Run 3401

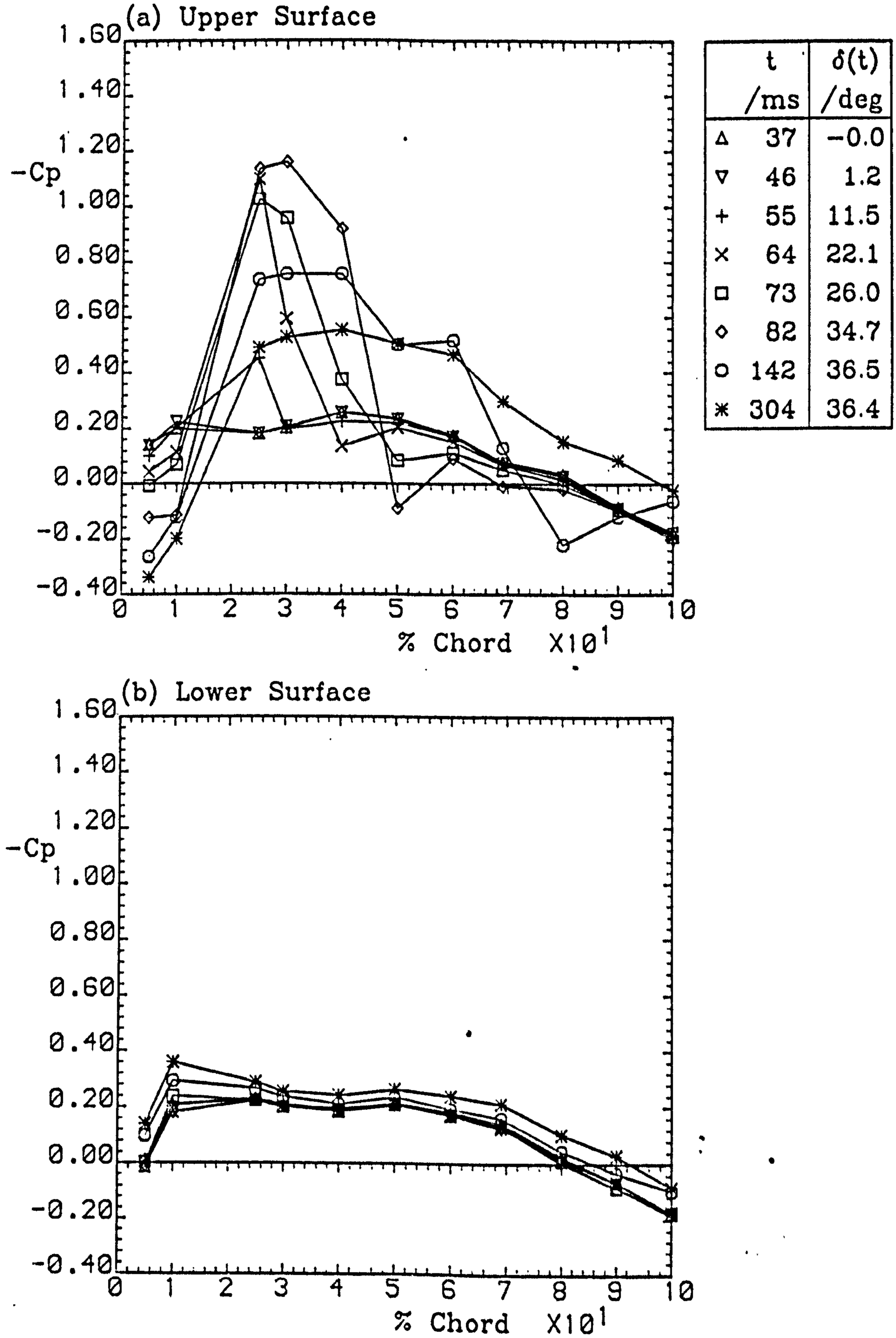

	t /ms	δ(t) /deg
△	37	-0.0
▽	46	1.2
+	55	11.5
×	64	22.1
□	73	26.0
◇	82	34.7
○	142	36.5
✳	304	36.4

Fig. 5.56 Time-varying pressure distributions

Run 3401

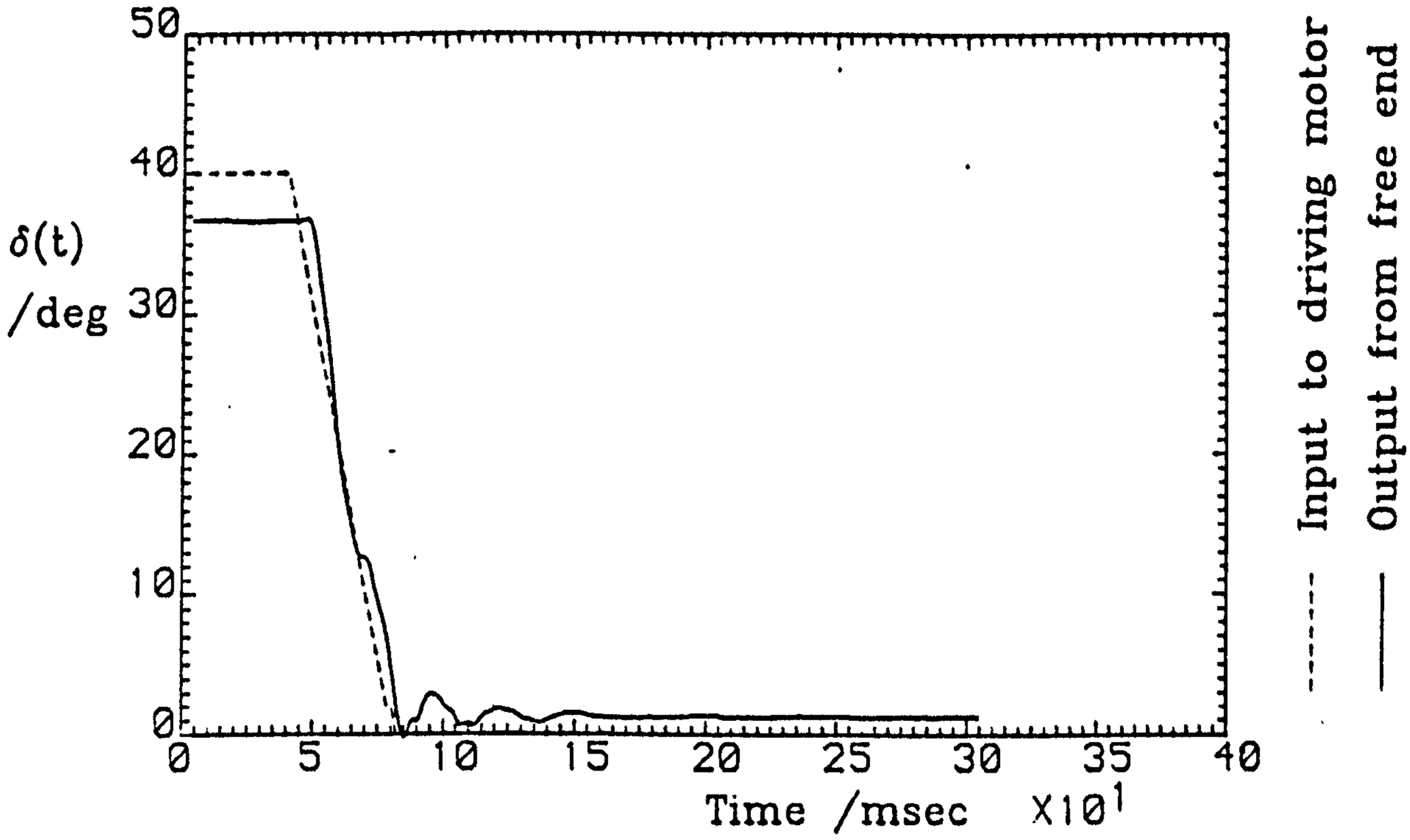

Fig. 5.57(a) Spoiler displacement trace

Spoiler configuration: Upper-surface,		
13% chord, gap opened, perforations closed		
α= 0.0°	U=20.0m/s	$\dot{\delta}$=990°/s

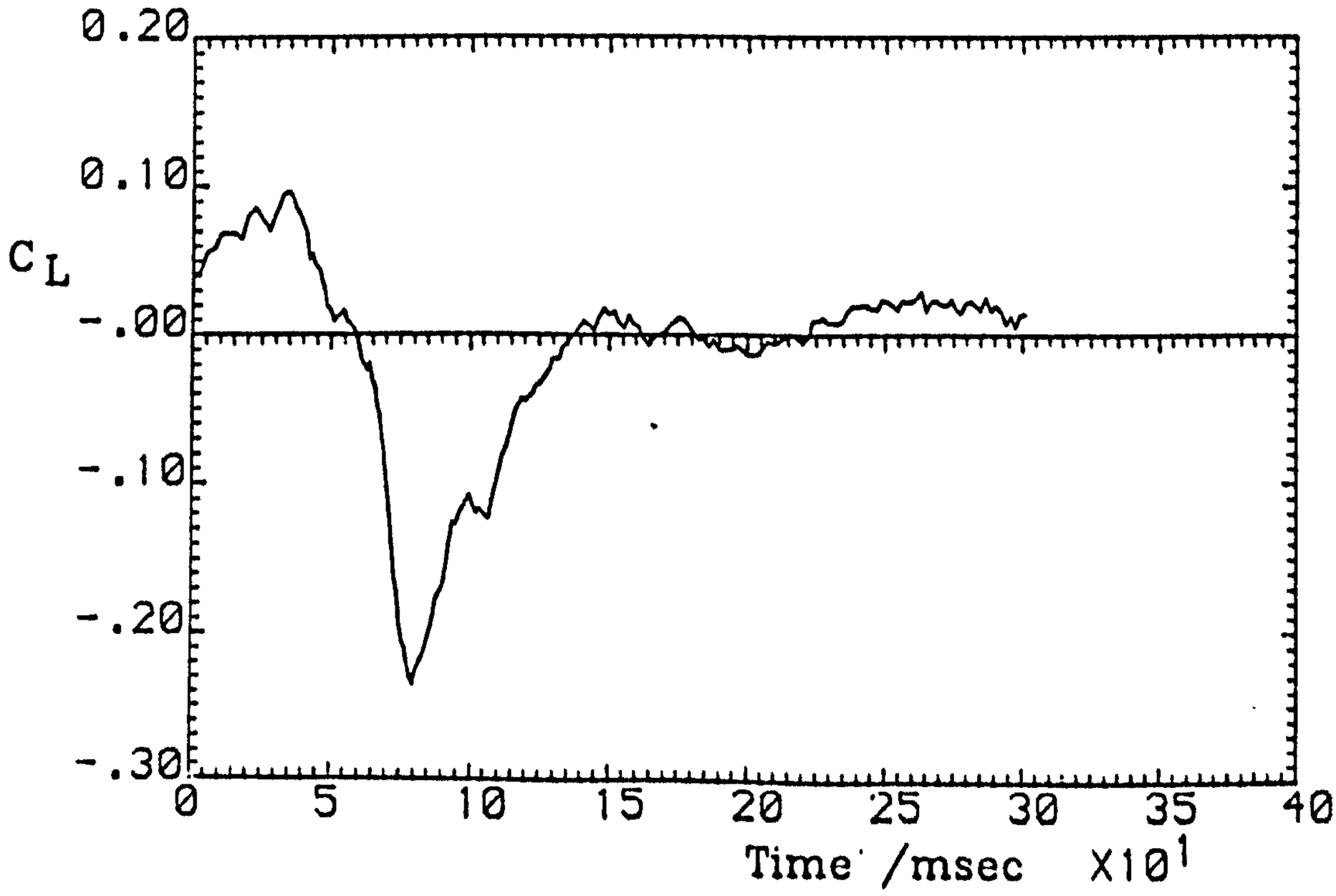

Fig. 5.57(b) Aerofoil lift time history

Run 3451

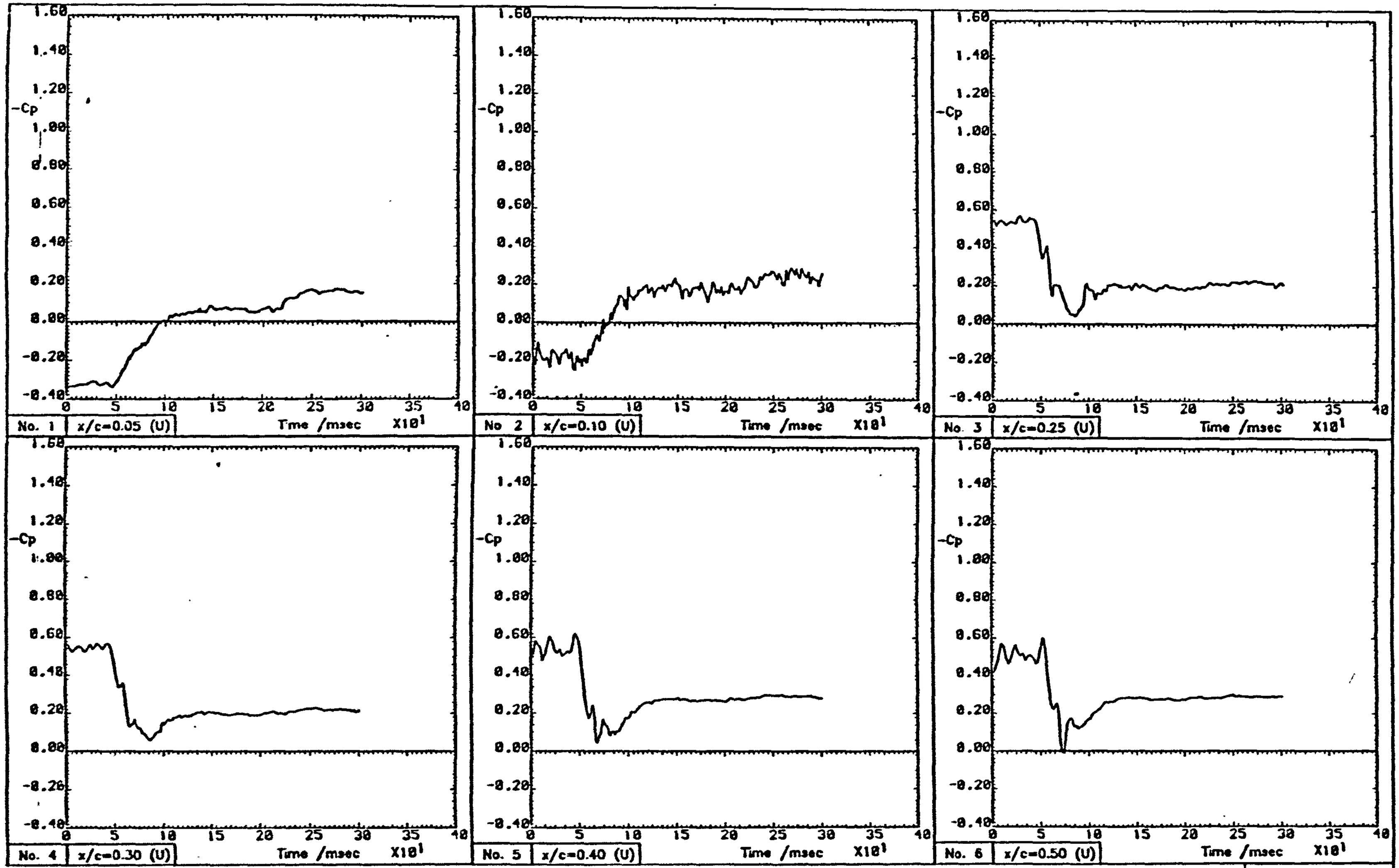

Fig. 5.58(a) Pressure signal time histories

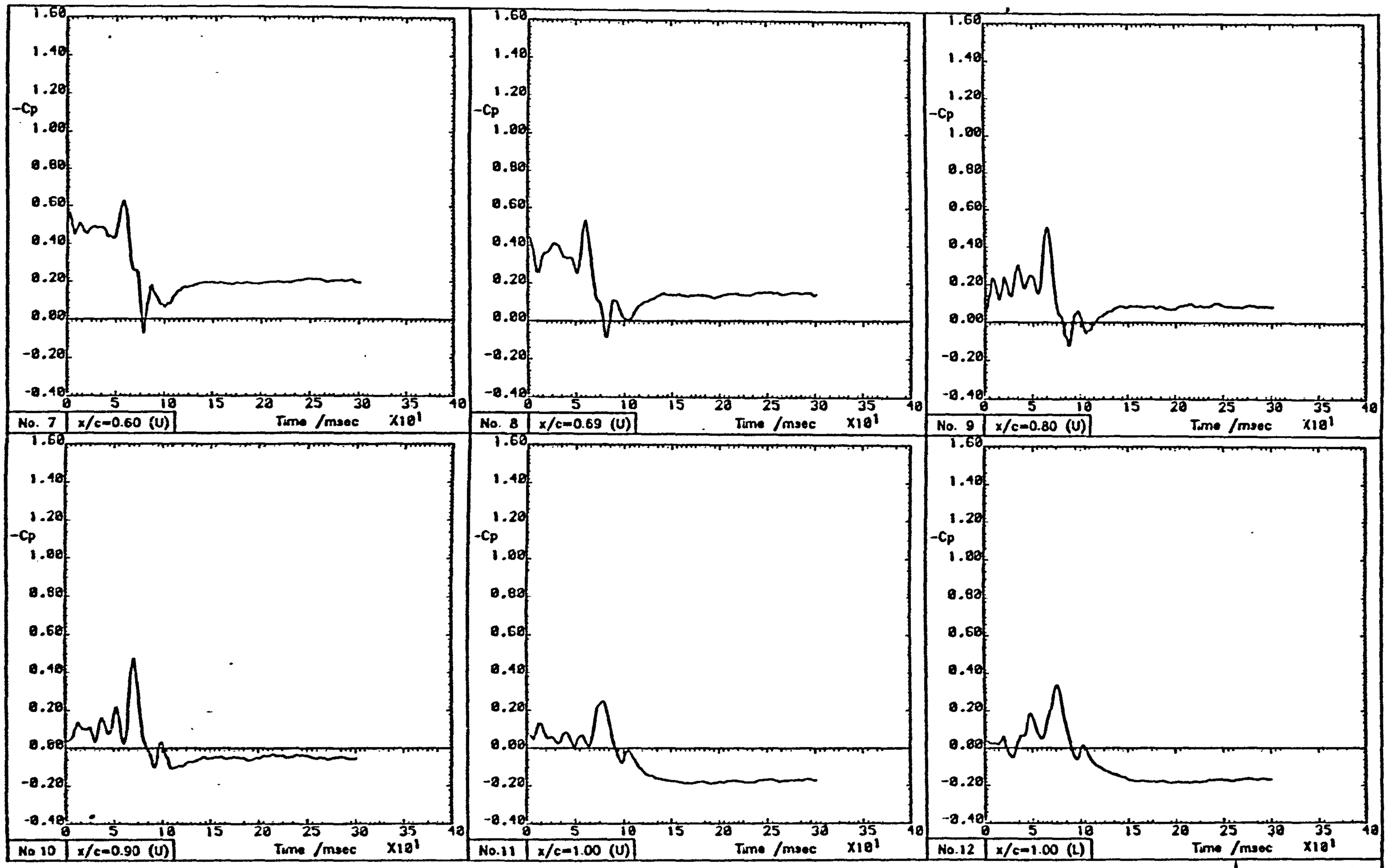

Fig. 5.58 (b) Pressure signal time histories

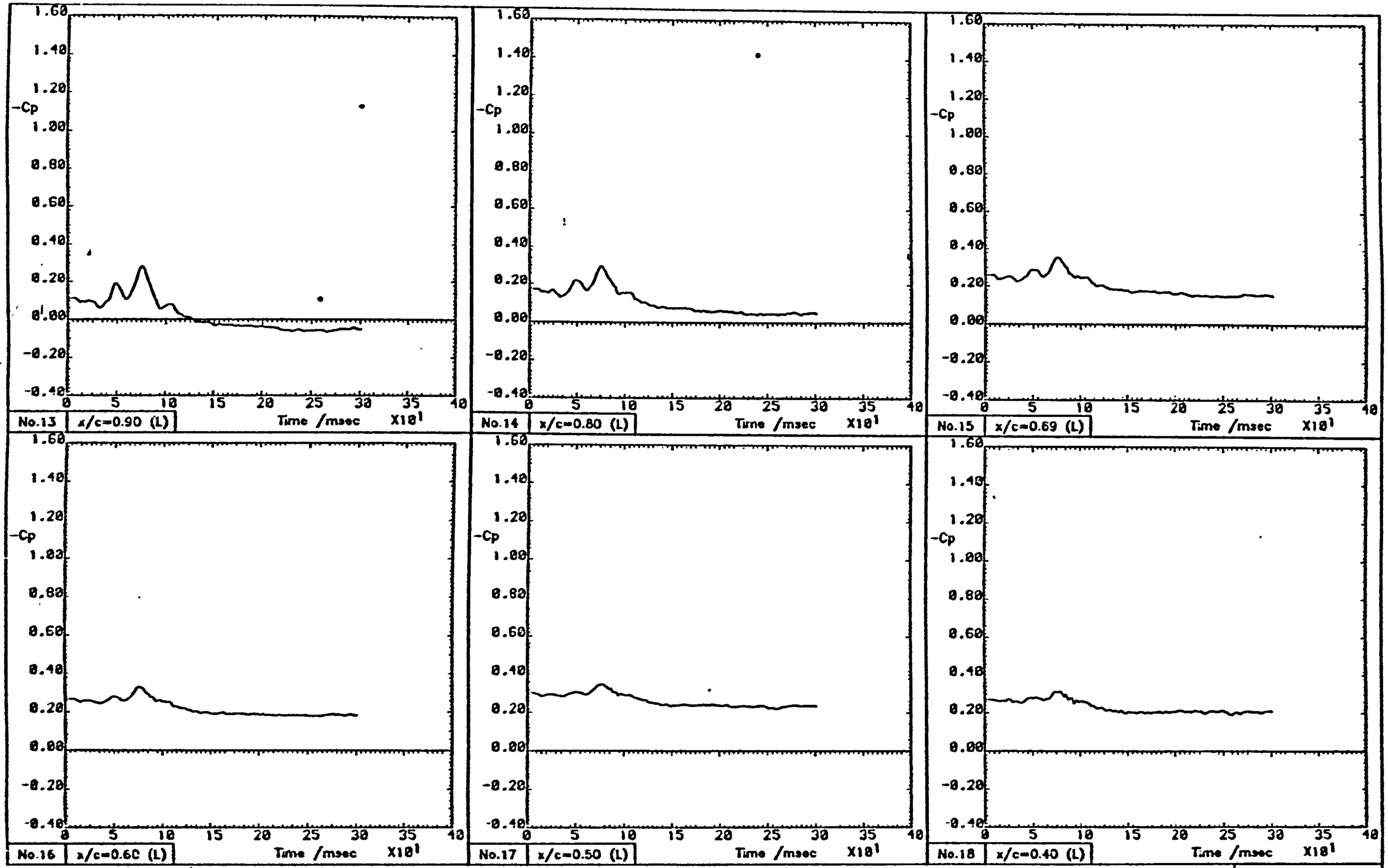

Fig. 5.58(c) Pressure signal time histories

Run 3451

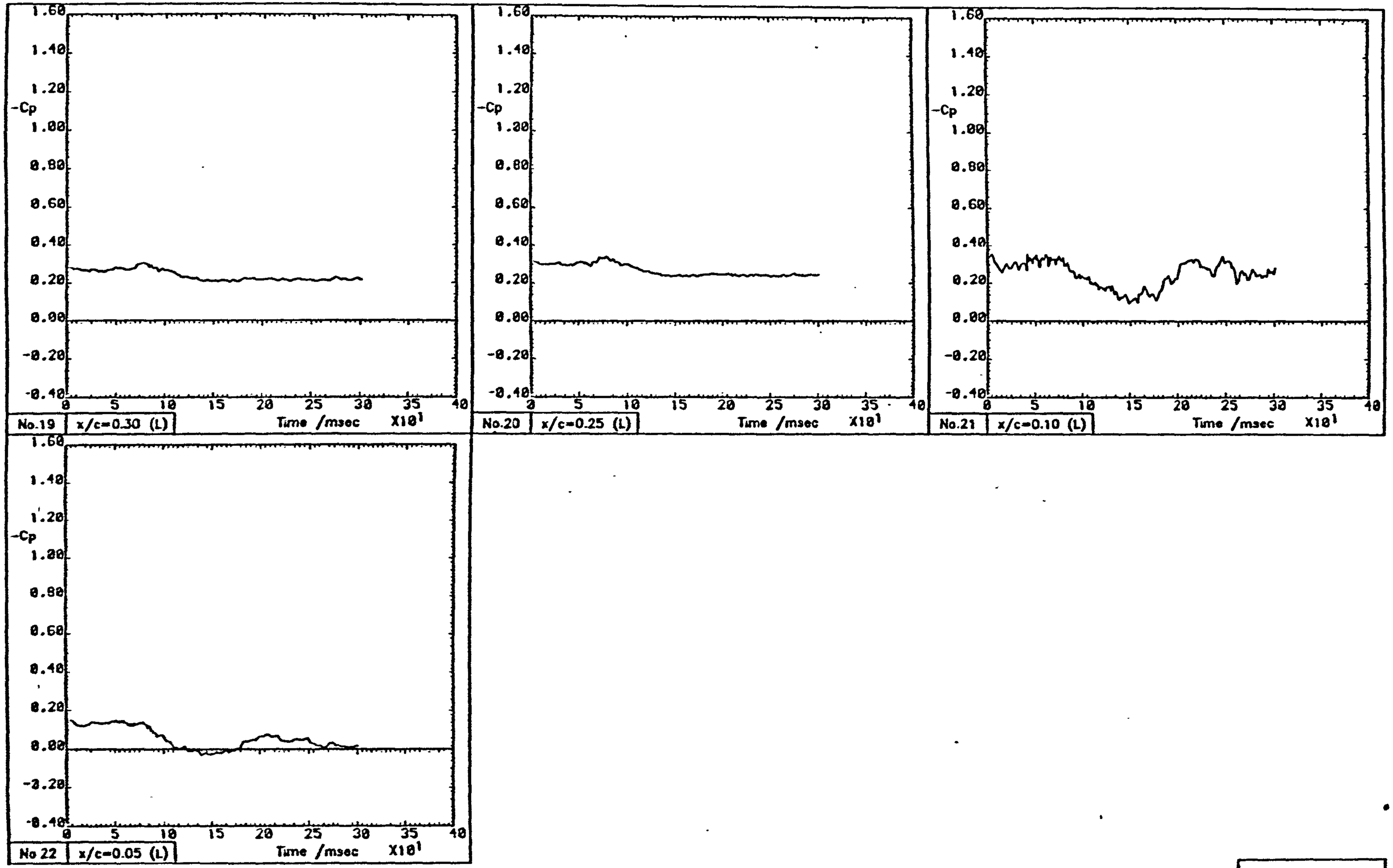

Fig. 5.58 (d) Pressure signal time histories

Run 3451

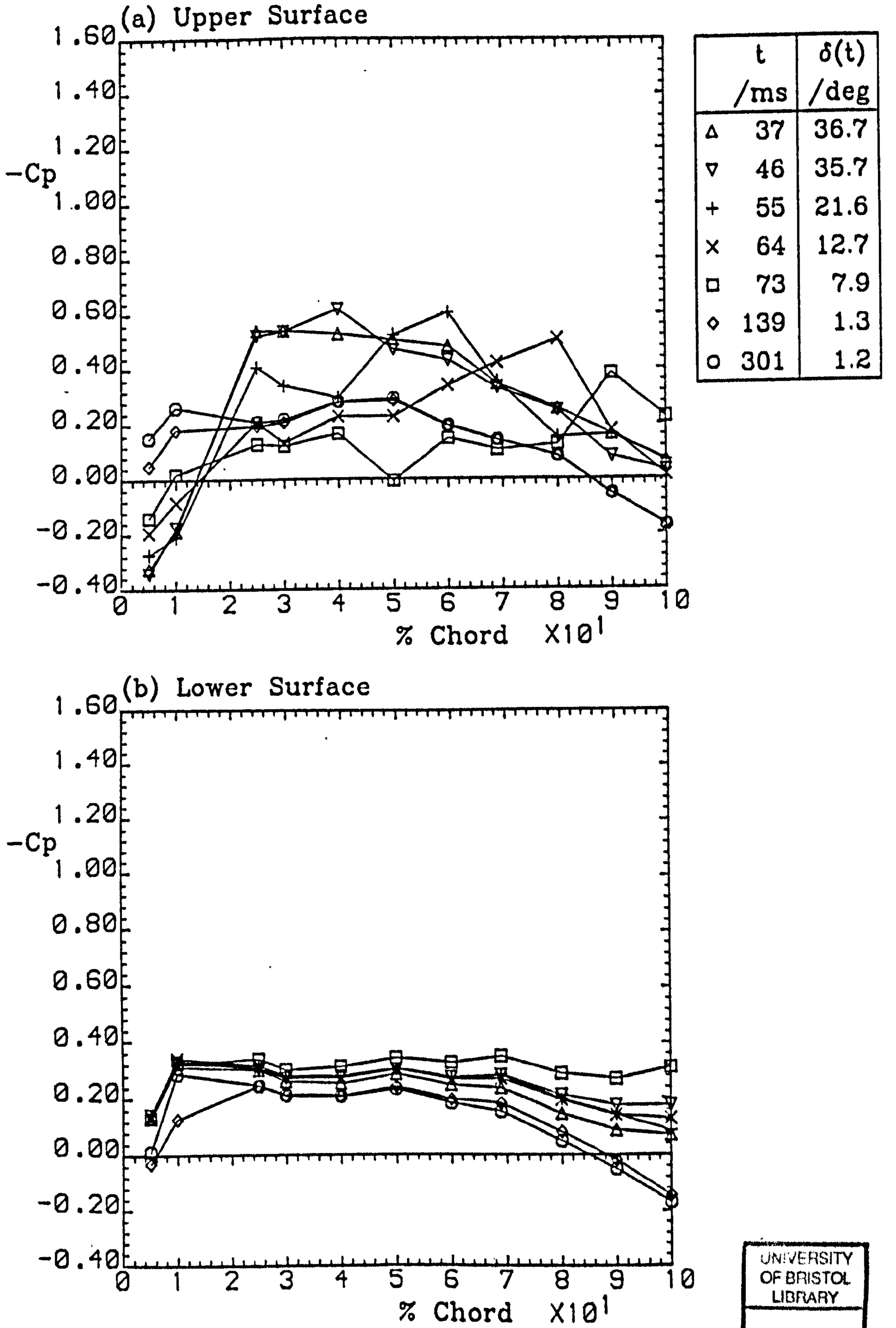

	t /ms	δ(t) /deg
△	37	36.7
▽	46	35.7
+	55	21.6
×	64	12.7
□	73	7.9
◇	139	1.3
○	301	1.2

UNIVERSITY OF BRISTOL LIBRARY
ENGINEERING

Run 3451

Fig. 5.59 Time-varying pressure distributions